Building and raising land: meandering rivers and filling estuaries

Steven A. H. Weisscher

255 UTRECHT STUDIES IN EARTH SCIENCES

Building and raising land: meandering rivers and filling estuaries

De vorming van nieuw land langs meanderende rivieren en riviermondingen

(met een samenvatting in het Nederlands)

P R O E F S C H R I F T

ter verkrijging van de graad van doctor aan de Universiteit Utrecht
op gezag van de rector magnificus, prof. dr. H.R.B.M. Kummeling,
ingevolge het besluit van het college voor promoties in het openbaar te verdedigen
op donderdag 1 september 2022 des middags te 12:15 uur

door

Steven Alexander Hubertus Weisscher

geboren op 23 december 1993 te Roosendaal en Nispen

Promotor:
Prof. dr M.G. Kleinhans

Copromotor:
Dr A.W. Baar

This work was financially supported by the European Research Council
(ERC Consolidator grant 647570).

Building and raising land: meandering rivers and filling estuaries

Promotor:
Prof. dr M.G. Kleinhans

Copromotor:
Dr A.W. Baar

Examination committee:
Prof. dr ir. K. Philippart
Royal Netherlands Institute for Sea Research, The Netherlands
Utrecht University, The Netherlands

Prof. dr I. Möller
Trinity College Dublin, Ireland

Prof. dr S. Temmerman
University of Antwerpen, Belgium

Dr A.J.F. Van der Spek
Deltares, The Netherlands

Prof. dr ir. A.J.F. Hoitink
Wageningen University, The Netherlands

Prof. dr T.J. Bouma
Royal Netherlands Institute for Sea Research, The Netherlands
Utrecht University, The Netherlands

ISBN 978-90-6266-623-2

Published by Faculty of Geosciences, Universiteit Utrecht, The Netherlands, in:
Utrecht Studies in Earth Sciences (USES), ISSN 2211-4335

Typeset using XeLaTeX

Cover: Tidal creek at Schiermonnikoog, the Netherlands, by Annerie Rutenfrans

Photography chapter covers: Kim van den Hoven [3] | Guus Weisscher [2, 5 & 6] | Steven Weisscher [1, 4 & 7]

Printed by Ipskamp Printing, Enschede, The Netherlands

Correspondence to: Steven Weisscher, steven@weisscher.nl

Utrecht Studies in Earth Sciences 255

Building and raising land: meandering rivers and filling estuaries

Steven Alexander Hubertus Weisscher

Utrecht 2022

Faculty of Geosciences, Utrecht University

Contents

明日は明日の風が吹く

Japanese proverb

(lit. “Tomorrow’s winds will blow tomorrow”)

“Tomorrow is another day.”

Summary

Estuaries form in drowned landscapes where rivers transition into the sea and come in a broad range of shapes and sizes. Previous efforts to categorise these tidal systems used the relative importance of rivers, waves and tides. However, this left differences due to the history of these systems largely unexplained, particularly the degree of estuary filling. Some estuaries have been completely filled, whilst others have been only partly filled or are still unfilled since sea-level rise slowed down during the Holocene. Until now, only two kinds of steady-state estuaries are recognised in the literature, namely (1) an unfilled lagoonal estuary with limited sediment supply and dynamics and (2) a completely filled estuary with an ideal upstream-converging shape.

A mechanism that could explain the diversity in estuary filling is well-known in rivers: floodplain formation. Fluvial studies showed that floodplain formation with mud and vegetation confines flow and fills accommodation, where a stronger tendency to form floodplains leads to narrower steady-state rivers that are meandering and laterally fixed, as opposed to wide and unconfined braiding. In this thesis, the parallels with estuaries are explored, where mud and vegetation are present in the form of mudflats and salt marshes. A recurring research question is to what extent these tidal floodplains influence the steady state of entire estuaries. Improved understanding of how estuaries evolve will lead to knowledge on how to design effective strategies of building and raising new land along estuaries to keep up with sea-level rise.

This thesis studied the effects of mud and vegetation on floodplain formation in meandering rivers and filling estuaries. Firstly, the necessary conditions for floodplain formation were studied for meandering rivers with chute channels (Chapter 2). Next, self-forming estuaries were created in the flume "the Metronome". As measurements of shallow flow in the experiments were practically infeasible, a flow model was tested and validated to derive data on water depth and flow velocity (Chapter 3). This model was used in the analyses of experiments of filling estuaries with mud and vegetation (Chapter 4) and sea-level rise (Chapter 5). Lastly, transitional polders between double dikes were modelled along the Western Scheldt Estuary (NL) to cause land-level rise (Chapter 6).

The river modelling with self-forming vegetated floodplains (Chapter 2) showed that a balance emerges between floodplain formation and destruction, and this balance determines the emergent channel and bar pattern. To reach this balance in a short model domain, a continuous inflow perturbation was necessary but had a negligible effect on the emergent channel and bar pattern. With increasing vegetation density, a continuum of rivers was formed between braided and meandering with chute channels.

By means of estuary experiments, it was studied (Chapter 4) to what extent such a balance in floodplain formation and destruction also influences the steady states of estuaries. The estuary experiments started as wide, deep lagoonal estuaries that filled in with fluvial and marine sediments. With only sand, the estuary filled sufficiently to form a multi-channel pattern with intertidal bars. Mud filled accommodation in the intertidal-to-supratidal reach. Compared to the experiments without vegetation, the vegetation channelised flow, which increased sediment transport in the upstream direction. Mud and vegetation narrowed the subtidal channels in the upstream direction, where the extent of intertidal and supratidal areas was governed by the balance between floodplain formation and destruction. This suggests that a range of steady states exist between the end-members of an unfilled and a completely filled estuary. Fast sea-level rise was applied in a new filling estuary experiment with otherwise the same conditions (Chapter 5) and caused sediment deposition closer to its marine and fluvial sources. As a result, the central part of the estuary became sediment-starved and subsequently drowned with fewer locations available for vegetation establishment.

Tidal floodplain formation fastened land-level rise in experiments and was tested further in a numerical model of the Western Scheldt Estuary (Chapter 6), where transitional polders (*in Dutch: wisselpolders*) are being considered to raise low-lying land. Four polders were added to the Western Scheldt and tested for different opening sequences and inlet widths. Findings showed land-level rise in all configurations. Transitional polders opened in an upstream-to-downstream sequence resulted in stronger shallowing of the estuary and hence in smaller tidal ranges than a downstream-to-upstream sequence, suggesting the opening sequence can play a part in managing flood risk. Polders opened later in a sequence temporarily experienced a lag in mud deposition, and net sand import was smaller for polders with a wide foreshore due to deeper inlet erosion.

This thesis proposes that tidal floodplains (i.e. mudflats and salt marshes) promote the filling of estuaries, where the balance between floodplain formation and destruction determines the steady state of an estuary. A stronger tendency to form floodplains results in a narrower estuary, similarly to how more extensive floodplains transform rivers from braided to meandering. Fast sea-level rise will probably enhance floodplain destruction in estuaries, which asks for effective strategies such as transitional polders to retain sediments, raise land and maintain ecologically valuable intertidal areas.

Samenvatting

Estuaria, ook wel riviermondingen genoemd, zijn waterrijke landschappen waar rivieren overgaan in de zee en komen voor in allerlei vormen en maten. Deze landschappen worden veelal gevormd door rivieren, golven en het getij, en de verhouding van deze drie invloeden gebruikt men doorgaans om riviermondingen onder te verdelen in verschillende klassen. Zo zijn er bijvoorbeeld riviermondingen die voornamelijk hun vorm te danken hebben aan de golven, terwijl andere juist grotendeels gevormd worden door het in- en uitgaande getij. Gezamenlijk voeren de rivieren, golven en het getij zand en slib aan, wat in veel gevallen zorgt voor de langzame opslibbing en verlanding van deze landschappen. Desondanks zijn deze drie invloeden niet toereikend om alle verschillen tussen riviermondingen te verklaren, en dan met name de mate van opvulling. Waar het ene estuarium grotendeels is afgevuld met zand en slib, zijn andere maar gedeeltelijk afgevuld of nog compleet ongevuld. Dit suggereert dat ook interne mechanismen belangrijk zijn voor de ontwikkeling van riviermondingen.

Een mechanisme dat de verschillen in de mate van opvulling van estuaria kan verklaren, komt uit de hoek van rivieren: de vorming van overstromingsvlakten (ook wel uiterwaarden genoemd). Eerder onderzoek in rivieren toonde aan dat de vorming van overstromingsvlakten met slib en planten de stroming vernauwt en het omliggende landschap opvult. Dit betekent dat een snelle vorming van uiterwaarden leidt tot een smalle geul die meandert of vast ligt in het landschap, in tegenstelling tot onbegrensde rivieren die juist breed zijn en uit meerdere geulen bestaan. In deze thesis beschrijf ik de parallellen tussen rivieren en riviermondingen, waarbij slib en vegetatie ook aanwezig zijn in riviermondingen in de vorm van slikken/wadplaten en schorren/kwelders. Een terugkerende onderzoeksvraag is in hoeverre de vorming van overstromingsvlakten de uiteindelijke vorm en grootte van riviermondingen bepaalt. Een beter begrip van hoe estuaria ontwikkelen kunnen we vervolgens gebruiken om effectieve maatregelen te ontwerpen om het land langs riviermondingen mee te laten groeien met de stijgende zeespiegel.

In deze thesis onderzocht ik de effecten van slib en vegetatie op de vorming van overstromingsvlakten in rivieren en estuaria. Eerst ging ik op zoek naar de condities die nodig zijn om uiterwaarden te laten ontstaan langs meanderende rivieren (hoofdstuk 2). Hierna liet ik gehele riviermondingen ontstaan op kleine schaal in een laboratorium. Aangezien het meten van de ondiepe getijdestroming niet mogelijk was in de experimenten, heb ik een computermodel opgezet en getest om waterdieptes en stroomsnelheden uit mijn schaalexperimenten te halen (hoofdstuk 3). Dit model kon ik vervolgens gebruiken om de experimenten van opvullende estuaria met slib en vegetatie (hoodstuk 4) en zeespiegelstijging (hoofdstuk 5) verder te analyseren. Als laatste paste ik de kennis van de eerdere hoofdstukken toe in computermodellen om hoger land (ook wel: landspiegelstijging) langs de Westerschelde te creëren (hoofdstuk 6).

Het modelleren van rivieren met begroeide uiterwaarden (hoofdstuk 2) liet zien dat er een balans ontstaat tussen de vorming en afbraak van uiterwaarden en dat deze balans het aantal geulen en zandbanken in de rivier bepaalt. Om deze balans in een computermodel te bereiken, liet ik het instroompunt van de rivier wiebelen. Deze verstoring was nodig om het meanderen op te starten, maar had verder geen noemenswaardig effect op hoe de rivier zich ontwikkelde. Verder toonde de modelstudie aan dat meer vegetatie leidt tot een overgang van een rivier met meedere geulen naar een rivier met een enkele, meanderende geul.

In schaalexperimenten van estuaria bestudeerde ik hoe de balans tussen de vorming en afbraak van overstromingsvlakten de uiteindelijke vorm van estuaria beïnvloedt (hoofdstuk 4). De experimenten begonnen als een brede, diepe, verdronken vallei met een riviertoevoer aan de bovenstroomse rand en een opening naar de zee aan de benedenstroomse rand. Vervolgens zorgde de aanvoer van zand en

slib vanuit de rivier en de zee voor de opvulling van het estuarium. Het zandige estuarium importeerde genoeg zand om hoge zandbanken te vormen met veel tussenliggende geulen. Slib vulde met name de ruimte in het gebied tussen de laag- en hoogwaterstand. Vegetatie zorgde voor een vernauwing van de getijdestroming, waardoor meer zand en slib naar het land werd vervoerd. De vorming van de modderige en begroeide overstromingsvlakten droeg bij aan het vernauwen van de diepe getijdegeulen en bepaalde de grootte van de slikken/wadplaten en schorren/kwelders. Dit betekent dat het interne mechanisme om overstromingsvlakten te vormen mede bepaalt in hoeverre een estuarium opvult. In een vervolgonderzoek (hoofdstuk 5) paste ik snelle zeespiegelstijging toe op eenzelfde experiment van een opvullende riviermonding met slib en vegetatie. De zeespiegelstijging zorgde ervoor dat zand en slib minder ver de riviermonding in werd vervoerd; oftewel, zand en slib hoopte op nabij de riviertoevoer en nabij het getijdegat (de connectie met de zee). Hierdoor ontstond een tekort aan sediment in het centrale gedeelte van de riviermonding, waardoor dit gedeelte steeds dieper werd en daar minder plekken waren waar vegetatie zich kon vestigen.

De vorming van overstromingsvlakten in riviermondingen leidde tot snellere landspiegelstijging in de experimenten en dit principe toetste ik in een computermodel van de Westerschelde (hoofdstuk 6). Momenteel denkt men na om langs de Westerschelde wisselpolders aan te leggen om het ingeklinkte land te verhogen. Wisselpolders zijn bestaande stukken land die tijdelijk worden vrijgegeven aan het getij. Zodra er voldoende zand en slib is ingevangen, kan de polder weer worden gesloten en uiteindelijk terugkeren naar z'n oorspronkelijke functie. In deze thesis voegde ik vier van deze polders toe aan de Westerschelde om te testen of de volgorde van het openen van deze polders, evenals de breedte van de inlaat, uitmaakt voor hoe snel zand en slib worden ingevangen. In alle scenario's was er sprake van landspiegelstijging. Het openen van wisselpolders van bovenstrooms naar benedenstrooms zorgde voor meer verondieping van het estuarium en daardoor voor een kleinere getijdeslag dan een openingsvolgorde van benedenstrooms naar bovenstrooms. Dit suggereert dat de volgorde van het openen van wisselpolders een rol kan spelen in het beheersen van overstromingsrisico's. Wisselpolders die als tweede of later werden geopend, hadden een tijdelijke vertraging in het invangen van slib. Verder was de aanvoer van zand naar een wisselpolder kleiner als deze achter een brede vooroever lag vanwege diepere erosie ter hoogte van de inlaat.

Met deze thesis stel ik voor dat overstromingsvlakten (slikken/wadplaten en schorren/kwelders) de opvulling van estuaria bevorderen, waarbij de balans tussen de vorming en afbraak van overstromingsvlakten de uiteindelijke vorm van een riviermonding bepaalt. De vorming van grotere overstromingsvlakten leidt tot smallere riviermondingen, vergelijkbaar met hoe dit in rivieren leidt tot smallere geulen die gaan meanderen. Snelle zeespiegelstijging zal waarschijnlijk de afbraak van overstromingsvlakten in riviermondingen vergroten. Dit vraagt dus om effectieve maatregelen, bijvoorbeeld wisselpolders, om landspiegelstijging te verwezenlijken en ecologisch belangrijke intergetijdegebieden tussen laag- en hoogwater te behouden.


1

Chapter 1 | Introduction

1.1 Context

Estuaries form in drowned, geologically inherited landscapes where rivers transition into the sea (Fig. 1.1) and come in an array of shapes and sizes. The transition from a river to the sea results in an along-channel gradient in an estuary from river-dominated discharge to tidal flow (e.g. Dalrymple et al., 1992). These river and tidal flows deliver sediment to an estuary, where it accumulates and is used to form intertidal bars, mudflats and salt marshes (Fig. 1.1). Hence, estuaries are commonly regarded as natural sinks for sediment (Dalrymple et al., 1992; Savenije, 2015; Dronkers, 2017).

Previous efforts to classify the many shapes of estuaries used the relative importance of rivers, waves and tides (Fig. 1.2) (Boyd et al., 1992; Yang et al., 2005). This led to the conceptual distinction between tide-dominated and wave-dominated estuaries, and (wave-dominated) lagoons that have a negligible river discharge and sediment input. These tidal environments are placed on a continuum between coastal tidal flats and strandplains without a river influence, and deltas (Fig. 1.2b). Yet, the broad classes of wave- and tide-dominated estuaries leave differences due to the history of these tidal systems largely unexplained, particularly the degree of estuary filling. Since sea-level rise slowed down during the Holocene, some estuaries have been completely filled, whilst others have been only partly filled or are still unfilled (e.g. Roy et al., 1980; Dalrymple et al., 1992; Féniès and Faugères, 1998; Clement et al., 2017; De Haas et al., 2018). As a result, there are large differences that remain unexplained in e.g. the areal extent of mudflats and salt marshes, and the channel and bar pattern, ranging from a multi-channel network to a single channel (see Fig. 4.1 for examples with different degrees of filling). A possible process that may further explain these difference in estuary morphology is estuary filling. The more an estuary is filled, the more mudflats and salt marshes and fewer, narrower tidal channels tend to be observed. However, the previous focus in literature on estuary filling from a geological perspective (e.g. Roy et al., 1980; Dalrymple et al., 1992) paid little attention to (1) how the process of estuary filling with sand, mud and vegetation takes place, and (2) how this influences the channel and bar pattern on a scale of entire estuaries.

A mechanism that could explain the diversity in estuary filling is well-known in rivers: floodplain formation. Rivers, similar to estuaries, fill their accommodation with sandy and muddy sediments and vegetation. Rivers tend to build floodplains of mud and vegetation which are raised by sediment supply during regular floods (Ferguson, 1987; Tal and Paola, 2010; Van Dijk et al., 2013a; 2013b). Meanwhile, laterally migrating channels and large floods rework part of the floodplains, resulting in a balance between floodplain formation and destruction (Fig. 1.1) (e.g. Braudrick et al., 2009; Van Oorschot et al., 2016). With decreasing stream power, this balance tilts towards stronger floodplain formation, which leads to narrower steady-state rivers (Nicholas, 2013). Accordingly, a continuum of steady-state rivers is recognised ranging from braided to meandering to laterally fixed (Leopold and Wolman, 1957; Kleinhans and Van den Berg, 2011) and from multi-channel to single-channel systems (Nanson and Knighton, 1996). For clarification, a steady state equilibrium is considered a geomorphic open system that self-maintains a constant form with continuous throughput of material and energy despite all but the largest perturbations (Thorn and Welford, 1994; Huggett, 2016). In geomorphological nomenclature, this state is commonly also referred to as 'dynamic equilibrium' (Zhou et al., 2017). However, general systems terminology prefers the term

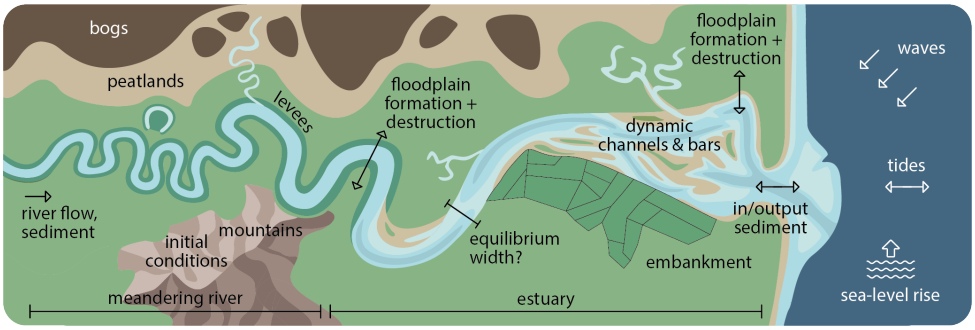

Figure 1.1 Conceptual model of the initial and boundary conditions that shape meandering rivers and estuaries, including river discharge, waves, tides, sea-level rise, inherited geological constraints and fluvial and marine sediment input. It remains unclear how these boundary conditions, together with muddy and vegetated floodplain formation and destruction and human impact, determine the steady state of estuaries in terms of the degree of estuary filling and associated channel width.

'steady state' for complex, open, entropy-driven systems to 'dynamic equilibrium', because the latter is considered more appropriate for closed systems (Thorn and Welford, 1994; Huggett, 2016).

So, the formation of muddy and vegetated floodplains influences the steady state of rivers by confining flow and filling accommodation. This raises the question whether mud and vegetation also influence the steady state of estuaries. Parallels can be drawn in floodplain formation between rivers and estuaries. Floods brings in fines (rivers: Kleinhans et al., 2018; tidal systems: Braat et al., 2017; 2019) and the decreasing inundation stress away from the main channels favours a gradient of thriving vegetation species (rivers: Van Oorschot et al., 2016; Solari et al., 2016; tidal systems: Brückner et al., 2019; Boechat Albernaz et al., 2020). Whilst rivers generally experience floods on a yearly basis, tidal environments have tidal flooding daily. The water levels associated with these daily floods depend on e.g. the spring-neap cycle and atmospheric controls, and contribute to the development of mudflats and salt marshes. On a scale of a single intertidal bar or flat, these "tidal floodplains" seem largely analogous to floodplains in rivers in how they influence the morphodynamics. Firstly, mudflats and salt marshes can cover mid-channel bars and flanks on the outer banks, where they confine tidal systems (Braat et al., 2017). Secondly, salt marshes stabilise the bed and increase the hydraulic roughness, which promotes sediment deposition and further filling of accommodation (Temmerman et al., 2007; Lokhorst et al., 2018; Brückner et al., 2019). Besides, salt marshes play a vital part in attenuating the tide, waves and storm surges (e.g. Gedan et al., 2011; Barbier et al., 2013; Duarte et al., 2013; Temmerman et al., 2013). However, on a scale of entire estuaries, it still remains to be investigated whether the two floodplain mechanisms of confining flow and filling accommodation also influence the steady state of estuaries.

This knowledge gap asks for a better grasp of the natural processes that shape estuaries. This is essential to determining the impact of human interventions, especially in light of future sea-level rise. Many estuaries were confined by land reclamation and embanked by dikes, which has worsened flood risk in two ways. Channel confinement increases the amplification of the tide, causing higher water levels during flood (e.g. Van der Spek, 1997; Friedrichs, 2010), and the dikes inhibit the accretion of sediment on floodplains that is needed to compensate for background subsidence (Berendsen, 2004; Kirwan and Megonigal, 2013). Consequently, channelised waterways and the sea slowly become super-elevated above the surrounding embanked floodplains (Chen et al., 2015), which leads to drowning issues and a vicious cycle of raising and reinforcing dikes to reduce flood risk (Pinter et al., 2008). Therefore, the current dike system is deemed unsustainable for river and estuary management (Castellarin et al., 2011; Remo et al., 2012) and the focus slowly switches to more "soft"

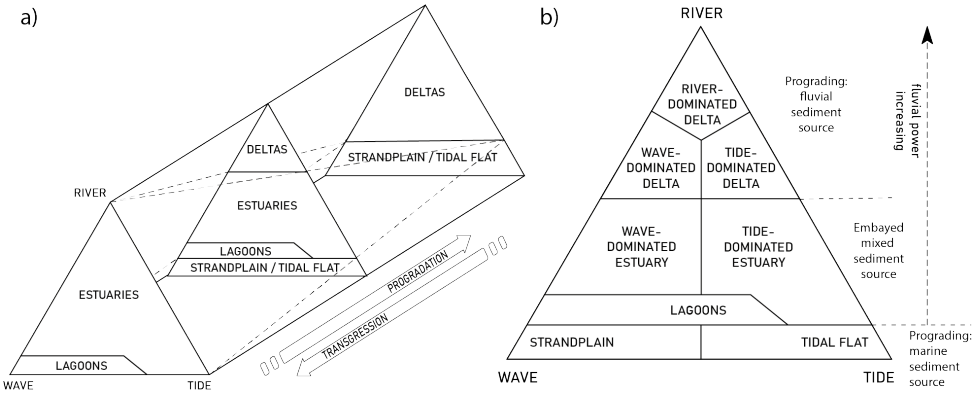

Figure 1.2 Classification of clastic coastal environments. (a) The three-dimensional prism, modified from Boyd et al. (1992), shows how the relative influence of rivers, waves and tides translates to different coastal environments of deltas, estuaries and coasts that may change over time under conditions of progradation and transgression. (b) An updated version of the prism, modified from Yang et al. (2005), that distinguishes between different kinds of estuaries and rivers based on their relative dominant forcing.

building-with-nature approaches that expand fluvial floodplains and intertidal storage area to reduce flood risk, drive land-level rise and improve biodiversity (e.g. Wolters et al., 2005; Rijke et al., 2012; Van der Deijl et al., 2017; Baptist et al., 2021; Gourgue et al., 2022). However, to oversee how these approaches, as well as dikes, dams and revetments, affect present-day managed estuaries, a deeper understanding is required of how estuaries naturally adapt to changing boundary conditions.

Therefore, this thesis first turns to landscape reconstructions of former and present-day estuaries in section 1.2, which form a geological archive of how estuaries developed under different initial and boundary conditions. This will form a basis for the development of hypotheses on which factors affect estuary filling and how this may affect the steady states of estuaries.

1.2 Coastal palaeo-landscape reconstructions

Reconstructions of former coastal landscapes show how estuaries started to fill as sea-level rise levelled off during the Middle Holocene around 8,000 years before present. These reconstructions revealed different kinds of estuary filling with sand, mud and vegetation depending on the boundary conditions (e.g. Heap and Nichol, 1997; Wilson et al., 2007; De Haas et al., 2018). For example, the classic facies models for wave-dominated estuaries (Roy et al., 1980; Nichol, 1991; Dalrymple et al., 1992) describe estuary filling of a muddy back-barrier basin overridden by a bay-head delta, salt marshes, floodplains and peatlands (Fig. 1.3). This development was found for large (40–100 km long) systems with little river discharge and sediment supply, and resulted in a progressively narrower estuary. In contrast, incised-valley fills with a large sand input from the rivers and the sea, such as the Manawatu valley (Clement et al., 2017), lack a muddy back-barrier deposit and instead have a thick tidal sand deposit with mud drapes formed by large tidal bars and flats. Alternatively, geologically constrained estuaries may lack a central basin deposit altogether (Abrahim et al., 2008), whilst in some alluvial estuaries the bay-head delta deposit is nearly absent (e.g. De Haas et al., 2018). These contrasting observations indicate that the initial and boundary conditions can have a profound influence on the filling of estuaries.

These initial and boundary conditions determine how much sediment is delivered to an estuary and how much accommodation needs to be filled. However, imported sediment also needs to be retained to cause estuary filling, and vegetation is considered to play an important part in this process. A well-studied example to illustrate the potential importance of vegetation is the Old Rhine Estuary in the Netherlands (Fig. 1.4) (e.g. Vos, 2015; De Haas et al., 2018; 2019). From an initially drowned back-barrier basin, it is hypothesised that rapidly expanding salt marshes and peatlands started to confine the estuary in a positive feedback loop (Beets and Van der Spek, 2000; De Haas et al., 2018; Pierik, 2021). The expanding patches of vegetation would dampen the tide and promote the deposition of fines, which decreased the tidal prism and favoured further vegetation expansion. In the end, a single narrow channel was left, bounded by vast peatlands and high bogs. After a river avulsion upstream, river discharge was strongly reduced and led to the closure and final filling of the Old Rhine Estuary.

Besides completely filled estuaries, there are still many estuaries that have been only partly filled (e.g. Arcachon Bay (FR); Féniès and Faugères, 1998; Allard et al., 2009), or are still unfilled (e.g. Georges Bay (AUS); Roy et al., 1980). Current understanding dictates that estuaries are ephemeral systems on a

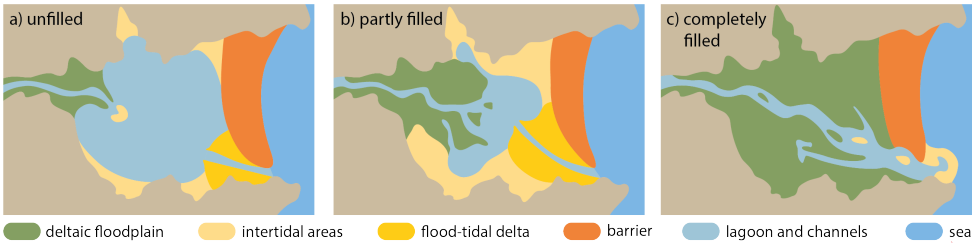

Figure 1.3 Conceptual model of estuary filling of an idealised wave-dominated estuary, modified from Roy et al. (1980). (a) A largely unfilled estuary with a fluvial bay-head delta protruding into a large low-energy lagoonal basin flanked by small intertidal areas. (b) A partly filled estuary with more intertidal areas and a larger bay-head delta and flood-tidal delta. (c) A completely filled estuary in which the confined estuary is mainly bounded by floodplains.

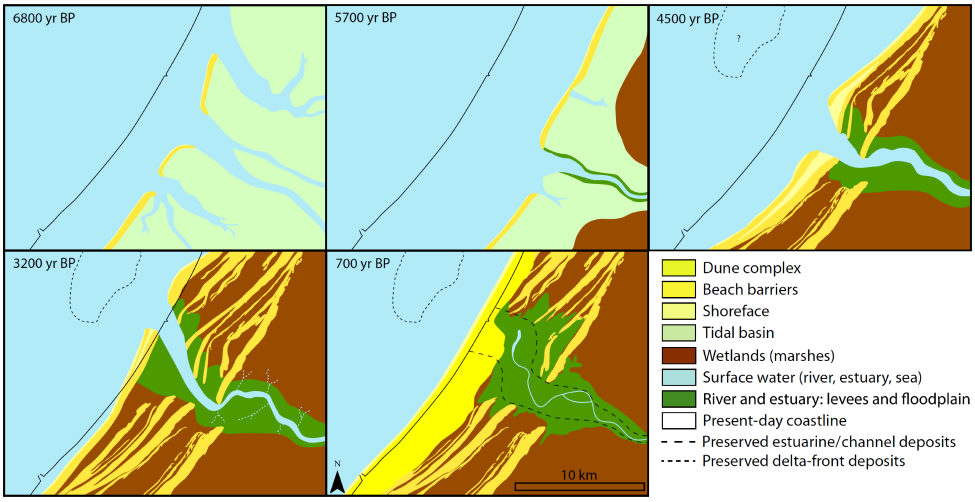

Figure 1.4 Palaeogeographic reconstruction of estuary filling of the Old Rhine Estuary in the Netherlands, modified from De Haas et al. (2019). Ages are in cal. y BP.

geological timescale of sea-level fluctuations and will inevitably fill over time (e.g. Dalrymple and Choi, 2007; De Haas et al., 2018). Then, it should follow logically that the duration of filling depends on the amount of sediment input, suggesting that unfilled and partly filled estuaries have not received sufficient sediment to cause complete estuary filling. However, a large sediment input is not a guarantee for rapid estuary filling as found, for example, for the Columbia River Estuary (USA), where accommodation remains partly unfilled due to wave action and fluvial sediment bypassing to the sea (Peterson, 2014). Other examples include the Arachon Bay Estuary (FR) (Féniès and Faugères, 1998; Allard et al., 2009) and the Ems-Dollard Estuary (NL/D) (Van Maren et al., 2016), which are partly filled estuaries that remained largely unchanged despite ample sediment availability. These observations show that also internal mechanisms that govern sediment retention are important and likely influence the stable state of estuaries.

At present, only two contrasting kinds of estuaries are considered to be in a stable state, assuming reasonably constant boundary conditions. The first is an unfilled estuary with a lagoonal basin that is largely below the threshold of motion (Fig. 1.3) (Roy et al., 1980). Unfilled estuaries typically form in deep (relative to the tidal amplitude) drowned valleys and remain largely unchanged because of weak tidal currents and negligible fluvial and marine sediment input (e.g. Dalrymple et al., 1992). The second is a completely filled estuary that ideally has a converging planform (Fig. 1.3) (Roy et al., 1980; Nichol, 1991; Dalrymple et al., 1992). This ideal, landward converging shape balances the decay of tidal energy by friction, resulting in a constant along-channel tidal amplitude, channel depth and flow velocity (Savenije, 2015), as well as a balanced ebb- and flood-directed sediment transport (Dronkers, 2017). A completely filled estuary with a convergent planform is considered a steady state (Savenije, 2015; Dronkers, 2017): a partly filled system develops flood-dominant transport which promotes filling if sediment is supplied from the upstream river or the sea, whereas an over-filled system develops ebb-dominance and sediment export that may lead to delta formation (Dalrymple et al., 1994; Savenije, 2015; Dronkers, 2017).

However, the current view that only unfilled and ideally converging estuaries can be in a steady state appears to deviate from numerous partly filled estuaries that largely remained unaltered in the past century despite ample sediment supply. Examples include the Arcachon Bay (FR) (Féniès and Faugères, 1998; Allard et al., 2009) and Ems-Dollard Estuary (NL/D) (Van Maren et al., 2016). These systems showed no distinct channel confinement towards an ideal converging shape that would be expected with ample sediment supply if only the unfilled and completely filled estuaries are steady states. Therefore, a hypothesis is that the tendency to form "tidal floodplains" (Fig. 1.1) determines the degree of estuary filling, which may imply also partly filled estuaries can attain a steady state.

In order to test this hypothesis, a proper understanding is needed of the driving mechanisms that capture and retain sediment to build and raise land. It is complicated to determine this from coastal landscape reconstructions and field observations due to the ever-changing boundary conditions, the practical impossibility to measure all relevant parameters and the reworking of former deposits. Therefore, current understanding on the driving mechanisms is mainly derived from experiments and numerical modelling, in which the effects of boundary conditions can be isolated, and is reviewed in the section 1.3.

1.3 Driving mechanisms for building and raising land

Current understanding of rivers and estuaries suggests that mud and vegetation play a crucial part in creating new land. Their effects on the morphodynamics were closely examined for rivers (see for review: Kleinhans, 2010) and were found to be similar for estuaries, as explained as follows. Firstly, mud fills accommodation by settling in low-energetic areas, including high bars, inactive channels, floodplains (in fluvial systems: Ferguson, 1987; Van Dijk et al., 2013a; Kleinhans et al., 2018) and

salt marshes (in tidal systems: Braat et al., 2017; 2019). Accordingly, mud confines flow and hampers channel incision that is the onset of braiding, as found for rivers (Braudrick et al., 2009; Van Dijk et al., 2013a) and estuaries (Braat et al., 2017; 2019). Secondly, vegetation hampers flow (Zong and Nepf, 2011), which confines flow in a main channel and allows for the capture of fines. Similar to mud, vegetation typically settles in low-energetic areas. However, recent numerical work in both rivers (Kleinhans et al., 2018) and estuaries (Brückner et al., 2019) showed that neither mud nor vegetation is necessary for the settling of the other, given the traits of the tested vegetation species in these studies.

Although the effects of mud and vegetation are known on a scale of a single intertidal bar or flat (e.g. Temmerman et al., 2007; Braat et al., 2019b), it remains unclear to what extent they contribute to estuary filling. Unlike in rivers, where morphology adapts to a channel forming discharge (Leopold and Wolman, 1957; Kleinhans and Van den Berg, 2011), estuary morphology in turn also influences the tidal discharge in a feedback loop (e.g. O'Brien, 1969; Jarrett, 1976). Therefore, some studies (Beets and Van der Spek, 2000; De Haas et al., 2018; Pierik et al., in prep.) suggested that rapidly expanding mudflats, salt marshes and peatlands may reduce tidal prism and effectively confine and ultimately fill an estuary (Fig. 1.4). Yet, this hypothesis remains largely untested in both scaled landscape experiments and numerical modelling (Boechat Albernaz and Kleinhans, in prep.) and would require the addition of mud and dynamic (live) vegetation that can establish, grow and perish. Recent advancements of mud and vegetation in scaled experiments (Baumgardner, 2016; Lokhorst et al., 2019) and numerical modelling (Van Ledden et al., 2004; Van Oorschot et al., 2016; Brückner et al., 2019) now allow for testing how "tidal floodplains" build and raise land.

Another mechanism that contributes to the filling of estuaries is flood-tidal asymmetry. This deformation of the tide may be imposed by the sea (for example on the North Sea; Dronkers, 1986; Wang et al., 1999) and also develops in estuaries dominated by tidal variation in channel depth, that is, where bottom friction results in a faster flood wave propagation relative to the ebb wave propagation (Speer and Aubrey, 1985; Blanton et al., 2002; Friedrichs, 2010; Moore et al., 2009). Consequently, sediment is net imported into an estuary because of sediment transport nonlinearity, resulting in increasing intertidal and supratidal area (e.g. Moore et al., 2009). Yet, this mechanism of flood-tidal asymmetry was not applied in previous scaled landscape experiments of estuaries (Leuven et al., 2018b; Braat et al., 2019a) and tidal basins (e.g. Reynolds, 1889; 1891; Tambroni et al., 2005; Stefanon et al., 2010; 2012), which is one of the reasons why previous experiments so far only produced ebb-dominant systems. Another reason for ebb-dominance in experiments is related to scaling problems, which were largely overcome with a new experiment setup (Kleinhans et al., 2014b; 2015; 2017) that will be addressed in the section 1.4.

1.4 Current methods to study rivers and estuaries

To determine how estuary filling is governed by muddy and vegetated floodplain formation, scaled landscape experiments and numerical modelling are useful methods to isolate individual parameters that may influence floodplain formation. Scale experiments use real materials and make the development of entire water landscapes more tangible but have to deal with scaling issues. Numerical modelling allows for quick sensitivity analyses of boundary conditions but requires parameterisation for natural processes and physical laws, not only for channels and bars but also for biogeomorphic floodplain processes. Therefore, these methods should be considered complementary in studying the development of rivers and estuaries. Below, the recent progress in these methods is reviewed that is relevant in the context of estuary filling with mud and vegetation.

Progress in scaled landscape experiments

Until recently, scaled landscape experiments of estuaries applied a periodic sea-level fluctuation to simulate tidal flow (Reynolds, 1889; 1891; Mayor-Mora, 1977; Tambroni et al., 2005; Tesser et al., 2007; Stefanon et al., 2010; 2012; Vlaswinkel and Cantelli, 2011; Iwasaki et al., 2013). Whilst such a driving force for tides resembles the natural situation, this classic method faces three scale problems: ebb-dominance, very low sediment mobility and strongly declining morphodynamics in the landward direction (Kleinhans et al., 2014b). These ramifications were largely overcome by a novel tilting method that periodically generates alternating slopes in the seaward and the landward direction, producing tidal flows with ample sediment transport in both the flood and ebb directions (Kleinhans et al., 2014b; 2015; 2017). Accordingly, sand-dominated estuaries could be reproduced on a laboratory scale with dynamic tidal bars and channels (Leuven et al., 2018b), mudflats (Braat et al., 2019a) and salt marshes (Kleinhans et al., 2022). Whilst these novel experiments showcased the development of initially narrow, exporting estuaries, in this thesis the periodically tilting flume setup was used to study the opposite, that is, the development of an initially wide, infilling estuary (Chapter 4). Consecutively, a similar experiment was conducted but with sea-level rise to determine its effect on the spatial and temporal patterns of sediment deposition and land formation (Chapter 6).

Data acquisition in scaled landscape experiments commonly concerns three parameters to quantify the hydro- and morphodynamics: bed elevation, water depth and flow velocity. Yet, the hydrodynamics are technically difficult to measure with the same spatial resolution as the bathymetry due to shallow water depths of at most a few centimetres. Therefore, shallow water depths are often inferred from dyed water colour saturation (e.g. Gran and Paola, 2001; Leuven et al., 2018b) or measured by means of laser scanning (e.g. Tambroni et al., 2005; Tesser et al., 2007; Stefanon et al., 2010; 2012) and photogrammetry, in case of unidirectional flow (Leduc et al., 2019). Flow velocity measurements are typically based on tracking particle seeds on the water surface (e.g. Mori and Chang, 2003; Leuven et al., 2018b; Braat et al., 2019a). However, these methods tend to be less accurate near vegetation, which blocks tracking particle seeds, and differently coloured sediments, which distort water depths inferred from water colour saturation. Accordingly, so far only one research group instead computed uniform flow velocity over a static bed elevation map of their tidal basin experiment with a numerical model (Tesser et al., 2007; Stefanon et al., 2010; 2012) in a similar fashion as modelling the hydrodynamics of real rivers and estuaries (e.g. Berends et al., 2019). This thesis will extend their numerical modelling method for unsteady, nonuniform flows (Chapter 3) to improve data acquisition in scaled landscape experiments with overall better spatial and temporal coverage.

Progress in numerical modelling

Numerical modelling is well-suited for sensitivity analyses and has often been applied in fluvial and tidal research. As for the modelling of meandering rivers, previous studies examined meander development and migration through one-dimensional (e.g. Camporeale et al., 2005; Lanzoni and Seminara, 2006; Perucca et al., 2007; Weiss, 2016) and two-dimensional modelling (e.g. Nicholas, 2013; Van Oorschot et al., 2016; Schuurman et al., 2016). Recent numerical work that excluded floodplain topography (Lanzoni and Seminara, 2006; Schuurman et al., 2016; Weiss, 2016) showed that a dynamic inflow perturbation is required to initiate and maintain meander dynamics with neck-cutoffs, following similar findings for meandering with chutes in scaled landscape experiments (Van Dijk et al., 2013a). Yet, it remains unclear how a dynamic inflow perturbation affects the meandering channel and bar pattern in terms of, for example, sinuosity and braiding index. Moreover, the numerical modelling of dynamic meandering with chutes remains under-investigated, for this requires a computationally expensive, two-dimensional approach that includes self-formed floodplain topography and allows for multiple channels over the cross-section. Given the advancements in computing power, this thesis will simulate a meandering river with chutes with self-formed

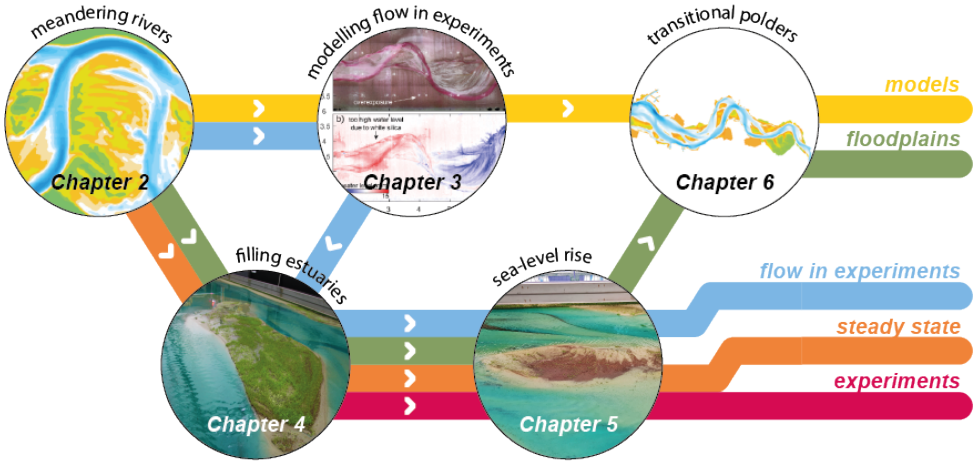

Figure 1.5 A metro-map overview of how the chapters in this thesis are linked via five story lines. These chapters together contributed to unravelling how muddy and vegetated floodplain formation influences the steady state of estuaries, which is the focus of this thesis, using numerical modelling and scale experiments.

vegetated floodplains to determine the effects of a dynamic inflow perturbation (Chapter 2). In the larger context of numerical modelling, this work will further clarify which boundary conditions are needed to reproduce biomorphodynamics with a natural variation in morphology.

Regarding the modelling of tidal systems, the effect of mud and vegetation remains underinvestigated on the long-term morphological development. So far, modelling efforts mainly included only sand to develop tidal basins (Marciano et al., 2005; Dissanayake et al., 2009) and estuaries (Van der Wegen and Roelvink, 2008) with similar channel and bar patterns as in nature. However, as most tidal models assume a planform with non-erodible boundaries (Lanzoni and Seminara, 2002), the dynamics are lost on the outer banks which are normally shaped by the building and destruction of mudflats and salt marshes. With the numerical hurdles overcome of modelling sand-mud interactions (e.g. Van Ledden et al., 2004) and dynamics vegetation (Van Oorschot et al., 2016; Brückner et al., 2019), steps were taken in fundamental research into the effects of mud (e.g. Braat et al., 2017) and vegetation (e.g. Lokhorst et al., 2018; Brückner et al., 2019; 2020) on estuary geometry and dynamics. Here, this thesis will apply the fundamental knowledge of sand-mud interactions to a societal relevant case of managed realignment to develop land-level rise (Chapter 5). Although single sites of managed realignment with mud and vegetation have been studied before (e.g. Wolters et al., 2005; Wheeler et al., 2008; Mossman et al., 2012; Kiesel et al., 2020; Gourgue et al., 2022), this thesis will specifically look into how an opening sequence of multiple managed realignments affects (1) their ability to import sediment and (2) the hydro- and morphodynamics in the main estuary.

1.5 Thesis outline

The main objective of this thesis is to improve the current understanding of how rivers and estuaries build and raise new land. To accomplish this objective, this thesis is split into three parts:

- The first part focuses on the necessary boundary conditions to reproduce natural morphodynamics in models and experiments.
- The second part aims at improving the current methods of acquiring hydrodynamic data in scaled landscape experiments.

- The third and main part studies how muddy and vegetated floodplain formation influences the steady state of rivers and estuaries by means of scaled landscape experiments and numerical modelling.

These objectives result in the two main story lines of "floodplain formation" and "steady state" that link the chapters of this thesis (Fig. 1.5). How floodplain formation influences a steady state is first investigated for a meandering river and then applied to estuaries. The main methods used in this thesis are "scaled landscape experiments" and "numerical modelling", which form another two story lines. The last story line is that of modelling "flow in experiments" to acquire more data on hydrodynamics in experiments that are otherwise difficult and time-consuming to measure in very shallow flows. Below, a brief overview is given of the chapters.

Chapter 2 explores how floodplain formation influences the channel pattern and dynamics of meandering rivers. This was studied through numerical modelling of a dynamic meandering river with chute cutoffs and self-formed, vegetated floodplains in the model Nays2D. This is a next step forward in determining which boundary conditions are necessary to develop dynamic rivers, estuaries and coasts in numerical models and scaled landscape experiments.

Chapter 3 tests and validates a numerical model to acquire flow data in scaled landscape experiments. This can substitute flow measurements, which tend to be complicated especially when vegetation and differently coloured sediments are used. To this end, the model Nays2D of Chapter 2 was tested on three published scale experiments: a meandering river, a braided river and a sandy estuary.

Chapter 4 shows the effect of mud and vegetation on the morphological development of filling estuaries in scaled landscape experiments. Flow data were derived from the model approach tested in Chapter 3 to describe the change in intertidal area and tidal prism during the experiments and how these changes were influenced by mud and vegetation.

Chapter 5 builds upon the filling estuary experiments in Chapter 4 and studies how sea-level rise will affect the hydro- and morphodynamics of future estuaries. A filling estuary was developed with self-forming floodplains of mud and vegetation and rapid sea-level rise. The model approach tested in Chapter 3 was used to obtain flow data to determine how sea-level rise affected the inundation period and flow velocity distributions.

Chapter 6 applies the concept of Chapters 4 and 5 of building and raising land by floodplains to a real large-scale estuary, i.e. the Western Scheldt Estuary in the Netherlands, using the numerical model Delft3D. Low-lying polders (i.e. "transitional polders") were added to the estuary in different sequences to determine how an opening sequence influences the import of sediment and the flood propagation along the estuary.

Chapter 7 combines the main findings of the previous chapters to fulfil the main research objectives of this thesis. The novel findings will be used to develop new hypotheses on the feasibility to keeping up with future sea-level rise. Also, implications are given on future estuary management. Finally, recommendations are given for future research into nature-based solutions for a more sustainable livelihood in coastal regions.

Chapter 2 | Upstream perturbation and floodplain formation effects on chute cutoff-dominated meandering river pattern and dynamics

Abstract

A sustained dynamic inflow perturbation and bar-floodplain conversion are considered crucial to dynamic meandering. Past experiments, one-dimensional modelling and linear theory have demonstrated that the initiation and persistence of dynamic meandering require a periodic transverse motion of the inflow. However, it remains unknown whether the period of the inflow perturbation affects self-formed meander dynamics. Here, we numerically study the effect of the inflow perturbation period on the development and meander dynamics of a chute-cutoff-dominated river, which requires two-dimensional modelling with vegetation forming floodplain on bars. We extended the morphodynamic model Nays2D with growth and mortality rules of vegetation to allow for meandering. We tested the effect of a transversely migrating inflow boundary by varying the perturbation period between runs over an order of magnitude around typical modelled meander periods. Following the cutoff cascade after initial meander formation from a straight channel, all runs with sufficient vegetation show series of growing meanders terminated by chute cutoffs. This generates an intricate channel belt topography with point bar complexes truncated by chutes, oxbow lakes, and scroll-bar-related vegetation age patterns. The sinuosity, braiding index and meander period, which emerge from the inherent biomorphological feedback loops, are unrelated to the inflow perturbation period, although the spin-up to dynamic equilibrium takes a longer time and distance for weak and absent inflow perturbations. This explains why, in previous experimental studies, dynamic meandering was only accomplished with a sustained upstream perturbation in flumes that were short relative to the meander wavelength. Our modelling of self-formed meander patterns is evidence that scroll-bar-dominated and chute-cutoff-dominated meanders develop from downstream convecting instabilities. This insight extends to many more fluvial, estuarine and coastal systems in morphological models and experiments, which require sustained dynamic perturbations to form complex patterns and develop natural dynamics.

Published as: Weisscher, S. A. H., Shimizu, Y., & Kleinhans, M. G. (2019). Upstream perturbation and floodplain formation effects on chute-cutoff-dominated meandering river pattern and dynamics. *Earth Surface Processes and Landforms, 44(11), 2156–2169*, DOI: 10.1002/esp.4638

2.1 Introduction

A meandering river forms an elaborate floodplain topography through meander initiation, expansion and cutoff (Hickin and Nanson, 1975; Hooke, 2004). The rate at which meanders migrate is commonly described as a function of bend sharpness, in which the migration rate increases towards an optimum and subsequently drops with increasing bend sharpness (e.g. Hickin and Nanson, 1975; Furbish, 1988; Crosato, 2009). While this approach focuses on individual bends, it is evident, for example from the River Otofuke in Japan (Fig. 2.1) and the River Allier in France (Kleinhans and Van den Berg, 2011), that the migration rate of one bend affects that of its downstream neighbours. Current understanding of such spatio-temporally radiating effects is that bend instabilities propagate in one, usually the downstream, direction rather than in both directions. However, the question is whether the period of such lateral instabilities, relative to the meander period, affects the degree of meandering dynamics. Furthermore, the implication of the downstream propagation of bend instabilities is that perturbations need to be imposed on the upstream boundary of all numerical models and experiments to maintain dynamic meandering (Lanzoni and Seminara, 2006; Van Dijk et al., 2012; Weiss, 2016). Yet, it remains unclear what the period of such perturbations would need to be and whether that affects the modelled meander migration rate and chute cutoff frequency.

Floodplain formation is thought to be the main necessary condition for dynamic meandering. However, due to the intricacies of floodplain formation, meandering, as opposed to braiding, has proven notoriously challenging to reproduce in numerical models (Nicholas, 2013; Van Oorschot et al., 2016; Schuurman et al., 2016) and laboratory landscape experiments (Braudrick et al., 2009; Tal and Paola, 2010; Van Dijk et al., 2012; 2013b). In the context of this study, a landscape experiment is a simulation of a fluvial, estuarine or coastal landscape with sediment mobility, morphodynamic processes and complexity comparable to those of natural systems (Kleinhans et al., 2014a). A landscape experiment is considered intermediate between a classic scale model by similarity rules and an analogue model. In absence of bank protection, unhindered widening results in bend cutoffs, mid-channel bars and braiding (Parker, 1976). In contrast, to maintain a single thread channel that can form meanders, the width-to-depth ratio of the channel needs to be small enough to inhibit the onset of mid-channel bars (Parker, 1976; Struiksma et al., 1985; Crosato and Mosselman, 2009; Kleinhans and Van den Berg, 2011), which requires that outer bend erosion is balanced by inner bend accretion (Van de Lageweg et al., 2014). Meandering may result from some form of strength in eroding outer banks (e.g. Leopold and Wolman, 1957; Ferguson, 1987; Kleinhans and Van den Berg, 2011), but recent modelling and past experiments suggest that meandering mainly requires floodplain formation on the point bar (see for review Solari et al., 2016). Accordingly, this encroachment on the point bar causes the focus of flow into the outer bend and reduces the tendency to incise chutes on the point bar that is the onset of braiding (Braudrick et al., 2009; Van Dijk et al., 2012; Van Oorschot et al., 2016; Kleinhans et al., 2018). Although floodplain formation occurs through floodplain sedimentation, vegetation establishment and the combination thereof, this study focuses on riparian vegetation as the bar-floodplain conversion agent.

Riparian vegetation interacts with fluvial morphodynamics in several ways. Firstly, added hydraulic drag by vegetation on the bars and floodplain causes flow to focus in a single thread channel (Van Oorschot et al., 2016). Secondly, vegetation enhances sediment deposition (Zong and Nepf, 2011; Corenblit et al., 2016; Kleinhans et al., 2018), thereby contributing to the vertical and lateral accretion of point bars (Stella et al., 2011; Van Dijk et al., 2013b). Thirdly, riparian vegetation increases bank stability via roots and the production of soil organic matter, which reduce outer bend erosion (Simon and Collinson, 2002; Braudrick et al., 2009; Tal and Paola, 2010). Local conditions determine the settling, growth and mortality of vegetation, while the feedback of vegetation on the hydromorphological pattern modifies these conditions and the resulting spatial and age distribution of vegetation (Simon and Collinson, 2002; Van Oorschot et al., 2016). Most two-dimensional

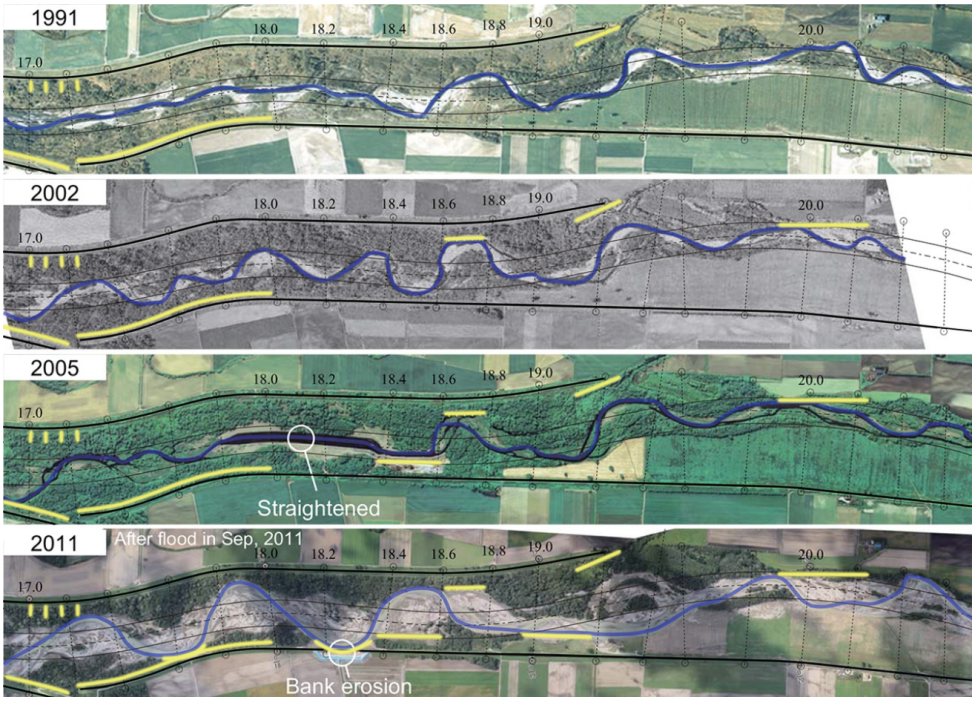

Figure 2.1 Time series of the River Otofuke in Hokkaido, Japan. Dikes (thick black lines) border the active channel belt and the thin black lines show the course of the river in the 1970s, after having been artificially straightened and widened. Scattered dikes and groynes constructed in the floodplain are given in yellow. Numbers indicate the distance in km from a downstream confluence. Flow is from the right to the left. (modified from Nagata et al., 2013)

morphodynamic model studies that incorporated vegetation parameterised it as static (see for review Solari et al., 2016); there are only two studies that applied dynamic vegetation, allowing multiple tree taxa to settle, grow and perish based on local hydraulic conditions (Van Oorschot et al., 2016; Kleinhans et al., 2018). This advancement resulted in a chute cutoff-dominated meandering pattern with a spatial and age distribution of vegetation similar to that in nature. However, these models initiated with a meandering topography and had a relative short domain relative to the meander wavelength, because the necessary conditions for sustained meandering were not studied.

The second necessary condition for sustained dynamic meandering in a model or experimental domain of limited length is a sustained dynamic upstream perturbation. Perturbations migrate and decay in the downstream direction as convective instabilities, as opposed to bidirectional absolute instabilities (Lanzoni and Seminara, 2006). Consequently, the dynamics of meandering rivers are found to decrease when no new perturbation is introduced at the upstream boundary, as observed in previous studies (e.g. Friedkin, 1945; Braudrick et al., 2009; Asahi et al., 2013). Conversely, landscape experiments showed that applying a periodic transverse inflow perturbation leads to dynamic chute cutoff-dominated meandering. This novel concept was adopted in few two-dimensional models (Nicholas, 2013; Schuurman et al., 2016; Van de Lageweg et al., 2016), which enabled the development of high amplitude dynamic meandering with neck cutoffs. Yet, some of these models oversimplify bar-floodplain conversion and exclude the self-formed floodplain topography from the flow by a minimum depth criterion, rendering these models quasi-one dimensional. However, spatial differences on the vegetated bars and floodplain are conducive to the development of chute cutoffs

and determine the location thereof (e.g. Fisk, 1947; Gay et al., 1998). This is crucial because chute cutoffs considerably limit sinuosity, and the impossibility thereof in one-dimensional and most two-dimensional models means that such models tend more easily to meandering than two-dimensional models with unconstrained fluvial plains that can be entirely reworked and reactivated. Moreover, the effect of the period of a periodic transverse inflow perturbation on the dynamics has not been tested in two-dimensional models and experiments. While absence of upstream perturbations reduces the dynamics and a slow perturbation perhaps simply acts as a weak forcing, it could be argued that relatively fast upstream perturbations are merely generating noise that causes braiding in the downstream direction. This reasoning leads to the hypothesis that there is an optimum perturbation rate at which meandering is most dynamic.

The objective of this study is to determine the effect of a periodic inflow perturbation on the river pattern and dynamics. To this end, we modelled a dynamic chute cutoff-dominated meandering river with a self-forming vegetated floodplain using the morphodynamic model Nays2D. We initiated the two-dimensional modelling with a straight channel on a rectangular fluvial plain with vegetation settling and with a domain length of about ten bends long, i.e., much larger than the typical meander wavelength. The inflow boundary was laterally moved at a range of celerities and the resulting meandering characteristics and dynamics were quantified.

The idealised model settings were inspired by the River Allier in France, located in a nature conservation area between Vichy and Moulins (Geerling et al., 2006; Kleinhans and Van den Berg, 2011), by the strongly managed River Otofuke in Japan (Nagata et al., 2014; Iwasaki et al., 2016), and by past landscape laboratory experiments by the Kleinhans research group (Table 2.1). Both these rivers and the experiment classify as meandering gravel-bed rivers with chute cutoffs. The Allier is one of few intermediately sized rivers in Europe that presently meanders freely and has natural discharge and sediment input variations, with peak discharge in winter. In contrast, the discharge of the Otofuke is partly regulated by a dam in its main tributary and strongly influenced by typhonic discharges in late summer, which occur on a decadal scale. Additionally, the river is laterally restricted by dikes bordering the active channel belt. While the Otofuke is allowed to meander and does show chute cutoffs, measures are frequently taken when expanding meanders threaten bank stability (Fig. 2.1). These measures included the construction of local dikes and groynes in the active floodplain. However, meanders quickly propagated in the downstream direction along such artificial obstacles and expanded significantly at locations where such obstacles were lacking, as has occurred during typhoon-induced floods in 2011 and 2016. Furthermore, measures were frequently destroyed during floods, so that all measures collectively provide spatio-temporally dynamic perturbations in the form of local topographic forcing for the meandering channel. The effect of this remains unclear and future river management of repeated interventions could benefit from a better understanding of such convection of spatial perturbations.

2.2 Morphodynamic model setup

2.2.1 Model description

We modelled a dynamic meandering river on a laboratory scale using Nays2D, starting from a straight channel. Nays2D is a physics-based numerical model that solves the depth-averaged nonlinear shallow water equations and computes bed load transport and bed level change (see Shimizu et al., 2013, for equations and numerical implementation), and it is predominantly used in fluvial research on both a natural and laboratory scale (e.g. Asahi et al., 2013; Van de Lageweg et al., 2016; Schuurman et al., 2016). Bed load transport was computed with the Meyer-Peter and Müller (1948) predictor. Sediment input at the inflow boundary was at local transport capacity in our idealised model to mitigate unwated effects of sediment deficit, which neglects possible effects in the

Table 2.1 Comparison between the naturally meandering River Allier (FR), the managed River Otofuke (JP), the landscape experiment by Van Dijk et al. (2012) and the river modelled on a laboratory scale of this study.

Parameter	Unit	Allier	Otofuke	Van Dijk et al. (2012)	this study
Mean annual flood discharge	m^3/s	500	161	1×10^{-3}	6.4×10^{-3}
Grain size	m	5×10^{-3}	60×10^{-3}	0.51×10^{-3}	0.76×10^{-3}
Channel width	m	75	25	0.3	0.5
Channel depth	m	1.2	1.8	0.015	0.04
Valley gradient	m/m	3.3×10^{-3}	6.7×10^{-3}	5.5×10^{-3}	2×10^{-3}
Aspect ratio (width/depth)	–	62.5	13.9	20	12.5
Shields mobility number	–	0.06	0.09	0.07	0.07
Froude number	–	0.18	0.67	0.58	0.4

River Otofuke due to upstream dams. The effect of the secondary flow on the sediment transport direction was parameterised from horizontal flow curvature (Engelund, 1974) to account for the three-dimensional effects of flow. Gravitational bank erosion processes were captured by a slope collapse module (Iwasaki et al., 2016) that administered a bed elevation correction in case of slope oversteepening while maintaining mass conservation. To generate a periodic inflow perturbation, the position of the grid cells with inflow was moved transversely at a constant displacement rate with a maximum amplitude of 0.75 m, similar to Van Dijk et al. (2012), while maintaining a constant inlet width and slope angle of its banks. The computational domain was 4.5 m wide and 30 m long, and the amplitude of the inflow perturbation was much smaller than the typical meander amplitude.

Vegetation colonisation and mortality were added to Nays2D. Every spring, vegetation colonised dry cells (i.e., with a water depth $h < 3$ mm) and was removed from the remaining cells when drowned. A second means of mortality was scour, which was tested year-round; vegetation was cleared away when the erosion depth exceeded the rooting depth (Table 2.2). The latter predominantly occurred on the outer bank of expanding meander bends, where bank failure exposed the roots. However, usually only part of the roots was exposed by bank failure, and the plant drowned and was subsequently removed the next spring. In our model, vegetation did not influence the critical angle for bank failure, and therefore meander migration was not limited in scenarios with very dense vegetation. The hydraulic drag that vegetation exerted on water flow was computed as follows, considering vegetation non-submerged under all flow conditions (Baptist et al., 2007):

$$C = \frac{1}{\sqrt{\frac{1}{C_b^2} + \frac{C_D m D h}{2g}}} \tag{2.1}$$

where C is the Chézy roughness coefficient including vegetation ($m^{0.5}/s$), C_b is the Chézy roughness of the bed ($m^{0.5}/s$), C_D is the drag coefficient ($-$), m is the stem density (m^{-2}), D is the stem diameter (m), h is the water depth (m) and g is the gravitational acceleration (9.81 m/s^2). Since we were not interested in the dynamics caused by vegetation life stages (Van Oorschot et al., 2016), vegetation density, drag and rooting depth were taken constant, that is, age-independent (see Table 2.2).

2.2.2 Model scenarios

A fixed rectilinear computational grid was used with 0.1 m square grid cells. The initial straight channel was 0.5 m wide and 0.04 m deep. The inlet had an initial lateral offset of $+0.4$ m, a fixed width of 0.5 m and fixed bank slopes of 45°, and inlet displacement commenced in the direction away from the valley axis. As the inlet was shifted laterally, the width-to-depth ratio of the inlet channel varied slightly, causing a minor oscillation of sediment input. We prescribed 432 cycles of a 50-minute hydrograph

Table 2.2 Default initial and boundary conditions.

Parameter	Value	Unit
Discharge Q (low-high)	2 - 6.4	L/s
Time step hydrodynamics/bed level change	0.02	s
Time step vegetation settling	50	min
Grain size	0.76×10^{-3}	m
Valley slope	2×10^{-3}	m/m
Inflow migration period T	170	h
Inflow migration amplitude	0.75	m
Drag coefficient vegetation C_D	1	–
Vegetation stem thickness D	0.5×10^{-3}	m
Rooting depth	0.03	m
Manning's n	0.02	$sm^{1/6}$

Table 2.3 Model scenarios. N1 is the default scenario. Three scenarios were also run on a finer grid with 5×5 cm square grid cells and are denoted with an 'F'.

Scenario	Stem density n (cm^{-2})	Inflow period T (h)
N1/N1F	2.5	170
Vegetation density scenarios		
N2	0	170
N3	0.1	170
N4	0.5	170
N5	1.28	170
N6	3.72	170
N7	5	170
N8/N8F	10	170
Inflow perturbation rate		
N9	2.5	*fixed*
N10	2.5	200
N11	2.5	127.5
N12	2.5	85
N13/N13F	2.5	42.5
N14	2.5	4.25

that was varied between 2 and 6.4 L/s. Each cycle represents a year in which the flow peaks in late summer, similar to the River Otofuke. In winter and spring, flow was near the beginning of motion.

The scale issue of sediment mobility must be resolved when a river is scaled down to a laboratory scale. Generally, in physical scale-experiments, a grain size is used that is larger than expected from the characteristic length scale of the channel to prevent cohesion and other scale effects, while the smaller water depth results in lower flow velocity and thus in lower sediment mobility (Kleinhans et al., 2014a). This discrepancy is overcome by employing a steeper valley gradient (e.g. Braudrick et al., 2009; Tal and Paola, 2010; Van Dijk et al., 2012). In this study, both the river dimensions and grain size were scaled down by a factor 80, which resulted in a uniform grain size $d_{50} = 0.76$ mm that was used in previous numerical models of the River Otofuke on a laboratory scale (Iwasaki, pers. comm.). This scaling factor is consistent with the linear grain size-dependence of the Shields mobility number, but the time-scaling from 365 days to 50 minutes in our model is a factor 10,500, which is over two orders larger. Time scales are problematic to determine, for they emerge from sediment transport and meander dynamics (Kleinhans et al., 2015a). Furthermore, the settling of vegetation every year implies and imposes a rate of morphodynamics. Returning to the issue of sediment mobility in our case, a

relatively steep valley gradient of 0.002 m/m^{-1} was applied to attain a sediment mobility of similar magnitude as in the Rivers Otofuke and Allier.

We conducted two series of scenarios, and several additional runs to test the effect of grid resolution (Table 2.3). Firstly, vegetation density was varied between 0 and 10 stems/cm^2 to determine its effect on the channel pattern and dynamics, with the objective to select a run with a sustained dynamic meandering river for the inflow perturbation tests. Most of these scenarios were run briefly for reasons of computational cost. Secondly, an array of inflow perturbation rates was applied to a model run with the selected vegetation density to examine whether the imposed perturbation rate forced the river dynamics. This included a control run without a dynamic inflow perturbation (N9). Additional scenarios were run to study the effect of a finer grid with 0.05 m square grid cells, while 0.1 m was the default resolution. To this end, we selected three scenarios, namely the default run (N1F), and the runs with largest vegetation density (N8F) and second fastest inflow perturbation (N13F), to test grid resolution dependence and to examine whether similar morphology and dynamics occur in extreme vegetation and perturbation cases. Data reduction as explained below was done in parallel to that of the coarse-grid scenarios.

2.2.3 Data analysis

The channel pattern and dynamics were qualitatively characterised by map comparisons of the bathymetry and of the spatial and age distribution of the vegetation, and quantitatively compared for the braiding index, sinuosity and meander period. Bathymetries were first detrended with the initial valley gradient. The upstream and downstream 5 m (50 cells) were disregarded to exclude boundary effects in case domain length-averaged parameters were computed. The braiding index was calculated as the spatially averaged number of channels that exceeded the mean cross-sectional Shields stress of the initial straight channel during low flow in each cross-section of the grid. Sinuosity was defined as the distance along the main channel relative to the domain length. The main channel was found as the filtered path of the minima of a map calculated as detrended bed elevation times flow velocity to the power three, which was empirically found to be the best indicator of channel position that excludes fast overbank flow and deep but abandoned channels. The meander period was determined on the lateral motion of seven cross-sections along the valley, and it was calculated as twice the time interval between two consecutive valley axis crossings, while filtering out intervals shorter than 5 hours and manually adding crossings in rare cases where the valley axis was not crossed by the migrating channel. The spin-up of the models was disregarded for determining the median and temporal variation of sinuosity, braiding index and meander period under dynamic equilibrium conditions; more specifically, in the initial stage with pristine floodplain, bends are still quasi-regular and cut through at approximately the same time. Following this sinuosity peak, the more irregular meanders cut through at different times to result in an overall lower sinuosity at dynamic equilibrium, as also found in Camporeale et al. (2005).

2.3 Results

2.3.1 General development

The fine-grid run of the default scenario (N1F), with intermediate stem density and inflow perturbation period, illustrates the development of the modelled dynamic meandering rivers with associated vegetation age patterns (Fig. 2.2; Movie S1, supporting information). Initially, the development of a non-migrating bar near the inlet caused localised erosion at the opposite bank, from which an alternate bar pattern advanced rapidly in the downstream direction. Subsequently, continued bank erosion, inner bank accretion and vegetation settling led to an increase in meander amplitude in the downstream direction that greatly exceeded the amplitude of the inflow

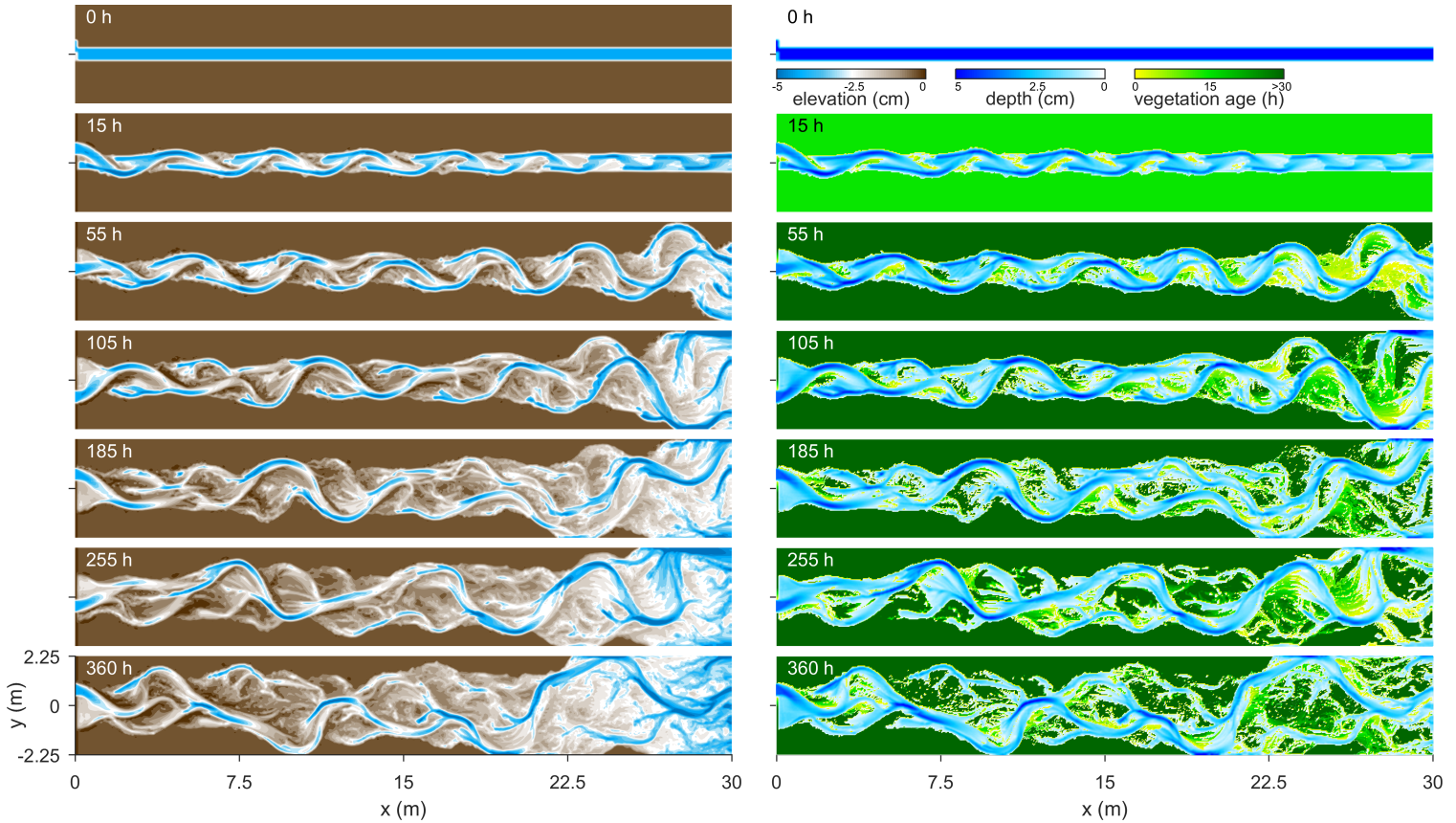

Figure 2.2 Development of river morphology in the default run N1F. Flow is from left to right. Left: bed elevation maps (DEMs) detrended by the initial valley slope. Right: water depth overlain by vegetation age.

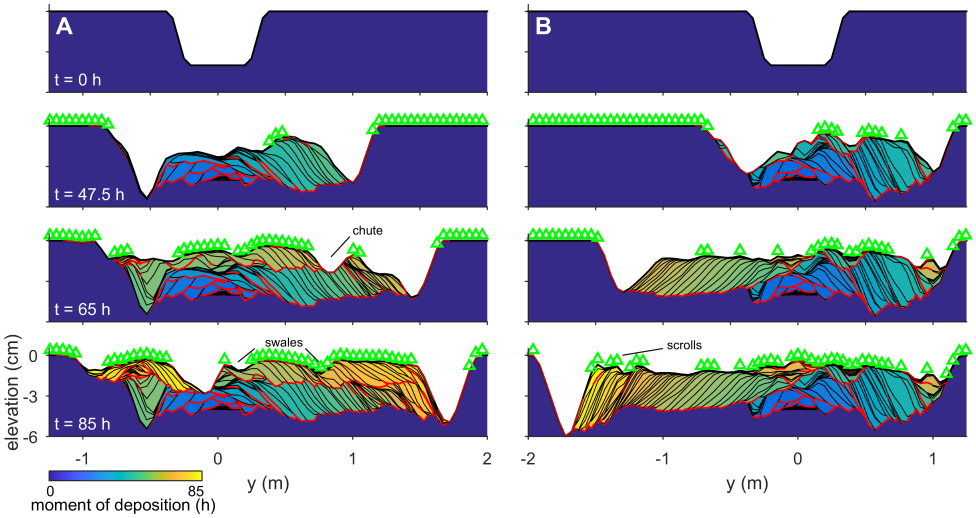

Figure 2.3 Examples of point bar development with lateral accretion surfaces, scrolls, swales and infill of a residual channel, which are indicative for meandering rivers. (a) Default model run N1F at $x = 23.65$ m; (b) Model run N13F (fast upstream perturbation) at $x = 22.85$ m. Vegetation is indicated by green triangles. Accretion surfaces and erosive contacts are indicated as black and red lines, respectively. The vertical exaggeration is 10.

perturbation. Meanwhile, the channel narrowed and deepened on the transition from alternate bars to meandering. Vegetation colonised the point bars as they expanded and migrated, which generated a scroll bar-related vegetation age pattern. Clearly, a sustained meandering pattern formed from an initially straight channel in the applied conditions with floodplain and sustained upstream perturbation.

The chute cutoffs developed as follows. Since the mean wavelength of the meanders grew larger than of the initial alternate bars, bends increasingly tightened. This bend sharpening reduced the channel gradient and caused increasing overbank flow. In consequence, incipient chutes formed at the upstream part of point bars, extended in the downstream direction and eventually cut off meander bends. The cutoff location on the point bar varied considerably, from chutes well across the entire point bar, far from the channel, to chutes through swales much nearer to the active channel. Interestingly, the river pattern changed intermittently between a weakly braided and a low-amplitude sinuous channel, which depended on the number of cutoffs, while the boundary conditions remained constant. Despite the occurrence of multiple cutoffs, the river generally tended towards a single thread channel with up to ten bends (Fig. 2.2).

The series of meander growth and cutoffs produced a complex morphology that was reflected in the stratigraphy of the channel belt (Fig. 2.3). For example, the development of a point bar was preserved as a set of lateral accretion surfaces, which are interpreted as non-erosive contacts in the sedimentological record and are considered characteristic of meandering river deposits. Abandoned meander bends were preserved as oxbow lakes in the channel belt and appeared to be filled in by splay deposits only when a chute or channel was in close proximity. When unfilled, such inactive channels sometimes reactivated by connecting with a chute at a later stage. In some model runs with a wide reworked floodplain, splay deposits contributed to the development of large outer bend levees (Fig. 2.4b). Erosive contacts were formed by the initiation and migration of chutes and channels as they reworked sediment of older deposits. For instance, the chute channel at y = 0.8 m in Fig. 2.3a ($t = 65$ h) eroded the top set of a still expanding point bar deposit and replaced it with a new point bar deposit before merging with

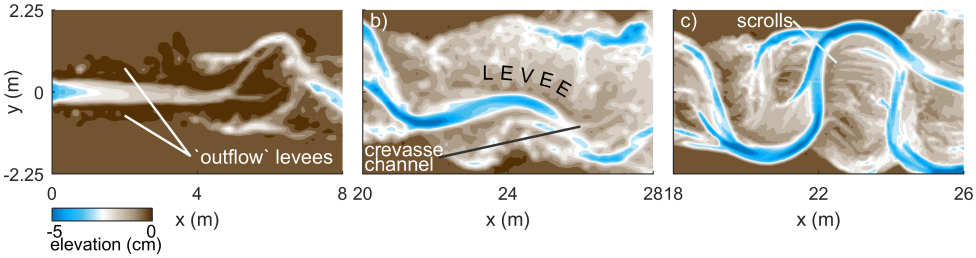

Figure 2.4 Illustrations of specific floodplain processes. (a) Levee formation along the channel just downstream of the fixed inflow location in scenario N9 at $t = 332.5$ h. (b) Outer bend levee formation on top of former point bar complexes by repeated splay deposits in scenario N12 ($T = 85$ h) at $t = 332.5$ h. (c) Scroll bars on a point bar of a highly sinuous channel section in fine grid scenario N13F ($T = 42.5$ h) at $t = 235$ h. The bifurcation at $x = 24$ m persists for a duration of ± 45 h. Flow is from left to right.

the former main channel. Thus, single generation meander bends occasionally had more than one set of lateral accretion surfaces.

2.3.2 Effect of vegetation density

Increasingly denser vegetation reshaped the river pattern from shallow weakly-braided to low-amplitude meandering with chutes (Fig. 2.5). Accordingly, the braiding index decreased from about 1.85 to 1.4 on average with a rather sharp transition at 1.28 stems/cm^2 (Fig. 2.6). Temporary higher braiding indices correlated with the development of chutes and the reactivation of former channels preceding (failed) chute cutoff. Furthermore, the sinuosity increased with vegetation density and showed larger variability due to meander expansion and cutoff. Generally, sinuosity first overshot before reaching a dynamic equilibrium between 1.15 and 1.4. There was a slight overestimation of sinuosity for the weakly-braided rivers, i.e., with a vegetation density ≤ 0.5 stems/cm^2, because the extracted main channel was the path of the most dominant channel in a network with on average two channels in the cross-section. In the most sinuous and densely vegetated channels, the meanders grew by localised erosion in the outer bends, which resulted in lateral expansion of the bends, followed by temporary semicircular scarps at the outer boundaries of the active channel belt (Fig. 2.5e-h). Cutoff of these bends resulted in oxbow lakes that were predominantly located at the edges of the channel belt. In contrast, less sinuous channels with sparse vegetation eroded the outer banks more gradually, and the bends that formed were short-lived and migrated in the downstream direction (Fig. 2.5a-d). Generally, dense vegetation hampered the onset of braiding by quickly colonising plug bars and by redirecting flow into the main channel.

To conclude, dynamic and sustained meandering rivers formed in scenarios with a vegetation density ≥ 2.5 stems/cm^2. Of these scenarios, scenario N1 (2.5 stems/cm^2) was used to test the effect of the inflow perturbation period.

2.3.3 Effect of the inflow perturbation period

The inflow perturbation period strongly influenced the position and meander period of the first bend ($x = 2$ m in Fig. 2.7). A relatively slow inflow perturbation caused cutoff of the forced alternate bar whenever the inflow passed the valley axis, which frequently initiated a cascade of cutoffs in the downstream direction. Such cutoff cascades were also observed in the time series of sinuosity, which gradually increased as bends expanded and abruptly dropped upon cutoff. However, for a relatively fast inflow perturbation, the forced alternate bar developed into a forced mid-channel bar. This bar pattern decayed in the downstream direction until a dynamically meandering single thread channel

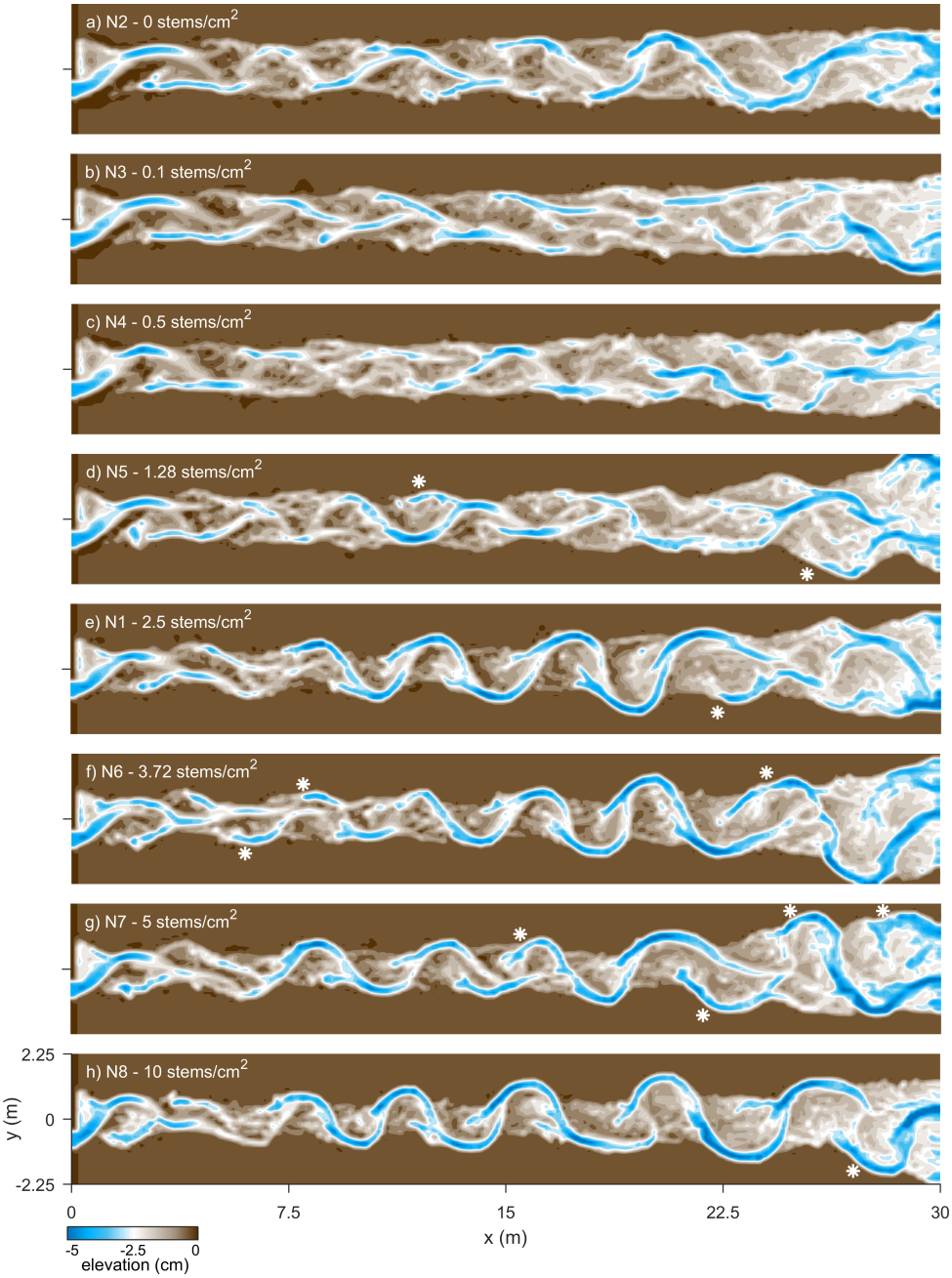

Figure 2.5 Maps of detrended bed elevation at $t = 100$ h for model runs with increasing vegetation density from top to bottom, showing a transition from weakly braided to meandering with chutes. Infrequently formed meander bends in (a–d) are generally short-lived. Examples of oxbow lakes are given as asterisks (*) in (d–h).

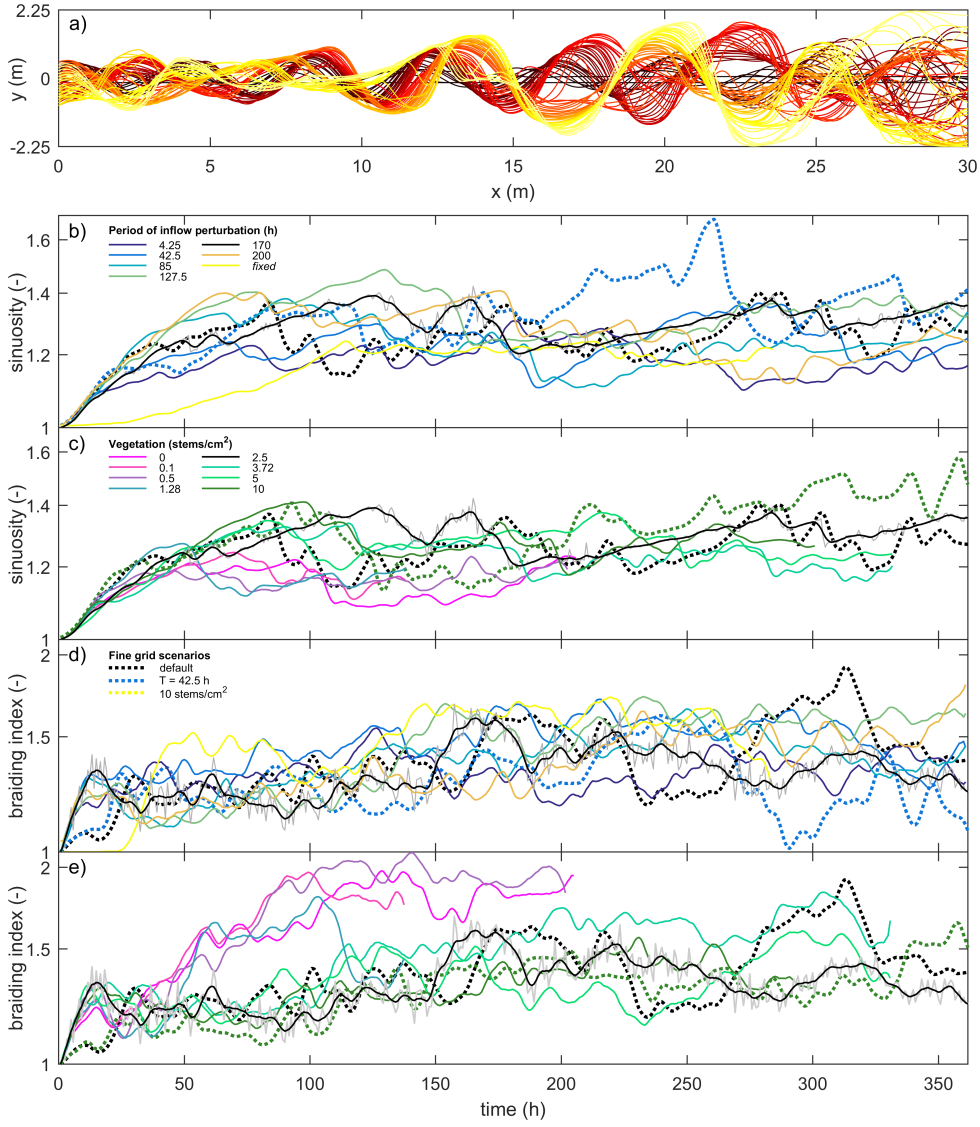

Figure 2.6 Quantification of river dynamics. (a) Channel centre lines of default run N1 showing meander extension, migration and chute cutoff. Time series of sinuosity for (b) different inflow perturbation periods and (c) vegetation density. Time series of braiding index for (d) different inflow perturbation periods and (e) vegetation density. Grey line for N1 illustrates sinuosity and braiding index before smoothing for clarity of presentation. Fine grid scenarios conducted to show resolution-independence of results are shown as dashed lines (see legend in d).

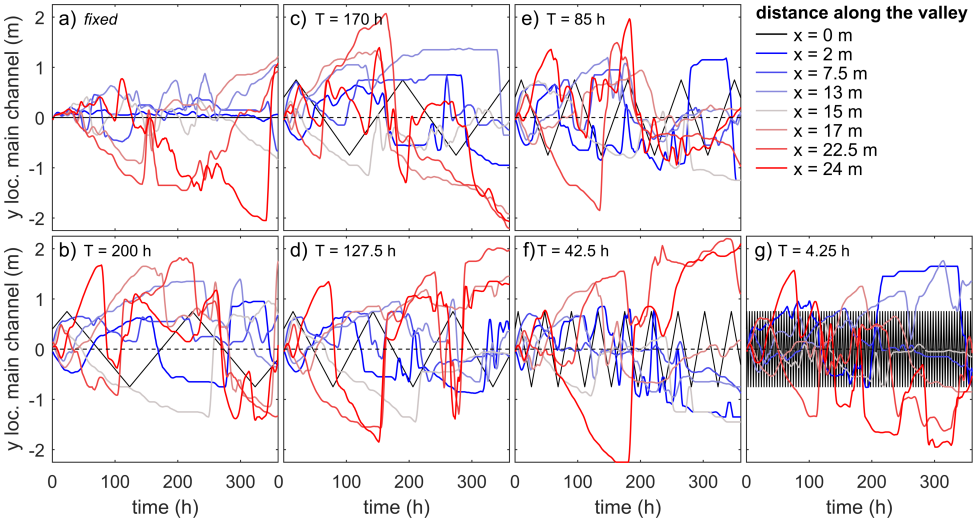

Figure 2.7 Lateral position of the main channel at several locations along the computational domain for different inlet perturbation periods for comparison with the regularly moving inlet position.

was attained. Over time, the mid-channel bar at $x = 2$ m widened and increased in height until one of the two channels became the dominant one, irrespective of the location of the inlet (e.g. $t > 275$ h in Fig. 2.7f). This resulted in a laterally steady inflow downstream of which new meanders were initiated. The amplitude of the first bend net increased and eventually exceeded the amplitude of the inflow perturbation.

The bends further downstream migrated uncoupled from the upstream boundary after spin-up of the model. This was demonstrated firstly by the initiation and cutoff of meanders being unrelated to the periodicity of the inflow perturbation (Fig. 2.7). Secondly, the braiding index and sinuosity were on average similar between scenarios (Fig. 2.6). Thirdly, the measured meander period showed no discernible relation with the inflow perturbation period (Fig. 2.8). As a result, large point bars could develop (Figs. 2.2, 2.3). Furthermore, the results suggest that fewer cutoffs occurred in scenarios with perturbation periods approximating the typical meander period, but this trend is not clearly significant.

Nonetheless, the dynamic inflow perturbation was necessary to attain and maintain dynamic meandering in the upstream part of the computational grid. This became apparent from scenario N9, in which a static inflow was used. At first, the channel of scenario N9 widened by lateral erosion of both banks. Since the inlet had a fixed width and therefore could not widen, an erratic flow perturbation was generated due to the sudden change in the width-to-depth ratio. However, as these perturbations were fairly small, it took approximately 15 m for them to grow and steer new perturbations that were the onset of small meanders (Fig. 2.7a). Also, a static inflow caused the development of levees bordering the main channel near the upstream boundary (Fig. 2.4a). This development stood in stark contrast to the scenarios that included a dynamic inflow perturbation, which developed large meanders close to the upstream boundary.

Perturbations in the modelled domain were found to propagate in the downstream direction. For example, we found that the expansion of a given bend often resulted in the hysteretic expansion of the next bend (Fig. 2.9a,b). However, this trend was not clearly observed for all bends. The predominantly downstream effect and strong tendency to form meanders was particularly evident following a cutoff cascade. A large point bar ($x = 9$ m at $t = 185$ h in Fig. 2.2) developed amidst a weakly braided network, which appeared to filter out the upstream perturbations, but itself caused a

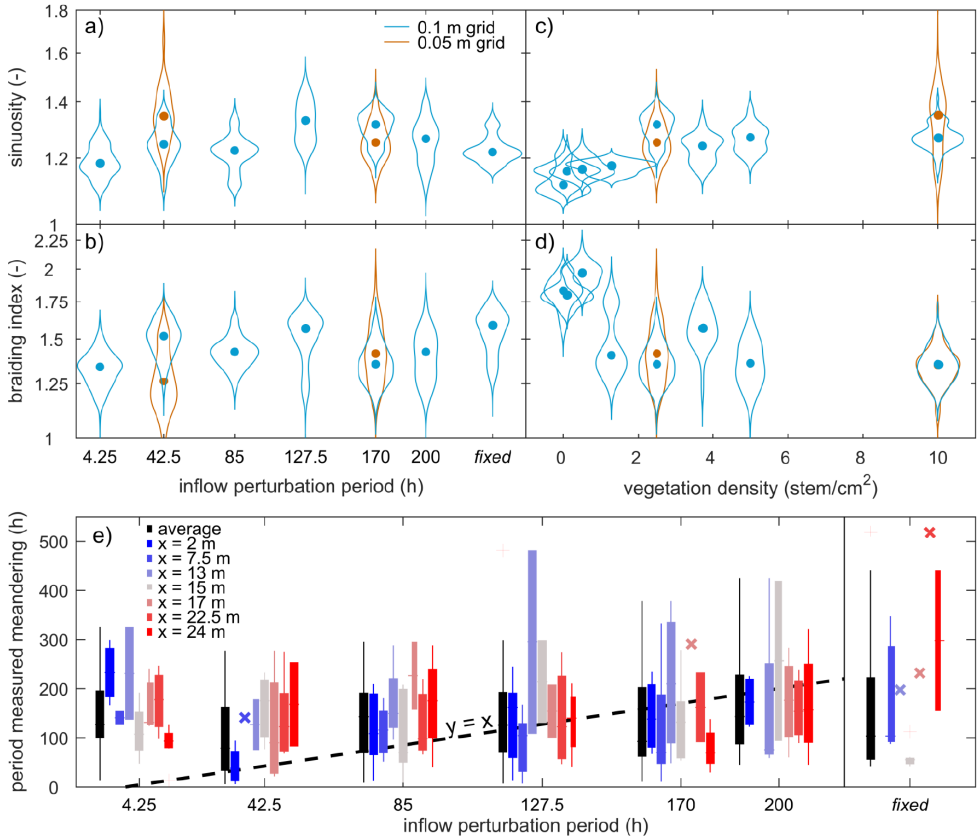

Figure 2.8 Near-independence of the internal river dynamics from the inflow perturbation rate. Violin plots show spatially-averaged sinuosity and braiding index as function of (a-b) the inflow perturbation period and (c-d) vegetation density, sampled from $t = 100$ h until the end of each model run. (e) No discernible correlation between the period of measured meandering and the period of inflow perturbation. Black bars show the average of seven locations along the valley, of which colours correspond to locations in Fig. 2.7. The $\times$ gives the meander period when only one could be measured, given model duration.

steady perturbation that led to meander bend formation in the downstream direction. Oddly, the filtered main channel path sometimes suggested that the cutoff of a bend resulted in the cutoff of its upstream neighbour (Fig. 2.9c,d). This would imply that perturbations in the modelled cutoff-dominated rivers could also propagate in the upstream direction. Upon further inspection, however, the morphological evolution showed that the chute on the upstream point bar was already forming before the chute on the downstream bar. The downstream bar was simply cut off effectively a few modelled years before its upstream neighbour, suggesting that the perceived upstream propagation was coincidental, rather than causally connected.

2.3.4 Effect of grid resolution

The meander-scale characteristics were independent of the grid resolution (Fig. 2.8), but the finer grid better resolved features well-known from the field. The finer grid enabled deeper incision, which contributed to lower width-to-depth ratios. Large tight bends exceeding π radials formed more frequently on a finer grid and were predominantly found in the downstream half of the domain.

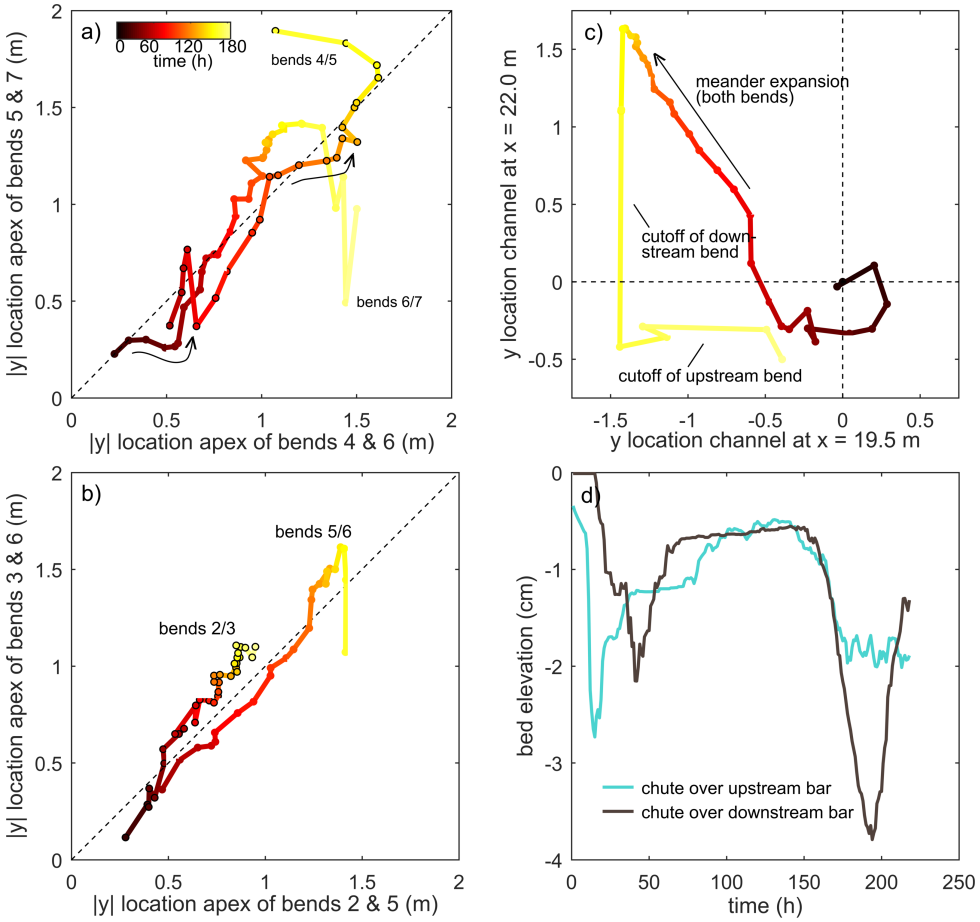

Figure 2.9 (a) Lateral expansion of two bends in scenario N10 ($T = 200$ h) causes hysteretic expansion of the downstream bend, resulting in concave curve sections, indicated by arrows. (b) Fairly straight lines of other bends in the same scenario indicate a lack of hysteretic expansion that would suggest a large convective instability. (c) Apparent upstream propagation of perturbation in N10, where cutoff of a downstream bend precedes cutoff of its upstream-neighbouring bend. (d) Chute channel over upstream point bar (blue; near $x = 19.5$ m) starts forming before the chute channel over the downstream point bar (black; near $x = 22.0$ m). "Black" becomes the dominant channel, whereas "blue" remains secondary and is not deeply incised (see text for explanation).

Additionally, point bars on the fine grid showed scrolls and swales and corresponding fine-grained vegetation age patterns (Figs. 2.2, 2.3, 2.4c), whereas these features were more obscure on a coarse grid.

Grid resolution also affected the distance over which the upstream perturbation effects dampened out. The second fastest perturbation scenario (N13F) showed dampening out over a shorter distance for a fine grid resolution than for a coarse resolution (N13); in particular, there were fewer mid-channel bars in the upstream reach, resulting in a distinctly lower braiding index and higher sinuosity for the finer grid scenario (Fig. 2.8). Interestingly, the largest sinuosity (1.7) was recorded in scenario N13F, for which the inflow perturbation was over an order of magnitude faster than the typical meander period (Fig. 2.6).

2.4 Discussion

Our model results demonstrate that both bar-floodplain conversion and a sustained dynamic inflow perturbation are needed to reach dynamic meandering in a domain of limited length. Bar-floodplain conversion causes a river pattern transition from braided to meandering, and the dynamic inflow perturbation leads to repeated meander initiation and cutoff close to the upstream boundary, unlike a static inflow. While this is in general agreement with previous findings (Lanzoni and Seminara, 2006; Van Dijk et al., 2012; Schuurman et al., 2016), the present results for the first time demonstrate that these are necessary and sufficient conditions for sustained meandering (1) for a large number of bends, unlike previous experiments (e.g. Van Dijk et al., 2012; 2013b); (2) for an initially straight channel, unlike previous modelling (e.g. Van Oorschot et al., 2016); and (3) for entirely self-formed floodplain, unlike one-dimensional meander simulators (Lanzoni and Seminara, 2006; Weiss, 2016) and two-dimensional modelling (Schuurman et al., 2016) in which floodplain was taken out of the domain.

The intricate channel belt topography of the simulated rivers is similar in many aspects to that of natural rivers, including features such as compound point bars, chutes, scroll-like vegetation age patterns and oxbow lakes (Figs. 2.2, 2.3, 2.4). These features appear better defined on a finer grid but are generally present at a lower grid resolution as well. The resulting stacked lateral accretion packages and the better preservation of meanders at the flanks of the valley are generally consistent with earlier modelling and experiments (Van de Lageweg et al., 2016).

Bar-floodplain conversion was crucial to redirecting flow off the point bars into a single thread channel with a low width-to-depth ratio (Tal and Paola, 2010; Van Dijk et al., 2012; Kleinhans et al., 2018). This resulted in bars forced by channel curvature that extended laterally as a consequence of localised outer bend erosion and inner bend accretion (Van de Lageweg et al., 2014). In contrast, in less sinuous channels with sparse vegetation, both the gradual erosion of the outer banks and downstream migration of bars suggest that bars migrated more freely. This behaviour implies that effective floodplain formation causes a meandering pattern. This finding with vegetation as bar-floodplain conversion agent bears resemblance to that of systems with floodplain formation through sedimentation of fines (Van Dijk et al., 2012; Matsubara et al., 2015) and the combination of fines and vegetation (Braudrick et al., 2009; Constantine et al., 2010; Kleinhans et al., 2018).

Previous research demonstrated that the river pattern is well predicted by combination of a form of stream power and grain size (Leopold and Wolman, 1957; Furbish, 1988; Kleinhans and Van den Berg, 2011). However, we show that the river pattern is significantly influenced by the degree of bar-floodplain conversion when potential stream power and grain size are invariable (Fig. 2.5). In nature, the stream power of a river sets the boundary conditions for vegetation in a biomorphological feedback loop, such as maximum flow velocity, flooding and desiccation time and water depth. Therefore, the flow regime of a river influences which vegetation species can flourish on the bars, banks and floodplains, which results in a measure of bar-floodplain conversion that is arguably closely related to stream power, as well as grain size. Variation in current relations of stream power, grain size and river pattern (Kleinhans and Van den Berg, 2011) could then be explained by other factors that affect vegetation species-specific settling, growth and mortality, such as climate and the availability of organic litter and nutrients (e.g. Baker, 1989; Bendix and Hupp, 2000).

The direct influence of the inflow perturbation period on meandering only extends to the first bend, while all other bends migrate uncoupled from the upstream boundary (Figs. 2.7, 2.8). This confirms previous research (Fig. 2.10) (Van Dijk et al., 2012; Schuurman et al., 2016) and is attributed to perturbations migrating in the downstream direction and dampening out within a few channel widths (Zolezzi and Seminara, 2001). New bar and bend instabilities are generated at every bend and especially large bends are able to filter out perturbations from upstream (Fig. 2.2) and create a steady perturbation that leads to the onset of meandering in the downstream direction. Consequently, the

initiation, migration and cutoff of all bends, apart from the first, are predominantly determined by the inherent biomorphological feedback loops. Also, the amplitude of the inflow perturbation is much smaller than the typical meander amplitude, which corroborates that the meandering dynamics are emergent behaviour rather than forced by the upstream boundary. Nonetheless, it seems that a perturbation period that approximates the typical meander period results in fewer cutoffs, which agrees with recent theory and modelling (Weiss, 2016). Furthermore, applying a periodically rotating rather than a transversely migrating perturbation will likely prevent the first bend and bar from being forced by the inflow perturbation (Weiss, 2016), perhaps reducing the number of cutoff cascades initiated by the inflow perturbation.

Inclusion of both finer sediments that could fill abandoned bends, and flow separation at abandoned meanders could have enhanced the persistent dynamic meandering, especially in the models with the fastest inflow perturbations. Firstly, the deposition of fines reduces the accommodation space on point bars by filling in chutes and oxbow lakes, contributing to thick cohesive deposits, and by draping the upper portions of point bars, which decreases bar erodibility. The extent to which such deposition may occur depends on the various plant species at hand, which differ between rivers (Simon and Collinson, 2002; Nicholas, 2013). Consequently, overbank flow is reduced that could otherwise lead to chute cutoff, as shown in mixed-load meandering rivers (Braudrick et al., 2009; Zinger et al., 2013; Kleinhans et al., 2018). Secondly, flow separation at abandoned meanders favours the development of a plug bar that reduces the tendency for chute cutoff (Constantine et al., 2010; Zinger et al., 2013). However, the modelling of flow separation requires much finer grids than is presently feasible; the fines grids required four months of single processor time on a state-of-the-art server PC.

Our findings show that morphology in state-of-the-art physics-based models requires continuous perturbation to maintain dynamics over the full length of the domain of limited length, which is in agreement with theory and experiments. This insight suggests the need for re-evaluation of previous experimental and numerical studies that were terminated before the decay of dynamics, triggered by initial disequilibrium and a static perturbation, could be observed (Friedkin, 1945; Braudrick et al., 2009). For meandering, our work shows that the perturbation period has a negligible effect on the river pattern and dynamics, but the dynamic perturbation must be sustained for the persistence of

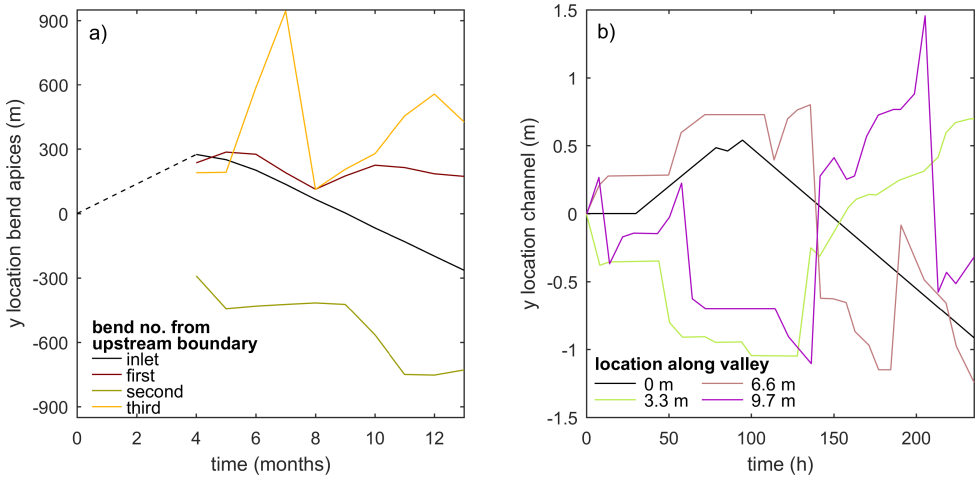

Figure 2.10 Results from previous studies showing that bends, apart from the first bend, migrate nearly independently from the inflow perturbation (a) in two dimensional modelling of high-amplitude meanders by Schuurman et al. (2016) and (b) in flume experiments by Van Dijk et al. (2012).

dynamic meandering over the full length of a domain of limited length. An appropriate period of the perturbation is of the order of magnitude of the natural dynamics, i.e., in our case the meander period.

The present findings also shed new light on the wide scatter observed in relations between meander bend migration and the bend radius normalised by the channel width R/B (e.g. Hickin and Nanson, 1975; Furbish, 1988; Crosato, 2009). The model results show that the growth and migration of bends resulted in tightening of their downstream neighbouring bends, which in turn affected the migration rate of the latter. Generally, tightened bends in our model migrated quickly. However, when bend tightening caused significant overbank flow, the discharge of the main channel decreased, which translated into a smaller strength to erode the outer bank (Van Dijk et al., 2012; 2014) and therefore in slower bend migration. Occasionally, this even caused a cascade in chute cutoffs as was also observed in the River Allier (Kleinhans and Van den Berg, 2011). The downstream propagating effects of bend tightening may explain part of the scatter observed in the aforementioned relations. Backwater and back-sedimentation effects could theoretically result in upstream propagation of perturbations (Hoyal and Sheets, 2009; Kleinhans et al., 2013), but such effects were not observed other than in accidental cases (Fig. 2.9).

In real-world context, external dynamic perturbations are generated by natural processes and repeated human intervention, while internal dynamic perturbations are caused by lateral channel motion at any point along an actively meandering river, contributing to the perpetuation of meandering. Examples of natural dynamic perturbations include an upstream braided river, mass movement from hillslopes and tributaries shedding water and sediment at different times (Van Dijk et al., 2012). Human intervention in rivers introduces new local perturbations that lead to meanders reforming over some downstream distance, probably similar to the distance between the first meander and the upstream boundary in our modelling. While many such measures are static (e.g. groynes, dikes), in contrast to 'soft' measures such as channel deepening and straightening, they may be destroyed over time, as has happened in the River Otofuke (Fig. 2.1). Consequently, both soft and hard measures collectively provide spatio-temporally dynamic perturbations in the form of local topographic forcing. Downstream of such forcing, the river returns to its inherent dynamic equilibrium. Nevertheless, downstream meander bends indirectly respond to upstream morphological change, implying that human intervention could steer unwanted meander expansion downstream or initiate a cutoff cascade (Hooke, 2004). This could contribute to unwanted faster flood wave propagation, but understanding of the propagation of instabilities can be used in remeandering practices. For example, erosion and deposition are redirected by periodically dumping sediment, retrieved from downstream sediment traps, on different sides of the upstream channel. Thus, the dumping causes a soft dynamic lateral perturbation, as was also demonstrated theoretically by Weiss (2016).

The effects of a sustained perturbation likely extend to other morphodynamic environments. For example, a similar conclusion has been drawn for rip currents in the coastal nearshore zone (Castelle and Ruessink, 2011). They found that a time-varying wave direction at the seaward boundary of the nearshore causes a natural variability of rip spacing, migration rate and direction (their Fig. 3). In contrast, when the wave forcing was constant, a steady state with constant wavelength is reached. The most striking dynamics that emerge with varying forcing are commonly observed in nature, i.e., the merging and splitting of bars leading to a change in the number or rip currents. However, no such patterns were reproduced by the model without continued perturbations enforced at one of the boundaries (Castelle and Ruessink, 2011). These findings strongly suggest that a dynamic perturbation on the boundary conditions is necessary in all physical and numerical models for fluvial, estuarine and coastal morphodynamics.

2.5 Conclusions

Morphodynamic modelling with Nays2D was conducted to determine the effect of a dynamic inflow perturbation on the river pattern and dynamics of a dynamic meandering river. This resulted in the following insights.

A dynamic inflow perturbation and bar-floodplain conversion are necessary and sufficient conditions to model dynamic chute cutoff-dominated meandering in numerical hydro-morphodynamic models and in laboratory landscape experiments with a domain of limited length.

Bar-floodplain conversion causes flow to channelise in a single sinuous channel with moderate sinuosity and therefore leads to the meandering river pattern. The model domain spanned about ten bends, which was sufficiently long to cause reformation of meanders following occasional shifts from meandering to weakly-braided in part of the domain due to chute cutoff cascades. The resulting sinuosity, braiding index and meander period are predominantly determined by the biomorphodynamic feedback loops, while the effect of the inflow perturbation period is negligible within an order of magnitude of the timescale of meander migration.

Nevertheless, the initiation and persistence of dynamic meandering requires a dynamic inflow perturbation or a sufficiently long domain, for bend and bar instabilities propagate in the downstream direction. Although the inflow perturbation period does not have a significant impact on the dynamic equilibrium river dynamics, a perturbation period of the order of magnitude of the main morphological time scale, here meander period, appears to be most appropriate. The implication is that all morphological models and landscape experiments for rivers, estuaries and coasts require perturbations on a boundary in order to model natural morphodynamics.

Acknowledgements

Comments by Bruce L Rhoads and an anonymous reviewer, and discussions with Wout van Dijk and Toshiki Iwasaki are gratefully acknowledged. The modelling was partly conducted by SAHW as part of his MSc internship with YS. SAHW and MGK were supported by the European Research Council (ERC Consolidator grant 647570 to MGK). The authors contributed in the following proportions to conception and design, modelling, analysis and conclusions, and manuscript preparation: SAHW(60%, 90%, 80%, 80%), YS(20%, 10%, 10%, 0%) and MGK(20%, 0%, 10%, 20%).


3

Chapter 3 | Complementing scale experiments of rivers and estuaries with numerically modelled hydrodynamics

Abstract

Physical scale experiments enhance our understanding of fluvial, tidal and coastal processes. However, it has proven challenging to acquire accurate and continuous data on water depth and flow velocity due to limitations of the measuring equipment and necessary simplifications during post-processing. A novel means to augment measurements is to numerically model flow over the experimental digital elevation models. We investigated to what extent the numerical hydrodynamic model Nays2D can reproduce unsteady, nonuniform shallow flow in scale experiments and under which conditions a model is preferred to measurements. To this end, we tested Nays2D for one tidal and two fluvial scale experiments and extended Nays2D to allow for flume tilting which is necessary to steer tidal flow. The modelled water depth and flow velocity closely resembled the measured data for locations where the quality of the measured data was most reliable, and model results may be improved by applying a spatially varying roughness. The implication of the experimental data-model integration is that conducting experiments requires fewer measurements and less post-processing in a simple, affordable and labour-inexpensive manner that results in continuous spatio-temporal data of better overall quality. Also, this integration will aid experimental design.

Published as: Weisscher, S. A. H., Boechat-Albernaz, M., Leuven, J. R. F. W., Van Dijk, W. M., Shimizu, Y., & Kleinhans, M. G. (2020). Complementing scale experiments of rivers and estuaries with numerically modelled hydrodynamics. *Earth Surface Dynamics, 8(4), 955–972*, DOI: 10.5194/esurf-8-955-2020

3.1 Introduction

Physical scale experiments greatly enhance our understanding of fluvial, estuarine and coastal processes and complement field observations and numerical models. The benefits of experiments that complement the other two means of research are twofold. Firstly, real material is used with its inherent laws and properties, as opposed to numerical models that require many parameters and approximations of laws for water flow, sediment transport (e.g. Meyer-Peter and Müller, 1948; Van Rijn, 2007; Baar et al., 2019) and lifeforms (e.g. Baptist et al., 2007; Van Oorschot et al., 2016). Secondly, experiments enable full control of the initial and boundary conditions and require little time to form entire systems, as opposed to the slow, ever-changing nature observed remotely or in the field.

The focus of this study is on landscape scale experiments that simulate morphodynamics with shallow water depths of at maximum a few centimetres, i.e. in or just above the viscous sublayer. This kind of scale experiments differs from classical hydraulic flume studies (e.g. Struiksma et al., 1985; Neary et al., 1999) and larger scaled experiments (e.g. Zanichelli et al., 2004; Siviglia et al., 2013) with water depths >10 cm in which flow data can be more easily measured with lasers and submerged flow meters (e.g. ADCP). In contrast, data collection in landscape experiments is often difficult, infrequent and hindered by various problems (Fig. 3.1).

Typical data collection in such experiments targets the following three elements: (1) the morphological development from overhead imagery and digital elevation models (DEMs) from laser scanning or stereo photography on a dry bed (e.g. Ashworth et al., 2004; Hoyal and Sheets, 2009;

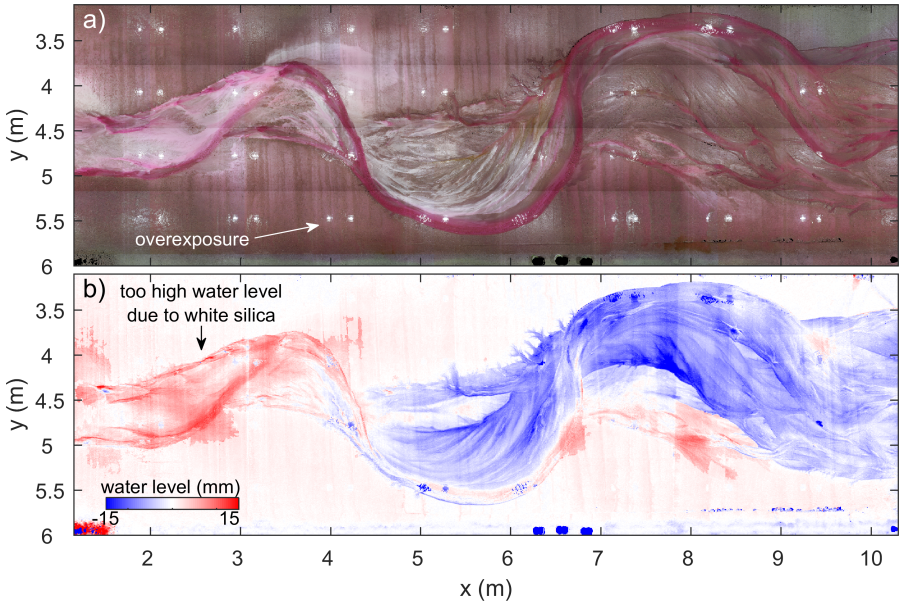

Figure 3.1 Exemplary data of a physical scale experiment of a meandering river by Van Dijk et al. (2013a) show how data extraction may be distorted. (a) Overhead imagery shows cases of light overexposure and the distribution of white silica flour. The water is dyed red where the water colour saturation is a measure of water depth. Flow is from left to right. (b) Water levels, based on measured bed elevations and water depths estimated from water colour saturation, are too high above the floodplain ($z = 0$ mm) at locations of abundant silica flour and too low at locations of overexposure.

Leduc et al., 2019); (2) water depth estimated from dye and light attenuation, possibly combined with absolute water level point measurements (e.g. Peakall et al., 2007; Tal and Paola, 2007; 2010), and; (3) flow velocity from particle imaging velocimetry on the water surface from floating particles or dye injections (e.g. Tambroni et al., 2005; Braudrick et al., 2009). Due to the shallow water depths in landscape experiments, it is technically difficult to conduct flow measurements by submerged instruments without disturbance of the sediment transport and with the same spatial resolution as of the bathymetry. To overcome the drawbacks of data collection and post-processing, there has so far been one research team (Tesser et al., 2007; Stefanon et al., 2010; 2012) that modelled water depth and flow velocity over DEMs of tidal basin scale experiments. However, the modelled data acquired by this novel method was not extensively validated against measured data and the model only applies for uniform flow conditions (Marani et al., 2003).

Here we explore the possibility of extending the numerical flow model application by Tesser et al. (2007) and Stefanon et al., (2010; 2012) for unsteady, nonuniform flows in landscape scale experiments. We aim to complement the measured morphological data with continuous, spatio-temporally dense numerical data of water depth, flow velocity and bed shear stress. On the one hand, this is a similar practice to modelling flow over the measured morphology of real rivers and estuaries (e.g. Berends et al., 2019), whilst here the shallow water equations need to be solved. On the other hand, this practice differs from remodelling the morphological development of a scale experiment (e.g. Struiksma et al., 1985), which are subject to all the combined errors of sediment transport predictors (Baar et al., 2019). The extended integration of experimental data and a numerical model would not only expand the possibilities for data analyses of a series of experiment bed scans, but would also open up fast methods of testing alternative experimental settings for either an experimental or idealised morphology. This would save valuable time in the laboratory, especially for long-lasting experiments that include vegetation (e.g. Braudrick et al., 2009; Van Dijk et al., 2013b; Lokhorst et al., 2019).

3.2 Review: Experimental Data Collection and Post-Processing Techniques

In order to quantify the hydro- and morphodynamics of a landscape scale experiment with shallow flow, the following three data types are commonly measured: dry bed elevation, water depth and flow velocity (Table 3.1). Below, the data collection and post-processing methods of these data are presented in conjunction with their drawbacks and achievable level of accuracy.

Firstly, bed elevation of experiments can be acquired through numerous techniques. These include a water level contour survey (Reynolds, 1889; 1891), a manual/digital point gauge survey (e.g. Friedkin, 1945; Peakall et al., 2007), 3D/laser and structured light (zSnapper®) scanning (e.g. Gran and Paola, 2001; Tambroni et al., 2005; Van de Lageweg et al., 2014; Kleinhans et al., 2014b; Marra et al., 2014), ultrasonic echosounding (e.g. Best and Ashworth, 1994; Hoyal and Sheets, 2009; Stefanon et al., 2010; 2012), and structure-from-motion (SfM) photogrammetry through which photos are geo-referenced to ground control points (Agisoft PhotoScan) (e.g. Westoby et al., 2012; Leduc et al., 2019). The most accurate technique is the point gauge survey ($\pm$ 0.1 mm) (Best and Ashworth, 1994), which does not require the flume to be drained. However, point gauging is terribly slow to get full coverage, as is the case for the water level contour survey, in which dry bed-water boundaries are registered for different water levels (Reynolds, 1889; 1891). In contrast, scanning, sounding and photogrammetry are much quicker and typically result in a vertical accuracy of $\pm$ 0.5 to 1 mm (Peakall et al., 2007; Leduc et al., 2019). Yet, these three techniques require a dry bed, apart from a few kinds of laser scanners (Tesser et al., 2007; Stefanon et al., 2010; 2012). Consequently, the bed may be disrupted during the draining and refilling of the flume. Also, vegetation hampers their

Table 3.1 Data collection techniques in fluvial and tidal scale experiments with erodible boundaries and flows shallower than a few centimetres. 'Overhead imagery' constitutes imagery or video from a camera at a fixed position that potentially allows for the classification of the experiment planform. Water depths 'est. from physics' are determined for a few cross-sections assuming uniform flow and a given discharge. 'SfM' is structure-from-motion photogrammetry. The field 'Remarks' contains additional sediments/vegetation on top of the main sediment that may interfere with overhead imagery analyses.

Paper	Type of experiment	Measurements					Remarks
		Overhead imagery	Elevation	DEM	Water depth	Flow velocity	
unidirectional flow							
Friedkin (1945)	meandering/braided river	x	point gauge	x	point gauge	-	silt, coal, loess
Schumm and Khan (1972)	alternating bars	-	point gauge	-	point gauge	-	kaolinite
Schumm et al. (1987)	alluvial fan	x	burial of pins	-	-	-	-
Ashmore (1991a; 1991b)	braided river	x	point gauge	-	point gauge	-	-
Ashworth et al. (1994)	braided river	x	point gauge	-	point gauge	-	-
Gran and Paola (2001)	braided river	x	laser/point gauge	x	water colour	PIV	vegetation
Ashworth et al. (2004)	braided river	x	laser	x	-	-	-
Peakall et al. (2007)	braided river	x	point gauge	-	point gauge	PIV	-
Tal and Paola (2007; 2010)	meandering river	x	laser	-	water colour	-	vegetation
Hoyal and Sheets (2009)	alluvial fan	x	ultrasound	x	est. from physics	dye	-
Van Dijk et al. (2009)	alluvial fan	x	SfM	x	est. from physics	-	-
Braudrick et al. (2009)	meandering river	x	laser	x	point gauge	dye	vegetation
Gardner and Ashmore (2011)	braided river	x	SfM	x	-	-	-
Van Dijk et al. (2012; 2013a)	meandering/braided river	x	laser	x	water colour	-	silica flour
Van Dijk et al. (2013b)	meandering river	x	laser	x	water colour	-	vegetation
Van de Lageweg et al. (2013; 2014)	meandering river	x	laser	x	water colour	-	silica flour
Leduc et al. (2019)	braided river	x	SfM	x	SfM	-	-
reversing flow							
Reynolds (1889; 1891)	estuary/tidal basin	-	contour-line	x	-	-	-
Mayor-Mora (1977)	tidal channel	x	point gauge	-	point gauge	-	-
Tambroni et al. (2005)	tidal channel	-	ultrasound	x	ultrasound	PIV	-
Tesser et al. (2007)	tidal basin	-	laser	x	ultrasound	model	-
Stefanon et al. (2010; 2012)	tidal basin	-	laser	x	ultrasound	model	-
Vlaswinkel and Cantelli (2011)	tidal basin	x	laser	x	bathymetry	-	-
Kleinhans et al. (2012; 2015b)	tidal basin	x	-	-	water colour	PIV	-
Iwasaki et al. (2013)	tidal basin	x	*unclear*	-	-	-	-
Kleinhans et al. (2014b)	tidal channel	x	zSnapper®	x	water colour	-	-
Braat et al. (2019a)	estuary	x	SfM	x	water colour	PIV	walnut shell
Leuven et al. (2018a)	estuary	x	SfM	x	-	PIV	-
Leuven and Kleinhans (2019)	tidal channel	x	SfM	x	water colour	PIV	-

accurate reading of the bed elevation (e.g. Gran and Paola, 2001). In consequence of these drawbacks, the number of DEMs is usually limited.

Secondly, water depth maps are acquired while the experiment runs in either of two approaches: water depth is derived from the dyed water colour saturation, or from measured water levels. As for the first approach on dye, the water colour saturation is an indicator of water depth that is recorded by overhead cameras (Carbonneau et al., 2006; Tal and Paola, 2007; 2010). To augment differences in colour saturation, some studies (e.g. Van Dijk et al., 2013a; Leuven et al., 2018b) converted the overhead RGB imagery to the CIE L*a*b* colour space; L* is a scale for luminosity, a* is a scale from green to red, and b* is a scale from blue to yellow. For calibration, the bed elevation of a map or transect is related to the corresponding values of colour saturation, after which a regression is used to convert the overhead imagery to water depth maps. Ideally, a regression is used that captures the exponential saturation of water colour with increasing water depth (Carbonneau et al., 2006). A high accuracy up to 1 mm is mentioned in literature (Tal and Paola, 2007; 2010), but may be much lower for substrates with mixed sediments with different colours and for lighting variations (Fig. 3.1) (e.g. Van Dijk et al., 2013a).

Alternatively, water depth is readily derived from water levels and bed elevations. Water levels are recorded as point measurements using an ultrasonic echosounder or water level gauge (e.g. Mayor-Mora, 1977; Tambroni et al., 2005) or are derived from SfM photogrammetry (Leduc et al., 2019). Although sounding and gauging are more time-consuming to get full coverage, the data has a much

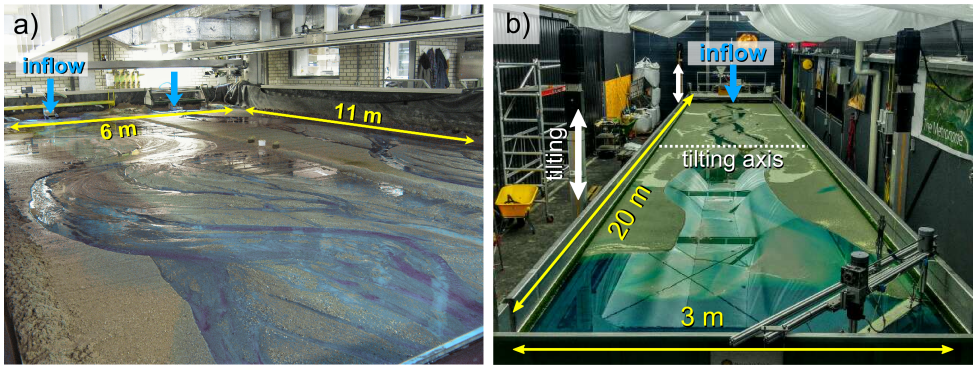

Figure 3.2 The flume setups of the two scale experiments tested in this study. (a) The Eurotank flume was used to simulate meandering and braided rivers in parallel on the left and right part of the flume, respectively (Van Dijk et al., 2013a). Water colour was converted to blue for visual comparison with (b) the second scale experiment in the tilting flume the Metronome that was used to simulate estuaries (Leuven et al., 2018b). The flume tilts over the short central axis, which steers flood and ebb flows that favour ample sediment transport in both tidal directions.

smaller claimed error of 0.2 mm (Tambroni et al., 2005). As for SfM photogrammetry, this only works up to present for unidirectional flow with rigorous calibration and has a vertical accuracy of 1 mm (Leduc et al., 2019). Additionally, few studies estimate water depth along cross-sections of the known bathymetry from uniform flow and an estimated discharge (Hoyal and Sheets, 2009; Van Dijk et al., 2009; Vlaswinkel and Cantelli, 2011).

Thirdly, flow velocity maps are created by tracking floating particles (Peakall et al., 2007; Kleinhans et al., 2017b), soap bubbles (Gran and Paola, 2001) and dye (Hoyal and Sheets, 2009; Braudrick et al., 2009) with overhead cameras. Either the data are partly manually digitised or a technique is used called particle imaging velocimetry (PIV) (e.g. Mori and Chang, 2003). Herein, small floating particles are seeded on the water surface, and their positions are recorded at a high frequency by overhead cameras. Subsequently, surface flow velocity and direction are computed by tracking the displacement of the particles from pairs of consecutive images. However, this technique falls flat for regions with either sparse or superabundant particles where it is infeasible either to get sufficient coverage or to track individual particles. Also, PIV particles may become stranded on bars, which culminates in much lower or absent measured flow velocities that are especially troublesome in tidal experiments (Leuven et al., 2018b). Another drawback is that the PIV particle removal is done by increasing the water depth and draining the flume, which may disrupt the bed. For this reason, PIV measurements cannot be done in experiments with vegetation and light-weight material, for the latter would be uprooted or displaced. This issue may be overcome by using soap bubbles (Gran and Paola, 2001). The error of PIV measurements of mean flow velocities may be as small as 0.5 pixel size if particle size and density are chosen correctly (Weitbrecht et al., 2002). Finally, measuring flow in the water column is infeasible with the available equipment reported in literature; this is due to the shallow water depth of at most a few cm in the type of physical scale experiments discussed here.

Thus far, only one research group has used a numerical model to create flow velocity maps for scale experiments with shallow flow (Tesser et al., 2007; Stefanon et al., 2010 2012). They used a tidal basin DEM and the boundary conditions as input and solved the Poisson boundary value problem, which is valid for systems where the water surface can be assumed horizontal (Marani et al., 2003). This resulted in maps of depth-averaged flow velocities over a tidal cycle. Although the model had been validated for the Venice Lagoon (e.g. Defina, 2000), the model was not calibrated for the experiment due to a lack of flow velocity measurements.

3.3 Methods

3.3.1 Selected Scale Experiments

Two fluvial experiments and one tidal experiment were selected for testing that are representative of other river flume setups with uni-directional flow (e.g. Ashmore, 1991; Tal and Paola, 2010; Braudrick et al., 2009) and for estuary flume setups with reversing flow (e.g. Reynolds, 1889; Tambroni et al., 2005; Braat et al., 2019a). Below, a brief review is given on the main findings and general setup of the selected experiments.

The fluvial experiments in the Eurotank flume by Van Dijk et al. (2013a) demonstrated the importance of cohesive floodplain formation for replicating a meandering channel in a physical scale-experiment. Floodplain formation by the deposition of fines was found to be sufficient to maintaining a sinuous, single-thread channel in the absence of vegetation. In contrast, a weakly braided river pattern developed in the control experiment without fines. Fines were represented by white, silt-sized silica flour that was added to the river discharge. Additionally, regular floods were applied to the river discharge to enhance the deposition of cohesive deposits on the floodplain, and the inflow was periodically perturbed to maintain meandering dynamics (Lanzoni and Seminara, 2006; Van Dijk et al., 2012; Chapter 2). The collected data constitutes overhead imagery and DEMs from line-laser altimetry. In parallel, floodplain has been formed experimentally with vegetation (Tal and Paola, 2010; Braudrick et al., 2009), but this requires parameterisation of vegetation that, although possible (Baptist et al., 2007; Chapter 2), introduces uncertainties that would hamper model-data comparison for this study.

The tidal experiment in the Metronome flume by Leuven et al. (2018b) showed the development of an entire estuary with erodible boundaries and self-formed bars on a laboratory scale. The self-formed estuary planform was characterised by along-channel alternations of shallow, wide sections that accommodated large bars, and deep bottlenecks where the main confluences were found. The Metronome flume tilts over the short central axis (Fig. 3.2), which differs from previous stationary flume setups with sea level fluctuations (Reynolds, 1889; 1891; Mayor-Mora, 1977; Tambroni et al., 2005; Tesser et al., 2007; Stefanon et al., 2010; 2012; Vlaswinkel and Cantelli, 2011; Iwasaki et al., 2013). The tilting motion periodically generates a slope in the landward direction during flood and a slope in the seaward direction during ebb, which result in tidal currents strong enough to move sediment along the entire estuary (Kleinhans et al., 2017b) (Suppl. Movie online). The collected data constitutes overhead imagery, DEMs from stereo-photography and flow measurements by large-scale particle imaging velocimetry (PIV) over a tidal cycle. Earlier experiments had tidal flow driven by slow sea level fluctuations, which is closer to the cause of tidal currents in nature but leads to lower sediment mobility (e.g. Tambroni et al., 2005; Stefanon et al., 2010). Moreover, such flows can be modelled with simpler flow models (Marani et al., 2003; Stefanon et al., 2010) that provide a less rigorous test of the numerical model applied here.

3.3.2 Numerical Model Nays2D

The numerical model Nays2D was selected to simulate water flow of fluvial and tidal landscape scale experiments for the following reasons. Firstly, Nays2D is one of few models that can account for shallow flow of at maximum a few centimetres deep. This is opposed to more common models for the simulation of large-scale fluvial and tidal morphodynamics (e.g. Delft3D) that often have build-in thresholds for minimum water depths. Secondly, Nays2D is open source (as opposed to e.g. FLOW-3D), so the technique tested in this study is freely available for third parties.

Nays2D solves the depth-averaged nonlinear shallow water equations, given by the following three equations in Cartesian coordinates, in which Eq. (3.1) is the preservation of mass and Eq. (3.2-3.3) are

the preservation of momentum in the streamwise and transverse direction, respectively:

$$\frac{\partial h}{\partial t} + \frac{\partial (h\bar{u})}{\partial x} + \frac{\partial (h\bar{v})}{\partial y} = 0 \tag{3.1}$$

$$\frac{\partial \bar{u}}{\partial t} + \bar{u}\frac{\partial \bar{u}}{\partial x} + \bar{v}\frac{\partial \bar{u}}{\partial y} + g\frac{\partial H}{\partial x} + \frac{g\bar{u}\sqrt{\bar{u}^2+\bar{v}^2}}{C^2 h} - \nu_t\left(\frac{\partial^2 \bar{u}}{\partial x^2} + \frac{\partial^2 \bar{u}}{\partial y^2}\right) = 0 \tag{3.2}$$

$$\frac{\partial \bar{v}}{\partial t} + \bar{u}\frac{\partial \bar{v}}{\partial x} + \bar{v}\frac{\partial \bar{v}}{\partial y} + g\frac{\partial H}{\partial y} + \frac{g\bar{v}\sqrt{\bar{u}^2+\bar{v}^2}}{C^2 h} - \nu_t\left(\frac{\partial^2 \bar{v}}{\partial x^2} + \frac{\partial^2 \bar{v}}{\partial y^2}\right) = 0 \tag{3.3}$$

in which t is time (s), $\bar{u}$ and $\bar{v}$ are the depth-averaged flow velocity (m s^{-1}) in the streamwise (x) and transverse (y) direction, H is the water level (m), h is the water depth (m), C is the Chezy roughness (m$^{0.5}$ s^{-1}), g is the acceleration due to Earth's gravity (m s^{-2}) and ν_t is the eddy viscosity coefficient (-). Eddy viscosity is approximated as

$$\nu_t = \frac{\kappa}{6} a u_* h + b \tag{3.4}$$

$$u_{*,x} = \sqrt{\frac{g\bar{u}\sqrt{\bar{u}^2+\bar{v}^2}}{C^2}} \quad \& \quad u_{*,y} = \sqrt{\frac{g\bar{v}\sqrt{\bar{u}^2+\bar{v}^2}}{C^2}} \tag{3.5}$$

in which $u_{*,x}$ and $u_{*,y}$ are the streamwise and transverse components of the shear velocity (m s^{-1}). The hydrodynamics were solved by dividing each time step into two parts, namely an advective part that was solved using a cubic-interpolated pseudoparticle (CIP) method, and a nonadvective part that was solved with a conventional finite difference method (Yabe et al., 1990). Since the aim of this study is to complement bathymetric data with hydrodynamic data rather than to reproduce the experiment, sediment transport and morphological updates were disregarded.

Input to Nays2D comprised a DEM of each experiment as initial condition and the corresponding boundary conditions (Fig. 3.3; Table 3.2). For the river modelling, the two DEMs (meandering and braided rivers) corresponded to the final flood stage; a constant bankfull discharge of 0.5 L s^{-1} entered at the upstream boundary, and the water level at the downstream boundary was derived from uniform flow. For the estuary modelling, the DEM was used that corresponded to tidal cycle number 5887 (see Leuven et al., 2018b), and a 0.1 L s^{-1} river discharge entered only during the ebb phase; DEMs at later stages could not be used since the ebb-tidal delta was incomplete due to the overhanging wave generator. The estuary DEM was interpolated to a coarser rectangular grid with 2.5×2.5 cm grid cells to limit model run time to at maximum one day. In agreement with modelling practices for natural systems (Arcement and Schneider, 1989), a spatially uniform Manning roughness coefficient of $n = 0.02$ s m$^{1/3}$ was applied of which the sensitivity will be assessed later. The Manning roughness coefficient is described as:

$$n = \frac{h^{1/6}}{C} \tag{3.6}$$

The reason for not using a spatially variable friction, which could be computed from maps of grain size, is that such maps would currently include all measurement errors due to lighting and sediment colour. If these errors are significantly reduced in future studies, spatially varying friction maps are a viable option. The model was cold started with an initial water slope equal to the valley slope of the DEM with initial flow velocities calculated from uniform flow.

Nays2D was extended to enable periodical tilting of the estuary DEM and the downstream water level boundary to drive tidal flow similar to the tilting flume the Metronome (Fig. 3.2). The domain was tilted sinusoidally with a period of 40 s and an amplitude of 0.075 m, meaning a maximum gradient

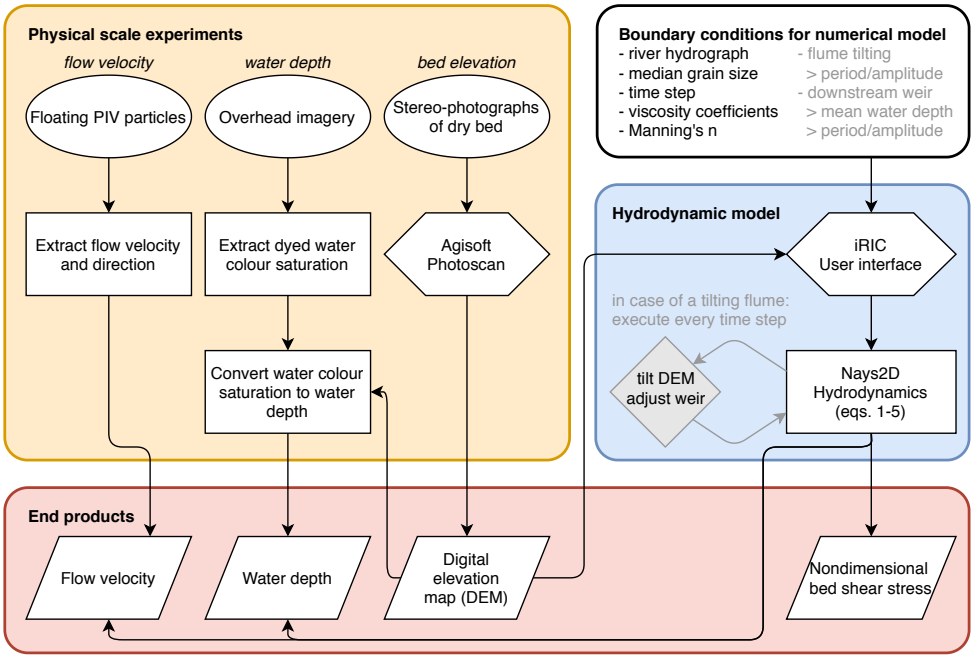

Figure 3.3 Workflow of integrating physical scale experiments and the numerical hydrodynamic model Nays2D to acquire water depth, flow velocity and sediment mobility maps (i.e., excluding point measurements). The DEM and corresponding boundary conditions are input to the model. Grey elements apply only to tilting flume experiments that simulate tidal systems. End products are on the bottom row and are indicators of hydrodynamics and morphological change.

of 0.0075 m m^{-1}. In the Metronome, the water level at the downstream boundary was set by a weir that moved in counterphase to the flume tilting so as to maintain a constant sea level of +0.065 m during tilting (see for explanation: Kleinhans et al., 2017b; Leuven et al., 2018b). As the experiment progressed, the weir amplitude was gradually reduced with the reduction of the length of the open sea due to the development of the large ebb-tidal delta; at tidal cycle number 5887, the weir had an amplitude of 0.004 m. To mimic the action of the weir in the model Nays2D, a sine function was imposed on the water depth at the downstream boundary, and the sea around the ebb-tidal delta was assigned a high diffusivity of $b = 0.02$ for numerical stability.

3.3.3 Data Analysis

Maps of water depth and flow velocity were compared to the measured data. For the two rivers, only water depth was compared, as flow velocity was not systematically measured other than sparse estimates of mid-channel flow (see Suppl. Fig. 3.13 for modelled flow velocity maps). To explore the causes of the water depth differences between the model and the experiments, the river planforms were classified into six classes (Suppl. Fig. 3.14). The first two classes comprised the locations of white silica flour and overhead light overexposure, which were based on the overhead imagery. The remaining four classes were morphological units with increasing levels of inundation, from a soaked bed with negligible water depth to a channel. These units were based on modelled flow, for which we used bed elevation times flow velocity to the power three that proved well to separate transporting channels from inactive ones (Chapter 2).

Table 3.2 Model settings and boundary conditions of the physical scale experiments in Nays2D. The first block of parameters is retrieved from the experiments, the second block is user-defined.

Parameter	Unit	Van Dijk et al. (2013a) *meandering/braided rivers*	Leuven et al. (2018b) *estuary*
River discharge	L s^{-1}	0.5	0.1
Grain size d_{50}	m	0.51×10^{-3}	0.55×10^{-3}
Downstream water level	m	*uniform flow*	0.065
Tilting period (flume & weir)	s	–	40
Tilting amplitude (flume)	m	–	0.075
Tilting amplitude (weir)	m	–	0.004
Time step	s	0.02	0.005
Manning's n	s $m^{1/3}$	0.02	0.02

Maximum and minimum water depths in the estuary experiment were compared to bracket the tidal conditions. The 16 overhead images taken during the tidal cycle were converted into measured water depth maps. To account for incoming light from a window at the seaward side of the flume, two conversions were formulated for the upstream and downstream boundaries that were linearly interpolated along the flume. The equation for the upstream boundary was $h = 1.43.10^{-7} \times Blueness^{-15.68} + 0.004$ and for the downstream boundary was $h = 2.41.10^{-2} \times Blueness^{-2.19} + 0.092$, where $Blueness$ is the b* band in the CIE L*a*b* colour space.

Surface flow velocity measurements of the estuary experiment were compared with modelled depth-averaged velocities. To this end, the modelled flow velocities were converted to surface flow velocity using

$$u_z = \frac{u_*}{\kappa} ln\left(\frac{z}{z_0}\right) \tag{3.7}$$

in which u_z is the flow velocity (m s^{-1}) at depth z (m), with depth-averaged flow velocity at $0.36\ h$, and z_0 is the zero-velocity level for rough flow (m). Modelled depth-averaged flow velocity and shear velocity were used to calculate z_0, from which u_z was calculated at the water surface. Grid cells lacking one or more of the 16 PIV measurements during the tidal cycle were filtered out to enable a fair comparison of experimental data and model throughout the entire tidal cycle. The comparison focused on morphologically relevant variables; these include the tidal flow velocity maxima during the ebb and flood phases, which are important for sand transport (Friedrichs, 2011), and the tidally averaged residual flows, which are important for mud transport (Postma, 1961; Groen, 1967).

Finally, the sensitivity to the Manning roughness coefficient was tested for the range $0.016 - 0.024$ s $m^{1/3}$ that agrees with common coefficients for sand (Arcement and Schneider, 1989). The mean absolute error (MAE) and mean bias error (MBA) quantify the difference between the model and the measurements. The MAE is computed as the average of absolute differences between the modelled and measured data. The MBA is computed as the average difference to quantify how much the model over- or underpredicts the measured data.

3.4 Results

3.4.1 Meandering and Braided Rivers

Water Depth

The modelled water depth resembles the measured data for both river types for locations where the quality of the experimental data is good (Figs. 3.4a-f, 3.5a-d; Suppl. Fig. 3.14). Similar to the

meandering river experiment, the model produces flow that is focused in a single sinuous channel, especially for $x > 4$ m (Suppl. Fig. 3.13), despite the multi-channel character of the DEM and the considerable overbank flow. This distinction of a main sinuous channel and swale channels is less distinct in the model for $x < 4$ m. This is also the domain range with slightly more modelled overbank flow over the floodplain compared to the experiment (Fig. 3.4c). The mean absolute error is small, albeit larger for the channels (MAE $= 1.73$ mm) than the low/high inundated areas (MAE $= 0.81$ mm), and the model bias error is negligible (MBE $< 0.1 \cdot$ MAE) (Fig. 3.5a,b), given a maximum water depth of 20 mm.

The braided river model reproduces the division of flow over about two channels with little overbank flow (Fig. 3.4d-f). However, the model predicts slightly more water flowing through the secondary channels and less through the main channel (for example the secondary channel around $x = 6$ m, $y = 1$ m in Fig. 3.4f). Overall, the model error is slightly larger than of the meandering river, with an MAE $= 2.31$ mm and MBE $= -0.65$ mm for channels and an MAE $= 1.30$ mm and MBE $= -0.25$ mm for low/high inundated areas (Fig. 3.5b,d); the bias errors indicate that modelled water depths are on average lower than the measured values for the braided river.

The modelled flow is more reliable at locations with abundant white silica flour where the measured data are quite inaccurate (Fig. 3.1b; Suppl. Fig. 3.14c). It is at these locations that the measured water levels, calculated as water depth from water colour added on the bathymetry, are unrealistically high above the surrounding floodplain. The reason for such large measured water depths for the upper meandering river (Fig. 3.4a-c) is that the white silica flour enhanced the colour contrast with respect to the yellowish sandy substrate. In consequence, higher redness values were recorded for floured regions on the a* band that Van Dijk et al. (2013a) used to estimate water depths. However, as this effect was unaccounted for during post-processing, too large water depths were assigned to these 'redder' areas.

3.4.2 Estuary

Water Depth

Periodic tilting of the estuary DEM that mimicked the motion of the tilting flume adequately reproduced the propagating behaviour of the tidal wave (Suppl. Movie online). Moreover, the modelled tidal wave caused maximum and minimum water depths close to those observed with an MAE $= 1.96$ mm for maximum water depths and an MAE $= 2.64$ mm for minimum water depths (Figs. 3.4g-l, 3.5e,f; Suppl. Figs. 3.15, 3.16). These errors are small compared to the largest water depths recorded in the estuary of about 35 mm.

Overprediction by the model mainly occurs at the ebb-tidal delta ($x > 18$ m in Fig. 3.4i,l). This is predominantly due to the difference of the downstream boundary conditions between the experiment and the model. In particular, the amount of water entering the flume during flood was somewhat limited by the pumping capacity in the experiment. In contrast, the influx of water in the model was determined with a uniform flow assumption, causing larger inflow that increased the water depths on the ebb-tidal delta. In turn, this larger influx likely contributed to the slightly larger maximum modelled water depths especially in the downstream half of the estuary.

Underprediction by the model is primarily ascribed to two factors, namely the chosen hydraulic roughness coefficient (model-based) and the water depth conversion from colour saturation (experimental data-based). Firstly, the observations clearly show that the tidal wave propagated faster in the deeper channels than over the shallow bars, causing flow to curl around bars (Suppl. Movie online). In the model, however, the partitioning of flow between channels and bars is less asymmetrical. In consequence, flood-dominant channels that end in a shoal may receive more modelled inflow over their shoal during ebb, resulting in overall slightly larger water depths (e.g. the red tidal channel at $x = 8$ m in Fig. 3.4l). This implies that the model diffusivity and/or hydraulic roughness on the bars are too small. Secondly, the experimental data-model comparison is sensitive

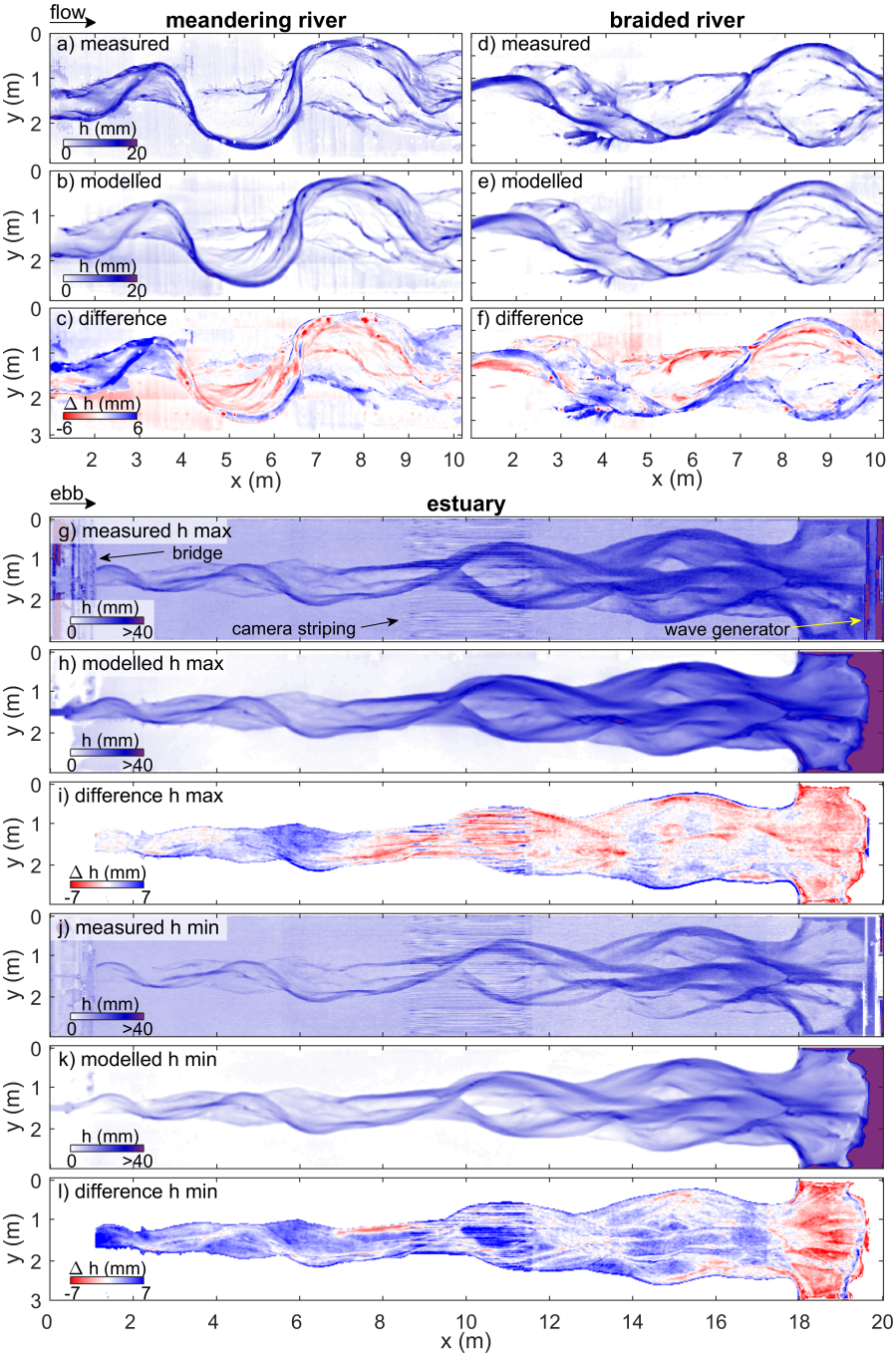

Figure 3.4 Measured and modelled water depth (a–c) for the meandering and (d–f) braided rivers by Van Dijk et al. (2013a) and (g–l) for the estuary by Leuven et al. (2018b). In case of the estuary, panels (g–i) show the maximum water depth during a tidal cycle, and panels (j–k) show the minimum water depth during a tidal cycle. Maps of difference are determined by subtraction of modelled from measured water depth.

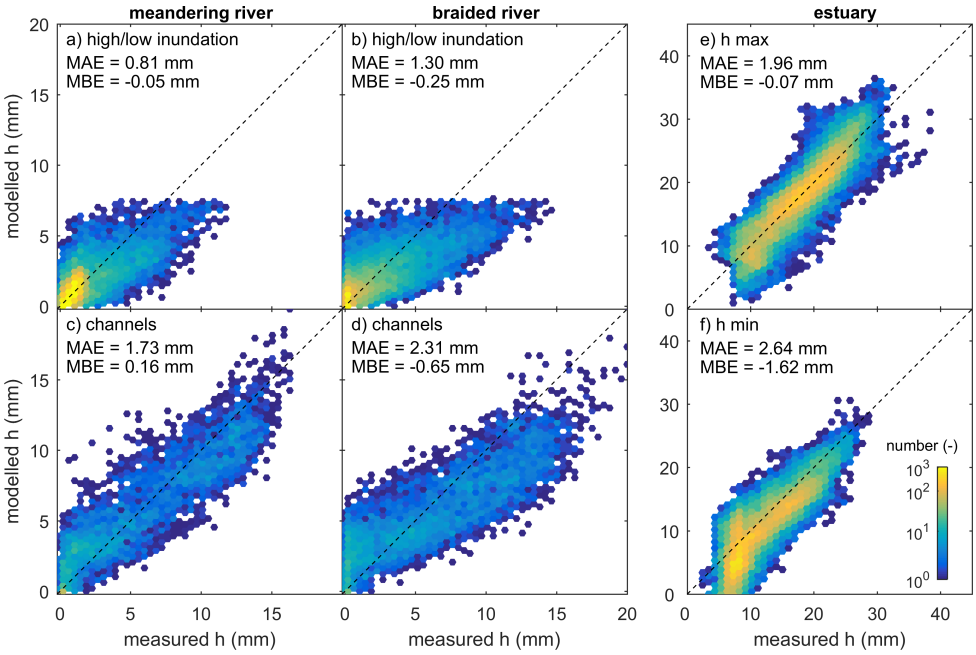

Figure 3.5 Comparison between measured and modelled water depths for different classes for the (a/c) meandering and (b/d) braided rivers, as well as for the (e) maximum and (f) minimum water depths in the estuary. The scatter density plots exclude floodplain and erroneous measured data (e.g. due to white silica flour), which are included in Suppl. Figs. 3.14 (rivers) and 3.15 (estuary). Colours indicate the occurrence frequency.

to the water depth conversions, which are less accurate for shallow water depths (Figs. 3.5f). Specifically, the nonlinear conversion equations used in this study and by Leuven et al. (2018b) overpredict water depths for very shallow flow (i.e., $h < 5$ mm; Fig. 3.5f)) so as to get the deeper water depths right. Therefore, measured water depths of very shallow flow over bars are too large, which explains most of the differences between model and experimental data for minimum water depths.

Ebb and Flood Flow

The modelled spatial pattern of peak flow velocities resembles that of the PIV measurements (Fig. 3.6). Both model and measurements show that peak ebb and flood flow are relatively large in channels and around bottlenecks, while they are relatively small on bars and in wider sections of the estuary. Furthermore, peak flow velocities decrease in the landward direction from $\pm$ 40 cm s^{-1} at the estuary mouth to $\pm$ 30 cm s^{-1} at $x = 2$ m (Fig. 3.7a,b). Over the entire tidal cycle, the model has a small MAE $=$ 6.45 cm s^{-1}, which is about 1/7 of the maximum surface flow velocity; in other words, the modelled order of magnitude is close to the measurements'. Also, a different manning roughness results in fairly similar water levels and flow velocities along the estuary, with slightly smaller flow velocities and water level variations for a higher roughness (Fig. 3.7b,c).

The model has full spatial cover, while experimental data are lacking particularly near the estuary mouth and for the shallower areas (Fig. 3.6a,b,e). Near the estuary mouth, PIV particles occasionally clumped together, which resulted in incorrect flow measurements that were excluded from comparison with the model. On the other hand, PIV measurements at shallow locations were discontinuous since the PIV particles either stranded on the bars or were drained to deeper waters. Consequently, flow velocity measurements on and around bars tend to be inaccurate, which explains the larger contrast of

modelled and measured velocities for shallower areas (Figs. 3.6, 3.8). For example, the model clearly shows the wetting and drying of a tidal bar with peak flow velocities half of those in a bordering channel (Fig. 3.8b). The measurements in the channel are about similar, but are unrealistic for the tidal bar; the PIV measurements suggest negligible flow which is incongruent with the recorded tidal water depth variations.

Residual flow maps of both modelled and measured flow show the expected ebb-dominance of channels and flood-dominance of bars, especially at their seaward sides (Fig. 3.9). Also, the two circulation cells measured on the ebb-tidal delta are well-reproduced by the model. However, the

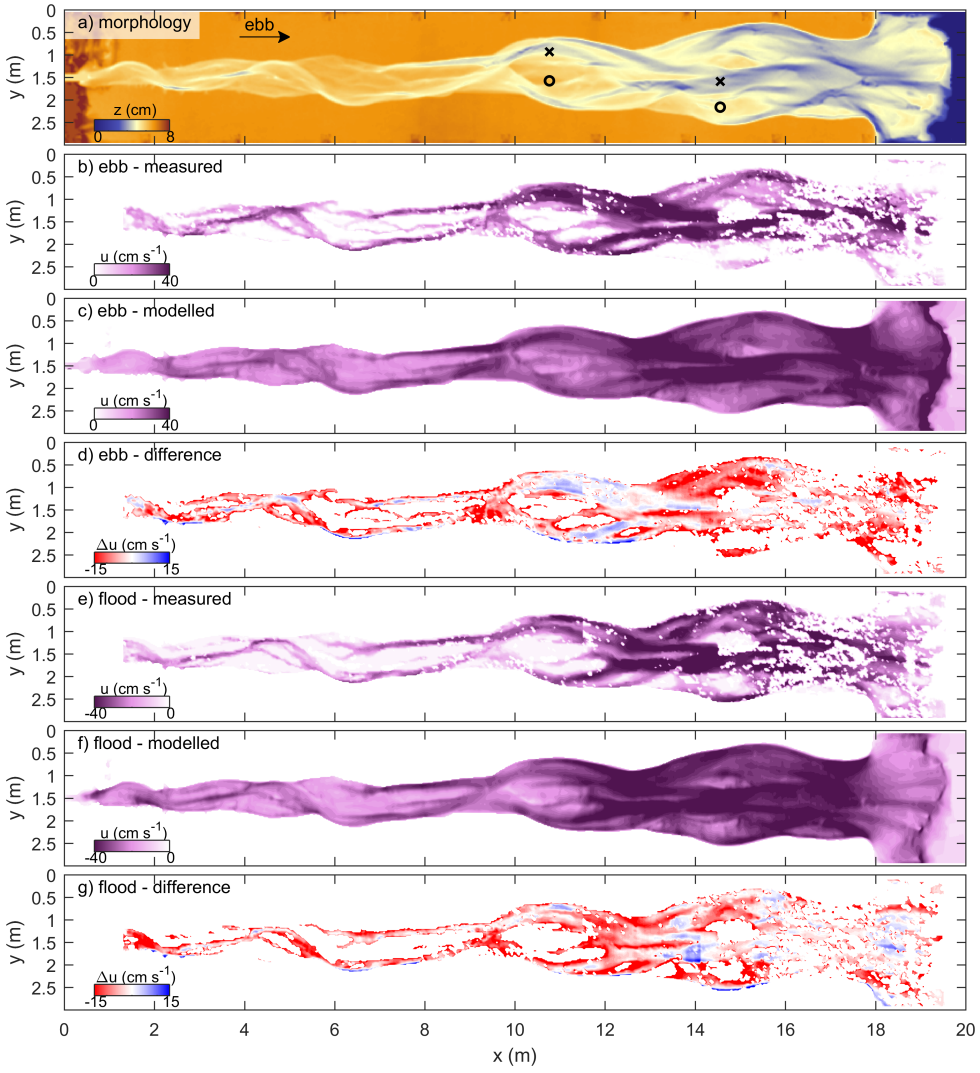

Figure 3.6 (b–d) Maximum ebb and (e–g) flood flow velocity with (a) the estuary morphology for reference. Maps of difference are determined by subtraction of modelled from measured surface flow velocity. 'X' and 'O' in (a) are the locations at which tidal stage diagrams were made in Fig. 3.8 of channels and shoals, respectively.

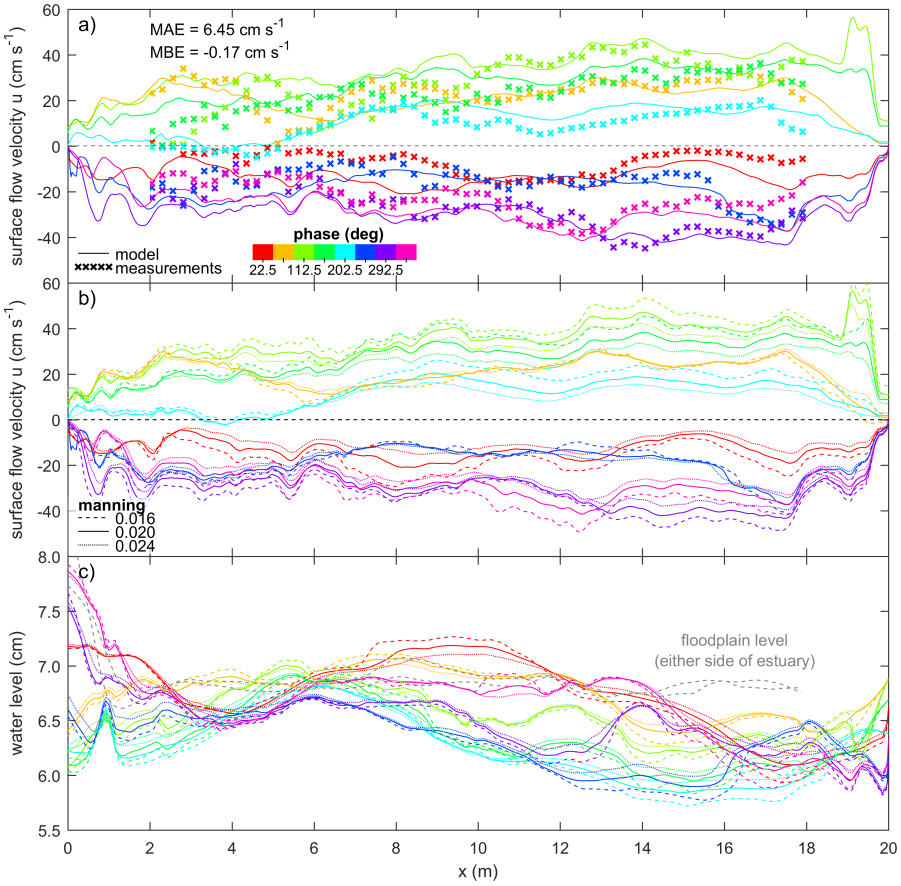

Figure 3.7 (a) Surface flow velocity along the estuary, given as the 90^{th} percentile of the streamwise flow velocity component. (b) The effect of Manning on the surface flow velocity and (c) the phase-dependent median water level of each cross-section along the estuary. Colours indicate the phase in the tidal cycle.

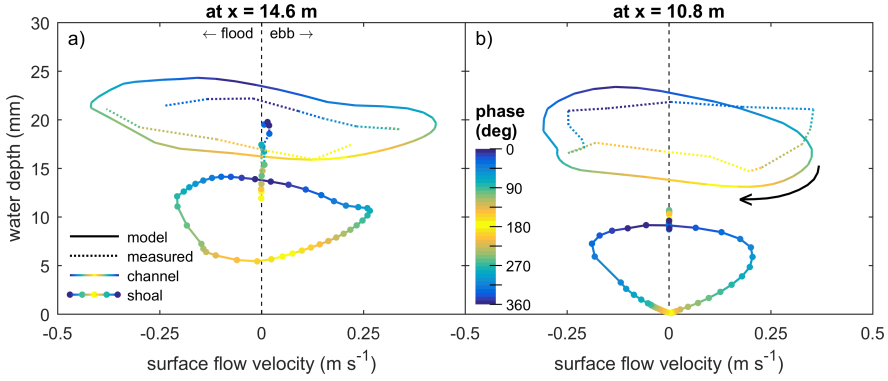

Figure 3.8 Tidal stage diagrams showing water depth versus surface flow velocity for a channel and shoal at (a) $x = 14.6$ m and (b) $x = 10.8$ m in Fig. 3.6a. Water depth and surface flow velocity were averaged for a 5x5 cell window. Colours indicate the phase in the tidal cycle.

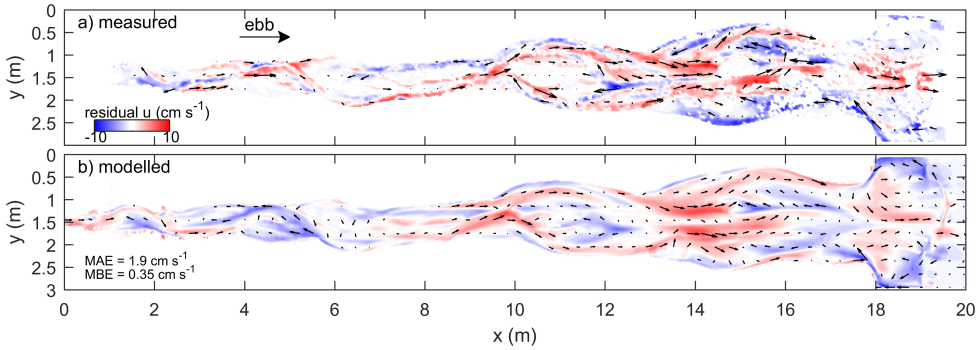

Figure 3.9 Residual surface flow velocity maps show similar spatial flow patterns and magnitudes between (a) the measured data and (b) model output, apart from the upstream 6 m. This upstream region was underseeded with PIV particles, which resulted in wrongly measured flow velocities. Therefore, computation of the mean absolute/bias errors was done for $x > 6$ m.

overall modelled residual flow is slightly less flood-dominated (MBE is positive) than the PIV-based residual flow. For example, the flood-dominance of the channel at $x = 14$ m is weaker but still recognisable in the modelled data (Fig. 3.9). Further landward, a discrepancy arises in that the model suggests that the channel and bar between $x = 4$ m and 6 m are flood-dominant, while the measurements show they are mainly ebb-dominant. Inspection of the raw PIV data shows that here the flood flow is underseeded with particles, suggesting that the measured data is inaccurate and leaving the model untested in this zone.

3.5 Discussion

The numerical hydrodynamic model Nays2D reproduces water depths and flow velocities for physical scale experiments with both unidirectional and reversing shallow flow (Figs. 3.4, 3.6, 3.9). The mean absolute error of modelled water depth is within 10 % maximum water depth (Fig. 3.5) and of modelled flow velocity is within 15 % maximum flow velocity (Fig. 3.7). In other words, the errors of modelled flow fall within the range of errors that was expected in the measured data. The model results are valuable because the spatio-temporal coverage and quality of experimental data are at present more limited in typical laboratory conditions for landscape experiments. Therefore, this experimental data-model integration opens up many opportunities for the analyses of hydrodynamics in experiments in a time-efficient, cost-effective and labour-inexpensive manner. Thus far, this integration has only been used to the authors' knowledge for one set of tidal scale experiments with erodible boundaries by Tesser et al. (2007) and Stefanon et al., (2010; 2012), who numerically computed flow velocity fields by solving the Poisson boundary value problem (Marani et al., 2003). In addition to their findings, the results of this study demonstrate that an experimental data-model integration extends to complex bathymetries with unsteady, nonuniform flows.

A major advantage of numerically modelled flow fields is the full coverage and the independence from imperfect lighting, particle seeding and empirical relations through which flow properties are inferred (e.g. Van Dijk et al., 2013a; Braat et al., 2019a). Additionally, the model adheres to continuity of flow, which is not the case for experimental data with errors, bias and uncertainty. Consequently, the modelled flow permits a much more accurate calculation of important flow parameters for system scaling and analysis.

One such an example is the computation of tidal prism. Tidal prism based on flow velocity and depth measurements is strongly underestimated by measurement error and missing values in shallow

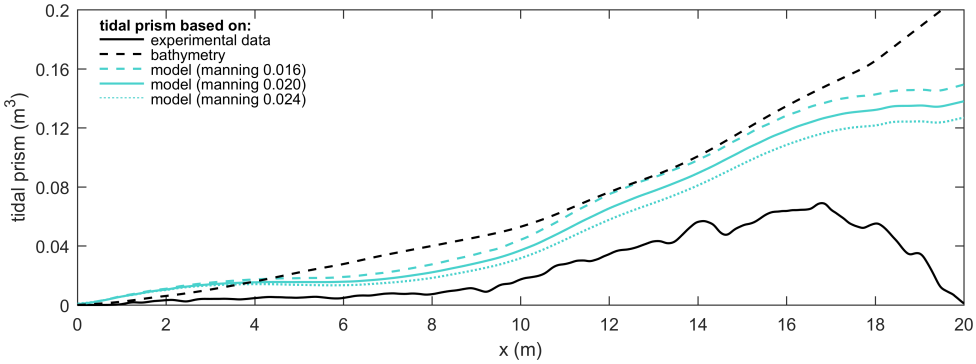

Figure 3.10 Tidal prism along the estuary based on experimental data, bathymetry and the model scenarios. Measured flow velocities were converted to depth-averaged velocities using Eq. (3.7). Tidal prism based on bathymetry (black dashed line) was computed as the cumulative volume of water along the estuary between high and low water levels imposed at the weir (i.e. with an amplitude of 4 mm) (cf. Braat et al., 2019a); this calculation ignores effects of friction and river inflow.

areas (Fig. 3.10). Alternatively, tidal prism could be computed using bathymetry and the cumulative volume of water between high and low water levels along the estuary, but this method ignores roughness effects and will result in an overestimation of tidal prism if the tide is a propagating wave, as opposed to a standing wave. The drawbacks of these computations are overcome by the model, which shows a steeper decrease of tidal prism in the landward direction due to roughness and a levelling-off towards the landward boundary, indicative of river inflow dominance (Fig. 3.10). Other important system-scale characteristics that can be derived from the modelled flow are e.g. tidal excursion length (e.g. Schramkowski et al., 2002) and the flow partitioning between multiple channels and bars (e.g. Bolla Pittaluga et al., 2003; Kleinhans et al., 2008). However, this does not mean that data need no longer be collected because the model may require calibration of e.g. hydraulic roughness.

The hydraulic roughness is commonly used to calibrate water levels and flow velocities in hydrodynamic models (e.g. Berends et al., 2019). Although a spatially constant Manning roughness of 0.02 s $m^{1/3}$ already produced satisfying hydrodynamics, the results could be improved by calibrating a spatially varying roughness; this is especially the case for experiments with wide sediment distributions or fines (e.g. Van Dijk et al., 2013a; Braat et al., 2019a). Such roughness maps could be generated from grain size maps based on overhead imagery, provided measurement errors due to lighting and sediment colour are greatly reduced. Using a spatially varying roughness may improve the partitioning of water at bifurcations over the downstream channels (for example the secondary channel in the braided river around $x = 6$ m [Fig. 3.4]). However, the partitioning of water over channels and bars also depends on which of the three classic assumptions of friction is applied, namely a constant Manning, Chezy or White-Colebrook roughness coefficient (Fig. 3.11). For example, using a constant Chezy instead of Manning would result in slightly slower flow in channels and faster flow over bars. In contrast, a constant White-Colebrook would produce faster flow in channels and slower flow over bars. In turn, these differences in flow velocity would have a considerable effect on the computed sediment mobility.

Sediment mobility is perhaps the most important measure of flow for morphodynamics (Kleinhans and Van den Berg, 2011) (Fig. 3.12), but it is difficult to acquire from experiments with shallow flow. Firstly, the nondimensional mobility number allows for the comparison to natural systems (Kleinhans, 2010). Secondly, it provides vital insight in sediment transport fields and morphological activity that is especially valuable for studying multi-channel systems and channel-bar margin interactions (De Vet et al., 2017; Van Dijk et al., 2018; Baar et al., 2019). For example, these data may be used to predict

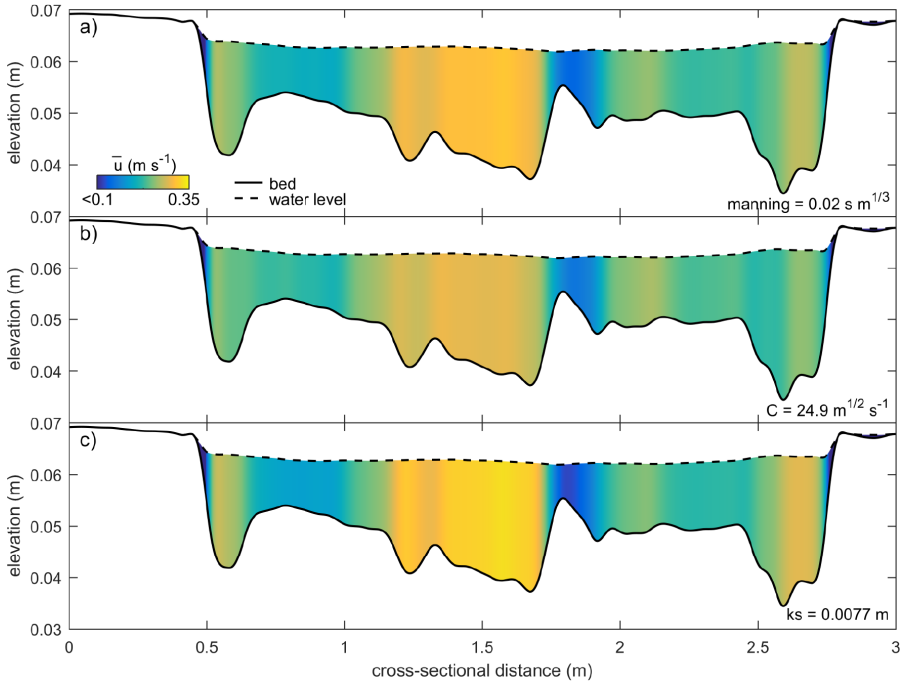

Figure 3.11 Effect of different hydraulic roughness predictors on the distribution of depth-averaged flow velocity $\bar{u}$ for (a) a constant Manning, (b) a constant Chezy C and (c) a constant grain roughness k_s (White-Colebrook). The cross-section is from the experimental estuary by Leuven et al. (2018b) at $x = 15.3$ m at maximum tilt in the ebb direction. Cross-sectional flow velocities were iterated for C and k_s assuming the same total discharge and water levels as modelled in this study with Manning.

future locations of erosion and deposition (Fig. 3.12a-d). Also, they may be indicative of grain size or may be coupled to grain size estimations from imagery (e.g. Gardner and Ashmore, 2011).

The model is potentially applicable in conditions where data collection is hampered, such as in vegetated experiments (e.g. Braudrick et al., 2009; Tal and Paola, 2007; 2010). Application on vegetation surfaces requires the vegetation to be filtered out of the DEMs and vegetation roughness effects to be added to the model (Baptist et al., 2007; Chapter 2). Consequently, experimental data could be enriched with water depth maps and particularly flow fields that are often absent (Table 3.1).

Water depth and sediment mobility maps enable unbiased classification of a river or estuary planform into inundation zones (Fig. 3.12g). For instance, this enables the study of the development of intertidal areas in estuaries, which are of key importance to a high biodiversity (e.g. Ysebaert et al., 2003). Moreover, such inundation classifications may effectively culminate in ecotopic maps that indicate at what locations which faunal and floral species would be likely to thrive. Finally, the model opens up a faster way of testing the design of a flume experiment. Whilst laboratory tests need to be done in series, the model allows for testing initial and boundary conditions in parallel. Based on the resulting flow fields and bed shear stress maps at the start of the modelled flume setups (sediment transport is not included), preferred flume settings may be readily derived and applied to the physical flume. Thus, probably fewer physical tests are required, which greatly reduces the total laboratory time. This is especially the case for experiments with different sediment mixtures and with vegetation, for which the flume needs to be emptied and cleaned after every run.

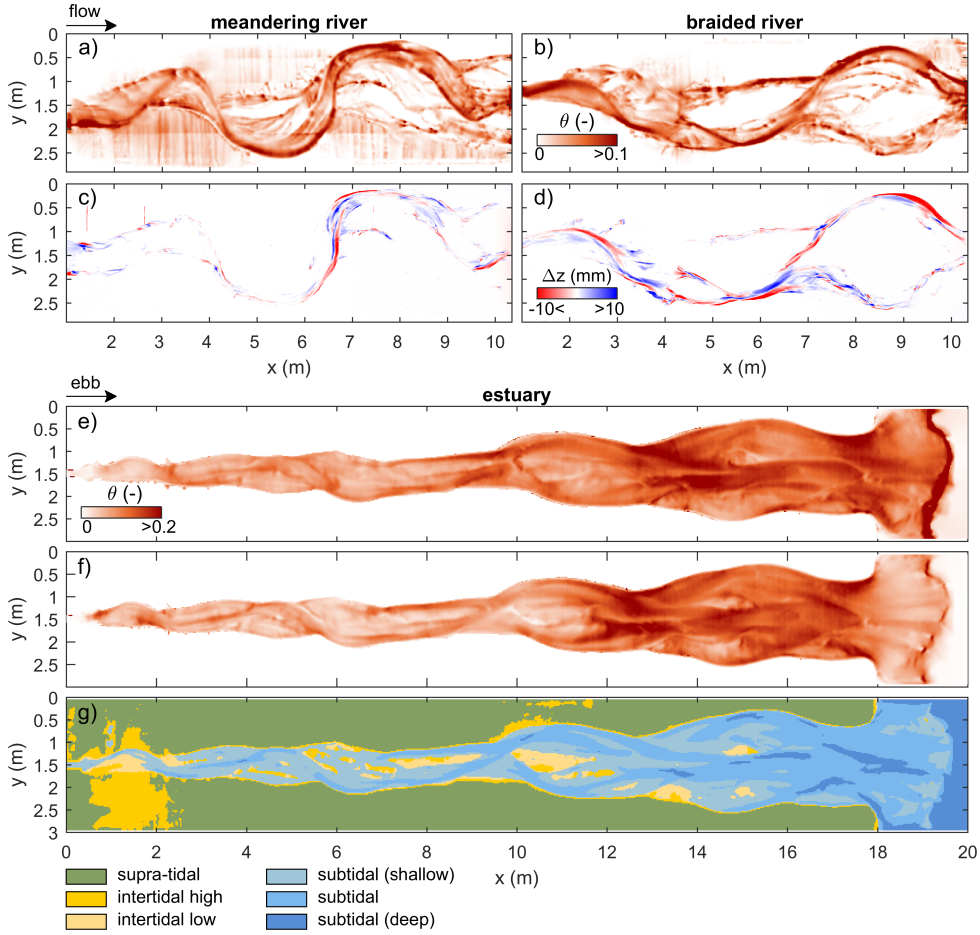

Figure 3.12 Complementary model data as maps of nondimensional bed shear stress (i.e. Shields numbers) and tidal zonation. (a) Shields numbers for the meandering and (b) braided rivers with (c–d) the corresponding elevation-difference DEMs with the next time step. (e) Maximum Shields numbers for the estuary in the ebb and (f) flood direction. (g) Classification of the estuary DEM in inundation classes based on modelled tidal flow. A similar classification is also applicable to unidirectional flow in rivers, as illustrated in Suppl. Suppl. Fig. 3.14a,f.

3.6 Conclusion

Hydrodynamic modelling with Nays2D simulates unsteady, nonuniform flows for physical scale experiments with unidirectional and reversing shallow flow. The modelling requires a DEM and the corresponding boundary conditions and produces continuous spatio-temporal data on water depth and flow velocity, whilst ignoring substrate colour differences, lighting overexposure and under or oversampling of floating PIV modules that usually decrease the quality of experimental data. Additionally, Nays2D computes sediment mobility, which is normally difficult to measure in shallow flows but is an important parameter for morphological activity and the comparison to natural systems.

The implication of this experimental data-model integration is that fewer measurements and less post-processing are required and are mainly meant for the calibration of model parameters such as

the hydraulic roughness. In turn, this integration opens up many opportunities for the analyses of hydro and morphodynamics in experiments. For example, the enhanced data enable the objective classification of the experiment planform into inundation classes which are potentially indicative of different ecotopes. Alternatively, the model allows for rigorous testing of different boundary conditions (e.g. discharge variability, sea level rise, vegetation) which could strongly reduce the time in the laboratory.

Open Research

Additional materials are available via https://doi.org/10.24416/UU01-CZV56M. The additional materials include the DEMs used in this study, the raw water depth and flow velocity data, the novel Nays2DMetronome solver specifically for tilting flumes, and a user manual for iRIC (i.e. the user interface for Nays2D). These also include four figures and a movie. Modelled data in this study were derived from numerical modelling that can be repeated with the open-source Nays2D model and the GUI iRIC, both of which are available at https://i-ric.org/en/download (Shimizu et al., 2013).

Acknowledgements

This research is supported by the European Research Council through the ERC Consolidator grant 647570 to M.G. Kleinhans and the Dutch Technology Foundation STW grant Vici 016.140.316/13710 to M.G. Kleinhans, which is part of the Netherlands Organisation for Scientific Research. This work is part of the Ph.D. research of S.A.H. Weisscher. We acknowledge L. Lacaze and M. Tal, whose reviews helped to improve the manuscript.

Supplementary material

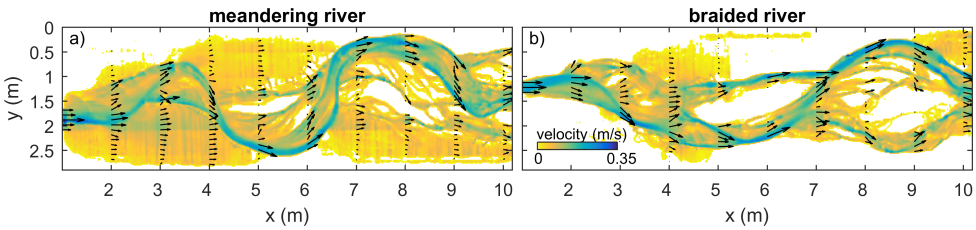

Figure 3.13 Modelled flow velocity for (a) the meandering and (b) the braided rivers by Van Dijk et al. (2013a).

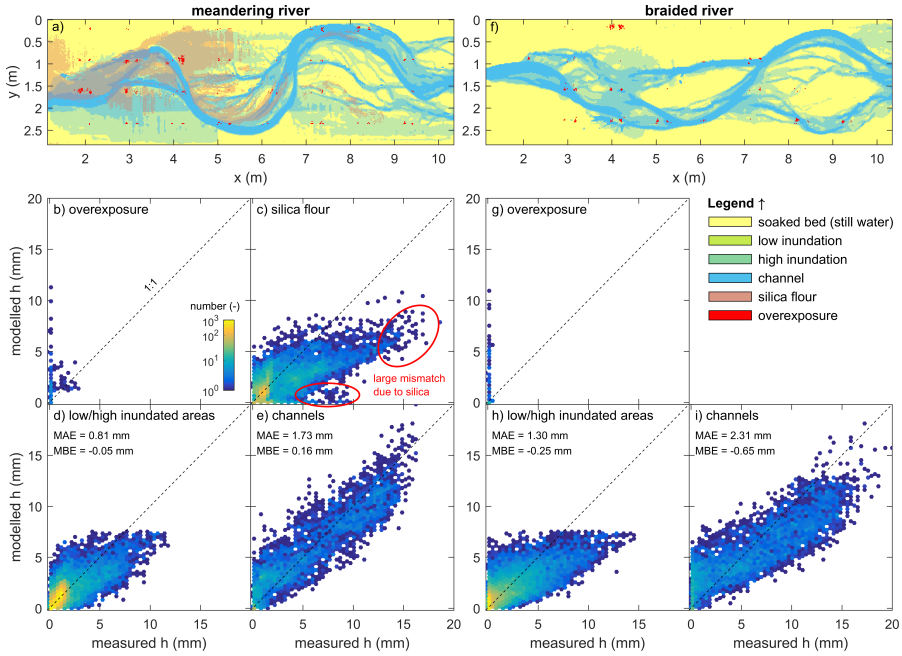

Figure 3.14 Inundation maps for the (a) meandering and (f) braided rivers by Van Dijk et al. (2013a), with modelled versus measured water depths divided into (b/g) cases of overexposure, (c) silica flour, (d/h) low/high inundated areas (i.e., submerged floodplain and bars, swale channels) and (e/i) channels. Large mismatches are in the measured data due to overhead light overexposure and white silica flour that distorts the extraction of measured water depth. Scatter density plots (d), (e), (h) and (i) are identical to those in Fig. 3.5.

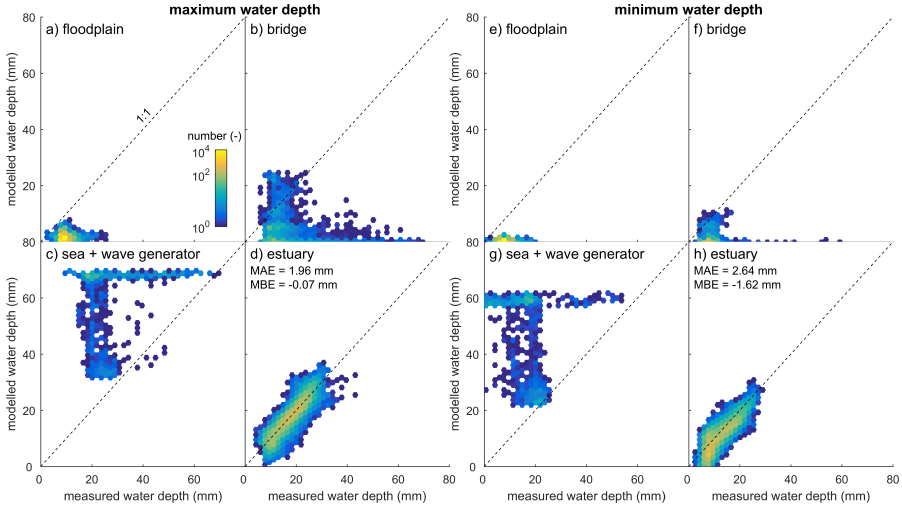

Figure 3.15 Same as Fig. 3.5e,f but also including cells with incorrect measured water depth corresponding to artificial obstructions (i.e. the bridge and wave generator) and the sea with artificial grass. The green grass distorts the water colour saturation with respect to the sand for which the colour conversion was calibrated. Consequently, measured water depths are underestimated for the sea part in the experiment.

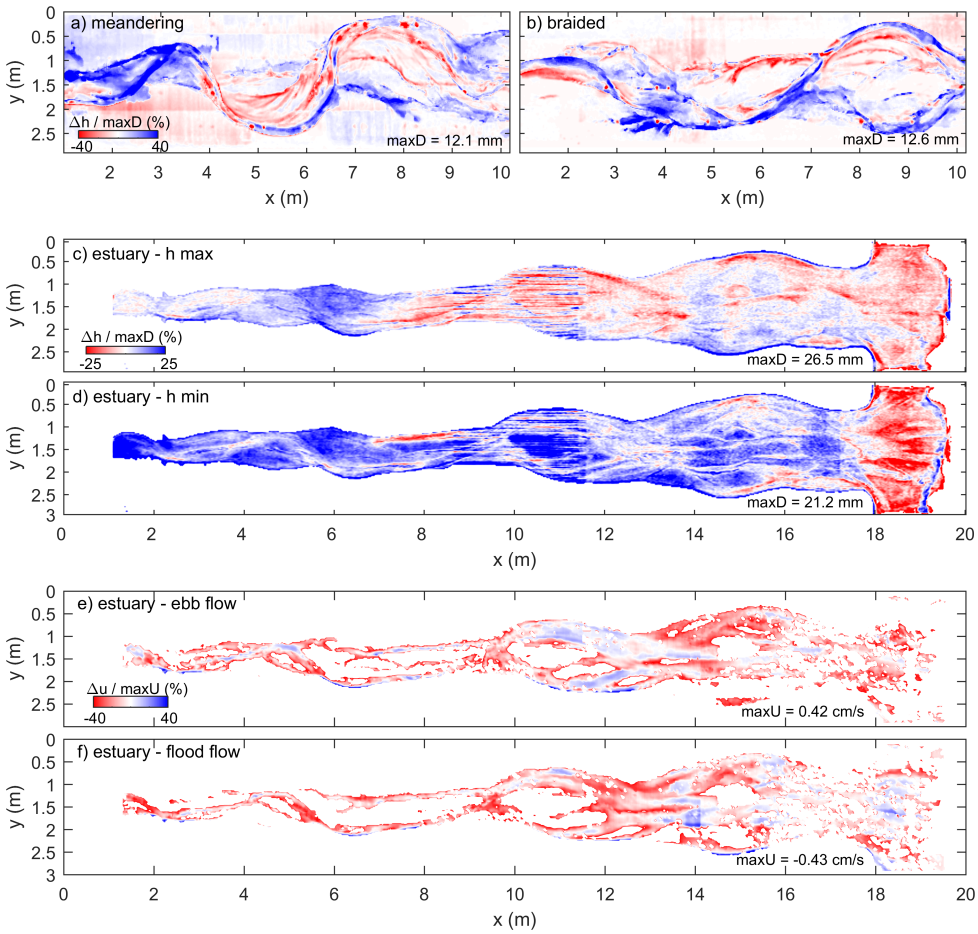

Figure 3.16 Same as difference maps of water depth in Fig. 3.4c,f and of flow velocity in Fig. 3.6d,g, but shown relative to maximum depth and maximum flow velocity. Maximum depth and flow velocity are determined as the 98^{th} percentile of the measured data.


4

Chapter 4 | Building and raising land: mud and vegetation effects in infilling estuaries

Abstract

Many Holocene estuaries were infilled to form convergent, single-channel systems, while others remained partially or wholly unfilled. This difference in the degree of infilling depends partly on the balance between fluvial and coastal sediment input and the hydrodynamics that can export sediment. However, it remains unclear to what degree this balance is tipped by mud supply and eco-engineering vegetation, and by what planform patterns the infilling proceeds. This study aims to explore experimentally how mud and vegetation change the degree and process of infilling, elevate and merge bars above intertidal levels and affect the planform of estuaries. To this end, three experiments were conducted in the Metronome, a flume that tilts periodically to create tidal currents, wherein forced tidal asymmetry resulted in net importing estuaries. In the second and third experiments, mud was supplied and in the third experiment seedlings were released of three vegetation species with eco-engineering traits at a laboratory scale. With only sand, the estuary fills sufficiently to form a multi-channel pattern with intertidal bars. Both mud and vegetation settle on intertidal bars and on the fluvial bay-head delta, thereby contributing to bar stabilisation and further estuary infilling, pointing at effective strategies to keep up with future sea-level rise. This reduces channel mobility and effectively narrows the summed subtidal channel width towards an ideally converging funnel shape. This seems especially effective where vegetation stabilises the mud. The experiments suggest that a range of steady states exists between the end-members of an unfilled and a completely infilled, ideal estuary.

Published as: Weisscher, S. A. H., Van den Hoven, K., Pierik, H.-J. & Kleinhans, M. G. (2022). Building and raising land: mud and vegetation effects in infilling estuaries. *Journal of Geophysical Research: Earth Surface, 127, 24 pp.*, DOI: 10.1029/2021JF006298

4.1 Introduction

As sea-level rise decelerated during the Middle Holocene, many estuaries started to infill and formed new land (e.g. Roy et al., 1980; Nichol, 1991; Van der Spek, 1995; Umitsu et al., 2001; Vos, 2015; Clement et al., 2017; De Haas et al., 2018; 2019). Yet, other estuaries were only partly infilled or remained unfilled, in part due to a lack of sediment (Fig. 4.1) (e.g. Roy et al., 1980; Allen, 2000; Zecchin et al., 2009). These observations led to the recognition of two contrasting kinds of steady-state estuaries. The first steady state is an unfilled estuary with a lagoonal basin that is largely below the threshold of motion (Roy et al., 1980). Here, the building of intertidal flats is inhibited by weak tidal currents, limited sediment availability and local, wind-generated waves (e.g. Dalrymple et al., 1992). Unfilled estuaries generally form in deep (relative to tidal amplitude), drowned valleys with negligible fluvial and marine sediment input (e.g. the Wagonga and Wapengo Lagoons, AUS; Fig. 4.1a,b) (Roy et al., 1980). The second steady state is a completely filled estuary that ideally has a converging planform (e.g. the Manawatu River, NZ; Fig. 4.1g) (Roy et al., 1980; Nichol, 1991; Dalrymple et al., 1992). In an ideal estuary, landward convergence balances the decay of tidal energy by friction, resulting in a constant along-channel tidal amplitude, channel depth and flow velocity (Savenije, 2015). Additionally, such an estuary has a balanced ebb- and flood-directed sediment transport (Dronkers, 2017). A completely filled estuary with a convergent planform is considered a steady state (Savenije, 2015; Dronkers, 2017): a partly filled system develops flood-dominant transport which promotes filling if sediment is supplied from the upstream river or the sea, whereas an over-filled system develops ebb-dominance and sediment export that may lead to delta formation (Dalrymple et al., 1994; Savenije, 2015; Dronkers, 2017).

Terminology of system dynamics

Here, a steady state equilibrium is considered a geomorphic open system that self-maintains a constant form with continuous throughput of material and energy despite all but the largest perturbations (Thorn and Welford, 1994; Huggett, 2016). In geomorphological nomenclature, this state is commonly also referred to as 'dynamic equilibrium' (Zhou et al., 2017). However, general systems terminology prefers the term 'steady state' for complex, open, entropy-driven systems to 'dynamic equilibrium', because the latter is considered more appropriate for closed systems (Thorn and Welford, 1994; Huggett, 2016). Here, perturbations on the boundary conditions often merely move an estuary marginally away from its current steady state, to which it is 'attracted'. Examples include both cyclic/seasonal perturbations such as the nodal cycle (Wang and Townend, 2012), and events such as river floods and storms (Townend et al., 2007; Swales et al., 2019).

Currently, the apparent dichotomy of the unfilled estuary and the ideal estuary raises the question whether estuaries have only two alternative steady states (or two 'attractors'). On the geological timescale of sea-level fluctuations, estuaries are considered ephemeral systems that will inevitably infill over time towards the presumed steady state of a single convergent channel, regardless of the transient patterns of lagoons, multi-channel networks, mudflats and salt marshes (e.g. Lanzoni and Seminara, 2002; Dalrymple and Choi, 2007; De Haas et al., 2018). Then, the duration of infill depends on the amount of fluvial and coastal sediment input, which are functions of offshore and hinterland conditions. This reasoning, which assumes only two alternative steady states, would indicate that many present-day systems (as in Fig. 4.1c-f) are not (yet) in a steady state, because they currently have multi-channel planforms and intermediate degrees of infilling. On the centennial timescale, however, this reasoning seems contrary to observational evidence for some estuaries that showed no apparent development towards a convergent channel over the past centuries, despite the availability of sediment. For instance, the tidal channels in the Arcachon Bay Estuary (FR) (Fig. 4.1c) have remained static and equal in number for centuries despite the abundance of marine sediment

Figure 4.1 Estuaries ranging from unfilled to infilled on different spatial scales. (a) Wagonga Lagoon (AUS) is an unfilled estuary (ria coast) with a large flood-tidal delta and two small bay-head deltas (on the left and bottom left). (b) Wapengo Lagoon (AUS) is a largely unfilled estuary (ria coast) with tidal flats adjacent to the flood-tidal delta (Nichol, 1991). (c) Arcachon Bay Estuary (FR) is a partly infilled estuary dominated by mudflats and has a small bay-head delta. (d) Rangitikei River (NZ) and (g) Manawatu River (NZ) are both infilled estuaries (Clement et al., 2017). (e) Tillamook Bay Estuary (USA) is a partly infilled estuary with bars/flats and has a small bay-head delta. (f) Carromore Lacken (IR) is a largely infilled estuary bounded by salt marshes and peatlands. In all images, river inflow is from the left and the sea is on the right.

(Féniès and Faugères, 1998; Allard et al., 2009). Another example is the Ems-Dollard Estuary (NL/D), which has a high suspended sediment concentration but shows no clear signs of filling of tidal basins bordering the channel since the 1900s (e.g. Van Maren et al., 2016). Some classifications of estuaries and embayments also recognise various states between entirely unfilled and completely filled (Allen, 2000; De Haas et al., 2018), but these concepts raise the question whether these are attractor states or merely one of many possible transient states.

Certain numerical and physical models suggest that partly filled estuaries can be in steady state. Recent numerical modelling (Braat et al., 2017) and scaled landscape experiments (Leuven et al., 2018b; Braat et al., 2019a) showed the development of a steady state in sand-bar dominated estuaries with multiple channels. These estuaries exhibited alternating wider sections with large bars and narrower sections with deep confluences, while the summed subtidal channel width developed towards a converging funnel shape (Leuven et al., 2018b). This was also observed in natural, multi-channel, ingressive estuaries like the Western Scheldt (NL) (Leuven et al., 2018b), as well as in infilling palaeo-estuaries like the Old Rhine Estuary (NL) (Pierik et al., 2017; De Haas et al., 2018; 2019) and the Shoalhaven River (AUS) (Roy et al., 1980). Conceptually, the approach of isolating the subtidal channels reduces an estuary to a one-dimensional system (Speer and Aubrey, 1985; Friedrichs and Aubrey, 1988), where the subtidal channels convey the flow momentum and the intertidal bars are conceptualized as having no other effect than being regions for water storage, just like shore-connected bars and tidal flats (Leuven et al., 2018d). Altogether, these examples in numerical modelling, experiments and field observations point at the possibility of a continuum of steady states with different degrees of infilling.

Floodplain-forming mechanisms

Mud and vegetation influence the local morphodynamics of estuaries through filling accommodation space and confining flow. More specifically, mud mainly settles as cohesive top layers on high-intertidal bars and flanking flats, which confine and funnel ingressive estuaries and reduce the migration rate of channels and bars (Braat et al., 2017; 2019a). As for salt marsh vegetation, this eco-engineering agent establishes on high-intertidal and supratidal areas, where the added hydraulic drag confines flow, stimulates sediment deposition and stabilises the bed (e.g. Temmerman et al., 2007; Lokhorst et al., 2018; Brückner et al., 2019). These mechanisms through which mud and vegetation fill and confine estuaries are analogous to the floodplain-forming mechanisms in rivers, where channel confinement causes a transition from braiding to meandering (e.g. Braudrick et al., 2009; Tal and Paola, 2010; Van Dijk et al., 2013a; Chapter 2). Accordingly, these mechanisms contribute to the building and raising of new land and are deemed necessary to reach the classic, ideally converging estuary (Savenije, 2015), whilst this converging planform is often imposed as non-erodible banks in numerical studies (e.g. Lanzoni and Seminara, 2002; Savenije, 2015; Dronkers, 2017; Olabarrieta et al., 2018).

The filling of accommodation space (in geological terms) and flood storage space (in tidal terms) may have a second effect: it reduces the tidal prism and may increase flood-dominance (e.g. O'Brien, 1969; Friedrichs, 1995). Previous studies hypothesised that quickly extending mudflats, salt marshes and peatlands may reduce tidal prism in a positive feedback loop (Beets and Van der Spek, 2000; De Haas et al., 2018). However, this hypothesis has not yet been clearly corroborated by the very few numerical studies and absent scale experiments that capture this long-term morphodynamic process. Conversely, continued filling and in particular the expansion of intertidal flats may also induce a switch from flood- to ebb-dominance (Speer and Aubrey, 1985; Dronkers, 1986; Fortunato and Oliveira, 2005), which hampers further filling and changes the estuary from a sink to a source, as is expected, for example, for the Dee Estuary (UK) (Moore et al., 2009). Accordingly, it remains unclear how mud and vegetation contribute to the two mechanisms of filling and confining wide lagoonal estuaries in drowned valleys on coastal plains and to what extent they modify the estuary planform during filling. For example,

in North-Western Europe, estuaries formed in the Middle Holocene on the drowned coastal plains by sedimentation and effects of vegetation, whilst sea-level rise and human-induced subsidence caused ingressions in the Late Holocene (Van der Spek, 1997; Gregoire et al., 2017; Pierik et al., 2017; De Haas et al., 2018).

In order to understand the morphological development of infilling estuaries, also in prospect of future sea-level rise, there is an urgent need to determine whether the degree of filling and the resulting planform of estuaries develop towards one possible steady state or whether there can be a range of possible steady states. Furthermore, it is unclear whether and how mud and vegetation enhance the filling of estuaries and whether they are necessary to reach a converging estuary planform. Here, this study experimentally investigates the filling processes of alluvial estuaries with and without mud and vegetation and places the results in the context of recent studies on multi-channel estuaries.

4.2 Methods

This study reports on three scaled landscape experiments of entire estuaries. These experiments comprise a control with only sand, a second experiment with sand and mud, and a third with sand, mud and live vegetation but otherwise the same conditions. The present experiments of infilling estuaries differ from past experiments in three ways, detailed below. Firstly, the initial bathymetry of the entire estuary is submerged during the tidal cycle except for the barriers, the banks and the uppermost area. This is different from Leuven et al. (2018b) and Braat et al. (2019a), who started with narrow converging estuaries that expanded over time by exporting sediment, which represented Late Holocene ingressive estuaries (De Haas et al., 2018). The present experimental estuaries were based on pilot experiments in a smaller flume (Suppl. 4.2) and designed to have modest infilling over time by sand import so as to determine the added effects of mud and vegetation. To accomplish sand import, an overtide was added to the principal tide to create tidal asymmetry conducive to flood-dominance (Kleinhans et al., 2017b), thereby simulating conditions found, for example, in the North Sea (Dronkers, 1986; De Haas et al., 2018). Secondly, mud was added to two experiments on both the fluvial and tidal boundaries, following Braat et al. (2019a). Thirdly, seeds of three vegetation species were added to the flow in one experiment to act as eco-engineering species (Lokhorst et al., 2019).

4.2.1 Experimental setup and procedure

Experiments were conducted in the tilting flume the Metronome. The 20 m long and 3 m wide flume tilts over the short central axis to generate tidal currents (Kleinhans et al., 2017b). While a periodic sea water level fluctuation to create tides is at first sight closer to the situation in nature, as in previous studies (e.g. Reynolds, 1889; Stefanon et al., 2010), this classic method leads to a number of scale problems, namely: very low sediment mobility, ebb-dominance and fast disappearing morphodynamics in the landward direction (Kleinhans et al., 2014b). The novel tilting method solves these issues by tilting, which generates periodically alternating flows and mobile sediment by a slope in the landward direction during flood and a slope in the seaward direction during ebb (Kleinhans et al., 2014b; 2015b; 2017b). Past experiments for the establishment of ingressive estuaries led, amongst others, to sand-dominated estuaries with dynamic tidal bars and channels (Leuven et al., 2018b) and mudflats (Braat et al., 2019a). Comparison between these experiments and natural estuaries showed that relative bar dimensions and the spatial mudflat distribution were largely similar.

The initial bathymetry was an idealised drowned river valley with a barrier coast (Fig. 4.2). The initial bed consisted of sand with a median grain size $d_{50} = 0.55$ mm, a $d_{10} = 0.32$ mm and a $d_{90} = 1.2$ mm to prevent hydraulic smooth conditions and unrealistically large scours (Kleinhans et al., 2017a). The sand bed was 17 m long, 3 m wide and had a bed thickness of 11 cm. Over the full length of the sand

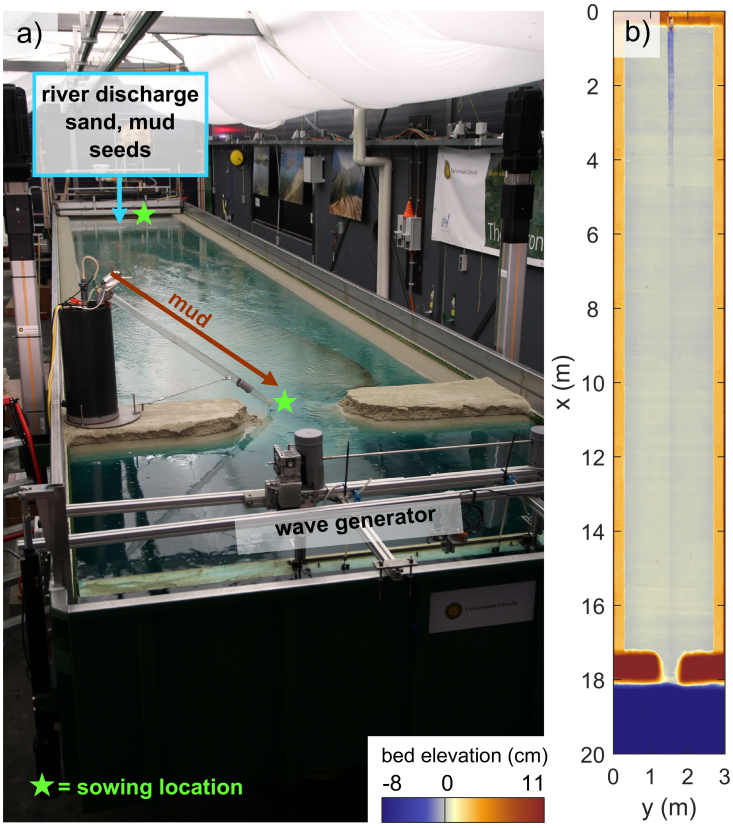

Figure 4.2 (a) The setup of the flume the Metronome. Crushed walnut was used as mud simulant and was released in pulses, one per tidal cycle, at the river and via a tube into the tidal inlet (brown arrow). Vegetation seeds were sowed via the river inflow and at the tidal inlet, after which they were distributed by tidal flow. (b) The initial bathymetry of the experiments was a rectangular estuary with a subtidal bed and high barrier islands. An initial river channel 0.16 cm wide and 1 cm deep was carved in the middle of the flat-floored valley, decreasing in depth in the seaward direction.

bed, a flat-floored valley was carved of 2.4 m wide and 3 cm deep with a central, straight river channel of 16 cm wide and 1 cm deep in the upstream 5 m of the basin that gradually shallowed to 0 cm in the downstream direction. At the tidal inlet, two sandy barrier 'islands' were constructed, each 1.15 m long, 0.6 m wide and 19 cm thick with 45° slopes. These excessively large barrier islands acted as a source of marine sandy sediment, for it was infeasible to mimic alongshore drift to provide sufficient marine sediment input (Van Rijn, 1997). The entire bed was set at a typical fluvial valley slope in landscape experiments of 0.001 m/m (Kleinhans et al., 2014a) by an offset tilt of the flume.

Flow conditions in the experiment were set to create a flood-dominated estuary. In many estuaries, the combination of river inflow and a semidiurnal M2 tide leads to sediment export, while the addition of an M4 overtide causes net import of sediment (Dronkers, 1986). These boundary conditions for water flow were reproduced in the experiments by imposing tidal asymmetry on the tilting (Kleinhans et al., 2017b). The principal tide was generated by tilting with a period of 40 s and a maximum slope of 0.006 m/m. The overtide had a period of 20 s and a maximum slope of 0.0012 m/m (i.e., 20% of the principal tidal constituent) and had a phase difference of 90°. With the addition of the offset slope of 0.001 m/m, the tilting had a maximum slope of 0.0062 m/m in landward direction during flood

and 0.0058 mm/m in seaward direction during ebb. There was free inflow and outflow of water at the seaward boundary, while a vertically moving weir ensured a constant water level at the shoreline of about 10 cm above the flume floor during tilting with a slight drop to 9 cm just after peak flood. The weir moved in the opposite phase of the tilt to keep the sea water surface horizontal while the flume bed tilted, in order to avoid emptying and filling of a tilting sea which would have caused large, unwanted water fluctuations at the shoreline (Kleinhans et al., 2017b). Waves were generated by a horizontal paddle at the seaward boundary with a frequency of 2 Hz and an amplitude of about 0.3 cm during the flood phase. These waves contributed to the mobilisation of sediment from the barrier islands and enhanced the landward transport on the ebb-tidal delta (for scaling, see online supplement in Leuven et al., 2018b). At the upstream boundary, a river discharge of 900 L/h was added to the estuary during the ebb phase only.

Sand and mud were added to the river, both at a rate of 0.4 L/h. The sand had the same grain size distribution as that of the initial bed, and the mud-like material comprised three equal parts of the following grain size classes: 0.45-0.8 mm, 0.8-1.3 mm and 1.3-1.7 mm. Crushed walnut shell with a density of 1350 kg/m^3 was used as mud simulant as in previous studies (Baumgardner, 2016; Braat et al., 2019a). This lightweight material can be transported in suspension and is slightly cohesive after deposition. A second nutshell feeder supplied crushed walnut shells in the tidal inlet at the start of every flood phase at a rate of 0.4 L/h to simulate the input of fines from the sea. As a result, a large range of sediment mobility was accomplished up to $\theta = 0.55$ during peak flood, where the Shields number $\theta = \tau/((\rho_s - \rho)gd_{50})$ with τ is bed shear stress, ρ_s and ρ are density of sand and water and g is the gravitational constant.

Vegetation protocol

Three species were selected with contrasting sensitivity to hydromorphological stresses and with contrasting eco-engineering effects on flow and sediment transport in laboratory landscape experiments. Based on Lokhorst et al. (2019), who tested 19 vegetation species for growth rate, hydraulic drag and rooting strength in cut-banks in Metronome-like conditions, the following three species were chosen with different eco-engineering traits: *Medicago sativa*, *Lotus pedunculatus* and *Veronica beccabunga*. These species sprout quickly, remain fairly small in the absence of nutrients, and are sensitive to the miniaturised hydroperiod in the experiments. *Medicago*, commonly known as alfalfa, has seeds that are transported as bed load, typically establishes in the vicinity of channels, and reduces bank erosion by dense, branching rooting. Therefore, alfalfa resembles riparian vegetation on (tidal) levees (Lokhorst et al., 2019). *Lotus* and *Veronica* represent reed-like and grass-like marsh vegetation in North-Western Europe, but their simple eco-engineering traits are also similar to those in estuaries with mangroves (Lokhorst et al., 2019). Since the tiny *Veronica* seeds are transported in suspension, *Veronica* usually establishes in higher and more distal parts of the estuary.

In the experiment with vegetation, seeds were supplied after the initial 1,000 tidal cycles both via the river and the tidal inlet at a 500 tidal cycle interval until the end of the experiment. In the design, a coverage of half the estuary (i.e. 19 m^2) was assumed to become vegetated by 6,000 tidal cycles with an average stem density of 10 stems/cm^2 and a germination probability of 0.5. Per sowing event, 80,000 seeds of *Medicago*, *Lotus* and *Veronica* each were supplied to the river and 80,000 seeds of *Lotus* and *Veronica* were supplied to the inlet.

Prior to sowing, seeds were soaked for 24 hours to stimulate sprouting. A sowing event commenced after dry bed scans (see section 4.2.2) and 10 tidal cycles for initial wetting. Next, over the course of 25 cycles, the fluvial mixture of seeds was added to the river discharge at one spoonful per cycle. Subsequently, the marine mixture of seeds was introduced just landward of the tidal inlet in the main channel over the course of 10 cycles at one spoonful per cycle. Finally, tilting continued for another 25 cycles to spread the seeds, based on the design tidal excursion length and on earlier tests, resulting in a total of 70 tidal cycles per sowing event.

Following a sowing event, the flume was stopped at its offset slope of 0.001 m/m for four days to allow for sprouting. A river baseflow of 300 L/h was applied to keep the tilted bed moist and the depth of the sea was increased to 10.8 cm to flood the channel and avoid sprouting in permanently submerged areas. Unfortunately, the high water table stimulated the growth of mould in low areas that received little river flow, increasing vegetation mortality (see Suppl. 4.3 for the protocols to suppress algae and fungi). Therefore, after 3500 cycles, the water depth of the sea was lowered to 10 cm during sprouting to minimise the mould.

4.2.2 Data collection and analysis

Time lapse photographs were shot by 7 AVG Mako (G-419C) colour cameras, positioned 3.7 m above the flume. The cameras had a resolution of 2048 by 2048 pixels and a fixed focal length of 12.5 mm, resulting in a pixel resolution on the sand bed of approximately 1.5 mm. Photographs were taken every tilting cycle at the end of flood when the flume was in a horizontal position. Before the images were stitched, the following corrections were applied to each image: noise removal, lens correction (vignette and distortion), geometric rectification and colour corrections. Blue dye was added to the water to get an indication of water depth, which was extracted from the time lapse imagery to get an approximation of the bathymetry development throughout the experiments (see Chapter 3 for review).

Digital elevation models (DEMs) were acquired by means of laser line scanning and stereo-photography. The laser line scanner had a horizontal resolution of 0.75 mm and a vertical resolution of about 0.2 mm (Van Dijk et al., 2013a). Since the accurate laser only covered the middle 2.4 m of the flume, somewhat less accurate stereo-photography was used to acquire the remaining side parts of the flume. Prior to DEM acquisition, the flume was drained slowly to minimise disrupting the bed, and overhead photographs were taken of the dry bed for image classification. Subsequently, the bed was scanned and oblique photographs were taken with a digital single-lens reflex camera and processed with structure-from-motion software (Agisoft Photoscan). Increments between DEMs increased as the experiments progressed and morphological change reduced. Firstly, DEMs were made with steps of 100 tilting cycles up to 500 cycles, followed by 8 DEMs with an interval of 250 cycles. Next, 5 DEMs were made with an interval of 500 cycles and the final 5 DEMs had an increment of 1,000 cycles, covering a total of 10,000 cycles. In the experiment with vegetation, DEMs were also taken just before a sowing event and right after a sprouting period to determine where vegetation had established or perished.

Flow measurements by instruments or particle image velocitmetry (PIV) is practically impossible in shallow flows, especially in the presence of vegetation. Therefore, flow data were acquired by the numerical model Nays2D, which was extended and validated in Chapter 3 to simulate tidal flow in scale experiments (see Suppl. 4.1). Nays2D takes as input a DEM and flow boundary conditions, applies the prescribed tilting motion of the flume and produces water depth and flow maps with a resolution of 2.5 by 2.5 cm over a tidal cycle. Vegetation was filtered out of the DEMs and added as increased hydraulic roughness, with a manning ranging from 0.02 s $m^{1/3}$ for bare sand up to 0.1675 s $m^{1/3}$ for dense vegetation (i.e., 20 stems/cm^2, 0.5 mm thick). The numerical output maps of Nays2D were made with increments of 1,000 cycles and were used to calculate sediment mobility, tidal prism and residual currents. Furthermore, the estuary was classified into subtidal, intertidal and supratidal depth ranges relevant for vegetation establishment and for basic interpretation of the hydrodynamics in terms of flood storage and momentum transfer (Friedrichs and Aubrey, 1988).

The tidal prism (P) and cross-sectional area (Ω) show an empirical, near-linear relation in natural tidal systems (e.g. O'Brien, 1931; 1969; Jarrett, 1976; Leuven et al., 2018a), but scaled tidal experiments appear biased and do not fit on these relations (Mayor-Mora, 1977; Seabergh et al., 2001; Stefanon et al., 2010). This bias is because the classic relationship $\Omega = kP^{\alpha}$, where k and α are

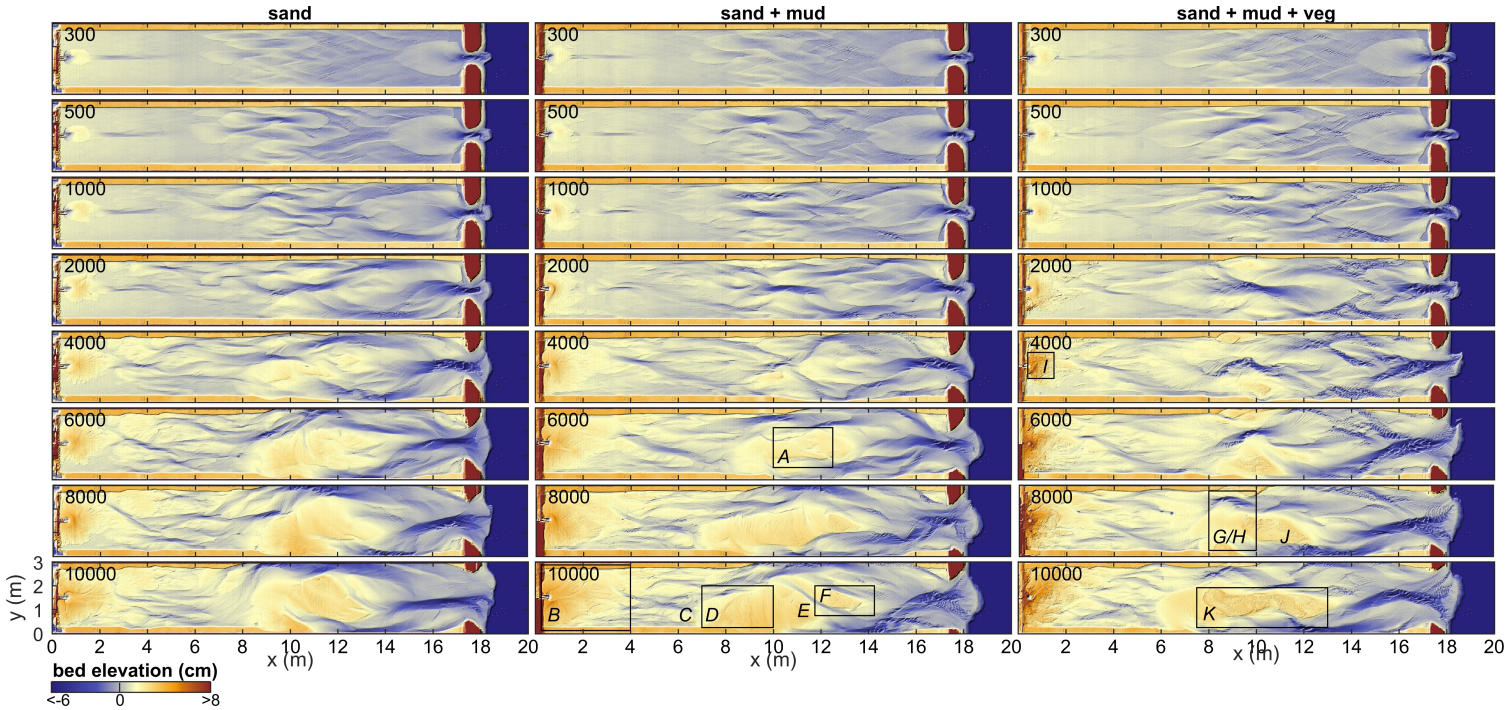

Figure 4.3 Morphological development of the infilling estuary experiments with only sand (left column), with mud (middle column) and with mud and vegetation (right column). Numbers indicate the tidal cycles. Letters correspond to the photographs in Fig. 4.5.

constants (see Leuven et al., 2018a, for review on parameter values), disregards friction effects that are much larger for small-scale tidal systems (Kleinhans et al., 2015b). The formulation by O'Brien (1969) accounts for these effects (also see the more complicated O'Brien-Jarrett-Marchi law: D'Alpaos et al., 2009; Stefanon et al., 2010). The O'Brien (1969) relation assumes that flood and ebb duration and peak flow velocities are equal and is given as follows:

$$P = \int_0^T au\, dt \tag{4.1}$$

with

$$u = U_{max} sin\left(\frac{2\pi t}{T}\right) \tag{4.2}$$

where t is time (s), a and u are the instantaneous cross-sectional area (m^2) and instantaneous, cross-sectionally averaged flow velocity (m/s), T is the tidal period (s) and U_{max} is the maximum value of u (m/s). Solving the integral results in

$$\Omega = cP^{\alpha} \tag{4.3}$$

where $c = \pi/(TU_{max})$ and α = 1. As a result, Eq. 4.3 allows for the comparison of natural tidal systems and experimental scale models (e.g. Seabergh et al., 2001).

4.3 Results

4.3.1 General estuary development

The general development of the three experiments is described as follows. Initially, a low-amplitude diamond-shaped bar pattern emerged in the middle of the estuary. This pattern quickly transformed within the first 300 to 500 tidal cycles into short discontinuous tidal channels that ended in shoals on both ends (Fig. 4.3). Meanwhile, a small ebb-tidal delta and a large flood-tidal delta formed near the inlet, and a bay-head delta started forming near the landward boundary.

Over time, the channels in the estuary deepened, widened and extended in both the landward and seaward direction while bars merged. Landward extension of the tidal channels created a series of terminal lobes that increased the mean bed elevation in the upper half of the estuary (Figs. 4.3, 4.4), whilst the channels and shoals extending seawards were highly dynamic and coalesced with the flood-tidal delta. Subtidal shoals typically separated ebb-dominated and flood-dominated channels, resulting in a mutually evasive tidal channel pattern. Continued growth and reorganisation of the tidal channels led to the development of three main confluence-diffluence nodes at $x = 4$, 10 and 17 m at around 2,000 tidal cycles. Between these confluences, there were on average two main channels flanking the banks of the estuary. It is at these locations that considerable bank erosion occurred, predominantly between $x = 10$ and 17 m where tidal currents were much stronger than between $x = 4$ and 10 m (Fig. 4.3). At the shoreline, barrier erosion was mainly driven by flood currents and waves, and most eroded sediment was transported in the landward direction. The waves contributed to the development of a subtidal shield on the ebb-tidal delta, flanked by flood-dominant channels. The bay-head delta aggraded and expanded by cyclic avulsion, starting with channel displacement, incision and extension after which the channel was backfilled and abandoned.

After about 6,000 tidal cycles, a large bar complex formed in the middle of the estuary by amalgamation of bars (Fig. 4.3). This bar complex rose partly above the high water level and focused tidal flow into two main channels. Given that the bar complex became supratidal and the maximum water level around the bar dropped, this suggested that the collective flow friction reduced whilst the channels developed and deepened. As for the two main flanking channels, the one at $y = 2.5$ m (Fig. 4.3) was more strongly ebb-dominated than the other at $y = 0.5$ m in all three experiments.

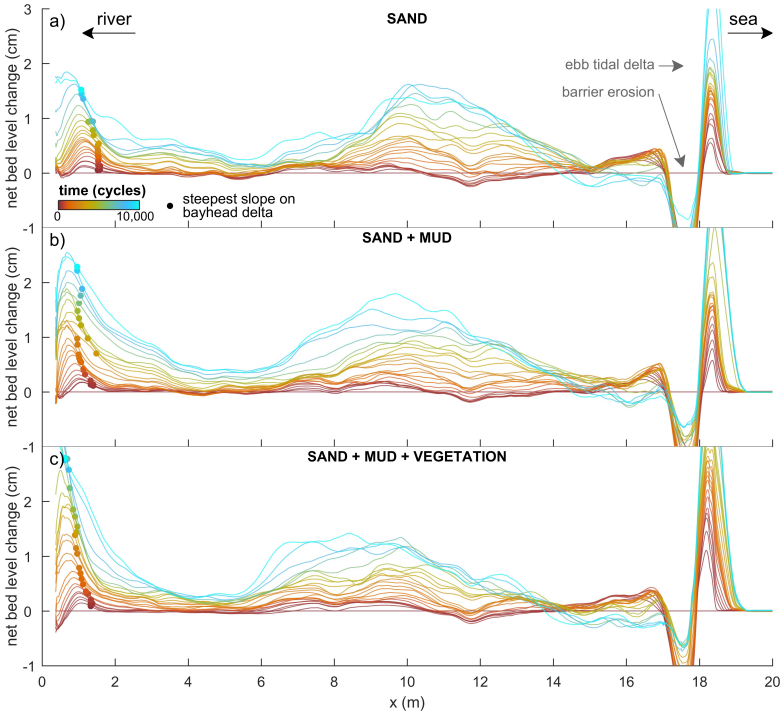

Figure 4.4 Mean cross-sectionally averaged bed level along the estuary for the experiments with (a) only sand, (b) with mud, and (c) with mud and vegetation. Unreworked banks and the barriers were excluded. Dots represent the location of the steepest downward slope on the bay-head delta (see text for discussion).

Over time, the growing bar complex was reworked repeatedly by cross-cutting channels formed by water level differences between the main channels flanking the bar (Fig. 4.3). This process caused sediment pulses into the main channels, and part of this sediment was transported in the landward direction, contributing to further infill (Fig. 4.4).

4.3.2 Mud distribution

Fluvial mud was mainly deposited on the bay-head delta in the first 3,500 tidal cycles (Figs. 4.5b, 4.6a-f), resulting in a higher and more prograded delta than in the sand-only experiment (Fig. 4.4). A small fraction of the mud was transported off the bay-head delta and transported to low-dynamic parts of the delta toe by tidal flows. Mud deposits were partly eroded by channel avulsion and overtopped by new sand and mud, resulting in multiple mud layers in the subsurface of the bay-head delta that were thicker, more abundant and more laterally continuous further away from the long axis of the flume (Suppl. 4.4). After 3,500 tidal cycles, landward migrating tidal channels reached and reworked part of the fluvial mud which was then transported to form intertidal mudflats mainly in the upstream half of the estuary (Figs. 4.5b-d, 4.6a-c). Meanwhile, the increased mud cover limited lateral migration of upstream channels compared to the sand-only experiment (see Supplementary videos).

Marine mud was transported partly into the estuary and partly out to sea to be deposited at the toe of the ebb-tidal delta. Very fine marine mud was swiftly transported in the landward direction and formed small mudflats in the upstream half of the estuary within the first 1,500 tidal cycles. Coarser mud (i.e. larger than about 1 mm) moved around subtidal shoals with net little transport in the landward

direction. Occasionally, this mud was trapped at the deep lee sides of subtidal bars and overridden by bar migration. Over time, many sandy tidal bars aggraded to intertidal elevations, which created new and higher sites for mudflat deposition (Fig. 4.7a); it took until 6,000 tidal cycles to reach this stage in the downstream half of the estuary (Figs. 4.5a, 4.8). Repeated visual inspection of movies (Suppl. Movies online) showed that most mudflats were completely reworked in about 2,000 tidal cycles, except for the mudflat at $x = 13$ m right between two confluences that had a longer lifespan of 3,000 tidal cycles (Fig. 4.5f). Mudflat reworking was slower than tidal bar erosion in the sand-only experiment and proceeded through small-scale erosive channels at their fringes (Fig. 4.5e), cross-cutting channels and large-scale channel migration. The re-mobilised mud led to new mudflats or was transported further into the estuary. Accordingly, the upstream half of the estuary became progressively muddier, with numerous mud-covered bars and mudflats merging with the bay-head delta (Figs. 4.5b, 4.6a-c, 4.8).

4.3.3 Vegetation patterns

Vegetation settling started on the low-energetic parts of the bay-head delta and on elongated shore-connected mudflats flanking tidal channels. As fluvial mud and plants increasingly focused flow into the channels, the light *Veronica* seeds were transported further into the estuary, from where

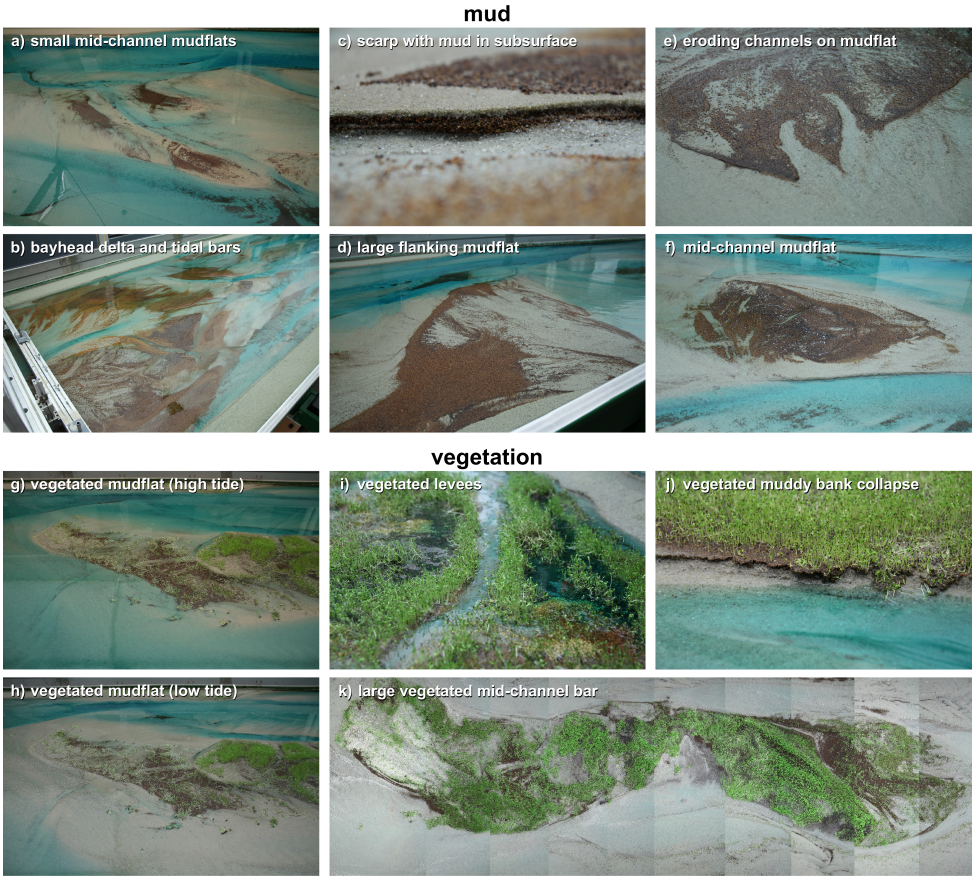

Figure 4.5 Photographs of (a–f) mud deposits and (g–k) vegetation in the experiments. The corresponding locations in the flume are indicated in Fig. 4.3.

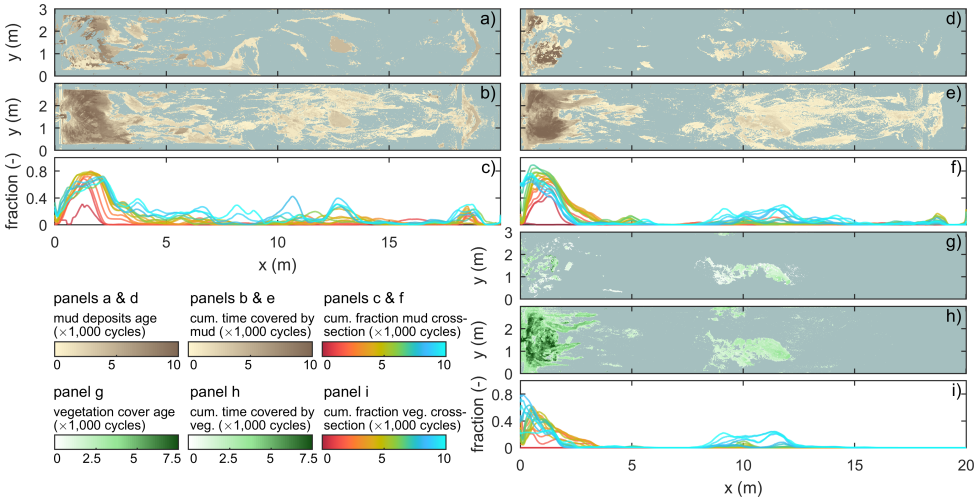

Figure 4.6 Mud and vegetation distribution throughout the second experiment with mud (left column) and the third experiment with mud and vegetation (right column). (a/d) Age of mud deposits at the surface at the end of the experiment. (b/e) Cumulative time over which the bed was covered with mud during the experiment. (c/f) Fraction over the cross-section that was covered with mud along the estuary over time. (g) Age of vegetation at the end of the experiment. (h) Cumulative time over which the bed was covered with vegetation during the experiment. (i) Fraction over the cross-section that was covered with vegetation along the estuary over time.

they dispersed to low-energetic zones near the bay-head delta. Additionally, the increased flow led to the development of more shoals on the landward end of tidal channels near the bay-head delta.

Fluvial mud and vegetation effectively filled the low-energetic region between the bay-head delta and the tidal channels, leaving one open channel of about 5 cm wide as a connection between the river inflow and the tide-dominated reach (Fig. 4.5i). Muddy, vegetated levees formed along this channel with predominantly *Medicago* and *Lotus*, whilst the sandy channel bed was slowly aggrading. The surrounding low-lying areas, here interpreted as fluvial floodplains, were covered with vegetation of all three species, with slightly more *Veronica* in the downstream direction. Given the increasing superposition of the channel above the surrounding landscape on the bay-head delta, crevasse splays occurred intermittently (Fig. 4.5i). Yet, few became successful avulsions due to the dense vegetation and absence of flood discharges, and most splay channels were backfilled with mud and covered by sparse vegetation. Distal floodplains often had deep stagnant water (i.e., > 0.5 cm), which in nature could facilitate peat formation. However, the selected species were unsuitable for peat formation and instead drowned and decayed (Fig. 4.5i), with some of the resultant organic matter being eroded later. The combination of reduced avulsion and local filling of accommodation space on the floodplains resulted in a more irregular bay-head delta shape than in the non-vegetated experiments.

As high-intertidal bars formed in the estuary after 2,000 tidal cycles (Fig. 4.8), they were sparsely colonised by *Veronica* and fewer *Lotus*, both mainly of marine origin. The vegetation sprouted on both muddy and sandy parts. *Veronica* usually established over a larger vertical range and ended up highest on the bars due to its smaller seed size. The vegetation sheltered regions that captured mud (Fig. 4.7b,c) and new seeds but little sand. However, no clear order was found in the establishment of mudflats vegetation, as one could lead to the other, and vice versa in other places. The first pioneering vegetation on bars was located close to the banks, where it first steered the flow to cause considerable erosion of the non-vegetated outer banks, after which the bars either merged with the outer banks or were eroded by migrating channels.

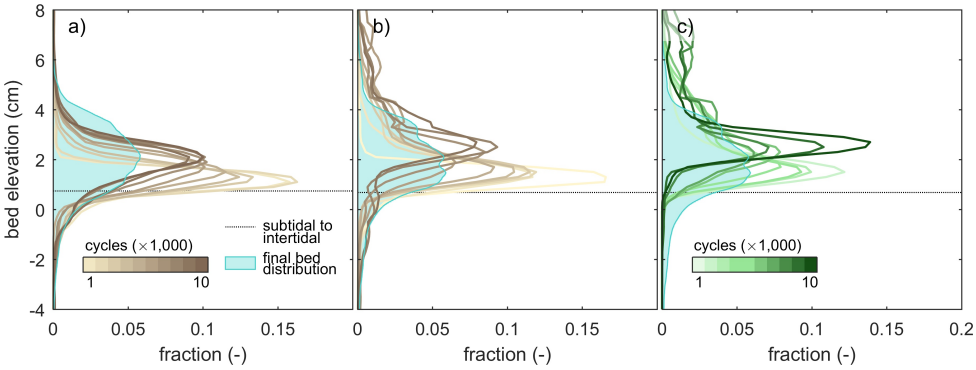

Figure 4.7 Mud and vegetation distribution as function of bed elevation over time in comparison to the bed level distribution at the end of the experiments. (a) The vertical distribution of mud in the experiment with mud and (b) in the experiment with mud and vegetation. (c) The vertical distribution of vegetation in the experiment with mud and vegetation. The boundary between subtidal and intertidal is the mean value for the entire basin.

Expanding tidal channels eroded and sandy bars buried the vegetated mudflats near the bay-head delta (around $x = 3$ m), strongly reducing the vegetation coverage after 5,000 tidal cycles. Fluvial sediment did not reach this area but was mainly trapped on the bay-head delta, which strongly grew in elevation compared to the non-vegetated experiments (Fig. 4.4). Most eroded vegetation was simply uprooted but some was preserved as layers of organic matter in the subsurface. Repeated visual inspection of movies showed that most muddy and sandy bars in the upstream half of the estuary were reworked within 1,000 tidal cycles, while only intertidal bars close to the vegetated bay-head delta covered by *Lotus* or *Medicago* persisted longer. As a result, vegetation was concentrated on the bay-head delta and small bars around $x = 10$ m during the first 6,000 tidal cycles (Fig. 4.6i).

Around 6,000 tidal cycles, vegetation started to establish on the large mid-channel bar in the central estuary that also formed in the non-vegetated experiments. At first, a small vegetated mudflat formed atop the bar that was in between the two main channels. Flood currents, particularly in the channel at $y = 0.5$ m, brought sediment to the landward side of the mid-channel bar where it was deposited as a shoal coalescing with the mid-channel bar (see 6,000 to 10,000 cycle panels in Fig. 4.3). This effectively increased bed elevations landward of the vegetated mudflat and created a new site for establishment, first by mudflats and *Veronica* and later also by *Lotus* and some *Medicago* (Fig. 4.5g,h). The vegetation inhibited flow and incision across the mid-channel bar and caused stronger tidal currents and deeper channels parallel to the bar. This resulted in the following three developments. Firstly, part of the mid-channel bar remained dry and was effectively turned into new supratidal land that narrowed the estuary (Fig. 4.8). Secondly, sediment was more efficiently transported through the main channels, which resulted in more landward expansion of the mid-channel bar than in the experiments without vegetation (Fig. 4.5k), as well as further infilling of the upstream range $x = 3-6$ m (Fig. 4.4c). Thirdly, the stronger currents started to steepen and erode the banks of the vegetated mid-channel bar (Fig. 4.5j). Seaward expansion of the bar was slower and commenced through the deposition of ridges covered by marine vegetation (*Veronica* and *Lotus*), followed by a mudflat on the back of the vegetated ridge once the bed had aggraded to high-intertidal levels. Near the end of the experiment, the water level difference between the ebb- and flood-dominated channels flanking the mid-channel bar had become so large that mud and vegetation near the middle of the bar were eroded and an incipient cutoff channel developed (Fig. 4.5k).

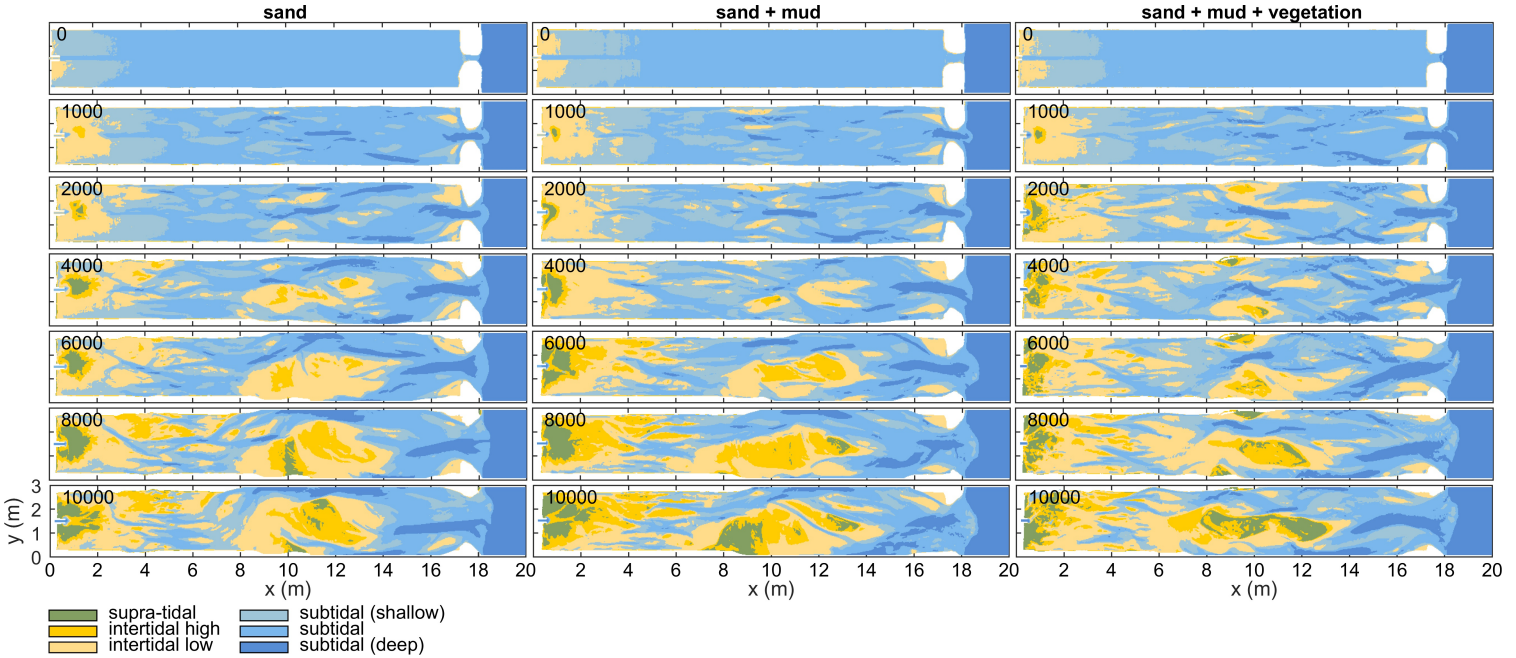

Figure 4.8 Development of subtidal, intertidal and supratidal area of the infilling estuary experiments with only sand (left column), with mud (middle column) and with mud and vegetation (right column). Numbers indicate the tidal cycles.

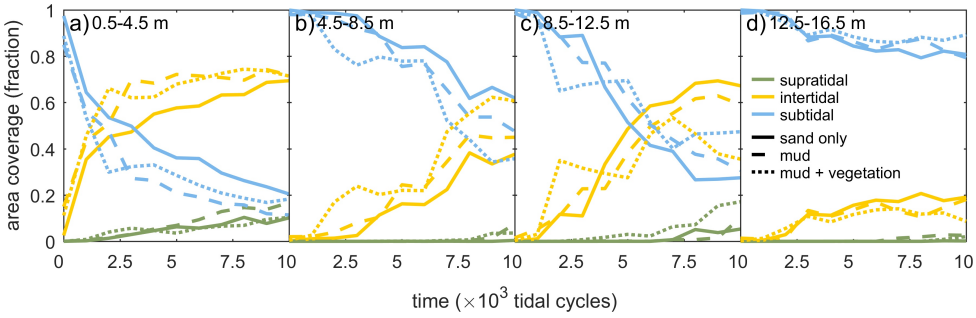

Figure 4.9 Subtidal, intertidal and supratidal area in four reaches of the estuary: (a) 0.5–4.5 m, (b) 4.5–8.5 m, (c) 8.5–12.5 m and (d) 12.5–16.5 m.

4.3.4 Infilling and development of a funnel-like shape

The intertidal and supratidal areas increased in all three experiments, showing a trend of estuary infilling (Figs. 4.8, 4.9). Mud and vegetation formed more intertidal area in the upstream half of the estuary, partly because more sediment was added, and caused faster development of supratidal areas (Fig. 4.9a-c). On the long vegetated bar (Fig. 4.5k), this development was at the cost of local intertidal area due to the deep, steeply-sloped channels next to the vegetated bar (Fig. 4.9c). However, as these deep channels proved very efficient in transporting sediment in the landward direction, the vegetated bar indirectly contributed to the accretion of more intertidal area in the upstream part of the estuary (Fig. 4.9b). Mudflats were typically found in regions classified as intertidal and supratidal, whilst vegetation predominantly occupied supratidal areas (Fig. 4.7).

Surprisingly, the rate of infilling in the 4.5–8.5 m reach was lower than in the seaward direction and on the bay-head delta upstream (compare Fig. 4.9b with a, c and d). Here, the subtidal and intertidal areas changed linearly over time, whilst the other reaches appeared to develop quicker towards a filled, steady state. This differentiation suggests that the coastal sediment supply and tidal currents mostly caused the infilling of the seaward half of the estuary, whilst the effects of fluvial input were limited to the bay-head delta. This is consistent with the along-channel development in flow asymmetry (Fig. 4.10d-f), which rapidly became mildly ebb-dominant on the bay-head delta, whilst the middle estuary remained flood-dominant throughout the experiments. At the tidal inlet, ebb-dominance increased rapidly with the progressive infilling of the estuary.

As intertidal and supratidal areas formed and expanded, the summed cross-sectional width of the subtidal channels approached a convergent funnel-like shape, especially in the experiments with mud and with mud and vegetation (Figs. 4.10, 4.12a). Fig. 4.12a indicates that the addition of vegetation led to a temporarily faster development towards a convergent shape especially during phases of expanding vegetation patches, i.e. between 2,000 and 4,000 cycles and after 6,000 cycles. The funnel-like shape was also evident from the linear-to-exponential decrease in tidal prism in the landward direction (Fig. 4.11). At the beginning of the experiments, the tidal prism increased in the upstream direction away from the tidal inlet, caused by a secondary tidal wave in the initially deep basin driven by the tilting. Minor differences in initial inlet width caused the difference in the initial profile of tidal prism between the experiments (Fig. 4.11). This effect quickly reduced over time as the inlet widened and the eroded sediment was captured in the estuary, which decreased sediment mobility (Fig. 4.13a-d) and cross-sectional area (Fig. 4.12b) in a morphodynamic feedback.

Sediment mobility further decreased as the experiments progressed, which is consistent with the observed estuary infilling (Fig. 4.13). This decrease in mobility was most prominent in the mud experiment. The vegetation experiment showed a decrease in mobility towards 5,000 cycles as also

seen in the other experiments, but, interestingly, this was followed by a small increase in surface area with channels with high sediment mobilities ($\theta > 0.1$) towards 10,000 cycles especially in the ebb direction (Fig. 4.13b-c). This trend is indicative of increased tidal penetration co-occurring with the flow confinement along the long supratidal bar.

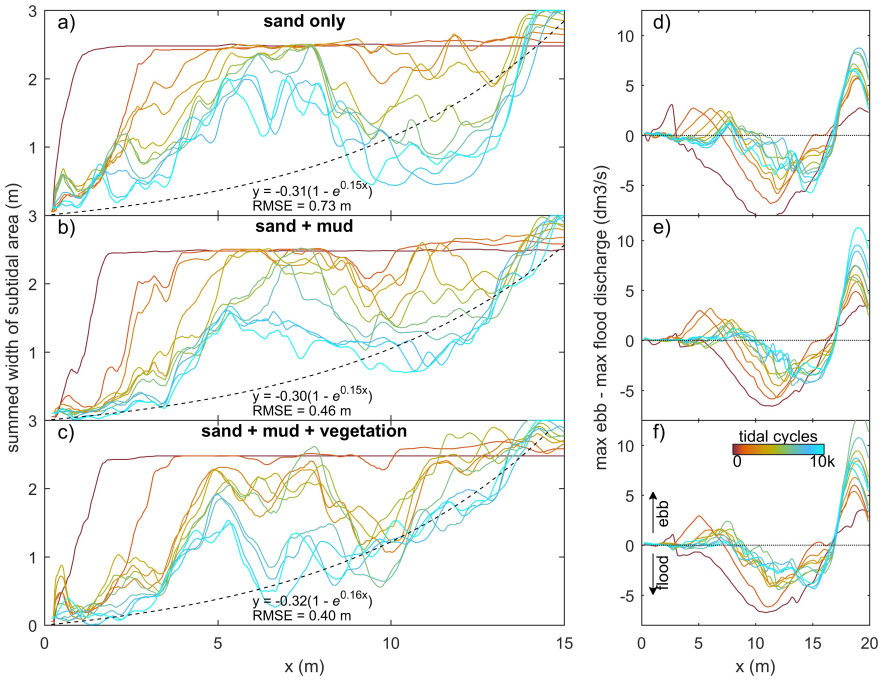

Figure 4.10 Summed width of subtidal area, showing the development towards a funnel-shaped estuary with exponentially converging width in especially the experiment with mud and vegetation. (a) The experiment with sand only, (b) sand and mud, and (c) sand, mud and vegetation. (d–f) Ebb or flood-dominance along the estuary over time. As subtidal area decreases over time, the experiments become less flood-dominant from the landward boundary.

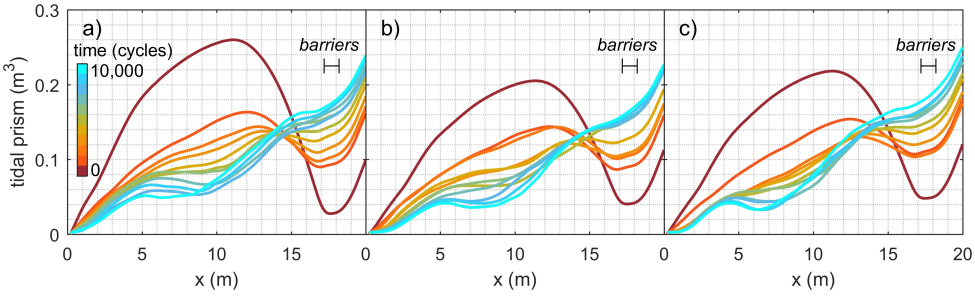

Figure 4.11 Tidal prism development along the estuary for the experiment (a) with sand only, (b) sand and mud, and (c) sand, mud and vegetation. Differences between the initial profiles of tidal prism were due to a minor inaccuracy of the initial inlet width (±3 cm difference between experiments) but had little effect on the long-term development.

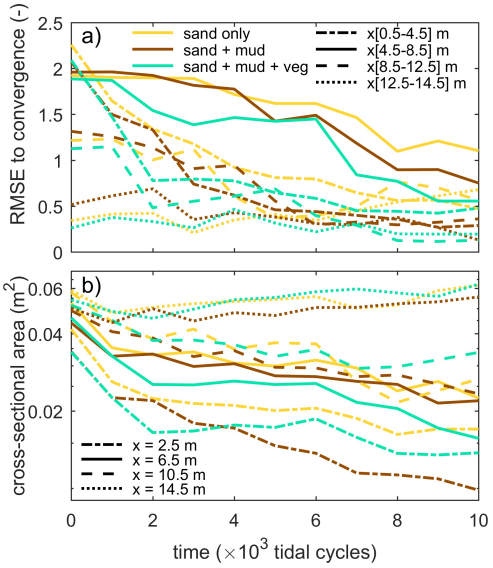

Figure 4.12 (a) RMSE of summed width of subtidal area to the convergence in Fig. 4.10a-c for four reaches along the estuary shows a quicker approach to subtidal channel convergence in the experiments with mud and with mud and vegetation. (b) cross-sectional area decreases more strongly towards the upstream boundary that is indicative of estuary infilling towards a convergent planform.

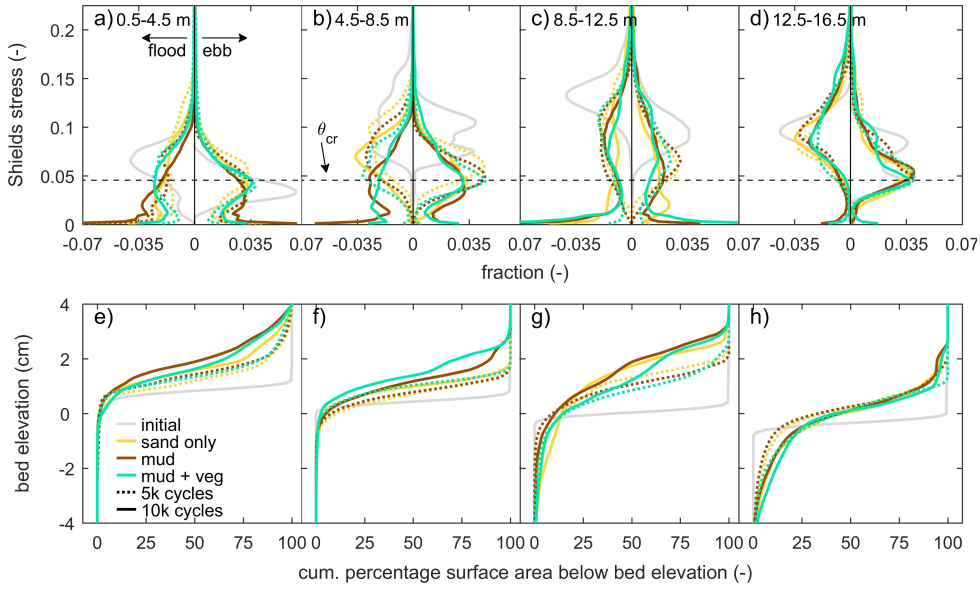

Figure 4.13 The distribution of maximum Shields stress in the flood and ebb direction, initially and at 5,000 and 10,000 cycles, split into four regions along the estuary: (a) 0.5–4.5 m, (b) 4.5–8.5 m, (c) 8.5–12.5 m and (d) 12.5–16.5 m. The critical Shields number (θ_{cr}) for beginning of sand motion is indicated as a horizontal dashed line. For the same reaches and times, the hypsometry development is given in (e–h).

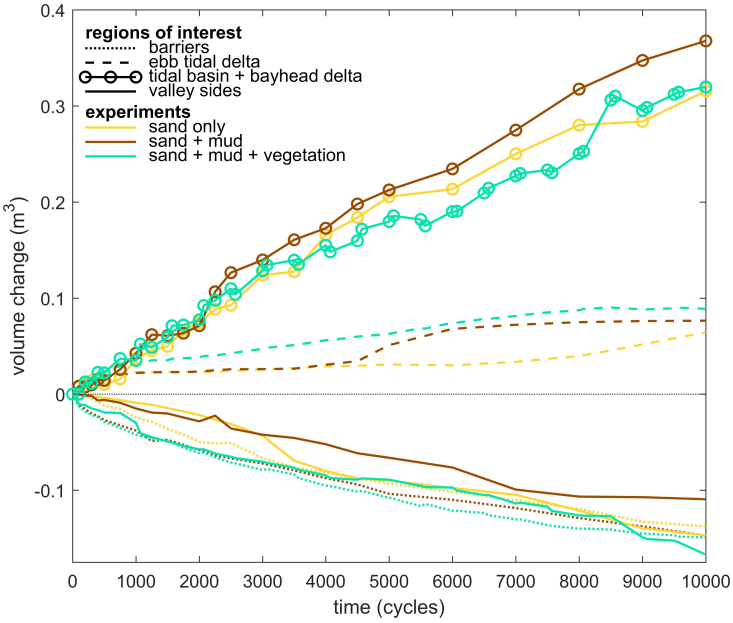

Figure 4.14 Sediment sources and sinks for the three experiments, split into four regions of interest: the barriers, the ebb-tidal delta, the estuary plus the bay-head delta, and the valley sides that eroded over time.

Apart from the fluvial sand input, most of the infilling resulted from reworking sediment already present in the initial bed. This sediment was firstly redistributed from the higher to the lower parts (Fig. 4.14). Secondly, sediment was moved upstream from the barriers, of which the erosion rate was comparable between the three experiments. The valley sides were least eroded in the experiment with mud. The sediment input by the river and from the eroded valley sides and barriers was about the same as the sediment gain in the estuary and the ebb-tidal delta. Overall, more sediment was deposited within the estuary in the mud experiment (Fig. 4.14) and this resulted in the most infilled estuary (also see Fig. 4.4).

4.4 Discussion

The general development in all three experiments is the infilling of a subtidal, unfilled estuary with sand, mud and even a minor amount of organic material. The experimental control on mud supply and vegetation allows for the analysis of mud and vegetation effects on the infilling trend and the morphodynamics. A generalisation to natural estuaries is followed by a conceptual model for steady states at varying degrees of infilling of wave-dominated and mixed-energy estuaries.

4.4.1 Mud and vegetation effects on estuary infilling

Mud promoted estuary infilling because it filled accommodation space from the landward boundary, which reduced the tidal prism in the upstream half of the estuary. This can be partly ascribed to mud being added as extra sediment. However, the low density and slightly cohesive properties of the mud enabled bars to elevate well into supratidal levels. The latter two effects led to limited lateral migration of the ebb-dominated tidal channels and a longer life span of the flood-dominated intertidal bars as cutoffs reduced. Consequently, mud could further infill the low-energetic regions of the estuary,

including the tops of intertidal bars (Fig. 4.5a,d-h) and topographical lows in the intertidal-to-supratidal range (Figs. 4.5b, 4.7a,b). This development made the estuary progressively muddier and shallower towards the landward boundary, which is consistent with observations in nature (e.g. Glenn, 1978; Baas et al., 2008; Van Maren et al., 2016), numerical modelling (Braat et al., 2017; Van de Lageweg et al., 2018; Lokhorst et al., 2018) and previous experiments in the Metronome (Braat et al., 2019a). Also, mud contributed to a seaward shift of the transition from flood-dominance to (weak) ebb-dominance downstream of the bay-head delta (Fig. 4.10e). Yet, mud in the experiments was generally not deposited as shore-connected mudflats that flank many natural estuaries (e.g. Dalrymple et al., 1992; Dalrymple and Choi, 2007), which was due to strong currents along the banks of the estuary. The formation of such shore-connected mudflats probably requires a broader range of suspended sediments (Braat et al., 2019a) and diurnal variability or a spring-neap cycle. This is analogous to how floods in meandering rivers create floodplains (e.g. Van Dijk et al., 2013a).

Vegetation captured part of the mud, which resulted in fewer and smaller mudflats compared to experiments without vegetation (Fig. 4.6). This process contributed to the quicker formation of supratidal areas particularly in the middle reach of the estuary and near the bay-head delta (Figs. 4.3, 4.8). While vegetation influenced, but did not determine, where mud settled in the estuary, neither mud nor vegetation was found necessary for the settling of the other. This observation agrees with both field observations (e.g. Van der Wal et al., 2008) and recent numerical modelling with mud and with dynamic vegetation (Braat et al., 2019b; Brückner et al., 2019). As emergent areas developed (Fig. 4.13e-h), vegetation in the experiment generally established in the supratidal range where it enhanced mud deposition (Fig. 4.7), in qualitative agreement with field observations (e.g. Allen, 2000; Temmerman et al., 2007; Mudd et al., 2009). Additionally, vegetation focused the flow between patches as also found in rivers (e.g. Luhar et al., 2008; Braudrick et al., 2009), resulting in channel formation on the bay-head delta (Fig. 4.5i) and in creek formation on the vegetated bars (Fig. 4.5g,h) in a similar fashion as on natural salt marshes (e.g. Temmerman et al., 2007). On the larger system-scale, vegetation indirectly caused more landward sediment transport especially after 8,000 cycles (Figs. 4.8a-c, 4.10, 4.13e-g, 4.14).

Tidal prism in the novel experiments scaled similarly to cross-sectional area as in natural estuaries (O'Brien, 1969; Jarrett, 1976; Byrne et al., 1980; Leuven et al., 2018a) and previous scale experiments (Mayor-Mora, 1977; Seabergh et al., 2001) (Fig. 4.15). However, while some numerical studies (Lanzoni and Seminara, 2002; Zhou et al., 2014) and scale experiments (Stefanon et al., 2010; 2012) show that the $P\Omega$ relation (Eq. 4.3) is approached in the initial phase of morphological evolution (not included in Fig. 4.15), this initial imbalance is absent in this study. This is probably caused by the tilting mechanism, which caused an initially large tidal prism within the basin that was larger than expected from the cross-sectional area at the inlet (Fig. 4.11). Nevertheless, the large tidal prism quickly reduced as the estuary filled with sediment eroded from the barrier, which also increased the mouth width. The inlet widening in the experiments was by design to generate unlimited marine sediment supply, as it was practically impossible to reproduce sediment exchange with the littoral zone in the experimental setup. Alternatively, the barriers could have been fixed but this would probably steer considerable bank erosion until the estuary drops below the threshold of motion. Regardless of the differences with nature, where the inlet tends to decrease as accommodation space is filled (e.g. O'Brien, 1931; 1969; Jarrett, 1976), the experimental estuaries converged.

While convergent, single-channel estuaries can have a balanced ebb- and flood-generated sediment transport (Savenije, 2015; Dronkers, 2017), many estuaries have a more complicated morphology. Recently, bar-dominated estuaries were shown to have, on average, a convergent shape if only the cross-sectional area of subtidal channels is considered (Leuven et al., 2018b). This is consistent with the one-dimensional flow model concept of Friedrichs and Aubrey (1988), in which the subtidal channels convey the momentum of flow and the intertidal zone only acts as flood storage to affect

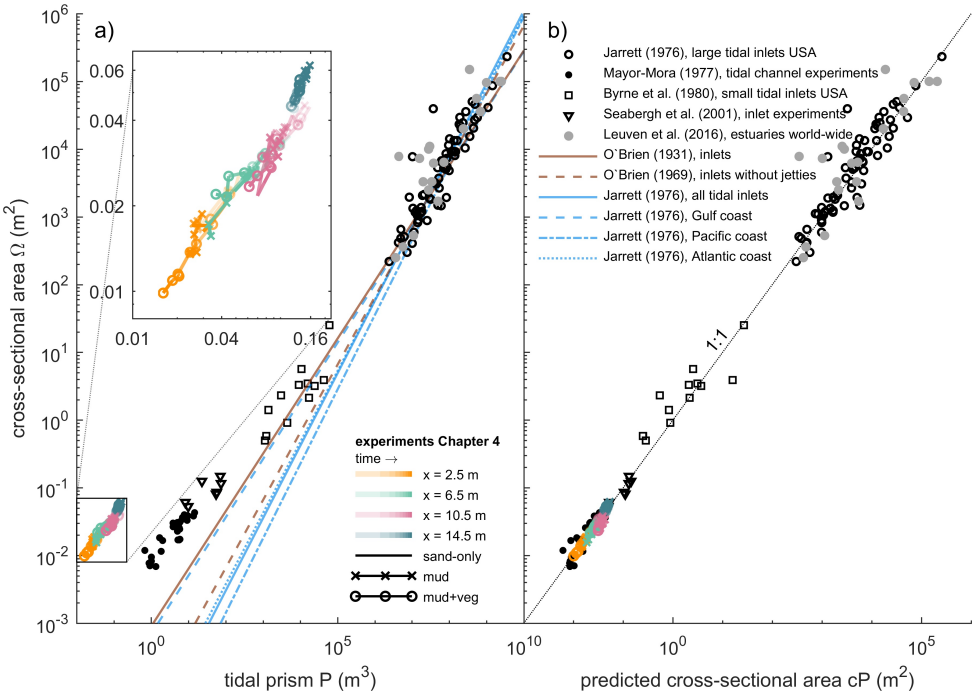

Figure 4.15 Development of cross-sectional area vs. tidal prism in comparison to natural tidal systems and previous scale experiments of tidal inlets. (a) Scale experiments deviate from the extrapolated relations that are based on natural tidal systems. The inset shows the temporal development for the three experiments of this study at four locations along the flume. (b) Cross-sectional area plotted against predicted cross-sectional area, which is tidal prism corrected for larger friction effects in scale experiments using $c = \pi/(TU_{max})$ (Eq. 4.1-4.3) (O'Brien, 1969; Seabergh et al., 2001). The graph shows similar behaviour for natural tidal systems and their down-scaled counterparts. Note: only data in the field data sets are plotted for which peak flow velocity at the tidal inlet/estuary mouth was available.

water surface amplitude and ebb-dominance. As such, a multi-channel estuary can be convergent in the subtidal cross-sectional channel area whilst this may not be directly apparent from the estuary morphology (Leuven et al., 2018d). The new experiments show that these empirical findings extend to wide infilling basins, where mud and vegetation quicken the self-confinement of the subtidal channels in experimental estuaries towards a funnel-like shape (Figs. 4.10, 4.12, 4.15). Indeed, at the end of all three experiments, the tidal prism at the mouth ($0.17 - 0.20$ m^3) was about similar to the final stage of previous experiments of muddy ingressive estuaries that developed by widening an initial narrow channel in the same flume (Braat et al., 2019a). The development to such a convergent shape in an initially wide, infilling basin is also found in palaeogeographical reconstructions of systems such as the Old Rhine Estuary (NL) (De Haas et al., 2018; 2019), the Oer-IJ Estuary (NL) (Vos et al., 2015) and the Shoalhaven River (AUS) (Roy et al., 1980). Together with previous findings, the new experiments show that a convergent shape with mid-channel bars can be considered an attractor state (cf. Thorn and Welford, 1994), as the subtidal channels of both ingressive and infilling estuaries tend to develop to such a shape.

The question is now to what degree the two mechanisms, filling and confining, contributed to the trend towards a multi-channel estuary that is on average convergent. Interestingly, the mud experiment was most infilled (Fig. 4.14), whilst the mud-vegetation experiment had developed slightly closer to

a convergent shape (Figs. 4.10, 4.12a). This convergent shape of the subtidal channels is somewhat obscured by an intricate pattern of intertidal bars and flats, compared to an ideal estuary. As these intertidal areas contribute to the tidal prism, mud and vegetation affected the subtidal channel and inlet dimensions of the whole system. At first, both mud and vegetation reduced tidal prism as overall higher bed elevations developed compared to the sand-only experiment (Figs. 4.4, 4.13), which caused friction-dominance over convergence effects (Dalrymple and Choi, 2007; Friedrichs, 2010). However, whilst the mud experiment continued to reduce tidal prism, the combination of mud and vegetation seemed to lead to a slight increase in tidal prism towards the end of the experiment (Fig. 4.11c). This apparent increase opposes current understanding that vegetation reduces tidal prism (FitzGerald et al., 2008; 2018) and more experiments are needed to determine whether the apparent increase in tidal prism, as well as the slightly more convergent shape, are significant or due to internal variability or unintended vegetation dynamics of the system.

The novel experiments fill a gap in the set of previous long-term morphodynamic modelling and experiments, which focused predominantly on ingressive estuaries (e.g. Van der Wegen and Roelvink, 2008; Leuven et al., 2018b; Braat et al., 2017; 2019a) on the one hand, and on tidal basins with too little fluvial input on the other. The new experiments showed that little floodplain sediment supply (i.e., mud) leads to a wide, multi-channel (braided) estuary, for example similar to the Oer-IJ Estuary (NL) (Vos et al., 2015). On the other hand, ample floodplain sediment supply contributed to a narrow estuary with levees and high floodplains that is closer to the classic, ideally converging estuary (Savenije, 2015). Furthermore, the experiments indicated a disconnect between the effects originating from the fluvial and marine boundary conditions. Specifically, the development of sub-, inter- and supratidal areas (Figs. 4.9, 4.12a) indicated that the bay-head delta reach and the downstream half of the estuary quickly approached a steady state, in contrast to the reach 4.5–8.5 m. It is the latter reach where the combined effects of the river and the tide on sediment supply (Fig. 4.11) are smallest and the morphological response to boundary conditions takes longest, as in the unfilled bay reach in the conceptual model of Dalrymple et al. (1992). Thus, as most reaches were at, or close to, a steady state (Fig. 4.12a), the experimental estuaries as a whole are considered close to a steady state as well.

4.4.2 A conceptual model for steady state morphology of estuaries

'Equilibrium' and 'steady state' are contested concepts in geology (Thorn and Welford, 1994; Zhou et al., 2017; Pierik, 2021), but are useful in the context of experiments and models with controlled boundary conditions. On the geological timescale of sea-level fluctuations, estuaries are considered ephemeral systems (Lanzoni and Seminara, 2002; Dalrymple and Choi, 2007; De Haas et al., 2018). However, on the centennial timescale, sandy estuaries have been argued to have two steady states given reasonably constant boundary conditions. The first is an unfilled estuary that is below the threshold of motion (Roy et al., 1980; Dalrymple et al., 1992), and the second is a filled estuary with bars and net converging channels. Depending on initial conditions such as valley dimensions, a filled estuary can be either a wide system with many channels or a narrower system with few channels and bars (Leuven et al., 2018b). Now, the new set of experiments suggests that also partly filled estuaries may attain a steady state.

The key concept that seems to determine to which steady state an estuary develops is the tendency to form floodplains, which is a function of variables including floodplain sediment supply, flood magnitude and frequency, tides, waves, and vegetation. Whilst the novel experiments all showed a fairly similar steady state, it is hypothesised that, for example, a higher floodplain sediment supply and more flood-resilient vegetation would probably lead to a narrower steady state. As a result, the different tendency for floodplain formation between estuaries allows for a continuum of steady states in terms of the channel planform, convergence and the degree of filling under reasonably constant boundary conditions on the centennial timescale. Here, the unfilled estuary and the ideal estuary are end-members on the continuum rather than the only two alternative steady states, which is presented

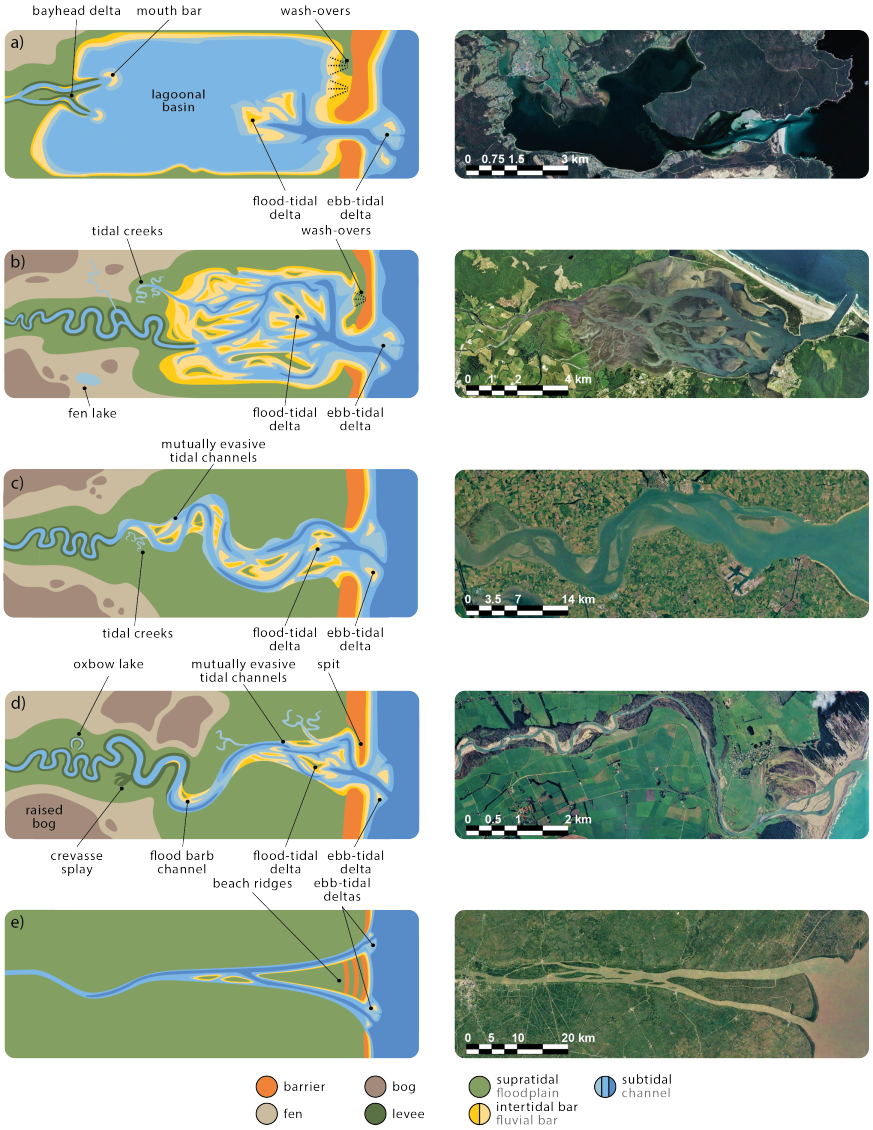

Figure 4.16 Conceptual models of (a/e) the two classic steady-state estuaries end-members between an unfilled estuary (after Dalrymple et al., 1992) and an ideal estuary (after Savenije, 2015) and (b–d) three examples of partly filled steady states with an increasing tendency to form floodplains, each with a natural estuary example in the right column. (a) The classic unfilled steady-state estuary. A natural example is the Georges Bay (AUS). (b) A partly filled steady state with a large number of tidal bars and channels and may be bound by salt marshes and peatlands, such as the Tillamook Bay Estuary (USA). (c) A partly filled steady state that is more confined than (b) with on average two tidal channels, as found for instance for the Western Scheldt (NL) (Leuven et al., 2018b). (d) A partly filled steady state that is strongly confined and quickly reduces to a single channel in the upstream direction. A natural example is the Tangimoana River (NZ). (e) The classic infilled steady-state estuary (Savenije, 2015; Dronkers, 2017). A natural example is the individual branches of the Mekong River (VT). Satellite imagery was retrieved from Google Earth.

in a new conceptual model (Fig. 4.16). In this model, the experiments of this study are somewhere between the Tillamook Bay Estuary (Fig. 4.16b) and Western Scheldt Estuary (Fig. 4.16c).

The possibility of many steady states between the conceptual unfilled estuary and the ideal estuary is consistent with the apparent steady states of some partly filled estuaries in nature. Examples include the Arcachon Bay Estuary (Fig. 4.1c) (Féniès and Faugères, 1998; Allard et al., 2009) and the Ems-Dollard Estuary (Van Maren et al., 2016). Both systems are in a partly filled state with multiple parallel channels that remain open regardless of ample sediment supply. Similar observations are made in estuaries with mangrove vegetation, such as in Darwin Harbour (AUS) (Woodroffe et al., 2016) and the Wapengo Lagoon (AUS) (Nichol, 1991). Another example is the multi-channel Western Scheldt Estuary, which has on average two tidal channels and mid-channel bar complexes that remain largely in place due to topographic forcing by the varied width of the estuary (Fig. 4.16c). The mechanisms leading to this steady estuary planform were demonstrated in previous Metronome experiments (Leuven et al., 2018b). On the timescale of formation of their experiments and of the Western Scheldt Estuary (Van der Spek, 1997), there was no apparent development towards a single convergent channel. Even with high mud supply, previous experimental estuaries remained multi-channel systems (Braat et al., 2019a). Nevertheless, the multiple channels were collectively convergent, which is consistent with the physical principles underlying the ideal estuary (Savenije, 2015).

This is not to say that any state can be stable, and that the stable width of estuaries is entirely unconstrained. Data from 68 estuaries show a surprisingly strong correlation between the width of the river upstream of the tidally influenced reach and the estuarine convergence length and the width of the mouth (Leuven et al., 2018c). The hydraulic geometry of channels in a tidal delta systematically vary with river discharge and tidal amplitude (Sassi et al., 2012), and channel dimensions in a rapidly shifting estuary with erodible banks generally correspond to those of the upstream river (Shimozono et al., 2019). How upstream river discharge controls the dimensions of estuaries is not clear and requires further work.

The antecedent landscape (i.e., the initial conditions) and boundary conditions both determine the degree of infilling and the steady state reached. Starting from a narrow, converging (ingressed) channel, previous experimental studies (Leuven et al., 2018b; Braat et al., 2019a) reached a multi-channel steady state resembling Fig. 4.16c through ingression, as opposed to the infilling cases in the present study. This contrast illustrates that the filling of estuaries is not necessarily a one-way process but depends on the boundary conditions, including relative sea-level, hydrodynamics, sediment supply and eco-engineering traits of vegetation. Moreover, these opposing ways of reaching a steady state have implications for the geological record that require further study. Ingressive estuaries generally only have facies of estuary filling at their margins (e.g. Vos, 2015), whilst infilling estuaries have infilling facies ranging much further outward of their present-day margins (e.g. Vos, 2015; Clement et al., 2017; De Haas et al., 2018).

The existence of a continuum of steady states raises the question whether large events and disturbances can cause a shift to another state. This is understudied, but published work suggests that storm and flooding events can have two contrasting impacts on estuary state. Events may set back the filling sequence in estuaries through erosion of predominantly intertidal and supratidal area (e.g. Mariotti et al., 2010) or events may temporarily increase the import of sediment derived from coastal erosion (e.g. Fruergaard et al., 2013). The effects of events and disturbances are often merely noise at the system scale and the estuary remains in its steady state; for instance, this has been shown for the Humber Estuary (UK) following a large river flood (Townend et al., 2007) and for the Firth of Thames (NZ) following storms and river floods (Swales et al., 2019). Similar findings apply at the smaller scale of salt marshes following hurricanes (FitzGerald and Hughes, 2019). In case the trigger is large enough, the resultant change in accommodation space can perhaps cause a shift towards another steady state. For example, this happened with the catastrophic formation of the Dollard tidal

embayment in the Ems Estuary, the Netherlands (Van Maren et al., 2016; De Haas et al., 2018; Pierik, 2021). A persistent change in boundary conditions could also force the system to another steady state (e.g. Pierik, 2021).

4.5 Conclusions

Physical scale experiments were conducted of infilling estuaries with mud and vegetation in the tilting flume the Metronome, which resulted in the following insights. Estuaries have a continuum of steady states between the classic concepts of the unfilled and completely infilled, ideally converging estuary. Intermediate cases can develop a converging planform with multiple channels. Mud and vegetation affect the degree of filling and the development of an overall converging system through two mechanisms: accretion in bars and system margins, and lateral confinement through flow concentration in channels. The first mechanism of filling increases the intertidal and supratidal area and reduces the tidal prism. The second mechanism of confining focuses flow into channels through increased bar elevation and hydraulic roughness caused by vegetation. Mud and especially vegetation elevated bars well above the mean high water level and increased the stability and longevity of bars. Mud contributed to overall slightly higher bed elevations, particularly on the bayhead delta and in the upstream basin. Vegetation reduced the mudflat area but led to faster bed level rise well into the supratidal range. The bar top stabilisation further reduced shortcut channels and bar removal. The combination of mud and vegetation proved conducive to narrowing of the wide estuary towards a convergent estuary, where the coastal and fluvial sediment supply and the plant properties determined the pacing of the confining processes.

Open Research

Additional materials are available in an online supplement and the data are available via https://doi.org/10.24416/UU01-R82TWE. The online supplement contains (Suppl. 4.1) a hydrodynamic modelling validation with Nays2D, (Suppl. 4.2) the main results of pilot experiments in a smaller flume, (Suppl. 4.3) an algae and fungi protocol, (Suppl. 4.4) photographs of cross-sections over the bay-head delta in the experiments with mud and with mud and vegetation, and three movies of the development of the experiments. The data package includes the DEMs acquired by stereo-photography and laser scanning, overhead imagery of the dry bed, input data for the model Nays2D, and the raw and processed output files of the hydrodynamic modelling. Consult the data package belonging to Chapter 3 for installation and use of the open-source model Nays2D.

Acknowledgements

This research is supported by the European Research Council (ERC Consolidator grant 647570 to M.G. Kleinhans). This work is part of the Ph.D. research of S.A.H. Weisscher. The pilot experiments in the Suppl. 4.2 were conducted by K. Van den Hoven as part of her MSc research. The experiments would have been impossible without excellent technical support. We thank Stuart McLelland and two anonymous reviewers, whose reviews helped to improve the manuscript.

Supplementary material

Supplement 4.1: Validation of Nays2D flow modelling

This study did an extra validation of the hydrodynamic numerical model Nays2D for estuary scale experiments, in addition to the earlier validation in Chapter 3. The reason for an extra validation was that the experimental setup of this study involved considerably larger tidal volumes than the estuary for which Nays2D was validated (Leuven et al., 2018b; Chapter 3). To this end, one Particle Imaging Velocimetry (PIV) measurement (cf. Leuven et al., 2018b) was conducted in this study at the end of the experiment with only sand to create residual flow velocity maps over a tidal cycle. In addition, water blueness values were extracted from the overhead imagery, which were used as indicator of water depths over a tidal cycle.

The tidal signal along the estuary was well reproduced by the numerical model. This is evident from the tidal zonation maps in Figure 4.17, which are derivatives of water depth variations; supra-tidal areas remain dry over a tidal cycle, intertidal areas are only submerged during flood and subtidal areas are flooded the entire tidal cycle. The numerical model resulted in slightly less intertidal area in the downstream half of the estuary, for example at the intertidal bar at $x = 16$ m and at the seaward side of the main mid-channel bar at $x = 14$ m (Suppl. Fig. 4.17). In contrast, slightly more intertidal area was modelled for the upstream half of the estuary, for example at the small mid-channel bar at $x = 7.5$ m and for the bayhead delta $x < 4$ m. The largest differences between the two maps were due to shortcomings of the overhead cameras. These are the striping at $x[8 - 11]$ m that results in less intertidal area in the measured maps, and the lighting difference of the downstream-most camera that results in the sharp edge between tidal zonation at $x = 19$ m.

Modelled residual flow shows a largely similar pattern to the measured values: the model shows there are two distinct ebb-dominated channels in the downstream half of the estuary at either side of the basin. The lower channel shows a slightly meandering ebb-tidal channel with small pockets of flood-dominant flow, which correspond with flood barbs in the morphology. The flood-dominant tidal channel from the ebb-tidal delta into the estuary splits upon reaching the large mid-channel bar at $x = 14$ m. This is fairly similar with the measurements, although many in-situ measurements are missing. There are notable differences in the upstream half of the estuary. Firstly, there is a large region

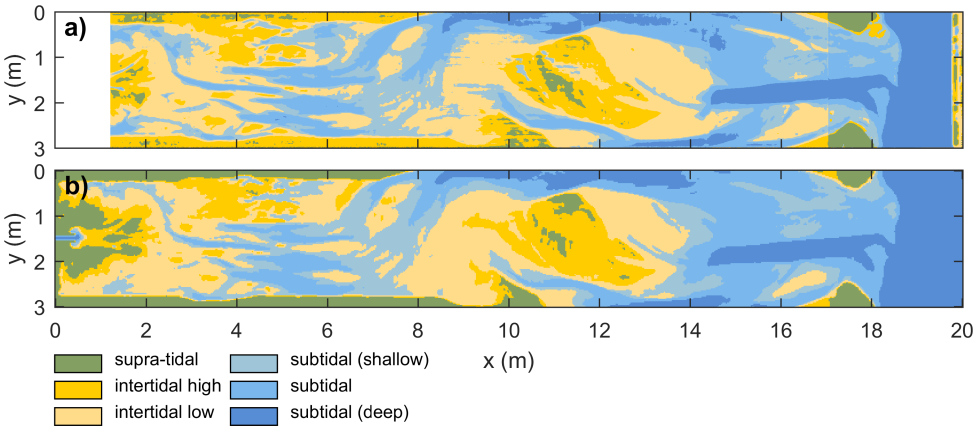

Figure 4.17 Tidal zonation maps of the end of the experiment with only sand based on (a) water colour saturation registered by overhead cameras and (b) numerically modelled flow in Nays2D. The upstream-most part of (a) was obstructed by the bridge and thus has no data. River inflow is at the left and the sea boundary is at the right.

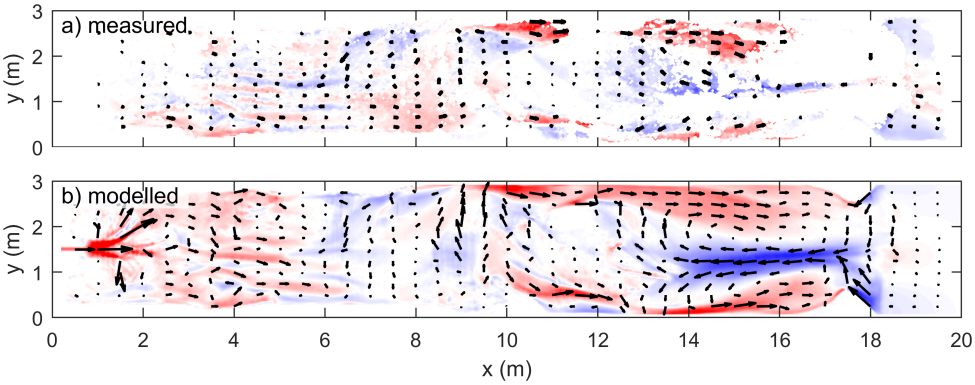

Figure 4.18 Residual tidal flow at the end of the experiment with only sand based on (a) Particle Imaging Velocimetry measurements and (b) modelled flow in the numerical model Nays2D. Residual flow measurements are only shown if more than three quarters of all measurements over a tidal cycle are available.

of slight ebb-dominance at $x = 8$ m, which is less distinct or absent in the modelled data. Additionally, the many parallel channels downstream of the bayhead delta ($x[2-6]$ m) are mostly ebb-dominant in the numerical model, whilst measurements indicate that about half of them are weakly flood-dominant.

Supplement 4.2: Pilot experiments in the mini-Metronome

Introduction

Preliminary to the Metronome experiments described in the main article, pilot runs were conducted in a smaller flume the mini-metronome. In the mini-metronome, a Holocene bar-built estuary was created to study the effect of vegetation on the formation of channels and bars in an evolving estuary. Different vegetation densities were studied to find the optimal vegetation input for the main Metronome experiments.

Methods

Three pilot runs were conducted in the flume the mini-metronome measuring 3.5 m by 1.2 m (developed by Kleinhans et al., 2014b; 2015b; Suppl. Fig. 4.19). Tilting the flume over the short central axis simulated a symmetrical tidal flow with a period of 34.0 s and an amplitude of 12.1 mm. A constant water level was maintained by continued in and outflow at the seaward boundary. At the river boundary, water enriched with sand was provided continuously. Once every tidal cycle, fluvial input was enriched with crushed walnut shells, representing silt and clay. Sand characteristics in the pilot runs were similar to characteristics in the Metronome, with median grain size d50 = 0.55 mm. However, walnut consisted of only two equal fractions: 0.20 mm and 1.2-1.7 mm. Sediment input per tidal cycle was 1.2 ml sand and 5.7 ml walnut.

In each simulation, initial morphology was a drowned river valley with two barriers next to the tidal inlet. The two barriers were locked in place by metal frames; hence the tidal inlet width was constant throughout the experiment. To represent the natural development of centuries to millennia each experiment was planned to run for 3,000 tidal cycles (Kleinhans et al., 2015a). The control experiment lacked vegetation. The other two experiments had vegetation introduced into an evolving estuary. Seeds of two species, *Medicago sativa* and *Lotus pedunculatus*, entered the basin hydrochorously at the river inlet every 500 tidal cycles. The two vegetation experiments differed in the number of seeds introduced at the river: 25.0 g *Medicago* seeds and 25.0 g *Lotus* seeds per

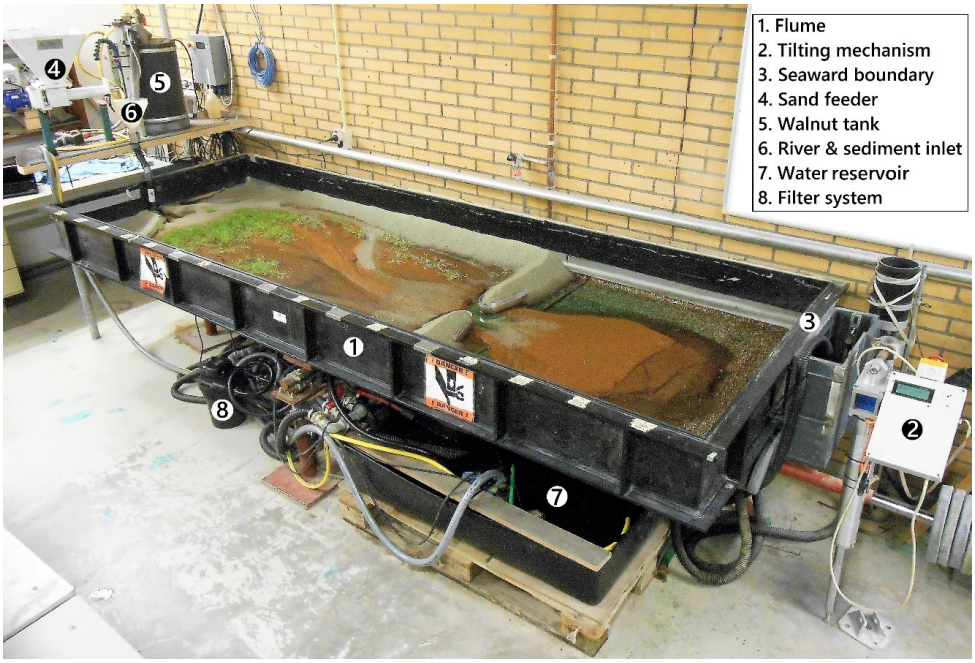

Figure 4.19 Setup of the flume the mini-metronome (after MSc thesis by K. van den Hoven).

vegetation cycle that resulted in a sparse cover and 80.0 g *Medicago* seeds and 80.0 g *Lotus* seeds per vegetation cycle that resulted in a dense cover. Due to a very high vegetation density, the dense vegetation experiment was aborted after 1,800 tidal cycles.

Vegetation growth and morphological development was studied quantitatively and qualitatively. Time-lapse photography in phase with the tide captured the entire flume in four positions every 4^{th} tidal cycle. Photographs represented flood, ebb, high water and low water. In addition, the estuary was carefully drained to scan the bed elevation and obtain detailed photographs, after time = 250 and after time = 500 tidal cycles, and subsequently at intervals of 100 tidal cycles. Bed elevation was scanned with a ViALUX 3d scanner consisting of a fringe projector and calibrated camera system, together termed: zSnapperTM. Photographs were taken with a digital single-lens reflex camera on a fixed frame above the flume.

Results

Initial morphological development was similar in all three pilot runs. During the first 500 tidal cycles walnut was deposited up to halfway the basin, small channels run parallel from the river inflow, and a sandy bay-head delta and ebb tidal delta evolved (top row in Suppl. Figs. 4.20, 4.21). The introduction of vegetation changed the estuarine morphology (Suppl. Figs. 4.20-4.22). Overall, vegetation establishment led to an increase in channel width and depth, and a decrease in braiding index. Sediment deposition per time step was highest during the dense vegetation run. The very dense vegetation captured sediment already in proximity of the river inflow. This is visualised by the highly elevated bay-head delta and a small ebb tidal delta (Suppl. Figs. 4.21, 4.22). With sparse vegetation, sediment could be transported throughout the tidal basin, so channels and bars increased in size and a large ebb tidal delta evolved (Suppl. Figs. 4.21, 4.22). After 2,500 tidal cycles, the main fluvial channel connected to the tidal channel.

Towards designing the Metronome experiments

The pilot runs in the mini-metronome flume provided insight into the eco-engineering effects of vegetation in Holocene estuary development. In the presence of vegetation, the estuarine system narrowed down when compared to the basin without vegetation. Vegetation captured sediment, so downstream sediment export reduced. Locally, vegetation patches created shelter for sediment deposition while areas with dense vegetation patches were static and hardly evolved over time. Vegetation density influenced estuary development. On the one hand, dense vegetation (Veg +++) led to a static system in which downstream sediment transport was inhibited. On the other hand, sparse

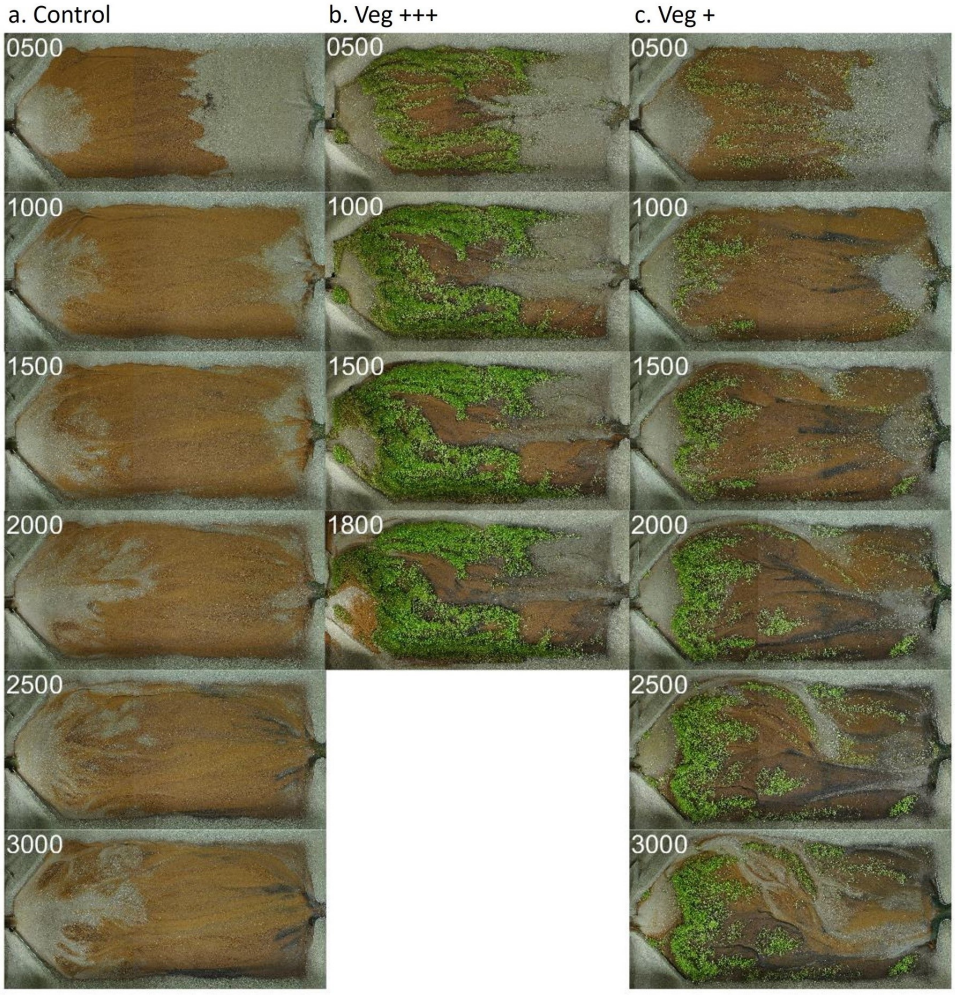

Figure 4.20 Basin top view with water drained from the flume in (a) the control run, (b) dense vegetation run, and (c) sparse vegetation run. In each photograph, left = river inflow, right = barriers with tidal inlet, and top left corner depicts the cumulative number of tidal cycles that the experiment was run, with the end stage in the final photograph of each column. Top row photographs were taken just before tide and river flow was started again after the first seeding (after MSc thesis by K. van den Hoven).

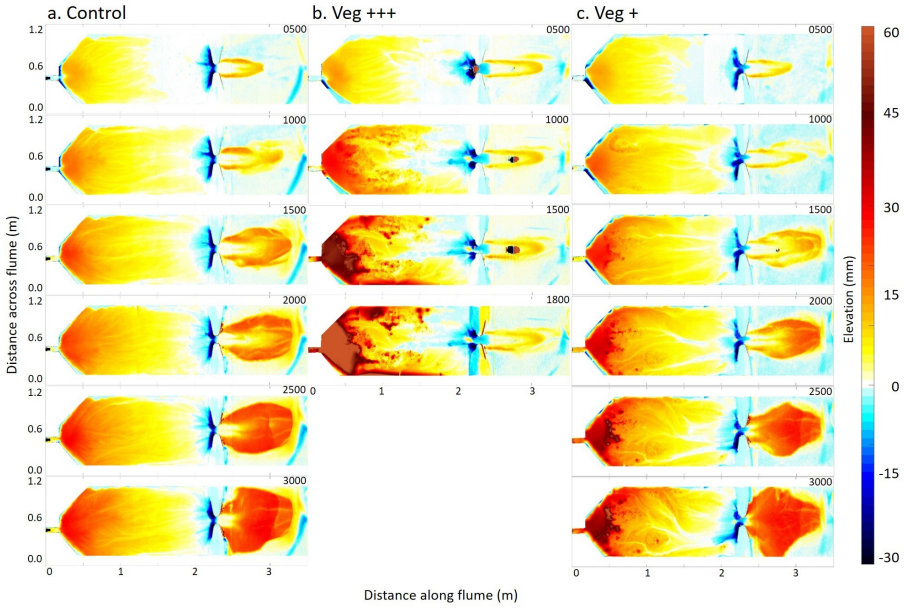

Figure 4.21 Bed elevation change for (a) the control run, (b) dense vegetation, and (c) sparse vegetation. Blue = erosion, white = unchanged, and yellow-brown = deposition. The darkest patches in (b) and (c) are due to incomplete correction for vegetation. In each panel, left = river inflow, right = the sea, and top right corner depicts the cumulative number of tidal cycles that the experiment was run, with the end stage in the final panel of each column. A small part of the flume was not captured by the zSnapperTM, so elevation data for the uttermost left and right side of the flume (top and bottom in each panel) is missing (after MSc thesis by K. van den Hoven).

vegetation (Veg +) created a dynamic system in which channels and bars evolved and adapted. The estuary with sparse vegetation evolved in a river-dominated and tide-dominated part (Suppl. Fig. 4.23).

The pilot runs contributed to the experimental set-up in the Metronome. In the pilot runs, differentiation of vegetation settlement was limited as both types of seeds were able to settle in similar locations, so in the Metronome experiments the smaller *Veronica beccabunga* was added to represent pioneer vegetation settlement. The pilot dense vegetation run showed it is important not to provide too much vegetation into the evolving estuary at once. Therefore, relatively small amounts of seeds were sowed through the river and tidal inlet in the Metronome. In addition, discharge was increased to enable continuous river flow through dense vegetation. In contrast to the pilot runs, extreme bayhead delta formation was limited in the Metronome by reducing fluvial sediment supply and adding marine sediment supply. Marine sediment was supplied by erosion of the sand barriers and by walnut input at the tidal inlet.

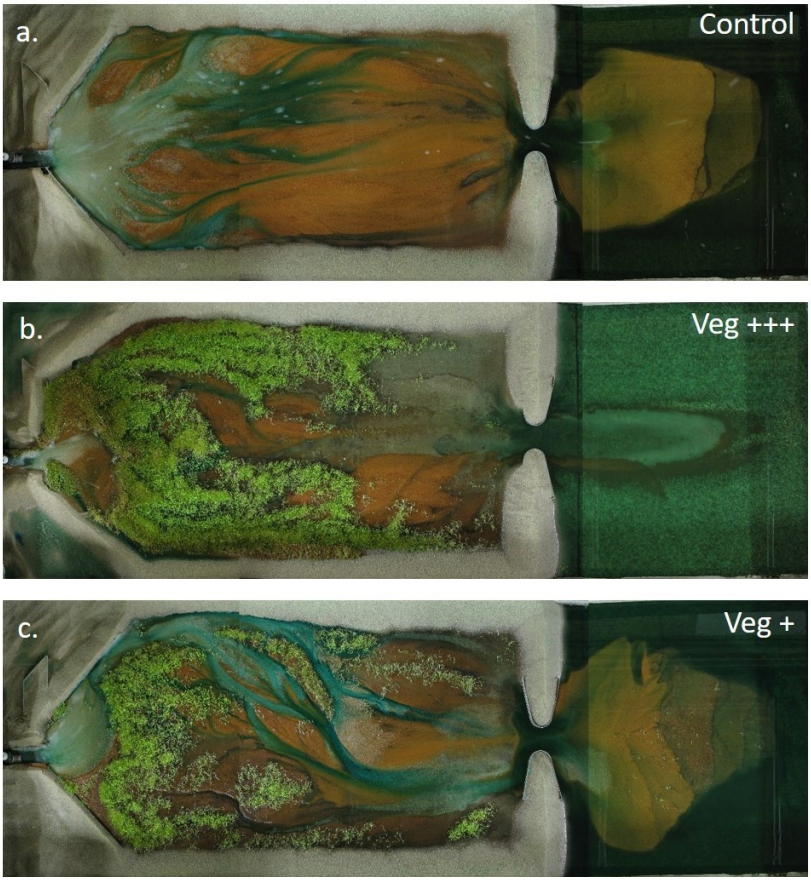

Figure 4.22 Flume top view for the (a) control run at 2,810 tidal cycles, (b) dense vegetation run at 1,595 tidal cycles, and (c) sparse vegetation run at 2,968 tidal cycles. Left is river inflow, right is sea with ebb tidal delta. Blue dyed water indicates channels (after MSc thesis by K. van den Hoven).

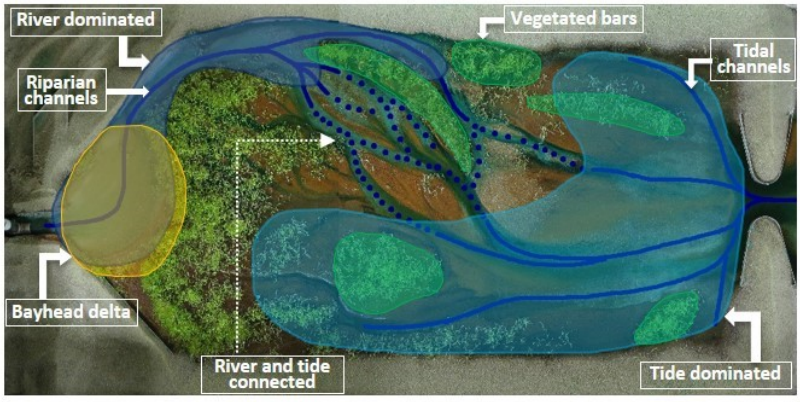

Figure 4.23 Estuary overview of experiment with sparse vegetation at tidal cycle 2,968 (after MSc thesis by K. van den Hoven).

Supplement 4.3: Algae and fungi protocol

Algal blooms were suppressed in the Metronome. 100 ml of anti-algae Algofin was added to the flume twice a week. Also, a bio-filter with active carbon was installed and outflow filters at either end of the flume were cleaned every time the flume was drained for scans so as to mitigate the growth of algae. Overall, algae had an insignificant effect on the morphodynamics, in line with Friedkin bank erosion tests under similar conditions in previous studies (Braat et al., 2019a).

In contrast, fungal growth posed a more serious problem to the morphological development in experiments with crushed nutshell. Fungi flourished in shallow regions of the estuary, especially when the flume was not tilting during scans and during days of vegetation sprouting. Consequently, the tops of tidal bars became very cohesive, more than could be attributed to the nutshell alone. This complication resulted in large scarps up to 2 cm when part of these bars were eroded, which occurred predominantly, but not exclusively, on tidal bars covered by nutshell in the upstream part of the estuary. Additionally, the threshold for motion was enhanced in the upstream part of the estuary by the fungi as the experiment progressed, which likely contributed to lower dynamics in later stages of development.

The growth of fungi was counteracted in two ways. Firstly, Pimafix^{TM} was added to the nutshell feeders to prevent fungi from flourishing inside the crushed nutshell. Second, the estuary bed was sprayed with water with low concentrations of tea tree oil and Pimafix^{TM}. Such spraying was done three times in the second experiment (sand and mud); intervals of no flow were relatively short, so fungal growth did not take large proportions. However, in the third experiment (sand, mud and vegetation) tilting was off repeatedly for four days to allow vegetation sprouting. To prevent fungi growth during the no-tilting periods, the upstream part of the estuary and brownish spots were sprayed every time the flume had been drained.

Supplement 4.4: Cross-sections over the bay-head delta

Suppl. Figs. 4.24 and 4.25 show cross-sections over the bay-head delta for x = 80, 120 and 160 cm. The mud experiment (Suppl. Fig. 4.24) clearly shows alternating layers of mud and sand. Mud abundance increases towards the valley edges and in the downstream direction on the bay-head delta. This trend is in contrast to the mud and vegetation experiment (Suppl. Fig. 4.25), where vegetation diverted flow and caused large spatial differences in mud and sand deposition. Therefore, there are fewer clear continuous mud layers in the subsurface and more local thick mud deposits, for example on the left in all cross-sections in Suppl. Fig. 4.25.

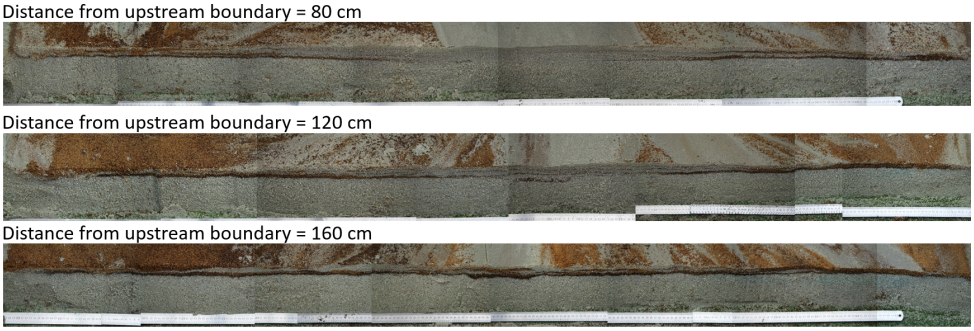

Figure 4.24 Cross-sections over the bay-head delta at x = 80, 120 and 160 cm in the mud experiment. Photos were taken facing the upstream direction. The top part of the cross-sections is the pristine surface.

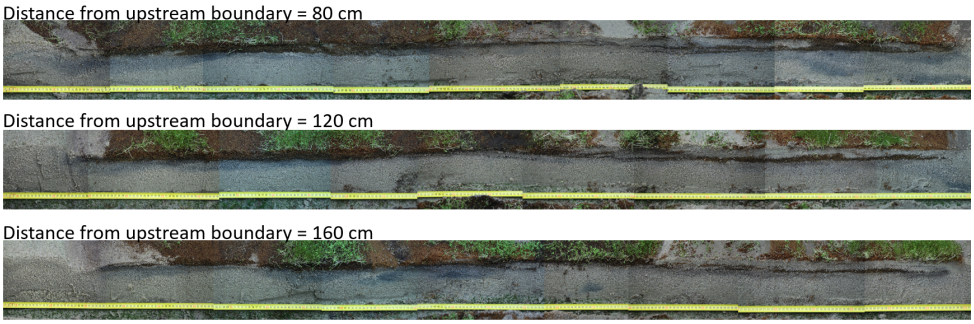

Figure 4.25 Cross-sections over the bay-head delta at x = 80, 120 and 160 cm in the mud and vegetation experiment. Photos were taken facing the upstream direction. The top part of the cross-sections is the pristine surface.


5

Chapter 5 | The effect of sea-level rise on estuary filling in scaled landscape experiments

Abstract

When sea-level rise slowed down in the middle Holocene, many estuaries filled the newly created accommodation, whilst others remained largely unfilled because of limited sediment supply. In view of the current and future rapid sea-level, the question arises how these systems will adapt and whether the land-level rise may keep up. Besides geological data and conceptual models of large-scale and long-term estuary infilling, little is known about the infilling process during sea-level rise on the decadal-to-centennial time scale that is relevant for society, for example in terms of prospected safety against coastal flooding. This study focuses on how sea-level rise affects the morphological and hydrodynamic development of infilling estuaries. To this end, scaled laboratory experiments were conducted in a tilting flume facility that creates bidirectional tidal currents and develops entire estuaries. A net importing estuary with sand, mud and vegetation was formed that was subjected to sea-level rise. Findings show that the bulk of imported sand deposited closer to the tidal inlet following sea-level rise than in an experiment without sea-level rise. The bay-head delta and the flood-tidal delta retained enough sediment to keep up with sea-level rise, whilst the tidal embayment in between drowned except for the highest vegetated bars. Sea-level rise also reduced vegetation survival and sprouting potential, as prolonged inundation increased mortality, negating the potential eco-engineering effect. This resulted in lower vegetation coverage with sea-level rise than under constant sea-level. These findings suggest that fast sea-level rise may cause natural systems to drown even if nearly sufficient sediment is available to fill the newly created accommodation, particularly the reach further away from the fluvial and marine sediment sources.

In review as: Weisscher, S. A. H., Adema, P. H., Rossius, J.-E. & Kleinhans, M. G. The effect of sea-level rise on estuary filling in scaled landscape experiments *The Depositional Record*

5.1 Introduction

During the Middle Holocene, many coastal regions drowned in response to rapid sea-level rise, which produced many estuaries around the world (Shi and Lamb, 1991; Hijma and Cohen, 2010; Vos, 2015; Job et al., 2021). In response to sea-level rise levelling off, part of these estuaries gradually filled and formed new land, whilst others only partly filled or remained unfilled (e.g. Roy et al., 1980). Conceptual models of estuary filling exist (Roy et al., 1980; Nichol, 1991; Dalrymple et al., 1992) but are inferred from the depositional record and focus on (multi)-millennial timescales. Generalised responses of estuaries to multi-millennial phases of sea-level rise and fall allow for two-dimensional predictions of lithofacies distributions, showing phases of coastal regression when the system shifts seaward and transgression when the system shifts landward. So, these qualitative models focus on the large-scale spatial and temporal development of filling estuaries and are therefore too general to determine changes in channel and bar patterns. Therefore, it remains unclear how the morphology on a scale of channels and bars in filling estuaries is affected by sea-level rise.

5.1.1 Holocene filling of tidal systems

Estuary filling depends on the following initial and boundary conditions and processes. Firstly, sediment is needed to fill an estuary, which is delivered by rivers and may be imported from the sea. Flood-dominant tidal asymmetry ensures that more sediment remains in an estuary and enhances sediment import from the sea (Friedrichs and Aubrey, 1988), contributing to estuary filling. Secondly, the eco-engineering effect of vegetation (De Haas et al., 2018; Brückner et al., 2019; Brückner et al., 2021; Chapter 4) increases the sediment trapping potential of estuaries, enhancing sediment retention. Mud helps fill accommodation and stabilises bar and channel positions (Braat et al., 2019a; Brückner et al., 2021). Thirdly, initial and boundary conditions such as inherited topography, subsidence, tidal amplitude at the estuary mouth and planform shape are also controlling estuary morphology (Leuven et al., 2019).

The Holocene evolution of the Dutch coastal landscape can serve as a case study for infilling systems under rapid sea-level rise conditions. Back-barrier basin deposits, e.g. like the Wadden Sea (NW Europe), are preserved in the coastal plain of the western Netherlands. The tidal basin morphology before 5,000 BP shows a system with moderate sediment supply, adjusting to rapid sea-level rise. At first, mostly sand is deposited in and along the channels. Later inter-channel areas rich in mud formed, stabilising the channels. Reed marshes concentrate along the basin margins and salt marshes are limited to the along channel mud flats and behind the barrier. Sea-level rise slowed down between 6,000 and 5,000 BP. At this point in time, sediment supply exceeded accommodation creation and the basin started to fill (Van der Spek and Beets, 1992). Only one tidal inlet was still open between 4,500 and 3,500 BP, followed by complete retreat of the sea from the basin by 3,275 BP (Roep and Van Regteren Altena, 1988). From nearly 100 years of bathymetric measurements in the Wadden Sea area, it shows that the tidal basin is currently importing enough sediment to keep up with sea-level rise. However, most imported sediment is being eroded from the ebb-tidal deltas seaward of the many tidal inlets, which decreases the sizes of these deltas. Sediment availability will likely determine if in the future the basin can silt up to keep up with sea-level rise or if it will drown. Because of the artificial hard barriers on the basin and barrier side, the coastline and barrier retreat and roll-over mechanisms will not occur (Van der Spek, 1994; Elias et al., 2012).

For the Netherlands, reconstructions of the coastal landscape and tidal systems were made for the Holocene (Vos, 2015; De Haas et al., 2018) (Fig. 5.1). The reconstruction by De Haas et al. (2018) highlights the importance of vegetation and mud in long-term estuary dynamics, as well as the necessity of having a river inflow that ensures the tidal inlet remains open. Most estuaries along the Dutch coast remained partly filled for most of the late Holocene despite ongoing (but slowing) sea-level rise, because of tidal asymmetry. The M4 tidal component on the North Sea leads to flood dominance in

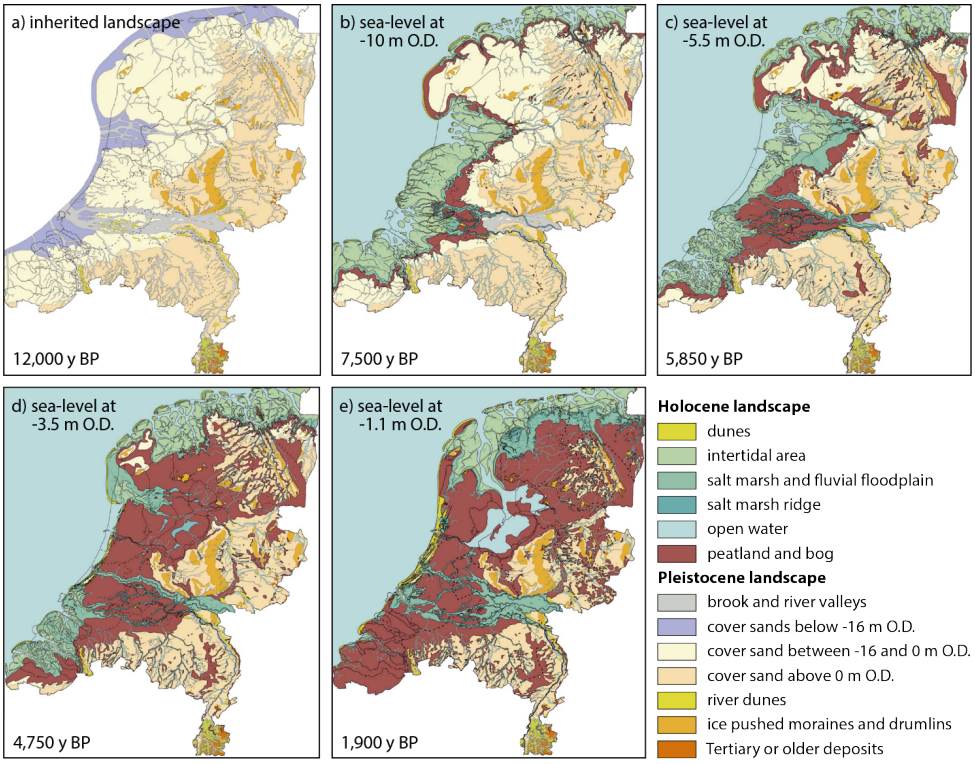

Figure 5.1 Evolution of the Dutch landscape from 12,000 BP to 1900 BP. Modified from Vos et al. (2018).

tidal systems, which brought sediment from the shallow sea floor into the estuaries and allowed these systems to keep up with sea-level rise (De Haas et al., 2018).

5.1.2 Accommodation and sediment supply

Long-term numerical modelling of estuaries showed that mud fills accommodation by stabilising bars and confining flow in channels (Braat et al., 2017; Brückner et al., 2021). This reduces channel and bar dynamics and confines the estuary with mudflats flanking the outer banks of an estuary. Moreover, tidal prism is reduced, which could promote a positive feedback loop of filling accommodation. Combination of mud, poorly sorted sand, vegetation and variations in water discharge (i.e. floods and tides) was found to form levees and crevasses, which also retain sediment (Boechat Albernaz et al., 2020). An increase in flood storage due to sea-level rise can cause flood dominance and import of sand from the ebb-tidal delta and adjacent coast, which mainly holds for shallow tidal basins (Du et al., 2018). Leuven et al. (2019) showed that small estuaries dominated by intertidal bars will likely face rapid sedimentation under sea-level rise, whilst large estuaries may face sediment starvation and drown.

There are very few scaled landscape experiments of tidal systems that include sea-level rise. The experiment by Stefanon et al. (2012) shows that sea-level rise enlarges the tidal channels and increases their cross-sectional area. Sea-level rise had a negligible effect on the overall channel and bar pattern, but this may be due to the low sea-level rise rate or the low sediment mobility in their experiment. To get a better understanding of possible morphological developments in estuaries that face sea-level rise,

this review turns to river delta experiments where the effects of sea-level rise have been more extensively investigated.

River delta experiments with sea-level rise demonstrated that the balance between sediment supply and accommodation creation determines the avulsion behaviour and stacking pattern of deltas (Van Heijst and Postmal, 2001; Paola, 2000; De Villiers et al., 2013). Sea-level rise reduces flow and sedimentation upstream from the coastline due to the backwater effect. This results in a delayed response in the downstream reach of a delta (Van Heijst and Postmal, 2001), which may range from a few kilometres for high-gradient rivers up to more than a hundred kilometres for the largest low-gradient rivers (Blum and Törnqvist, 2000; Hoyal and Sheets, 2009). On a scale level above that of individual channels and at a scale of the entire delta surface, delta experiments indicated that a step-wise retreat of delta lobes during transgression (i.e., autostepping) is largely unrelated to upstream processes, including sediment input and water discharge, and is mainly caused by sea-level rise (Muto and Steel, 2001). The steps can form by lobe avulsions followed by a short period of reduced transgression, or even limited progradation, in an overall transgressive system. Similar behaviour was found for Martian deltas in crater lakes in response to lake filling (De Villiers et al., 2013). The generic insight learnt from these experiments is that back-stepping occurs in a drowning environment, which from a sedimentary perspective still leads to sediment deposition whilst from the perspective of land formation, drowning is the same effect as erosion.

The limited number of scale experiments of estuaries with ongoing channel and bar dynamics (Leuven et al., 2018b; Braat et al., 2019a; Kleinhans et al., 2022; Chapter 4) highlight the effects of mud and vegetation on channel and bar dynamics. Both mud and vegetation reduce tidal prism by elevating bars and confining channels. As vegetation limits flow over bars, flow becomes focused in deeper channels that tend to migrate faster (Kleinhans et al., 2022). So far, only the experiments in Chapter 4 produced net filling estuaries, developing from a drowned wide river valley. Especially vegetation proved effective at confining the collective subtidal channels in the upstream direction, whilst mud and vegetation filled accommodation mainly in the upstream half of the estuary. This resulted in high bars and new land, which contributed in a positive feedback loop to a linear-to-concave decrease in tidal prism in the upstream direction. Put differently, this development suggests that mud and vegetation enable bars to grow above the water table. Depending on the balance between sediment supply and the sea-level rise rate, these areas could potentially keep up with mild sea-level rise or could exhibit reduction in analogy with back-stepping.

5.1.3 Objective and hypotheses

The objective is to determine the effects of rapid sea-level rise on the morphological response of an filling estuary. To this end, laboratory experiments were conducted wherein entire estuaries were formed with sand, mud and vegetation on an initially drowned river valley. By design, the experiment was set up to receive slightly less sediment than needed to compensate for new accommodation created by sea-level rise. Hypothetically, this left three possible scenarios of morphological response. Firstly, the entire system may drown, with subtidal areas rapidly expanding at the expense of intertidal and supratidal areas. Secondly, parts of the system may aggrade to maintain a stable average depth, whilst other parts further away from a sediment source will drown (i.e., the central part of the estuary). Thirdly, the system may shift landward. Then, channel and bar patterns will shift upstream, provided there is enough space. This scenario likely means the drowning of the downstream part of the estuary.

5.2 Methods and materials

This study presents the findings of two scaled landscape experiments of estuaries in which the effect of sea-level rise was isolated. The first experiment was a control without sea-level rise of a filling estuary with sand, mud and live vegetation. This control experiment was also reported in Chapter 4, in which it was found that mud alone and vegetation with mud quickened the building and raising of new land as compared to an experiment with only sand. The novel, second experiment was a filling estuary with sea-level rise but otherwise the same conditions.

5.2.1 Flume experiments

The experiments were done in the "Metronome", a 20 m long and 3 m wide flume that drives tidal currents by periodic tilting over its short central axis (Kleinhans et al., 2017b). This novel tilting method solves a number of scale problems that former experiments with periodic sea-level fluctuations experienced, such as ebb-dominance and very low sediment mobility (e.g. Reynolds, 1889; Stefanon et al., 2010; 2012). To date, the tilting setup enabled the development of tidal basins (Kleinhans et al., 2015b), ingressive estuaries with sand (Leuven et al., 2018b), mud (Braat et al., 2019a), vegetation (Kleinhans et al., 2022) and channel dredging (Van Dijk et al., 2021), as well as filling estuaries with mud and vegetation (Chapter 4).

The initial setting of the experimental estuaries resembled an idealised drowned river valley with an open barrier coast and a long lagoon relative to the tidal excursion length (Fig. 5.2), designed to be similar to Chapter 4. In a sand bed of 17 m long, 3 m wide and 0.11 m thick, a flat-floored valley was carved of 2.4 m wide by 0.03 m deep over the full length of the sand bed. The initial sand bed had a median grain size $d_{50} = 0.55$ mm and a coarse tail of $d_{90} = 1.2$ mm to prevent the development of unrealistically large scours (Kleinhans et al., 2017a). The tidal inlet was bordered by two large, sandy barrier islands which were designed to erode over time and act as a source of marine sediment, as alongshore drift was impractical to reproduce in the flume. The flume had an offset tilt of 0.001 m/m, which is a typical fluvial valley slope in landscape experiments (Kleinhans et al., 2014a). A central, straight river channel in the upstream reach of the control experiment had a negligible effect on channelising river flow (Chapter 4) and was therefore left out in the new experiment with sea-level rise.

The boundary conditions were conducive to filling of the estuary. The flume was tilted with a 40 s tidal period and an overtide of 20 s for flood dominance. The tilting slope amplitude of the principal tide was 0.0012 m/m and the overtide had an amplitude of 0.006 m/m with a phase difference of 90°. Combined with the initial offset slope of 0.001 m/m, this resulted in a maximum slope of 0.0062 m/m in the upstream direction during flood and 0.0058 m/m in the downstream direction during ebb. At the downstream boundary, a weir moved in the opposite phase of the flume tilting to ensure a constant water head at sea to prevent a water surge during flood and channel incision during ebb. Also, a horizontal paddle generated waves with a frequency of 2 Hz and an amplitude of about 3 mm (for scaling, see supplement to Leuven et al., 2018b). At the upstream boundary, a river discharge of 900 L/h entered the estuary during ebb with a feed of sand and mud, both at a rate 0.4 L/h. Mud was simulated as crushed walnut shell with a density of 1350 kg/m^3 and a grain size ranging from 0.45 to 1.7 mm, conform to previous studies (Baumgardner, 2016). Mud was also added at 0.4 L/h at the tidal inlet at the start of every flood to simulate fines from the sea.

Sea-level rise was implemented in the new experiment in 1 mm increments every 1,000 tidal cycles, starting from 3,000 cycles. This culminated in 7 mm sea-level rise by the end of the experiment at 10,000 cycles, which corresponds to approximately a 12 % water depth increase of the 60 mm deep tidal inlet channel. Accordingly, a volume of 45 L of accommodation was created every 1,000 cycles, which was by design slightly larger than the total sediment feed (±13 L sand and mud) plus the maximum

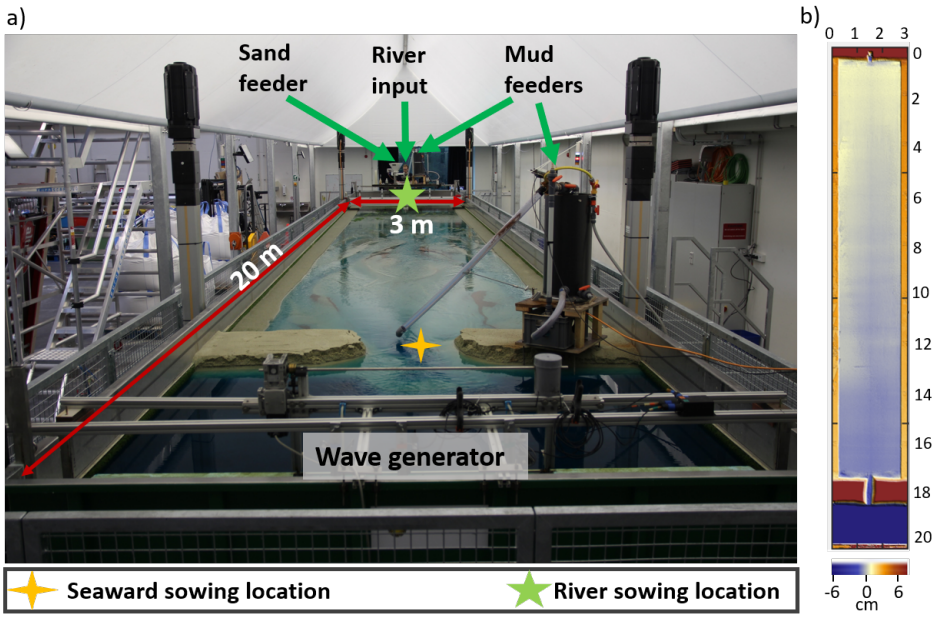

Figure 5.2 (a) Experimental setup of the experiment. The photo was taken at 2,000 cycles into the sea-level rise experiment. (b) Digital elevation model of the initial bathymetry of the experiment.

potential barrier erosion of 25 L. Therefore, based on the filling and creation of accommodation, a slightly transgressive estuary was expected to develop.

5.2.2 Seed distribution

Three vegetation species were selected with different eco-engineering effects in a laboratory scale experiment (Lokhorst et al., 2019): *Medicago sativa*, commonly known as Alfalfa, *Lotus pedunculatus* and *Veronica beccabunga*. Alfalfa represented riparian vegetation, and *Lotus* and *Veronica* resembled reed- and grass-like marsh vegetation (Lokhorst et al., 2019). Seeds were supplied every 500 cycles after an initial 1,000 cycles spin-up, before which no intertidal area existed where vegetation could establish. The number of seeds was calculated to obtain an average coverage with significant vegetation-induced flow resistance by the end of the experiment at 10,000 cycles with an average stem density of 0.25 stems/cm^2. In total, 80,000 Alfalfa seeds and 40,000 seeds of both *Lotus* and *Veronica* were supplied to the river and 40,000 seeds of *Lotus* and *Veronica* supplied to the inlet. This amounts to a total of 240,000 seeds on an approximate surface area of 2.4 by 17 m, or a maximum seeding density of 0.59 seeds/cm^2. With a germination probability of 0.5 and a possible fraction of the surface covered by vegetation, say 0.2, this would amount to 1.5 stems/cm^2, this would about double the total flow resistance in vegetated areas compared to the bare bed surface (Lokhorst et al., 2019), which is sufficient to affect the partitioning of flow over vegetated and bare areas (Kleinhans et al., 2022). While this is about half the number of seeds of *Lotus* and *Veronica* compared to the experiment in Chapter 4, the actual plant density is mainly limited by air temperature, mould, and seed loss by burial, which we managed to control better in the second experiment. Moreover, vegetation settling and mortality are mainly determined by inundation duration, which is linked to the degree to which estuary filling can keep up with sea-level rise, and by erosion due to morphodynamics, which is also linked to depth. Increased trapping is less likely in the present setup, which is flood-dominant and

captures most sand and mud anyway (Chapter 4). As such, vegetation is mainly expected to affect, and be affected by, the pattern and dynamics of the tidal bars.

Each sowing event took 70 tidal cycles to enable distribution of seeds by the flow but avoid most loss, similar to the protocol in Chapter 4. After 10 cycles for initial wetting of the bed following bed scans, pre-soaked seeds were released in the river outlet over 25 cycles. Next, seeds were added just upstream of the inlet during the flood phases over the course of 10 cycles, followed by a final 25 cycles to allow the seeds to spread throughout the estuary. The flume was then stopped at its offset slope of 0.001 m/m for four days to allow for sprouting before the experiment could continue. During sprouting time, the sea was at the current mean sea-level and a low 300 L/h river discharge entered the estuary to produce throughflow.

5.2.3 Data analysis

Orthophotos and digital elevation models (DEMs) were made every 1,000 tidal cycles by means of stereo-photography of the dry bed. Before shooting stereo photos with a digital single-lens reflex camera, the Metronome was drained slowly without disturbing the bed. The images were processed in Agisoft Metashape (structure-from-motion software) to create DEMs with a 5 by 5 mm resolution. Most vegetation, apart from dense patches on the bay-head delta, was filtered out using a low-pass 5% (percentile) filter with a 35 by 35 mm window. To quantify the hydrodynamics, tidal flow was modelled using the numerical model Nays2D (Chapter 3) following the method in Chapter 4. Nays2D takes as input a DEM and the corresponding boundary conditions and produces maps of water depth and flow velocity, from which inundation duration and distributions of flow velocity were calculated.

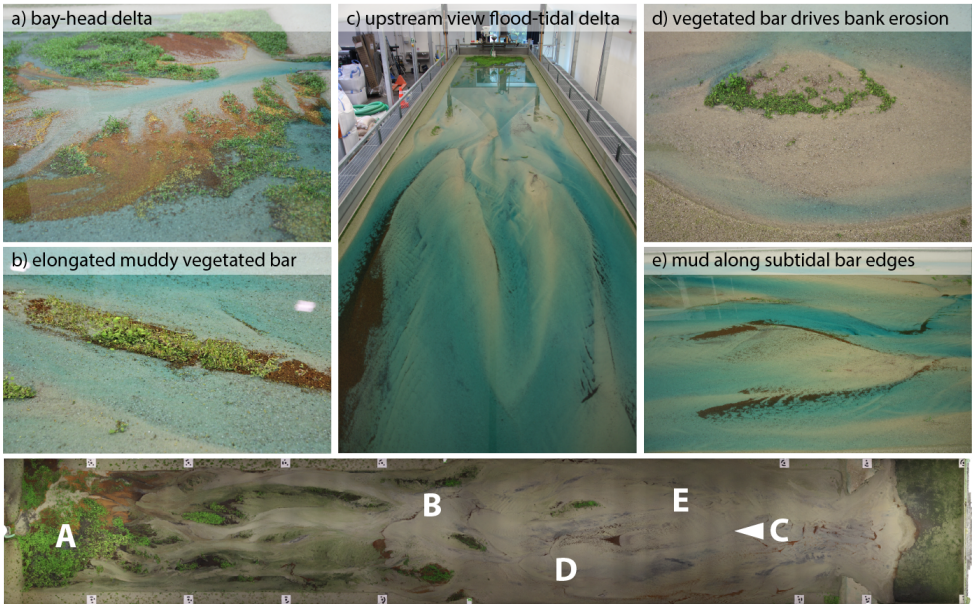

Figure 5.3 Photographs of mud and vegetation in the sea-level rise experiment. Letters in the orthophoto correspond to positions of the photographs.

5.3 Results

5.3.1 General estuary development

The general development of the estuary with sea-level rise is described as follows. At first, short discontinuous tidal channels, separated by low-amplitude bars, formed in the downstream half of the estuary (Fig. 5.4). From this initial low-amplitude, submerged channel and bar pattern, a large flood-tidal delta developed near the tidal inlet together with a small ebb-tidal delta barely extending into the sea. Continued inlet widening by the waves and the incoming tide eroded sediment that was predominantly transported onto the flood-tidal delta. Meanwhile, the upstream, landward half of the estuary remained largely unaltered in the first 3,000 tidal cycles, apart from a vegetated bay-head delta forming from the landward boundary (Fig. 5.3). At first, Alfalfa established on the bay-head delta within the first 1,000 tidal cycles, followed by *Lotus* and *Veronica* whose seeds were either germinating slower, captured by existing vegetation or transported to other low-energetic regions on the bay-head delta. Shortly after vegetation establishment, a first avulsion occurred on the bay-head delta at 2,000 cycles, resulting in a new main channel with several active branches.

After sea-level rise commenced at 3,000 tidal cycles, the focus of sediment deposition remained on the bay-head delta (x=0–3 m) and the flood-tidal delta (x=10–17 m) throughout the experiment (Figs. 5.4, 5.5b). Most fluvial sand and mud was retained and protected by the dense vegetation, whilst most marine sand and mud elevated the flood-tidal delta. Hence, only little sediment was transported further upstream. Upstream transport commenced mainly in the form of lobate bars, or terminal lobes, at the upstream ends of landward extending tidal channels (Figs. 5.4, e.g. from 10 to 8 m at 1,000 to 3,000 cycles), landward of which the basin morphology hardly changed. The little sediment imported beyond the flood delta was not nearly enough to avoid the drowning of the initially already deep subtidal bay in the range x=3–8 m (Figs. 5.4, 5.7f,h). This region remained largely subtidal until 6,000 cycles (Fig. 5.7d,f). The few intertidal and supratidal areas that formed along the estuary where sparsely colonised by *Lotus* and *Veronica* (Fig. 5.3) and covered with mudflats. Yet, most mud was

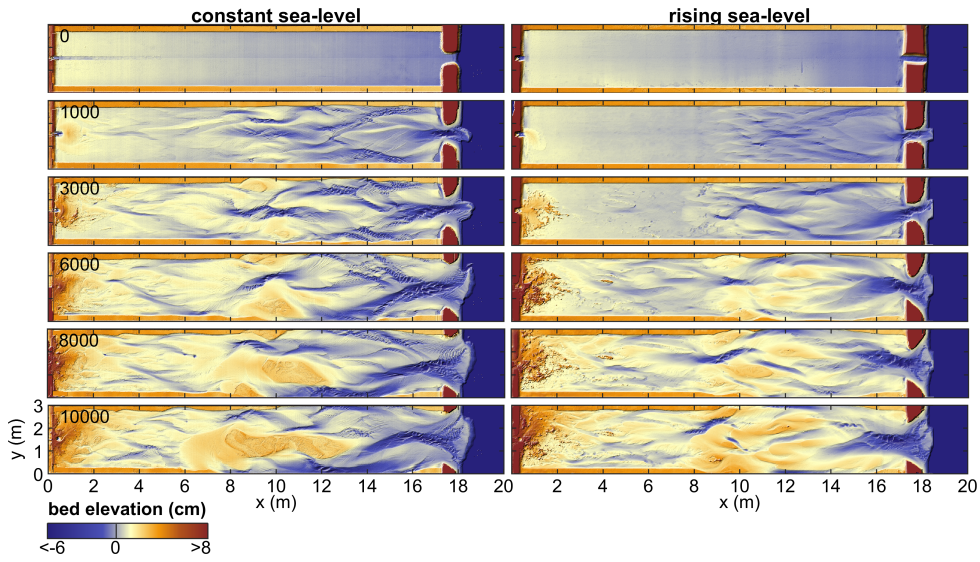

Figure 5.4 Digital elevation models of the experiments with a constant sea-level (left column) and with sea-level rise (right column), excluding vegetation.

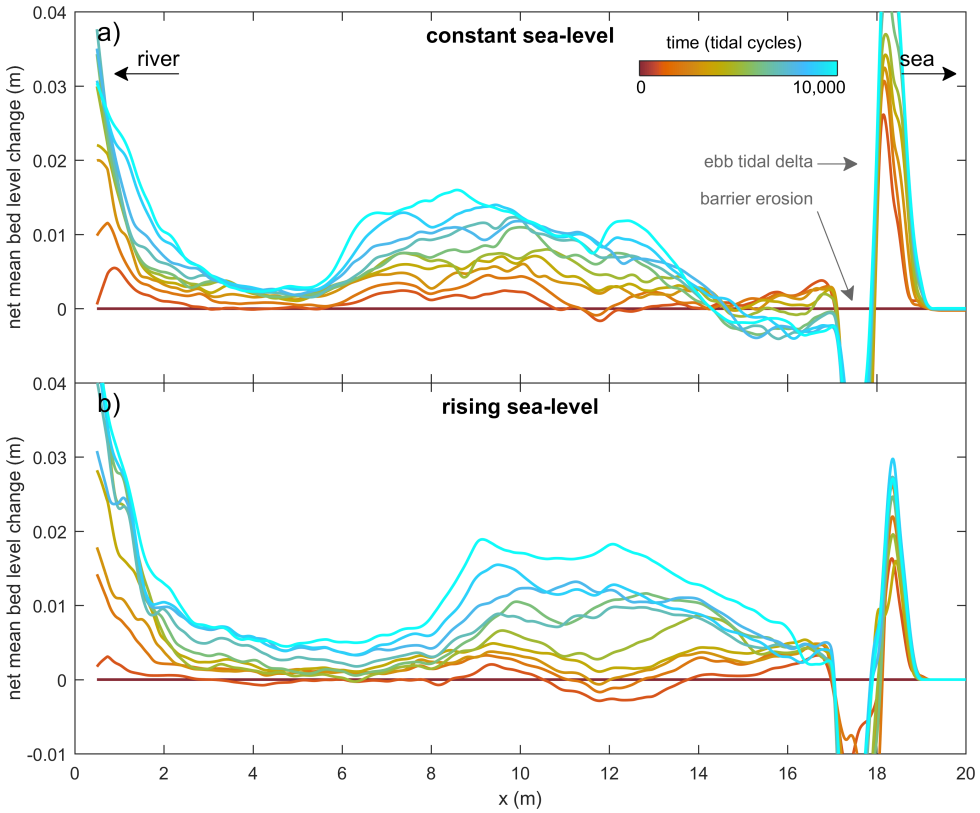

Figure 5.5 Mean bed level change (a) along the experiment with constant sea-level (Chapter 4) and (b) the new experiment with sea-level rise. Calculations exclude the unreworked outer banks of the estuary.

overridden by migrating sand bars and preserved in the subsurface. Also, prolonged inundation due to sea-level rise caused considerable mortality of the vegetation on the bay-head delta and bar tops.

From 6,000 tidal cycles onward, the estuary developed increasingly more intertidal area. This created new sites for vegetation establishment and mudflat deposition just downstream of the bay-head delta and near the flood-tidal delta (Fig. 5.3). Yet, only very few muddy and vegetated bars elevated into the supratidal elevation reach. Generally, vegetation near the flood-tidal delta seemed sparser and on average younger than near the bay-head delta, suggesting a faster turn-over rate of intertidal vegetation. Also, a large channel confluence had formed around $x = 10$ m, which deepened and produced a pulse of sediment further upstream into the deep subtidal bay at x=3–8 m (Figs. 5.4, 5.5b). This caused slightly higher bed levels in the upstream half of the estuary but was largely insufficient to reach an intertidal elevation.

5.3.2 Effect of sea-level rise

Comparison with the constant sea-level experiment shows that sea-level rise impacted the morphological development in the following ways. Firstly, sea-level rise created new accommodation that prompted the bulk of imported marine sediments to be deposited closer to the tidal inlet (Fig. 5.4). Consequently, less sediment was transported further upstream during the first 6,000 tidal cycles. Afterwards, the development of a large confluence landward of the flood delta in the sea-level

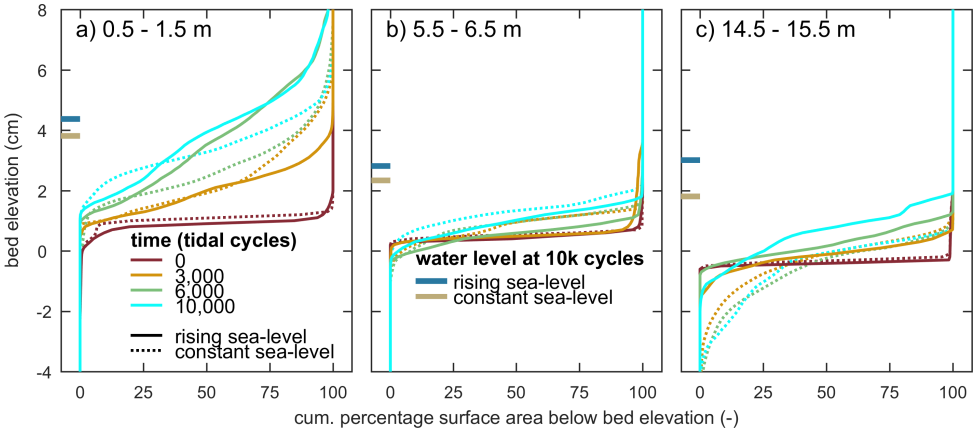

Figure 5.6 Development of cumulative bed elevation distribution for the experiment with constant sea-level and the experiment with rising sea-level (a) for the bay-head delta, (b) the drowned bay and (c) the downstream part of the flood-tidal delta. The bed elevation profiles exclude the unreworked outer banks along the estuary and include the valley slope. Mean water levels are given for the final time step at 10,000 cycles and derived from numerical modelling in Nays2D.

rise experiment scoured bed sediment that was transported towards the subtidal bay. Although this resulted in slightly higher mean bed elevations for the range x=3–8 m in the sea-level rise experiment, it proved insufficient to develop large intertidal and supratidal areas like in the constant sea-level experiment because of sea-level rise (Fig. 5.7).

Secondly, prolonged inundation time (Fig. 5.7) due to sea-level rise increased plant mortality and limited the area suitable for vegetation establishment. Consequently, less vegetation established and survived in the middle of the estuary, which concurred with faster channel migration and resulted in a net loss of vegetation in the second half of the experiment. In contrast, vegetation on the bay-head delta was more abundant in the sea-level rise experiment. However, this difference could also be due to the poorer control of mould in the experiment without sea-level rise. For the middle estuary (Fig. 5.8), the intertidal area nearly doubles for the sea-level rise experiments at the original sea level, whereas the intertidal area hardly changed when the constant sea level experiment was exposed to instantaneous sea-level rise as most loss in intertidal area was compensated for by the conversion of supratidal to intertidal. On the other hand, the loss of supratidal area under instantaneous sea-level rise was much larger than the gain of supratidal area for the sea-level rise experiment under the original sea level (Fig. 5.8), showing that the middle estuary aggraded higher under sea-level rise than under constant sea level, but with less supratidal and vegetated area.

Thirdly, flow velocity was on average larger with less spatial variation when a sea-level rise was imposed (Fig. 5.9), consistent with the expectation of drowning. As a further test of this notion, an equally large but instantaneous sea-level rise was imposed in the numerical model on the final bathymetry of the estuary experiment with constant sea-level. This resulted in so much deepening that supratidal area nearly disappeared and intertidal area was much reduced (Fig. 5.9i). Likewise, a numerical test of flow without sea-level rise imposed on the final bathymetry of the experiment with sea-level rise shows a considerable increase of intertidal and supratidal area along the entire estuary. The occurrence of larger flow velocities under sea-level rise point at reduced friction mainly due to larger water depths. Additionally, morphological complexity influenced the flow pattern, as the abundant intertidal and supratidal areas in the constant sea-level experiment (Fig. 5.7a-d) resulted in much more spatial variation in flow velocity than in the sea-level rise experiment (Fig. 5.7e-h). This was particularly clear for the subtidal bay in the range x=4.5–8.5 m (Fig. 5.9e-h).

5.4 Discussion

The experiment of a net importing estuary with sand, mud, live vegetation and sea-level rise showed that imported sediment stayed closer to its fluvial and marine sources than in a control experiment with constant sea-level (Chapter 4). As a result, the central estuary between the bay-head delta and flood-tidal delta drowned, and vegetation was mostly limited to the bay-head delta. Below, the trends in the experiments are compared to models and observations in various environments and implications are inferred for estuarine responses to future sea-level rise.

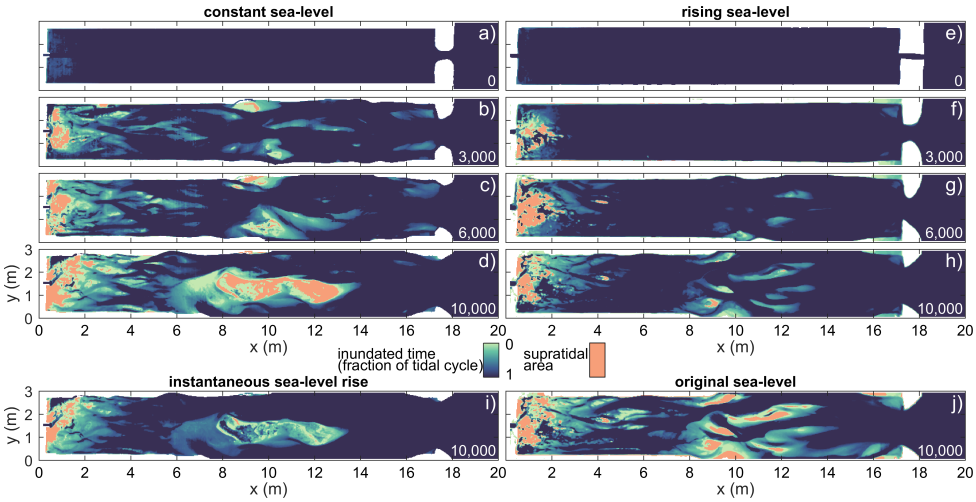

Figure 5.7 Maps of inundation duration normalised by the tidal period for the experiment with constant sea-level (left column) and the experiment with sea-level rise (right column). Panel (i) shows the inundation duration if an instantaneous 7 mm sea-level rise was imposed on the final time step of the experiment with constant sea-level. Panel (j) shows the inundation duration for the final time step of the experiment with sea-level rise if the original sea-level is imposed (i.e. an instantaneous 7 mm sea-level lowering).

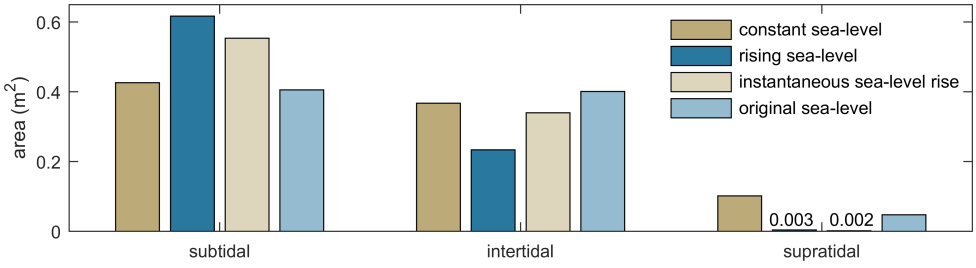

Figure 5.8 Effect of sea-level rise on subtidal, intertidal and supratidal area for the reach x=6–14 m, plotted for the final time step of the constant sea-level and the rising sea-level experiments. Also, the hypothetical distribution of the tidal zones are given for the constant sea-level experiment with instantaneous sea-level rise, and for the rising sea-level experiment with its original sea-level to cross-reference their development.

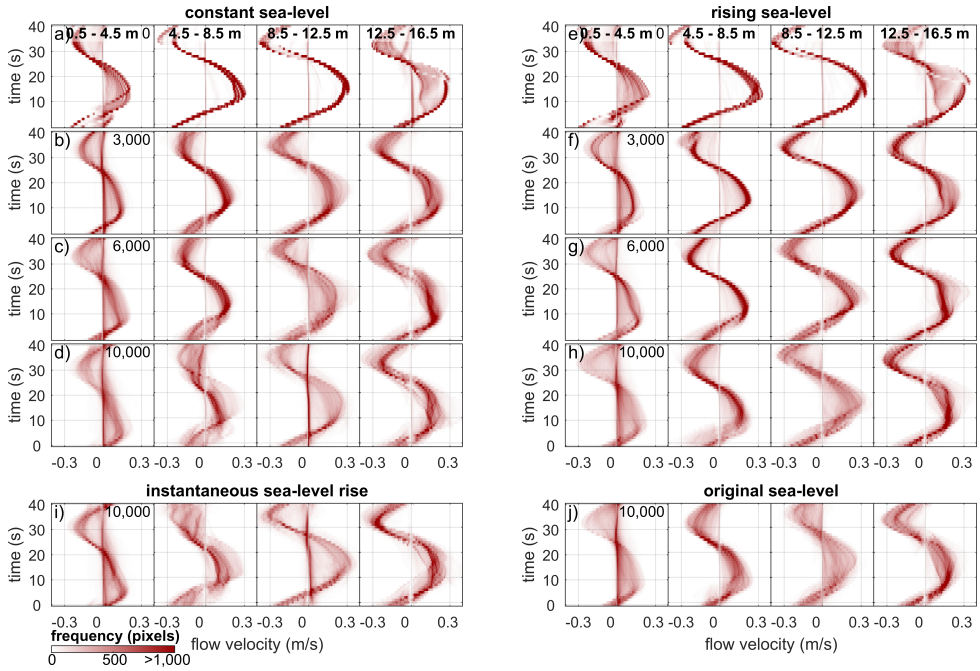

Figure 5.9 Distributions of flow velocity over time in four reaches along the estuary. Panel (i) shows the flow velocities if an instantaneous 7 mm sea-level rise was imposed on the final time step of the experiment with constant sea-level. Panel (j) shows the flow velocities for the final time step of the experiment with sea-level rise if the original sea-level is imposed (i.e. an instantaneous 7 mm sea-level lowering).

5.4.1 Estuary drowning

The experiment showed that sea-level rise influenced the locations for sediment deposition along an estuary (Figs. 5.4, 5.5). More specifically, the bay-head delta and flood-tidal delta continued to receive sediment from the nearby fluvial and marine sources, whilst the middle-to-upstream reach of the estuary experienced sediment starvation and drowned (Fig. 5.7). In the case of a constant sea-level, the development of bars was limited by water depth as shallower flow led to reduced sediment mobility and less vertical accretion. Hence, any additional imported sediment was transported further into the basin to drive land-level rise along the entire estuary. This limitation by water depth was also found for braided sand-bed rivers, in which bar complexes are predominantly formed by lateral channel migration (Van de Lageweg et al., 2013; Schuurman et al., 2013). However, braided rivers have ample sediment and about constant discharge for a given reach, whilst the experimental estuaries started unfilled and had a landward decreasing tidal prism. Therefore, vertical accretion in the middle estuary was also in part limited by sediment availability, especially so in the sea-level rise experiment where accommodation increased over time. Both the bay-head delta and the flood-tidal delta showed mild back-stepping under sea-level rise, caused by sediment deposition progressively closer to the sources of the river and the tidal inlet. This resulted in a clear disconnect between the fluvial and marine sediments in the middle estuary, which then drowned. This disconnect probably also explains why the subtidal channels did not collectively converge in the landward direction like in the constant sea-level experiment (Fig. 5.7) (Chapter 4).

Sea-level rise negated the eco-engineering effect of the vegetation and limited the area suitable for vegetation establishment. Accordingly, vegetated bars remained small, typically had a shorter lifespan

and were separated by subtidal channels. Although the number of *Lotus* and *Veronica* patches was larger under sea-level rise conditions, their collective abundance within the estuary was considerably smaller. Hence, the patches proved less effective at focusing tidal flow and increasing landward sediment transport as seen in the constant sea-level experiment. The patches promoted mud deposition at their rims and foreshores, yet neither mud nor vegetation was necessary for the settling of the other, conform to field data (Van der Wal et al., 2008) and numerical modelling (e.g. Brückner et al., 2019). This deposition pattern is similar to natural salt marshes (Vandenbruwaene et al., 2015; Schwarz et al., 2018), where mud deposition may quickly reduce onto the salt marsh, which sometimes results in topographical lows bounded by narrow levees. In nature, such a morphology is likely more prone to quick removal of vegetation by a rising sea-level and may also contribute to less suitable area for vegetation establishment after drowning (Mariotti and Fagherazzi, 2010).

Flow velocities increased and became more spatially uniform as the estuary drowned in the sea-level rise experiment. Such spatial uniformity is also found in natural unfilled estuaries, where flow velocity generally decreases upon entering a wide and deep subtidal bay (e.g. Roy et al., 1980; Dalrymple et al., 1992). In nature, tidal prism decreases in the landward direction, but in a tilting flume it can also increase (Kleinhans et al., 2017b). In both ingressive and infilling experimental estuaries, the tidal prism quickly develops a landward decreasing trend (compare Braat et al., 2019a and Chapter 4). However, in the experiment with sea-level rise, the infilling could not keep up and, as a result, the tidal action and morphodynamics may have been larger in the subtidal bay than expected in nature. Furthermore, the flood-tidal delta and the bay-head delta showed a tendency of back-stepping towards their respective sediment source, which seems unlikely to be caused by slightly larger tidal currents in the subtidal bay where the flow is much deeper than on the deltas. The new experiment indicates that also a flood-tidal delta may undergo a form of back-stepping or retreat closer to its source of marine sediment upon relative sea-level rise (Fig. 5.5). This retreat did not show distinct lobes that deltas form, which may relate to the tidal currents over the flood-tidal delta.

The estuary drowning in the experiment resembles palaeogeographic reconstruction cases of coastal drowning in the Early Holocene (e.g. Allen and Posamentier, 1993; Vos, 2015). An example that became progressively more unfilled in response to sea-level rise is the Gironde River valley during the Middle Holocene (Allen and Posamentier, 1993; Dalrymple et al., 1992). This system showed a clear disconnect between the marine flood-tidal delta and the more fluvial bay-head delta, with few intertidal flats and salt marshes bordering the subtidal bay. Nonetheless, the deep subtidal bay of the Gironde Estuary was largely muddy, which differs from the generally sandy subtidal bay in the experiments. This difference is likely due to a relatively smaller input of fines into the inlet and into the river combined with a large trapping efficiency of the vegetated bay-head delta in the experiment. Since the sea-level rise experiment was mainly shaped by tides and waves and only a little by the river, a more significant fluvial influence would probably result in a larger sediment flux towards the central estuary and slower drowning.

The experimental estuary was set in an initially wide drowned valley, which may respond differently to sea-level rise than confined estuaries. In wide drowned valleys, the erosive power of the tidal flow drastically reduces upon entering the estuary, which implies that estuary filling largely depends on fluvial and marine sediment input (Roy et al., 1980) and expanding salt marshes (e.g. Beets and Van der Spek, 2000; De Haas et al., 2018). Conversely, the converging shape of confined estuaries leads to strong flow velocities along an estuary. Therefore, estuary reaches that face sediment starvation are hypothesised to experience outer bank erosion to elevate bars and channels if fluvial and marine sediment supply is insufficient (Leuven et al., 2019), which requires further work.

5.5 Conclusion

Rapid sea-level rise causes imported sediment deposition closer to its marine and fluvial sources in scale experiments of infilling estuaries. Sea-level rise created additional accommodation, but insufficient sediment was transported beyond the river-fed bay-head delta and eroded from the coastal barriers to fill all accommodation despite an increased tidal discharge due to sea-level rise. Consequently, intertidal and supratidal areas mostly drowned in the central reach of the estuary. Locally, vegetation stabilised bars and facilitated vertical accretion, but sea-level rise compromised the eco-engineering effects of vegetation by longer inundation times and increased channel migration. Mud was mostly deposited on the bay-head delta and the declining intertidal flats. The hypothesis of a landward shift of depositional units was not observed in the sea-level rise experiment. Instead, sea-level rise caused sediment supply closer to its fluvial and marine sources, which resulted in the bay-head delta and flood-tidal delta keeping up with sea-level rise. Therefore, the central reach of the estuary received insufficient sediment to compensate for the newly created accommodation by sea-level rise and drowned. This suggests that keeping pace with sea-level rise not only depends on the sea-level rise rate, but also on the length of a tidal system and antecedent conditions such as river valley width.


6

Chapter 6 | Transitional polders along estuaries: driving land-level rise and reducing flood propagation

Abstract

Dikes are the conventional means of flood defence along rivers and estuaries. However, dikes gradually lead to the superelevation of waterbodies compared to the subsiding embanked areas, resulting in a rapidly increasing unstable situation under sea-level rise. Therefore, future flood management requires new, sustainable strategies that not only minimise flood risk, but also steer land-level rise. An example is a transitional polder, where a dike-protected area is temporarily reopened to the tide to capture sediment until it has risen well above mean sea-level, after which it could be returned to its original function. This study explores how the sequence of opening transitional polders affects sediment capture and large-scale estuary dynamics through 2D modelling in Delft3D. To this end, different opening sequences were tested along a large estuary, using the Western Scheldt (NL) as an example. Findings show land-level rise in all permutations. However, polders opened later in an opening sequence temporarily experience a lag in muddy sediment capture, most likely due to a deficit in fines. Opening polders located more upstream alone or at the start of an opening sequence generally causes a stronger reduction in mean tidal range than opening more downstream-located polders. This is explained by increased friction due to (1) locally added intertidal width and (2) shallowing of the main channels because of increased flood dominance. An upstream-to-downstream opening sequence caused the greatest reduction in mean tidal range, but this is negligible compared to the increase in tidal range due to historic dredging within the estuary for navigational purposes. Further work is needed to determine how dredging, closure of transitional polders and storm surges may negate this benefit to flood safety.

published as: Weisscher, S. A. H., Baar, A. W., Van Belzen, J., Bouma, T. J. & Kleinhans, M. G. (2022). Transitional polders between double dikes: driving land-level rise and reducing flood propagation. *Nature-Based Solutions*, 2, 100022, 15 pp.

6.1 Introduction

A rising sea-level, large peak discharges and land-subsidence pose an increasing flood risk for millions of people living along estuaries and coastlines (Syvitski et al., 2009; Minderhoud et al., 2017). Rivers and estuaries are commonly fixed and squeezed between dikes to protect the hinterland against flooding and to provide more arable and habitable land. However, dikes impede natural floodplain aggradation that would otherwise balance background subsidence (Berendsen, 2004; Kirwan and Megonigal, 2013; Auerbach et al., 2015), which may result in land subsidence that is worsened further by groundwater extraction practices (Syvitski et al., 2009; Minderhoud et al., 2017). As a result, water bodies become superelevated above the land (e.g. Chen et al., 2015), which strongly increases flood risk especially in light of future sea-level rise (Nicholls et al., 2018). So, the conventional management of mainly heightening and widening hard structures such as dikes is no longer a sustainable solution (Kiedrzyńska et al., 2015; Munsch et al., 2017; Schuerch et al., 2018). Hence, new strategies under the collective of "managed realignment" are being investigated that combine green and grey infrastructure to minimise flood risk and drive land-level rise through natural processes and natural ecosystems (e.g. Temmerman et al., 2013; Esteves, 2014; Zhu et al., 2020).

Managed realignment involves the landward relocation of a primary flood defence to an existing or new landward flood defence to restore tidal exchange on former embanked areas (French, 2006). This landward relocation of primary flood defences has been realised and studied for a variety of reasons (see for review: Esteves, 2014), including: flood protection (e.g. Symonds and Collins, 2007; Kadiri et al., 2011), increased intertidal habitat (e.g. Wheeler et al., 2008; Vuik et al., 2016), controlled tidal restoration (e.g. Cox et al., 2006; Oosterlee et al., 2020) and managed retreat (e.g. Abel et al., 2011). Tidal exchange may be restored by lowering, removing or breaching part of the former primary dike and can be regulated via culverts and sluices. Subsequently, tidal flows deliver sediment to the low-lying de-embanked land where it contributes to land-level rise. Corresponding rates of land-level rise range from a few millimetres to tens of centimetres per year and level off over time as the inundation period decreases (Temmerman et al., 2003; Morris, 2012). Yet, it has proven challenging to predict actual accretion rates and determine how these depend on e.g. sediment supply and salt marsh vegetation (e.g. Fagherazzi et al., 2012; Gourgue et al., 2022). Over time, sediment accretion contributes to the development of ecologically rich intertidal flats and salt marshes (Pethick, 2002; Woodruff et al., 2013). For example, managed realignment at the Sieperda polder (Eertman et al., 2002) and the Wallasea Island (Dixon et al., 2008; Kadiri et al., 2011) promoted the formation of high vegetated foreshores that stabilised the shoreline and reduced flood risk by attenuating waves and

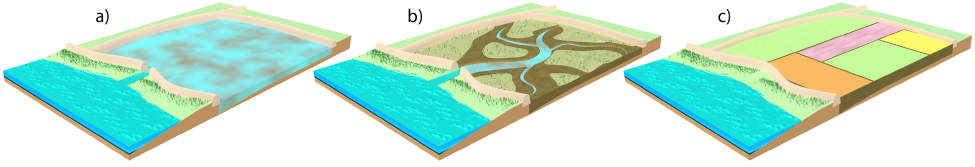

Figure 6.1 Conceptual box models of a transitional polder between double dikes. (a) Dikes inhibit sediment deposition and land-level rise on embanked land which may lead to subsidence and land elevations below sea-level. To cause land-level rise, transitional polders can be formed by artificially breaching a dike to reintroduce the tide. (b) As time progresses, sediment is net imported by tidal flow which elevates a transitional polder into an intertidal-to-supratidal reach. (c) After sufficient sediment import and land-level rise, the transitional polder may be closed off and returned to its original function, for example, as arable land. The inland dike remains the primary dike for flood defence, and the cycle of opening and closing may be started anew to keep up with relative sea-level rise.

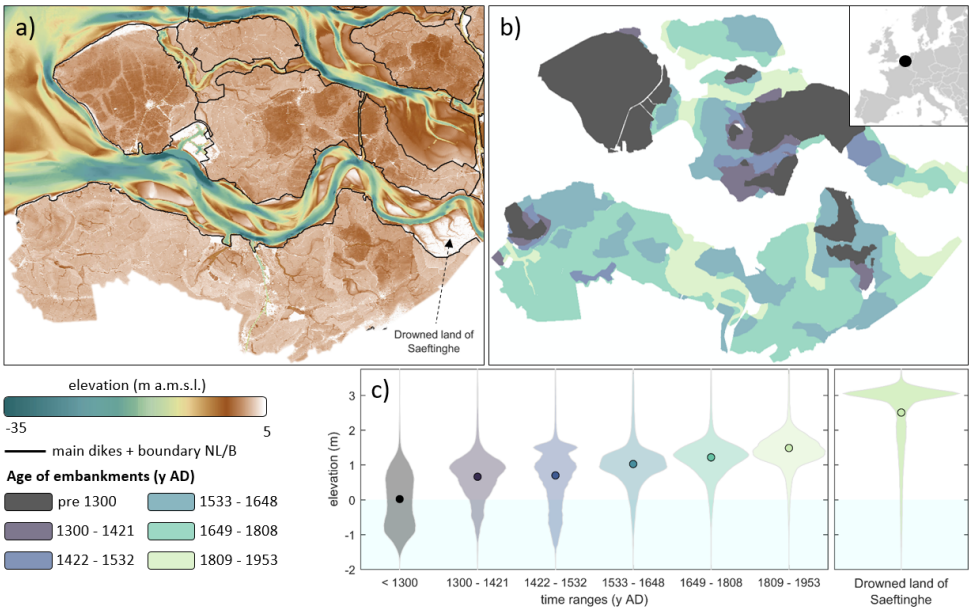

Figure 6.2 Overview of land reclamations along the Western Scheldt Estuary. (a) Map of bed elevation of the area near the Western Scheldt Estuary. Note that the highest bed elevations along the estuary are found outside the main dikes (exluding the barrier coast and the harbour near the estuary mouth). (b) Age of embanked areas along the Western Scheldt Estuary. Uncoloured regions represent unreclaimed land. The geographical location is given in an inset. (c) Violin distribution plots of bed elevations split per age of embankment, showing older polders have a lower bed elevation than younger ones. For reference, an unembanked salt marsh named "Drowned Land of Saeftinghe" is shown for comparison, which has a much higher bed elevation.

storm surges (e.g. Möller et al., 1996; Zhu et al., 2020). Nevertheless, many managed realignment sites have a lower biodiversity (Wolters et al., 2005; Mossman et al., 2012) and less diverse topography (Lawrence et al., 2018) compared to natural tidal marshes, which may be linked to rapid sediment accretion (Elschot and Bakker, 2016) and limited tidal exchange (Masselink et al., 2017). Alternatively, tidal exchange may be regulated such that sediment delivery is kept at a minimum, so the site of managed realignment acts as a floodbasin to reduce high water levels during storm surges, for example for the Kruibeke–Bazel–Rupelmonde polders along the Scheldt Estuary (Cox et al., 2006).

A novel strategy that resembles current managed realignment projects is the concept of a transitional polder between double dikes (Zhu et al., 2020; Van Belzen et al., 2021) and will be the focus of this study. Managed realignment sites are intended to remain open to the tide indefinitely to maintain their functions of e.g. flood protection and habitat (e.g. Pethick, 2002; Wolters et al., 2005; Esteves, 2014). So, the land is permanently lost for anthropogenic use, which can be problematic in low-lying deltas with limited space availability, where people do not want to give up valuable space. Hence, in contrast to managed realignment, a transitional polder is intended to be only temporarily opened to the tide to elevate the land. After sufficient land-level rise into a supratidal regime, the transitional polder will be closed off from the tide to restore its original anthropogenic function of e.g. agriculture on the newly elevated land (Zhu et al., 2020; Van Belzen et al., 2021). Following a controlled dike breach (Fig. 6.1a), a low-energy floodbasin is formed that promotes sediment deposition and salt marsh establishment (Woodruff et al., 2013). Continued filling elevates a transitional polder well into a supratidal regime especially if vegetation is present (Fig. 6.1b) (Allen,

2000; Morris et al., 2002; Kirwan et al., 2010; Fagherazzi et al., 2012). So far, this process is essentially similar to managed realignment projects that also had their seaward dikes breached, either by storms (e.g. Eertman et al., 2002; French, 2006) or by planned efforts (e.g. Dixon et al., 2008; Gourgue et al., 2022). Recent numerical modelling (Gourgue et al., 2022) suggests a supratidal salt marsh may cover an initially low-intertidal polder within 50 years, but longer time spans may be needed for systems without abundant suspended sediment supply and pre-carved channels to better distribute the sediment. The third and final step is the closure of the inlet (Fig. 6.1c), after which the original function of the embanked area is restored whilst the inland dike remains the primary dike for flood defence, resembling the practice of Tidal River Management in Bangladesh (e.g. Adnan et al., 2020). The result is a high and wide body of sediment in front of the primary inland dike that is protected by a secondary seaward dike and greatly reduces inundation of the low-lying hinterland in case of a dike failure (King and Lester, 1995; Zhu et al., 2020). Also, ecologically important habitats that have formed during the phase of land-level rise (Fig. 6.1b) will be lost upon inlet closure (Fig. 6.1c), so multiple transitional polders in different phases or a combination of different managed realignment strategies may be needed to maintain biodiversity and ecosystem integrity, but this analysis is beyond the scope of this study.

Building and raising new land in a transitional polder differs fundamentally from land reclamation. Land reclamation is mainly conducted to increase the extent of arable and habitable land by the embankment of high foreshores, either developed naturally (Kirwan et al., 2010; Vuik et al., 2016) or stimulated by artificial obstacles to promote accretion (Dijkema, 1987; Vos and Van Kesteren, 2000; Pethick, 2002), as has happened in many estuaries around the world (e.g. Sherwood et al., 1990; Van der Spek, 1997; Birch et al., 2009; Ahlhorn et al., 2012). This confines an estuary, which amplifies the tidal range (Van der Spek, 1997) and narrows shore-connected tidal flats and foreshores, leading to less wave attenuation and a higher risk of dike breaching (e.g. King and Lester, 1995; Möller et al., 1996; 2014; Zhu et al., 2020; Zhang et al., 2021). Moreover, estuary confinement reduces the landward-directed sediment import by tidal asymmetry, which leads to natural channel deepening in large friction-dominated estuaries (Nnafie et al., 2018; 2019) as observed in e.g. the Weser Estuary (Ahlhorn et al., 2012), the Columbia River Estuary (Sherwood et al., 1990) and the Western Scheldt Estuary (Van der Spek, 1997) prior to large-scale dredging. In absence of sediment input, the newly gained land becomes subjected to sediment compaction and background subsidence (Van de Broek et al., 2019; Oosterlee et al., 2020; Van Putte et al., 2020). As a result, younger reclaimed lands tend to be highest and oldest tend to be lowest (Fig. 6.2), making the latter most prone to inundation. In contrast, the strategy of transitional polders aims at lowering flood risk by raising already existing land to a supratidal elevation before returning it to its original function. To maintain flood safety, transitional polders may need cycles of inlet opening and closing to capture new sediment to compensate for land subsidence and eustatic sea-level rise.

So far, most deliberate de-embankments in estuaries were smaller than 400 ha and were single efforts in individual tidal systems (Wolters et al., 2005; Van den Hoven et al., 2022). Therefore, little is known about how the location of a transitional polder along an estuary influences the import of sand and mud and the tides with an estuary. 1D numerical modelling of estuaries suggests a local widening of intertidal storage area, which can be interpreted as a transitional polder, dampens the tidal range and increases tidal prism (e.g. Friedrichs, 2010; Leuven et al., 2018d). Yet, it remains unclear how such altered tidal characteristics influence the channel and bar pattern within an estuary, which requires two-dimensional modelling. Recent numerical modelling (Nnafie et al., 2018; 2019) showed that added floodbasins (about 10 m deep) along the Western Scheldt Estuary locally change the tidal flow and sediment transport patterns within the estuary, causing the development of a shoal in front of a floodbasin inlet. Such a shoal is analogous to a local ebb-tidal delta and its size becomes larger with a wider floodbasin inlet and relocates the main estuary channel further away from the outer banks (Nnafie et al., 2018). This raises questions (1) whether a similar shoal will develop in case of

much shallower transitional polders and (2) whether such a development will limit the desired sediment import into the corresponding transitional polder.

Finally, as increasingly more de-embankment projects are being considered, it is necessary to study how multiple transitional polders will function. In particular, it remains an open question how a planned sequence of opening transitional polders affects their ability to bring about land-level rise, needed to reduce flood risk. This exploratory study aims to investigate this question using the Western Scheldt Estuary (NL) as an example of a typically large estuary and simulates the effect of different opening sequences of four transitional polders along the estuary by means of two-dimensional modelling in Delft3D. Opened polders were not closed again, so the insights of opening multiple polders are also relevant for current and future managed realignment projects that focus on e.g. attaining a rich biodiversity and carbon sequestration (Temmink et al., 2022). Here, only sand and mud is considered, disregarding bioturbation by benthos, salt marsh vegetation dynamics and dredging for navigational purposes.

6.2 Case study: Western Scheldt Estuary

This study uses the Western Scheldt Estuary as an example for reasons of data availability and recent aspirations of applying transitional polders (Van Belzen et al., 2021). The multi-channel estuary is located in the southwestern part of the Netherlands (Fig. 6.2) and is on average convergent. This convergent shape is largely the result of large-scale land reclamations since the 14^{th} century, which transformed the highly branched estuary with large intertidal flats and salt marshes into the convergent shape of today (Fig. 6.2). This drastically decreased the intertidal and supratidal areas (Van der Spek, 1997) which are vital for habitat, breeding grounds and biodiversity (e.g. Benoit and Askins, 2002). Additionally, the increased channel convergence amplified the tidal range (Coen, 1988). Currently, the mean tidal range increases from 3.5–4 m at the estuary mouth to nearly 5.5 m at the city of Antwerp. The tidal prism at the mouth of the estuary is about 1×10^9 m^3 and the yearly averaged river discharge is 120 m^3/s (Van Dijk et al., 2021). Sediment input via the river is negligible and mainly depends on littoral drift and flood-dominant tidal flows, a condition that has been prevalent for a few thousand years (e.g. Van der Spek, 1997).

The large-scale land reclamation in the past points at ample sediment supply in the Western Scheldt Estuary that was needed to elevate intertidal bars and flats into a supratidal regime before embankment was possible. This potential for land-level rise is especially evident from the "Drowned Land of Saeftinghe". This former embanked area was breached by storms and intentionally breached during the Eighty Years' War in the late 16^{th} century and became part of the estuary again (hence "drowned"). Over time, new intertidal flats and salt marshes started developing as sediment was net imported (Jongepier et al., 2015; Vos, 2015). This naturally elevated most of the formerly drowned land into a supratidal regime with a median elevation of 3 m above mean sea-level (Fig. 6.2a,c). Irony is in the name, as this 3580 ha "drowned land" is currently the highest parcel of land in the region, being 4 m higher than the lowest embanked areas (Fig. 6.2a,c). This development of land-level rise equals observations of recently breached embanked areas in the same estuary (e.g. Eertman et al., 2002). Similar developments elsewhere are seen to follow an unintended dike breach, where, given sufficient sediment supply, land-level rise may allow re-embankment (Kleinhans et al., 2010).

The estuary is dredged to maintain access for ships to the port of Antwerp. Small-scale dredging has been done since the 20^{th} century and was intensified with three major deepening events (in the 1970s, 1990s and 2010s) to accommodate increasingly larger ships and maintenance dredging to maintain the newly desired channel depth (e.g. Van der Spek, 1997; Jeuken and Wang, 2010; Van Dijk et al., 2021). The resultant deeper continuous channel further amplified the tide, increasing tidal range at the port of Antwerp by roughly 0.5 m between the 1970s and the 2000s (Coen, 1988; Jeuken, 2000). Current

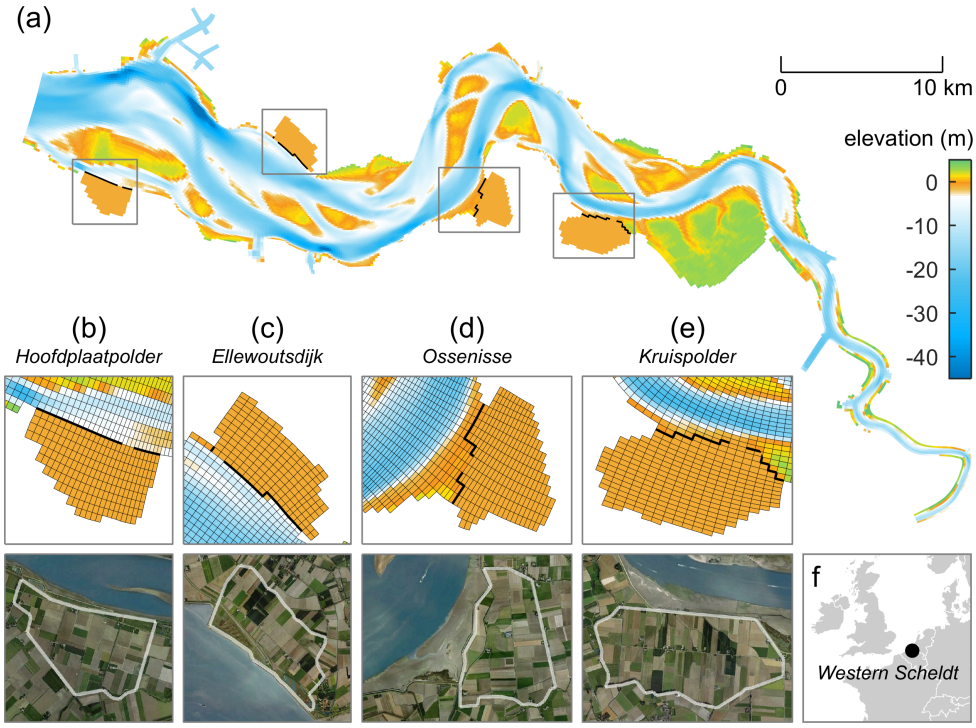

Figure 6.3 (a) The NeVla model schematisation of the Western Scheldt Estuary (NL/B) in the numerical model Delft3D (after e.g. Maximova et al., 2009; Grasmeijer et al., 2013; Vroom et al., 2015) including four added transitional polders outlined in the squares. (b–e) A zoom of the numerical grid and a satellite image (Google Earth; accessed: April 2021) of the four transitional polders. The average grid cell size in the transitional polders is 160 m^2. (f) The location of the estuary.

disposal activities near intertidal flats aim at "maintaining the steady state of the multi-channel system and preserve ecologically valuable intertidal habitats" (e.g. Depreiter et al., 2015; Plancke et al., 2010).

6.3 Methods

The morphodynamic modelling was done using Delft3D FLOW2D3D version 6.02.13.7658 from tag 7545 (Deltares, 2020). Delft3D is an open source numerical model that solves the non-linear shallow water equations (see Lesser et al., 2004, for equations and numerical implementation). Here, the depth-averaged flow version was used, which has been widely tested and used in studies on the morphodynamics of rivers (e.g. Van Oorschot et al., 2016) and estuaries (e.g. Dam et al., 2016). Delft3D includes a stratigraphical module that enables the modelling of sediment mixtures of sand and mud (Van Kessel et al., 2011; Braat et al., 2017).

6.3.1 Model setup and scenarios

The model domain of this study is part of the curvilinear NeVla-Delft3D schematisation of the Western Scheldt Estuary, which was calibrated for hydrodynamics (e.g. Maximova et al., 2009; Vroom et al., 2015) and morphology (Grasmeijer et al., 2013; Schrijvershof and Vroom, 2016). The original NeVla-Delft3D schematisation covers part of the North Sea and the Western Scheldt Estuary up to the city of Ghent in Belgium, which is the upstream limit of tidal influence. Here, a nested model was used to reduce computational time. The computational domain stretched from the city of Antwerp to

the estuary mouth at the city of Vlissingen (Fig. 6.3a) and comprised grid cell sizes ranging from 30 to 300 m. To assess the implementation of transitional polders, four small grids were added to the computational domain (Fig. 6.3) (Table 6.1). The polders had an assumed initial bed elevation of -1 m NAP (i.e., the Amsterdam ordnance datum, close to mean sea-level at the Dutch coast), which is equal to the lowest polders along the Western Scheldt (Fig. 6.2c) and within the intertidal range. The four transitional polders were inspired by Van Belzen et al. (2021) and selected based on the following criteria. Firstly, the transitional polders reached at maximum 2 km inland to limit the fetch for locally generated waves in real-life, although wave modelling was not accounted for in the model. Secondly, the minimal area was set to 4 km^2, i.e. equally large or larger than most current de-embanked areas (see for review: Wolters et al., 2005; Van den Hoven et al., 2022), to have an observable effect on tidal wave propagation in the estuary. Thirdly, the locations for the transitional polders-to-be lacked urban buildings, industry and solar panels to have a minimal impact on society. Dikes between the transitional polders and the estuary were implemented as thin dams in the model domain that prevented flow and sediment exchange between two adjacent cells, limiting flow interaction to $\pm$200 m wide inlets between the transitional polder and the main estuary (Fig. 6.3).

Flow conditions at the upstream and downstream boundaries of the model were determined by time series in the Western Scheldt Estuary of water levels at the estuary mouth and water discharges at the river inflow over the first 10 months of the year 2013 (Van Dijk et al., 2019). These boundary conditions are considered representative for typical hydrodynamic forcing of this system and captured seasonal and diurnal variability, spring-neap cycles and storm surges. River discharge was partitioned over the upstream boundary to mitigate strong channel incision. Also, this partitioning allowed the discharge to be varied sinusoidally over time from one bank to the other to cause natural inflow perturbations (Schuurman et al., 2016; Chapter 2).

Sediment was modelled as a mixture of one sand fraction and one mud fraction using the stratigraphic module by Van Kessel et al. (2011) (sediment characteristics are listed in Table 6.2). This module tracks the spatial and temporal bed composition in layers of a user-defined thickness, here 0.05 m. The initial bed consisted of a uniform mixture of 95% sand and 5% mud. Sand was supplied

Table 6.1 Spatial characteristics of the selected sites to implement controlled floodbasins.

Site	Area (km^2)	Distance to mouth (km)
Hoofdplaatpolder	4.61	14
Ellewoutsdijk West	4.38	22
Ossenisse South	5.10	34
Kruispolder	7.43	49

Table 6.2 Sediment characteristics, after Braat et al. (2017).

Sediment property	Value	Unit
sand		
median grain size	2×10^{-4}	m
specific density	2650	kg/m^3
dry bed density	1600	kg/m^3
transverse bed slope parameter α_{bn}	30	-
mud		
settling velocity	2.5×10^{-4}	m/s
critical bed shear stress for erosion	0.2	N/m^2
erosion parameter	1×10^{-4}	kg/m^3s
specific bed density	2650	kg/m^3
dry bed density	1600	kg/m^3

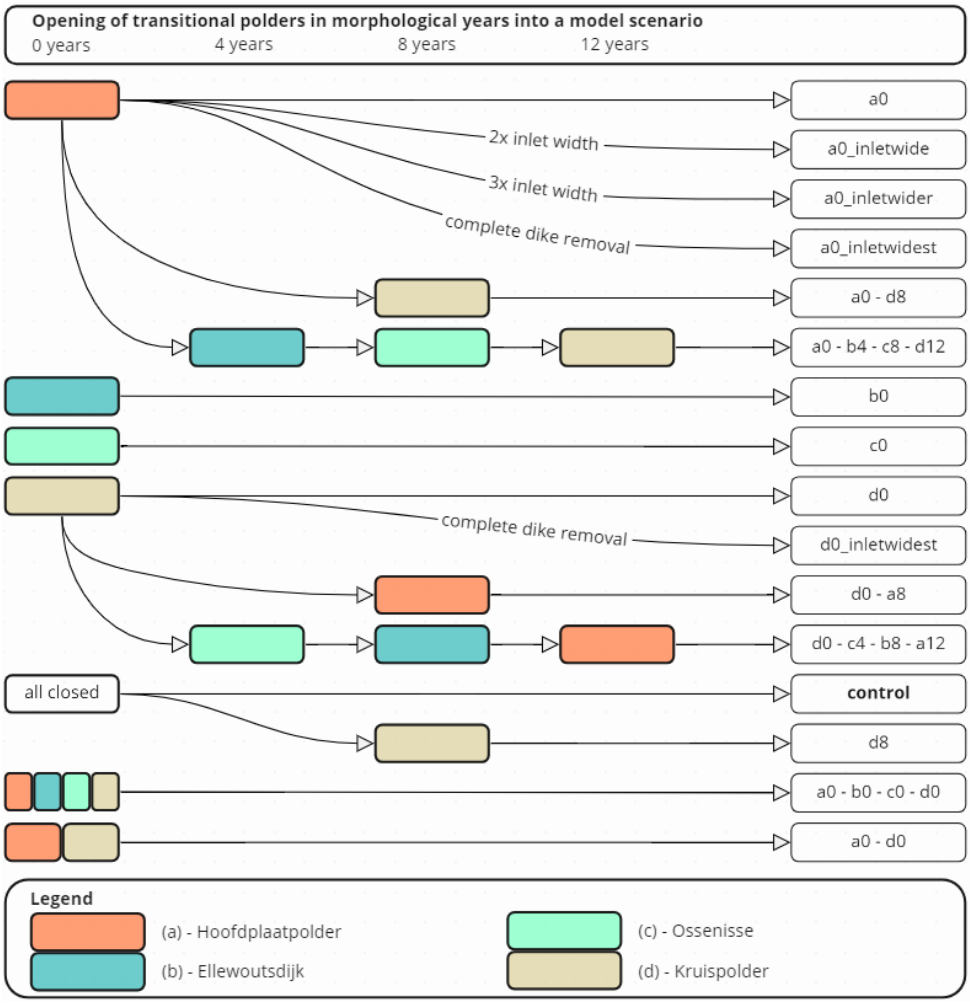

Figure 6.4 Overview of the 16 model scenarios with the scenario name in the right-most column. Transitional polders were opened at the start or after 4, 8 or 12 morphological years. In the scenario name, transitional polders are denoted from downstream to upstream as "a", "b", "c" and "d", and the suffix (0, 4, 8 and 12) denote after how many years they were opened. Annotations indicate when a wider inlet to a transitional polder was applied, where "complete dike removal" is essentially the widest inlet possible.

at both the upstream and downstream boundaries as an equilibrium concentration boundary condition; this means sand supply was equal to the transport capacity of the flow to prevent erosion or deposition at the boundaries. Mud was supplied at both boundaries at a constant concentration of 0.04 kg/m^3 to acquire mud concentrations throughout the estuary matching field observations (Van Kessel and Vanlede, 2010). Mud was treated as a cohesive sediment, for which the amount of erosion and deposition was determined by the Partheniades-Krone formulation (Partheniades, 1965) and depended on user-defined critical bed shear stresses. Here, the erosion shear stress was set to 0.2 N/m^2 and the deposition by settling of mud was set to occur in all flow conditions (following Braat et al., 2017). For simplicity, a constant 2.5×10^{-4}m/s settling velocity was assumed for mud,

disregarding that the settling velocity is influenced by flocculation, a process that depends on concentration, biochemistry, residence time, turbulence, salinity, season and pH (e.g. Mietta et al., 2009). The settling velocity is similar to previous numerical modelling in estuaries (e.g. Braat et al., 2017; Brückner et al., 2020) and is typical for fluvial mud (Temmerman et al., 2003) and on the low side for marine mud.

Sediment transport was calculated using the Van Rijn (2007) predictor (TRANSPOR2004), which is well-suited for sediment mixtures of bedload and suspended load and applicable to tidal environments. The downslope sediment transport on transverse bed slopes was parameterised using an α_{bn} of 30, following Baar et al. (2019). The Manning bed roughness was spatially variable along the estuary (cf. Nnafie et al., 2018; Brückner et al., 2021; Van Dijk et al., 2021) and varied between 0.02 and 0.028 s/m^3. To speed up the numerical computation, the bed level change calculated after every hydrodynamic time step was multiplied with a factor of 20. Such a morphological acceleration factor is common practice in long-term morphological modelling (e.g. Lesser et al., 2004; Van der Wegen and Roelvink, 2008; Dissanayake et al., 2009) and enables a faster computation of longer timescales. In the case of this study, this means that the 10 hydrodynamic months of 2013 (Van Dijk et al., 2019) resulted in 16.6 morphological years.

In total, 16 scenarios were run in which the opening of transitional polders was systematically varied (Fig. 6.4). These include scenarios of different configurations of transitional polders (1) opened throughout a scenario, (2) opened after 4, 8 or 12 morphological years, and (3) with a larger inlet width. The analysis focused on the morphological development within the transitional polders and their effect on tidal range, tidal prism and morphology along the estuary. For clarity, the terms "upstream" and "downstream" are used for along-estuary directions and "seaward" and "landward" are used for cross-sectional directions.

6.4 Results

This section will first describe the general development of the scenarios in which only one of four transitional polders was open. Next, the effect is presented of different opening sequences of transitional polders on their sediment capture and the estuary hydrodynamics.

6.4.1 Effect of individual polders

All transitional polders showed a net gain in bed elevation once they were opened to the tide (Figs. 6.5, 6.6, 6.7a–d). Typically, highest gains in elevation were found in the centre of the transitional polders in the form of a sandy flood-tidal delta. Mud generally settled at the lee side of the flood-tidal delta and at the low-energetic edges of the polders (Fig. 6.6i–l). The most upstream and downstream polders, i.e. *Kruispolder* and *Hoofdplaatpolder*, were most efficient at importing sediment, with 25 % of their area having been elevated by more than 2 m after 16.6 morphological years. Interestingly, whilst sand primarily accounted for the elevation gain in most transitional polders, mud accounted for more than half in case of *Ellewoutsdijk* (Fig. 6.7a–d). As mud concentrations at the inlet of *Ellewoutsdijk* were within range of the other inlets (Fig. S1), the enhanced trapping efficiency of mud could be largely ascribed to the elongated shape of *Ellewoutsdijk*.

The location of a transitional polder influenced the tidal range and tidal prism. In the control run without transitional polders, the mean tidal range amplified in the upstream direction from 4 m at the mouth to 6 m near the city of Antwerp (Fig. 6.8b). Opening of a transitional polder changed this amplification, with the direction of change depending on the location of a polder. That is, a polder located more upstream led to a strong reduction in tidal range (Fig. 6.9c), while in contrast, the most downstream transitional polder slightly increased the tidal range. The temporal development of tidal range along the estuary in Fig. 6.8c indicates that the reduction in mean tidal range (1) increases over

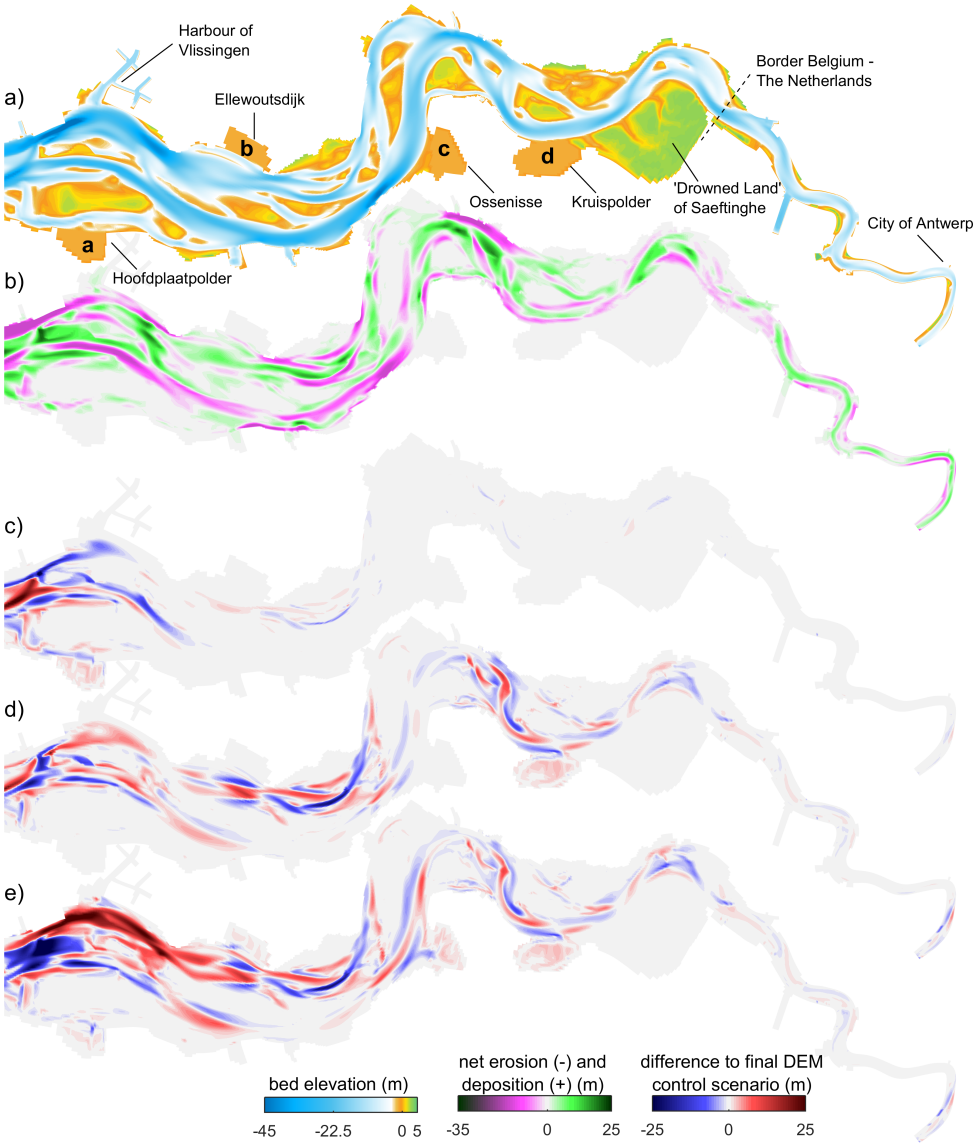

Figure 6.5 (a) Bathymetry and (b) morphological change in the estuary after 16.6 years for the control scenario where all transitional polders remained closed. The difference is shown between the final bathymetry of the control scenario and (c) scenario a0 in which the downstream-most polder was open (d) scenario d0 in which the upstream-most polder was open and (e) scenario d0–c4–b8–a12 in which all polders were opened in a sequence from upstream to downstream.

time and (2) increases during larger amplified spring-neap cycles becomes more pronounced during temporarily higher mean tidal ranges related to yearly variations in tidal forcing (see temporal change in the amplitude of spring-neap cycles in Fig. 6.8a). Tidal prism was increased downstream of an opened transitional polder due to the added intertidal storage volume (Fig. 6.9d). The smallest gain in tidal prism correlated to the smallest polder *Ellewoutsdijk* (Table 6.1). Interestingly, the upstream-most

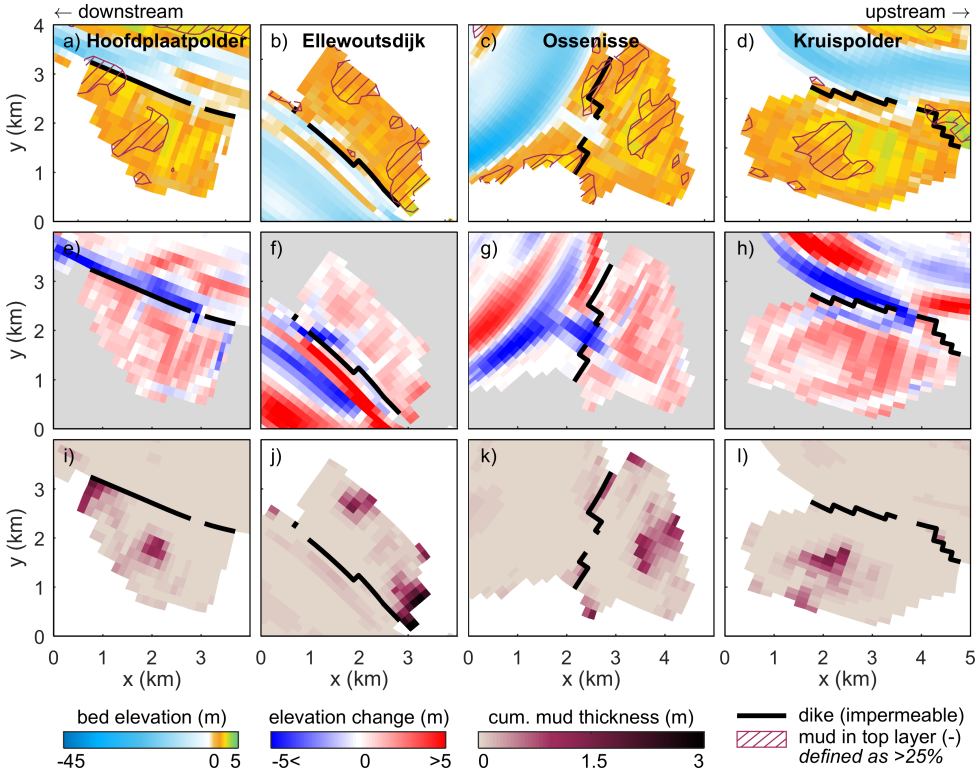

Figure 6.6 Morphological development in the transitional polders for the four scenarios in which only one transitional polder was open with a default inlet width. (a–d) The final bed elevation after 16.6 morphological years plus the presence of mud in the top 0.05 m layer. (e–h) Bed elevation change, expressed as the final bathymetry of subplots (a–d) compared to the final bathymetry of the control scenario in which no transitional polder was opened. (i–l) Cumulative mud layer thickness after 16.6 morphological years of new mud deposits, disregarding mud in the unreworked sediment (i.e. 5 % mud in the initial sediment bed). Mud-related compaction was not included in the modelling.

polder *Kruispolder* resulted in a locally increased tidal prism, while the other more downstream polders resulted in a roughly constant increase up to the estuary mouth (Fig. 6.9d).

In the control scenario when no transitional polders were opened, small intertidal bars formed in the downstream half of the estuary (Fig. 6.5). The channel bed in the upstream reach of the estuary aggraded by a few metres mainly because of fluvial sediment input and erosion of flanking sand bars. This resulted in a shallower but slightly wider channel. Along the entire estuary, sills formed in the main channel (in absence of dredging) especially near large bends (Fig. 6.6). Consequently, the main channel was split into discontinuous, mutually evasive channel sections, for example seen at the channel bend northeast of the "Drowned Land of Saeftinghe". Despite some channel migration and sill formation, the bed elevation distribution remained largely constant in the middle reach between the Dutch-Belgian border and the (in the control scenario unopened) transitional polder at *Ossenisse*. Downstream of this polder, morphological change was largest, including strong channel incision of the main channel and a major shift of the main channel south of the harbour of Vlissingen (Fig. 6.6).

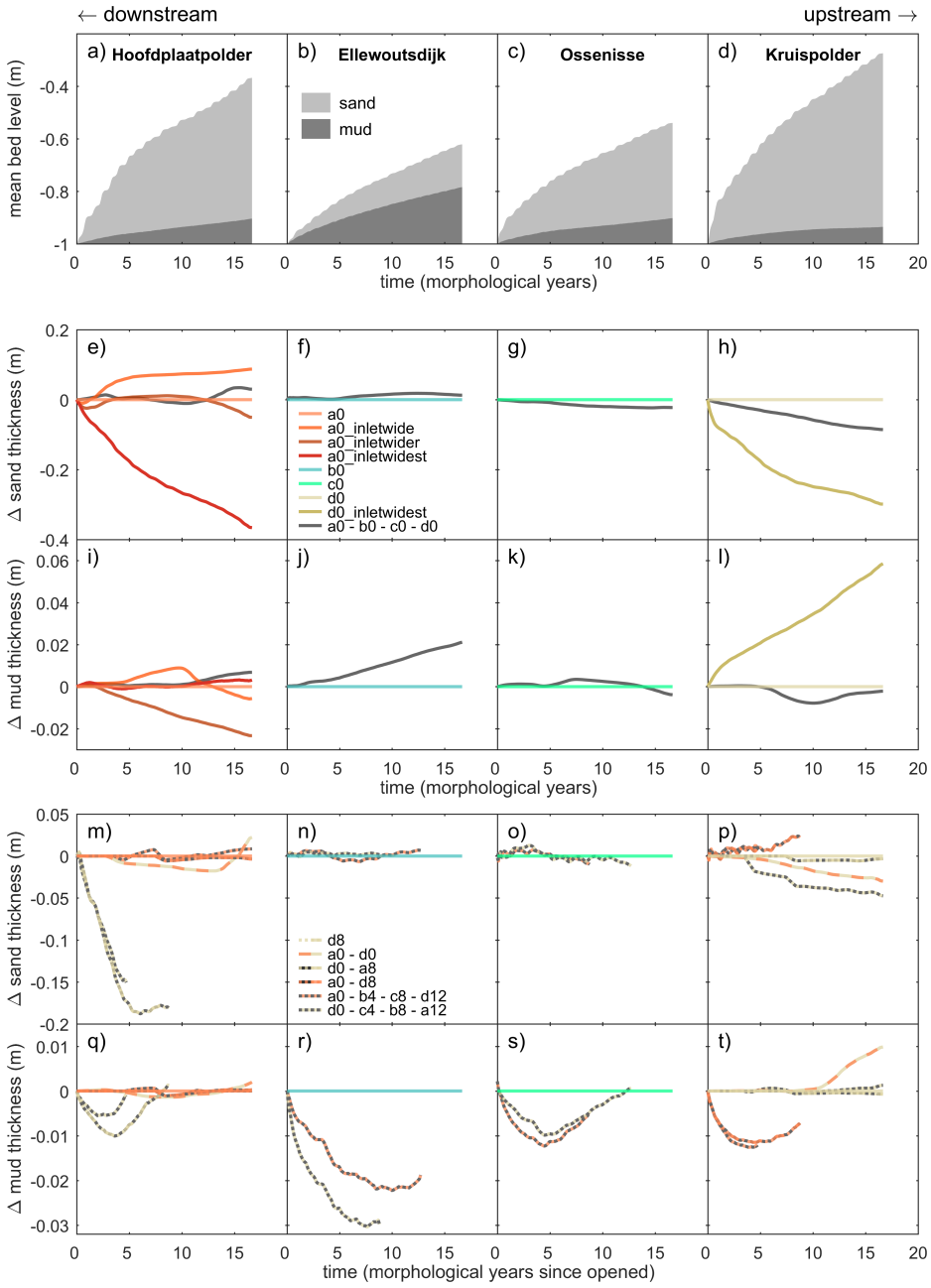

Figure 6.7 Development of (a–d) mean bed level, attributed to sand and mud deposits, for the four scenarios in which only one transitional polder was open with a default inlet width (i.e. a0, b0, c0, d0). Panels (e–t) show the difference in mean sand and mud thickness compared to panels (a–d), where panels (e–l) show scenarios with one or all polders opened at the start of a model run, and panels (m–t) show scenarios with opening sequences of multiple transitional polders. Note the smaller y axis for panels (m–t).

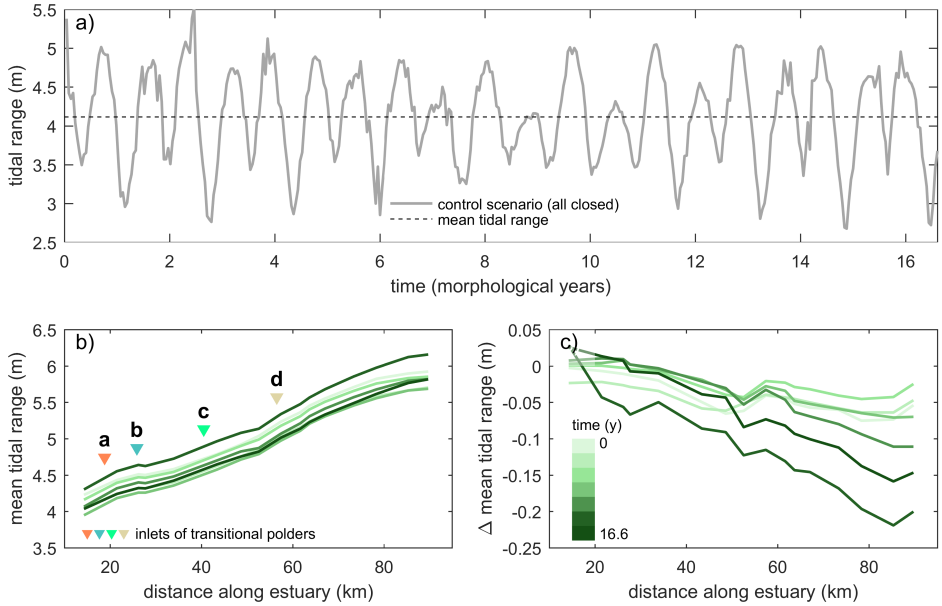

Figure 6.8 Development of tidal range. (a) Time series of tidal range at the estuary mouth for the control scenario in which no transitional polder was open. (b) Mean tidal range per spring-neap cycle along the estuary for the control scenario. (c) As an example, the difference in mean tidal range between scenario d0 and the control scenario, showing an increasingly smaller tidal range when the upstream-most transitional polder is open. Final along-estuary trends for all scenarios are given in Fig. 6.9c,e.

6.4.2 Effect of opening sequences

Transitional polders that were opened later in a sequence had a smaller import of mud compared to when they were opened at the start of a scenario (Fig. 6.7q–t). Nonetheless, this lag in mud import was only temporal and decreased over time, as is evident from the temporal development of the mean mud thickness in the transitional polders (Fig. 6.7q–t). In contrast, most sequences had a negligible effect on import of sand, with deviations in Fig. 6.7m–p of about two orders of magnitude smaller than the sand deposits of scenarios with only one transitional polder in Fig. 6.7a–d. The two exceptions to this trend at *Hoofdplaatpolder* (Fig. 6.7m) were linked to a shore-connected bar migrating in front of the inlet before the inlet was opened. This bar migration happened in all scenarios, but while early openings allowed for sufficient reworking to ensure a shallow channel connection to the main channels, an entirely new channel had to be carved through the foreshore after opening at 12 morphological years. This led to deeper inlet incision (Fig. 6.6e) and therefore lower mean bed elevations (Fig. 6.7m). Furthermore, this development partly explained the lower mean bed elevation at *Ossenisse* (Figs. 6.6e, 6.7c), where a wide foreshore is in front of the inlet in all scenarios at all times.

Tidal range and, to a lesser extent, tidal prism were influenced by an opening sequence. Typically, tidal prism increased downstream of an open transitional polder due to added volume storage (Fig. 6.9d). The opening of all polders simultaneously or from downstream to upstream resulted in the largest increase in tidal prism. Fig. 6.9e shows that an opening sequence from upstream to downstream reduced tidal range considerably, while the other way around tidal range hardly reduced or even increased in the upstream half of the model domain. This trend was more pronounced in the sequences with four open polders but also present in the sequences with only the two outermost polders (Fig. 6.9e). However, Fig. 6.10 shows it was probably not the added storage volume of the transitional polders but instead their impact on estuary morphology that influenced the tidal range.

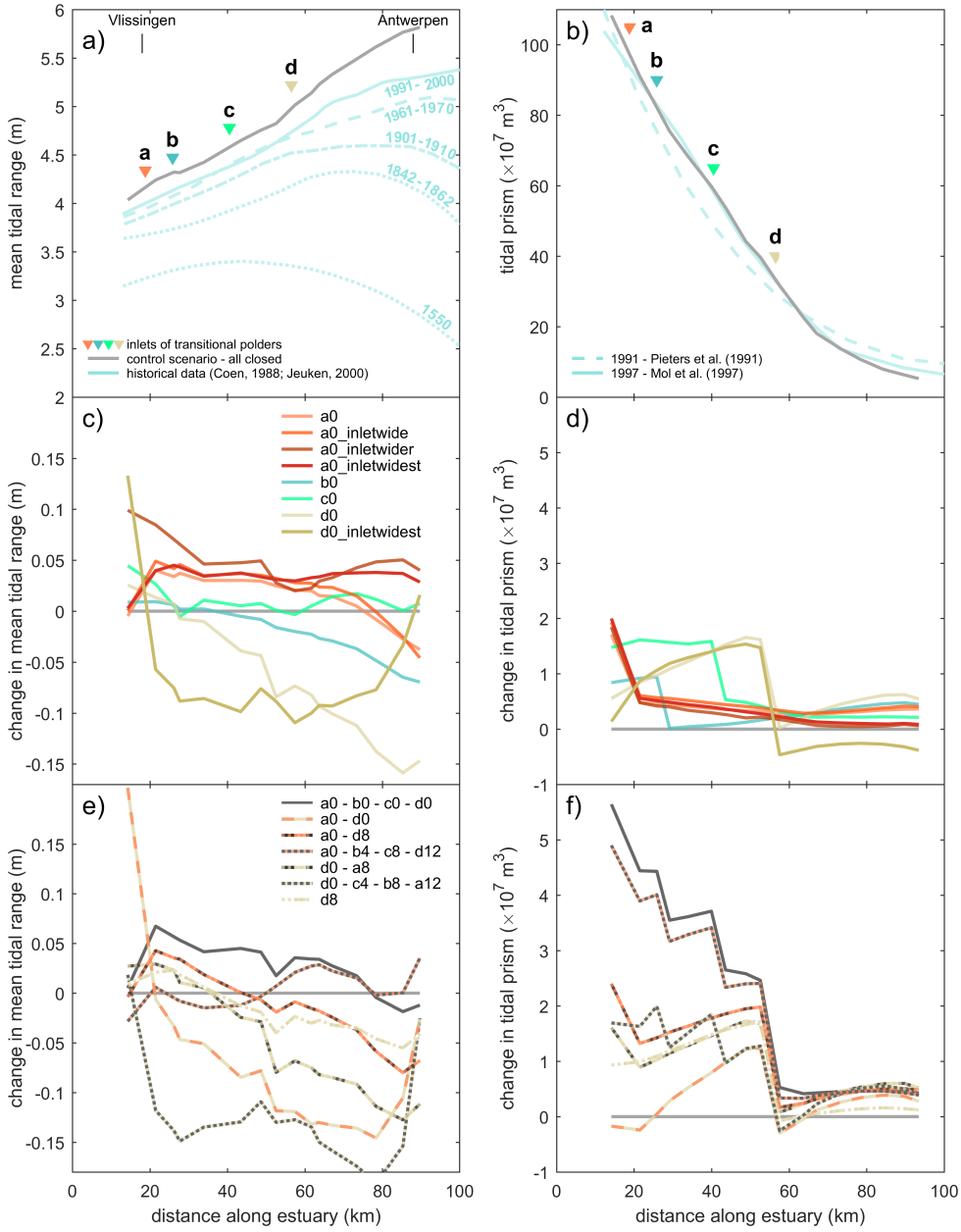

Figure 6.9 Tidal range and tidal prism along the Western Scheldt Estuary. (a) Tidal range and (b) tidal prism, averaged over the last two spring-neap tidal cycles, for the control scenario without transitional polders together with historical data (Coen, 1988; Jeuken, 2000). (c) Change in tidal amplitude and (d) tidal prism if any one transitional polder was open throughout the model run. (e) Change in tidal amplitude and (f) tidal prism for scenarios with an opening sequence of transitional polders.

For example, most opening sequences starting with *Kruispolder* exhibited channel shallowing just downstream of the *Kruispolder* inlet and in the downstream 20 km of the domain. In contrast, opening sequences starting with *Hoofdplaatpolder* resulted in channel deepening in the downstream 15 km (Fig. 6.10). Therefore, the incoming tide experienced less friction that enabled larger tidal ranges in scenarios with channel deepening, whilst channel shallowing produced more friction that led to smaller tidal ranges (Fig. 6.9c,e).

6.4.3 Effect of inlet width

Inlet width had a considerable effect on the net import of mud and sand. Scenarios including the most downstream transitional polder *Hoofdplaatpolder* (Fig. 6.7e) hinted at an optimum inlet width for sand import around twice the default inlet width and a reduction of sand import by about half upon complete dike removal. This trend of reduced sand import is similar for the most upstream transitional polder *Kruispolder* (Fig. 6.7h). However, complete dike removal caused nearly a doubling of mud deposition in the most upstream polder, whilst the most downstream polder experienced less mud deposition (Fig. 6.7i,l). This is probably related to the shape of the transitional polders, which extended further landward for the upstream-most polder with lower flow velocities near the landward boundary.

Also tidal range was affected by inlet width. Whilst the opening of most transitional polders contributed to a similar or smaller tidal range, the transitional polder closest to the seaward boundary instead increased tidal range once opened (Fig. 6.9c). This increase was more pronounced if larger inlet widths were used. However, this increasing trend stood in contrast to the most upstream transitional polder, where complete dike removal resulted in a much smaller tidal range throughout most of the estuary (Fig. 6.9c). As for tidal prism, it was largely unaffected by different inlet widths.

6.5 Discussion

This study reports on the numerical modelling of four transitional polders between double dikes along the Western Scheldt Estuary. The incentive to applying transitional polders was to import sandy and muddy sediments to cause land-level rise that could strongly reduce flood risk (Zhu et al., 2020; Van Belzen et al., 2021). Here, this potential for sediment import, as well as the effect on estuary morphology and tidal wave propagation, was tested for four polders opened (1) alone, (2) in a sequence and (3) with increasingly larger inlet widths. These effects are placed in the context of current estuary management that includes managed realignment and dredging, after which implications are inferred for flood risk management

6.5.1 Effects of transitional polders

The general morphology in a transitional polder developed towards a landward extending sandy flood-tidal delta with thin mud deposits at the lee side of the delta and at the rims of the polder (Fig. 6.6). This seaward-to-landward filling resembles the initial stages of filling in tidal basins with sand, mud and live vegetation (Boechat Albernaz and Kleinhans, in prep.). However, such filling differs from field observations (e.g. Eertman et al., 2002; Dixon et al., 2008; Lawrence et al., 2018) and models (Spearman, 2011; Gourgue et al., 2022) of managed realignment projects, where mud-dominated filling typically starts at the landward rims of managed realignment site and progresses in the seaward direction. A possible explanation lies in the initial bed elevation of the transitional polders, which was at a much lower elevation (i.e. -1 m below mean sea-level) with respect to the tidal range than many managed realignment sites. This low initial elevation was selected based on the lowest embanked areas along the Western Scheldt Estuary (Fig. 6.2) and therefore first required sand import before tidal conditions were weak enough to achieve mud-dominant filling from the rims. Additionally, a landward-to-seaward filling is often ascribed to

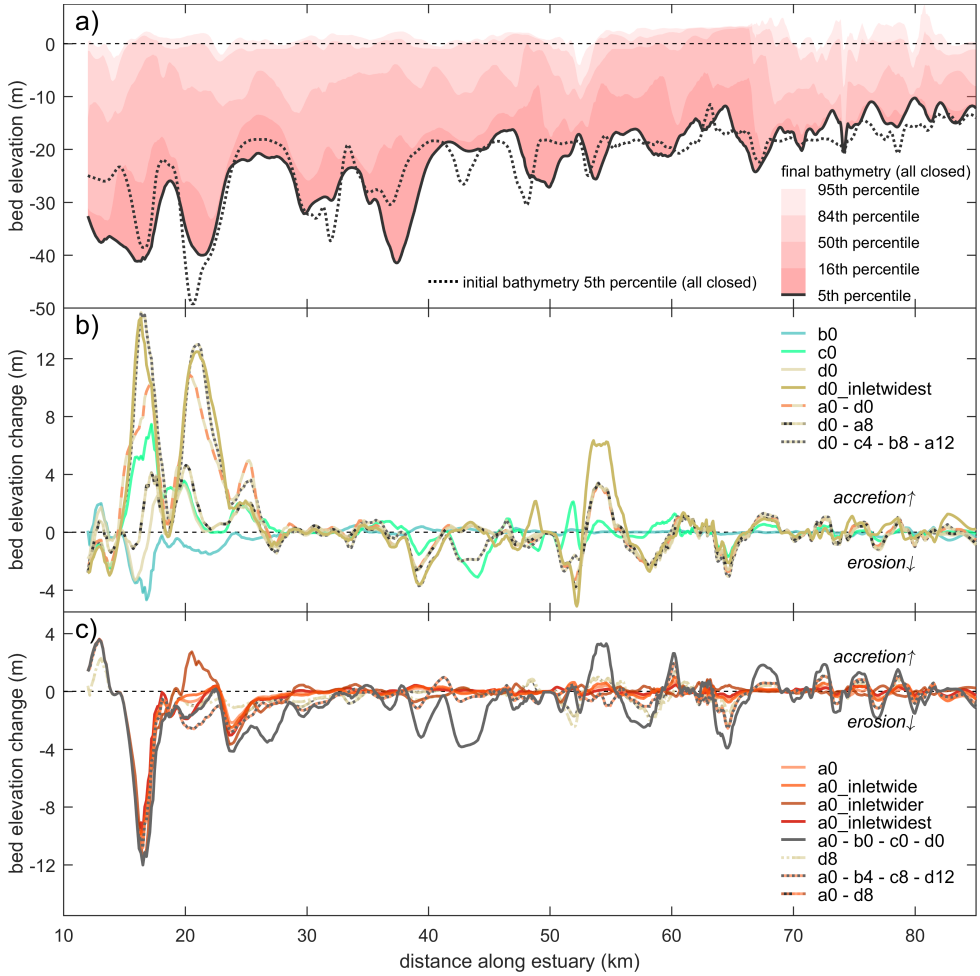

Figure 6.10 Channel depth along the estuary over time. (a) Bathymetry expressed as bed elevation percentiles. The initial bathymetry curve shows the 5^{th} percentile, which represents the main channels. (b/c) Differences in bed elevation shown as the 5^{th} percentile compared to the control run presented in (a). (b) shows scenarios that experienced net channel shallowing (accretion) and (c) shows scenarios that experienced net channel deepening (erosion).

laterally expanding salt marshes that capture mud and stabilise the bed (Gourgue et al., 2022), but such vegetation dynamics were beyond the scope of this study. As opposed to this study, some managed realignment sites had an initial channel network excavated to improve drainage and jump-start the formation of creeks and channels (e.g. Williams and Orr, 2002; Wallace et al., 2005; Gourgue et al., 2022). These channels may allow focused transport and import of sediments and stimulate land-level rise, but when located too high or low with respect to the tidal range, such pre-carved channels have little effect on the trend of landward-to-seaward filling in managed realignment, for example in the Tijuana Estuary, USA (Wallace et al., 2005).

The effects of a single transitional polder can be described in relation to its location relative to the local estuary morphology and its location along the estuary. Firstly, the location relative to the estuary morphology, in particular the presence of a wide foreshore or shore-connected bar,

influenced the import of sand. The presence of a wide foreshore or shore-connected bar coincided with strong inlet channel erosion that net reduced the sand import in the first years after opening. Inlet erosion upon a deliberate or storm-induced dike breach was also observed for managed realignment sites landward of well-established vegetated foreshores, e.g. "the Freiston shore" in The Wash Estuary (UK) (Symonds and Collins, 2005; Symonds and Collins, 2007). Regarding the Freiston shore, inlet erosion was ascribed to an elevation drop into a lower-lying basin, causing fast inflow and slow outflow during high spring tide, and most reworked sediment was net imported into the basin, situated high in the tidal range (Symonds and Collins, 2005; Symonds and Collins, 2007). In contrast, the transitional polders in this study were below mean sea-level and therefore experienced stronger ebb currents and ebb-directed sediment transport, which explains the smaller net import of sediment compared to the Freiston shore. Nonetheless, in practice, such a wide (vegetated) foreshore or shore-connected bar is probably preferred as this attenuates waves and reduces the risk of the outer dike breaching (King and Lester, 1995; Möller et al., 1996; Zhu et al., 2020). Mud import appeared generally unaffected by the local estuary morphology and was instead predominantly governed by the local suspended sediment concentration. In this study, the suspended sediment concentrations were largely similar for the domain of the four selected polders (Fig. S1). Yet, higher concentrations and correspondingly higher accretion rates are expected for sites closer to the turbidity maximum further upstream. Moreover, adding flocculation (Mietta et al., 2009) and mud-fixating lifeforms (Brückner et al., 2020), which depend on e.g. salinity and biochemistry that vary along-estuary, may also alter mud accretion rates and cause a stronger along-estuary trend in mud deposition if included.

Secondly, the along-estuary location had a strong impact on estuary morphology, where a more upstream polder resulted in more cumulative erosion and deposition in the main estuary (Fig. 6.6c,d). This is explained by the added intertidal storage volume, which increases tidal prism from the estuary mouth up to the inlet of a transitional polder (Fig. 6.9d), conform to previous one-dimensional modelling of estuaries (Leuven et al., 2018d). Yet, it remains an open question if the increase in morphological change downstream of a polder inlet is mainly caused by a larger tidal prism or whether perturbations also travel from the polder inlet in the downstream direction. This would be in contrast to the current theory of macro cells in tidal systems (e.g. Van Dijk et al., 2019; Sonke et al., 2022), which suggests that perturbations do not propagate to other downstream or upstream macro cells. This question requires further work. Another consequence of added intertidal storage volume is a reduction in tidal range that becomes more pronounced for transitional polders located further upstream (Figs. 6.8c, 6.9c). This is associated with the net converging estuary width, which means a similarly sized transitional polder further upstream leads to a relative larger gain in intertidal area that can dampen the tide (Friedrichs, 2010). And although a reduction in tidal range 0.1 to 0.2 m may appear small, this is significant for flood defences that are constructed to a centimetre accuracy. Yet, when compared to a 0.5 m tidal range increase at Antwerp, Belgium, between the 1970s and 2000s (Coen, 1988; Jeuken, 2000) due to dredging (Van der Spek, 1997; Jeuken and Wang, 2010; Van Dijk et al., 2021), transitional polders are of a lesser influence. Regarding the amount of sediment import into the transitional polders, the along-estuary location appeared to be of negligible influence as the modelled suspended sediment concentrations were largely similar for the estuary reach that contained the four polders (Fig. S1), in line with previous modelling of the same estuary (e.g. Braat et al., 2019a; Brückner et al., 2020).

The opening sequence of multiple transitional polders generally had little effect on the import of sand (Fig. 6.7m-p). This excludes effects of migrating shore-connected bars which induced channel inlet erosion and less sand import for the downstream-most polder *Hoofdplaatpolder* when opened after 12 years (Fig. 6.7m). On the other hand, mud import was temporarily lagging behind in transitional polders opened later in a sequence compared with when they were opened at the start of a scenario (Fig. 6.7q–t). As this lag was only temporal, the four transitional polders appeared not to compete for mud import in the current setup of a sand-dominated estuary. However, it remains unclear if this also

applies to later stages of filling beyond the modelled time, as more mud is taken out of the estuary and preserved in the transitional polders.

Scenarios including the most upstream transitional polder *Kruispolder* typically developed shallower main channels in the middle-to-downstream reach of the estuary (Fig. 6.10b). In contrast, deepest channels were formed in scenarios without transitional polders or with only the downstream-most polder *Hoofdplaatpolder* (Fig. 6.10c). This appears similar to historical records (e.g. Sherwood et al., 1990; Ahlhorn et al., 2012) in which land reclamation and progressive embankment (i.e. fewer transitional polders) were linked to a natural channel deepening and consequently a larger tidal range. Long-term numerical modelling (Nnafie et al., 2019) corroborates this modelled trend for estuaries with moderate-to-high friction and ascribed this to a decrease in sediment import driven by tidal asymmetry. Consequently, the altered estuary morphology affects the amplification of the incoming tide. Shallower channels increase friction that reduces the tidal range, while deeper channels lead to a larger tidal range (Friedrichs and Aubrey, 1988). Generally, the trend of channel shallowing or deepening was dominated by the first polder in a sequence (i.e. deepening for the downstream-most polder and increasingly more shallowing for polders further upstream). However, this does not explain the outlier of scenario "d8", where opening of the upstream-most *Kruispolder* after 8 years instead resulted in channel deepening and remains an open question.

The inlet width and geometry of the transitional polder mainly affected the net import of sand and mud (Fig. 6.7e,h,i,l). This is understandable, as a smaller inlet width focuses and increases flow velocities at the inlet up to a point where the friction of the inlet width becomes a limiting factor; an example is the managed realignment at Alkborough, where a 20 m narrow inlet greatly limits tidal exchange and the input of sediments (Wheeler et al., 2008). Consequently, transitional polders with complete dike removal experienced weaker tidal exchange flows and significantly less sand import (Fig. 6.7e,h). As for mud, the distance to the inlet strongly correlated with mud deposits, simply because more distal parts have weaker tidal flows that favour net mud deposition. This is conform to tidal restoration sites, where low-energy intertidal areas furthest away from the inlet generally retain most of the deposited mud (e.g. Eertman et al., 2002; Jongepier et al., 2015), a process that is promoted by salt marsh vegetation (e.g. Schwarz et al., 2015; Temmerman et al., 2007). Nnafie et al. (2018) showed a wider inlet width of subtidal secondary basins results in a larger shoal development just seaward of the inlet, which "pushes" the channel away from the outer banks. However, such a shoal development was not clearly observed in the modelling of the shallow, intertidal transitional polders with complete dike removal. This absence may be caused by the smaller and shallower geometry of the transitional polders or a relatively short modelling time of 16.6 morphological years. Yet, the modelling time-span was sufficient to develop a flood-tidal delta in the transitional polder (Fig. 6.6).

The flow conditions in this study excluded large storm surges and the modelling of waves, but their effects on land-level rise can be inferred from observations at managed realignments. Examples at Tollesbury (UK) (Watts et al., 2003) and Chowderness (UK) (Morris, 2013) show that locally generated waves and waves entering via a narrow inlet are generally not energetic enough to erode newly deposited sediments due to a limited fetch. In contrast, unsheltered sites of realignment experience slower salt marsh establishment (e.g. Morris, 2013). Accordingly, only model scenarios with complete outer dike removal will probably have less land-level rise when wave modelling was included, where the balance between sediment delivery and lateral erosion by waves affects the extent of the salt marsh (e.g. Fagherazzi et al., 2013). As for storm surges, these events are a main cause for dike failure and the creation of new unplanned sites for managed realignment (e.g. French, 2006; Jongepier et al., 2015; Vos, 2015). Yet, on a longer, centennial timescale of estuary filling, storm surges are not regarded as a limiting factor for sediment accretion in sheltered foreshores and floodbasins, evident from e.g. the extensive historical formation of supratidal salt marshes of the Western Scheldt

(Van der Spek, 1997; Vos, 2015). How storm surges will affect the shallowing of the main tidal channels in the estuary due to added floodbasins remains underinvestigated and benefits from future studies.

6.5.2 Implications for estuary management

The modelling excluded dredging, which has a strong influence on the estuary morphology and is linked to strongly increasing the tidal range in the Western Scheldt (e.g. Coen, 1988; Van der Spek, 1997; Jeuken, 2000) (Fig. 6.9a). In comparison, the transitional polders have a decreasing, albeit much smaller effect on the tidal range by causing the estuary channels to shallow (Figs. 6.8c,e, 6.10). This would reduce flood risk. However, the natural shallowing of channels will most likely be negated by maintenance dredging to maintain a deep fairway connection to harbours further upstream. Additionally, this suggests that continued dredging will probably prevent the development of mutually evasive tidal channels in the main fairway (Van Dijk et al., 2021) as modelled in this study, for instance, at the estuary bend northwest of the "Drowned Land of Saeftinghe" (Fig. 6.6a). Consequently, it remains to be investigated to what extent dredging, adapted to local issues, may negate the tidal range reduction by transitional polders, which is especially relevant for determining future flood risk.

In light of future sea-level rise, large estuaries in terms of convergence length and channel depth will likely experience drowning of ecologically invaluable intertidal and supratidal areas (Leuven et al., 2019; Chapter 5). Transitional polders may be part of the solution to limit estuary drowning, enhance flood safety on its margins, and restore ecological habitat area. The opening of multiple transitional polders, especially ones further upstream, increases the flood-dominant import of marine sediment. Not only will this sediment be used to build and raise land in the transitional polders, but it may also allow already existing intertidal area to keep up with sea-level rise. Storm surges are dangerous events in terms of flood risk that were unaccounted for in this study. Nevertheless, this study indicated that transitional polders dampen larger mean tidal ranges more strongly (Fig. 6.8c). This suggests that transitional polders may contribute to lower flood risks during storm surges as well, which is in line with findings for managed realignment sites (e.g. Temmerman et al., 2013; Bouma et al., 2014; Van den Hoven et al., 2022), and requires further work.

6.6 Conclusion

Numerical modelling was conducted of transitional polders between double dikes along the Western Scheldt Estuary in the Netherlands using different opening sequences and inlet widths, which led to the following findings that is also relevant for other managed realignment practices. Land-level rise occurred in all transitional polders in all scenarios by net import of sand and mud, but transitional polders opened later in a sequence experienced a temporal lag in net mud import, probably due to a deficit in fines. Polders located more upstream typically led to smaller tidal range that was attributed to two mechanisms. Firstly, the added intertidal width caused more friction that reduced tidal amplification. Secondly, the opening of more upstream polders led to natural channel shallowing particularly in the downstream reach of the estuary, which further reduced tidal amplification and improved flood safety. The modelling suggests an upstream-to-downstream opening sequence reduces tidal range strongest. However, further work is needed to determine to what extent redirected dredging activities, closure of transitional polders and the inclusion of storm surges may negate this benefit to flood safety.

Open Research

Additional materials are available in an online supplement and in an online data package. The online supplement contains a supplementary figure (Suppl. Fig. 6.11). The data package includes the Delft3D files needed to run the scenarios presented in this paper and is available at: https://public.yoda.uu.nl/geo/UU01/ISQ31Y.html. Delft3D is an open source code available at this site (https://oss.deltares.nl).

Acknowledgements

We acknowledge two anonymous reviewers whose comments helped to improve the manuscript. This research is supported by the European Research Council through the ERC Consolidator grant 647570 to Maarten G. Kleinhans. This work is part of the PhD research of Steven A. H. Weisscher.

Supplementary material

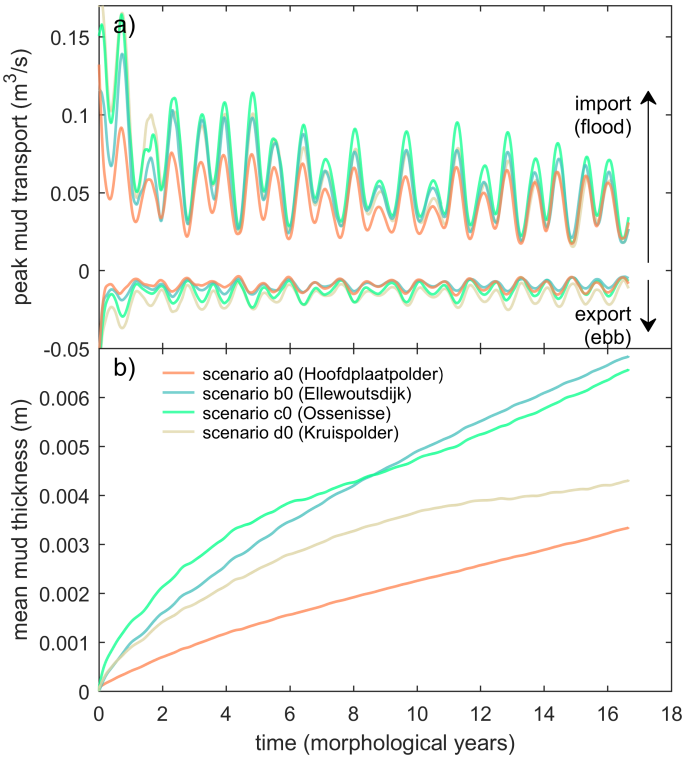

Figure 6.11 (a) Suspended mud import during peak flood and export during peak ebb shows that a transitional polder location has little influence on the magnitude of mud transport at a polder inlet and (b) on the net import. a0 (i.e. *Hoofdplaatpolder*) is the most downstream polder and d0 (i.e. Kruispolder) is the most upstream polder. For further clarification on the scenario name, the reader is referred to Fig. 6.4

Chapter 7 | Synthesis

The main aim of this thesis was to determine how mud and vegetation influence the steady state of estuaries. Mud and vegetation are known to build floodplains in rivers and "tidal floodplains" in estuaries in the form of mudflats and salt marshes. In rivers, floodplains confine channels and fill accommodation, which alters the stable state of rivers. As rivers merge into estuaries around the fluvial-tidal transition, it was hypothesised that "tidal floodplains" may also influence the steady state of estuaries. This could explain the differences in the degree of estuary filling, which remained largely unexplained by previous classifications of estuaries using the relative importance of rivers, waves and tides (Boyd et al., 1992; Yang et al., 2005). Therefore, this thesis studied whether and how muddy and vegetated tidal floodplains also influence the stable states of entire estuaries using scale experiments and numerical modelling.

This synthesis describes first how the thesis deepens the current understanding of floodplain formation in rivers and estuaries. Then, the main findings are combined to infer implications and develop hypotheses that are relevant in the context of estuary management and future sea-level rise. Finally, the synthesis concludes with recommendations for future studies.

7.1 Main conclusions

7.1.1 Floodplain formation

In rivers, floodplain formation by mud and vegetation are thought to confine channels and fill accommodation (e.g. Braudrick et al., 2009; Nicholas, 2013), resulting in a transition from braided to meandering to laterally fixed rivers (Leopold and Wolman, 1957; Nanson and Knighton, 1996). Commonly, these transitions in river pattern are well predicted using a form of stream power and grain size (Furbish, 1988; Kleinhans and Van den Berg, 2011). However, this thesis (Chapter 2) proves that a river pattern is also governed by the tendency to form floodplains when stream power and grain size are invariable. Still, stream power and grain size set the boundary conditions for vegetation establishment and mortality (e.g. Simon and Collinson, 2002; Van Oorschot et al., 2016) and so are arguably closely related to floodplain formation. Then, variation in current relations to predict river pattern could be explained by additional factors influencing vegetation, such as climate and the availability of nutrients (e.g. Baker, 1989; Bendix and Hupp, 2000).

Until now it remained an open question whether "tidal floodplains" in the form of mudflats and salt marshes also confine channels and fill accommodation similar to fluvial floodplains. This seemed plausible as fluvial floodplains transfigure into mudflats and salt marshes as a river enters its downstream tide-influenced reach. Recent scale experiments (Braat et al., 2019a; Kleinhans et al., 2022) and numerical models (Braat et al., 2017) confirmed that the confining and filling effects also apply to tidal floodplains in ingressive, exporting estuaries. Mud and vegetation contributed to narrower systems with less lateral expansion. However, the contribution of mud and vegetation to net importing estuaries remained largely untested (Boechat Albernaz and Kleinhans, in prep.), yet may be key to explaining the diversity of estuary filling. This thesis for the first time presents scaled landscape experiments of filling estuaries and tested the effects of mud and vegetation on estuary filling (Chapter 4). From an initially drowned river valley, an infilling estuary developed by net import of

fluvial and marine sediments under flood-dominant tidal conditions. Added mud filled topographical lows in the intertidal-to-supratidal reach and caused a faster development of higher and more supratidal bars because of its low-density and slightly cohesive properties. This is conform field data and numerical modelling on a scale of a single flat (e.g. Braat et al., 2019b; Gourgue et al., 2022) and on a scale of an entire estuary (Braat et al., 2017). Vegetation proved especially effective at channelising flow, which confined the subtidal channels and contributed to more sediment transport in the landward direction.

The confining and filling mechanisms by mud and vegetation led to narrower multi-channel estuaries in the experiments (Chapter 4). Commonly, estuaries are described to have an ideal shape where the floodplain-bounded channel converges in the landward direction (Savenije, 2015; Dronkers, 2017). Field observations indicated that a deviation from this ideal shape is a reliable indicator for the location and size of bars (Townend, 2012; Leuven et al., 2018a). Then, it seems that it is the subtidal channels that develop towards a converging planform and not necessarily the outer banks. Chapter 4 confirms this hypothesis experimentally, showing that such a converging planform of the subtidal channels also develops in wide filling estuaries with floodplain formation regardless of tidal bar and tidal flat geometry. Furthermore, the tendency to form floodplains governs the amount of intertidal and supratidal area, where more mudflats and salt marshes culminated in a narrower estuary (see Fig. 4.10). Therefore, this thesis proposes that different tendencies for floodplain formation enable a continuum of partly filled estuaries that can reach a steady state on a centennial timescale, assuming reasonably constant boundary conditions. This is consistent with some partly filled estuaries such as the Arcachon Bay (Féniès and Faugères, 1998; Allard et al., 2009) and Ems-Dollard Estuary (Van Maren et al., 2016), which have been in an apparent steady state in the past century despite ample sediment supply.

The concept of filling accommodation along estuaries has received increasing attention over the past decades in the form of managed realignment projects (e.g. Wolters et al., 2005; Esteves, 2014; Van den Hoven et al., 2022). Many sites for managed realignment were created by storm-induced dike breaches (e.g. French, 1999), but increasingly more sites are being proactively designed. As some managed realignments show a great potential for land-level rise (Eertman et al., 2002; Jongepier et al., 2015), managed realignment can also be used to elevate low-lying reclaimed land, after which it may return to its original function of e.g. arable land. This novel strategy is called a transitional polder between double dikes and aims to reduce flood risk. So far, most artificially designed managed realignments were singular efforts, which raised the question how the opening of multiple sites at once or in a sequence would affect flood risk and estuary morphodynamics. This was investigated in Chapter 6 using four transitional polders along the Western Scheldt Estuary. The numerical findings indicated that all configurations of transitional polders, having an initial elevation of -1 m ordnance datum, showed a net gain in bed elevation. Yet, transitional polders opened later in a sequence temporarily lagged behind in mud deposition. In contrast, sand import was not influenced by the opening sequence but mainly by the local estuary morphology: a wide foreshore led to deeper inlet erosion and therefore a smaller net import of sand. Still, in practice, wide (vegetated) foreshores will probably be preferred as these attenuate waves and protect the dike (Möller et al., 1996; Zhu et al., 2020; Zhang et al., 2021). Lastly, an upstream-to-downstream opening sequence increased flood dominance and resulted in a stronger shallowing of the estuary channels compared to a downstream-to-upstream sequence. Consequently, opening transitional polders from upstream to downstream strongly reduced tidal range, suggesting that the opening sequence can play an integral part in managing flood risk.

7.1.2 Effect of sea-level rise

The scaled landscape experiments of filling estuaries in Chapter 4 showed that mud and vegetation form floodplains that confine channels and fill accommodation. This resulted in partly filled estuaries

that were close to a steady state with constant boundary conditions. However, with sea-level on the rise and expected to reach up to 1 to 2 m higher by 2100 (Bamber et al., 2019; Horton et al., 2020), a proper understanding is needed of how the balance between floodplain formation and destruction will change. This will help to predict how estuaries will respond to sea-level rise, which is essential as these environments fulfil many ecosystem services, including habitat and nursery grounds, coastal protection and carbon sequestration (e.g. Chmura et al., 2003; Barbier, 2007; 2011). Recent work (Du et al., 2018; Leuven et al., 2019) suggested that large and small estuaries (in terms of convergence length and channel depth) will respond differently to sea-level rise. Where small, friction-dominated systems are mostly prone to larger tidal amplification and flood risk, larger systems which are less dominated by friction will likely face sediment starvation and loss in intertidal and supratidal areas.

Scaled landscape experiments in Chapter 5 confirmed this hypothesis for large, deep estuaries and showed estuary drowning in response to rapid sea-level rise. From an initially drowned river valley, a filling estuary was formed that was subjected to sea-level rise. The increase in accommodation caused sediment to be deposited closer to its fluvial and marine sources to compensate for the increasing water depth. Accordingly, most sediment input was used to elevate the bay-head delta and the flood-tidal delta, whilst little was transported into the central part of the estuary. And since tidal flows in this part of the estuary were to weak to erode the outer banks to compensate for the loss in sediment input and wind-driven waves that may drive bank erosion were absent, the central part of the estuary drowned. Consequently, vegetation had fewer locations to settle, which negated its eco-engineering abilities to elevate bars and promote landward transport of sediment. The result was a wider and deeper estuary with less spatial variation in flow velocity and fewer intertidal and supratidal areas.

7.2 Implications for building and raising land

7.2.1 The estuary-delta continuum

This thesis shows that mud and vegetation build and raise tidal floodplains that confine channels and fill accommodation in estuaries. This internal mechanism of floodplain formation and destruction influences the degree of filling, where a stronger tendency for floodplain formation leads to narrower steady-state systems with fewer channels over the cross-section (Chapter 4). The estuary experiments of Chapter 4 with mud and live vegetation developed towards a partly filled steady state with on average two main tidal channels over the cross-section that were net convergent in the upstream direction. Then, a stronger tendency for floodplain formation, for example through a larger mud supply and stronger vegetation, will likely result in progressively more filling towards a completely filled and confined steady state (Savenije, 2015; Dronkers, 2017). This suggests that estuaries can be in a range of steady states that are in balance with floodplain formation.

This finding that estuaries can be in a range of steady states between unfilled and completely filled differs with previous literature in two main ways. Firstly, the estuary experiments in Chapter 4 indicate that the filling of estuaries is not solely governed by the boundary conditions of e.g. sediment input, fluvial discharge and tidal flow but also by internal mechanisms such as floodplain formation (Fig. 1.1). This may explain why some partly filled estuaries are in an apparent steady state despite ample sediment supply, such as the Columbia River Estuary (USA) (Peterson, 2014), the Arcachon Bay Estuary (FR) (Féniès and Faugères, 1998; Allard et al., 2009) and the Ems-Dollard Estuary (NL/D) (Van Maren et al., 2016). The importance of internal mechanisms such as floodplain formation and destruction differs from the previous understanding that estuary filling strongly correlates with sediment supply, based on the ephemeral nature of estuaries on a geological timescale of sea-level fluctuations (Lanzoni and Seminara, 2006; Dalrymple and Choi, 2007; De Haas et al., 2018). Secondly, alluvial estuaries have been argued in literature to have two contrasting kinds of steady states on a centennial timescale, namely an unfilled lagoonal system largely below the threshold of motion (Roy et al., 1980; Dalrymple et al., 1992)

and a completely filled, confined system (Savenije, 2015; Dronkers, 2017). Now, estuary experiments in Chapter 4 and by Leuven et al. (2018b) suggest that also partly filled estuaries may attain a steady state where the degree of filling depends on flood dominance and the tendency to form floodplains, given reasonably constant boundary conditions. This corroborates observations in partly filled estuaries that showed no distinct channel confinement towards an ideal converging shape (e.g. Féniès and Faugères, 1998; Peterson, 2014; Van Maren et al., 2016) that would be expected with ample sediment supply if only an unfilled and completely filled estuary can be a steady state.

A main aim of the thesis was to explain the broad range in estuary shapes and sizes. Previous efforts classified estuaries based on the relative importance of rivers, waves and tides (Boyd et al., 1992; Yang et al., 2005). However, this left largely unexplained why the channel and bar pattern varies between a multi-channel network and a single channel in different estuaries. Estuary filling was found to have a considerable influence on the channel and bar pattern based on the experiments in Chapters 4 & 5, field observations and stratigraphic box models (Roy et al., 1980; Nichol, 1991; Dalrymple et al., 1992). For instance, unfilled wave-dominated estuaries typically have a large lagoonal basin that is mostly devoid of bars due to weak tidal currents. Conversely, partly filled estuaries such as the Tillamook Bay Estuary (USA) exhibit a channel and bar pattern resembling a braided river, and completely filled estuaries such as the Manawatu River (NZ, Clement et al., 2017) and the Mekong River (VT) resemble more meandering and laterally fixed rivers. So, more filling leads to narrower steady-state estuaries with fewer channels and bars over the cross-section. Especially the difference between partly filled and completely filled estuaries was previously disregarded in classifications (Fig. 1.2), although the observed channel and bar pattern may be very different between these kinds of estuaries.

Therefore, a revised classification of estuaries is proposed in Fig. 7.1a that includes the distinction between partly filled and completely filled estuaries. The original classification was based on Boyd et al. (1992) and later updated by Yang et al. (2005), in which estuaries and deltas were placed on a continuum. Estuaries and deltas can change into one another by means of progradation and transgression, which is driven by changes in relative sea-level and sediment supply. Another factor that influences estuary filling and therefore progradation is the tendency to form floodplains. Here, the classification regards the entire (drowned) valley for classifying estuaries and deltas, which in this context means that a bay-head delta in a lagoon is considered part of an unfilled estuary instead of a river-dominated delta. The experiments of Chapter 4 follow the red arrow through the diagram in Fig. 7.1 from an unfilled lagoon to a partly filled wave-dominated estuary. On a longer timescale and under conditions of progressive filling, the estuary would develop towards a completely filled wave-dominated estuary and ultimately an overfilled wave-dominated delta.

The projected development of estuary filling along the red arrow in Fig. 7.1 seems to increase in river dominance but actually maintains an equal importance of rivers, waves and tides. This is, because the ternary diagrams also include clastic coastal environments that lack a river influence altogether: strandplains and coastal tidal flats (Boyd et al., 1992; Yang et al., 2005). This exposes a minor flaw in these ternary diagrams, which are intended to classify coastal environments based on the independent, quantitative and measurable influence of rivers, waves and tides. For example, the filling of a lagoon with river inflow with constant influence of rivers, waves and tides will probably develop into a wave-dominated delta and not a strandplain as may be inferred from the ternary diagrams (Fig. 7.1a). This means also a measure for progradation or filling is required to pinpoint a coastal environment. This measure for the degree of filling is influenced by floodplain formation, which are both so far difficult to express quantitatively. For example, the degree of filling may be expressed as a surface or volume fraction of the estuary that is supratidal or higher but requires knowledge of the initial unfilled extent or volume which is not always readily available. Therefore, it remains ambiguous how to come to an objective classification of coastal environments.

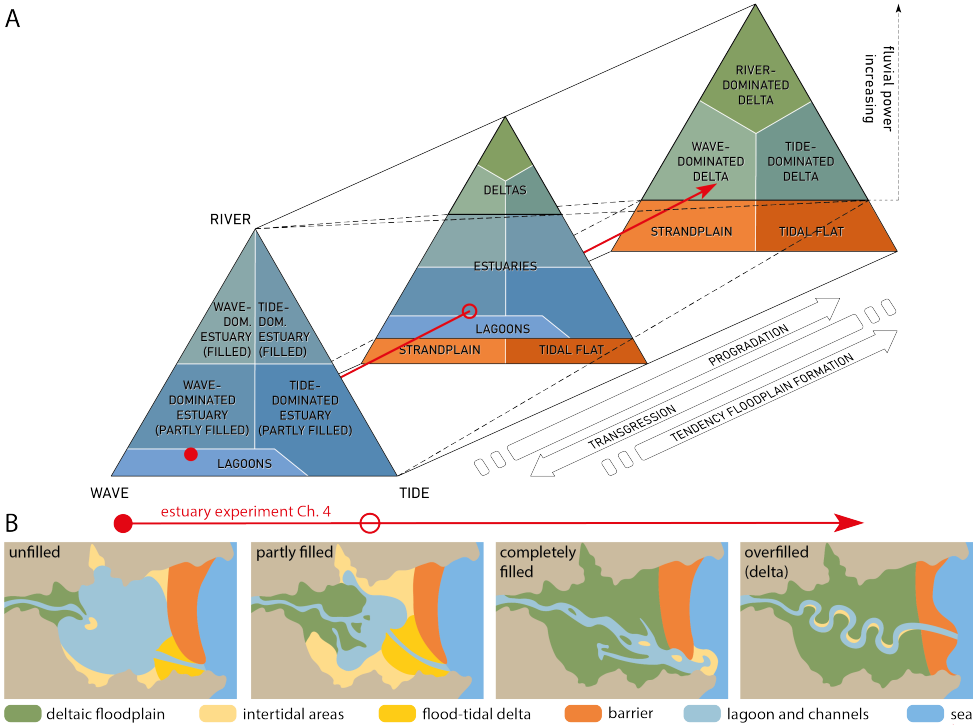

Figure 7.1 (a) A revision of the classification of coastal environments with different forcing of waves, tides and rivers (Fig. 1.2) that now also distinguishes between partly filled and completely filled estuaries (modified from Boyd et al. (1992) and Yang et al. (2005)). The red arrow indicates the estuary filling of the experimental estuaries in Chapter 4 from an unfilled lagoon to a partly filled wave-dominated estuary and extrapolates towards an overfilled wave-dominated delta. The relative forcing of waves, tides and rivers remains equal along this arrow, as the lower trapezoid of strandplain and tidal flat lacks river forcing. (b) A conceptual model of wave-dominated estuaries on a continuum from underfilled to overfilled along the red arrow in panel (a), where the first three panels are modified from Roy et al. (1980) (Fig. 1.3).

7.2.2 Estuary and coastal management

Tidal floodplain formation not only affects the shape of estuaries but also contributes to the building and raising of new land. Mud and salt marsh vegetation elevate bars and flats into a supratidal reach, which forms wide vegetated foreshores at the outer banks of an estuary. This natural development of high foreshores has proven to be opportune for land embankment in the past centuries (e.g. Vos and Van Kesteren, 2000; Pethick, 2002; Birch et al., 2009; Ahlhorn et al., 2012), which extended the area of land suited for agriculture and urbanisation. However, embankment in the past has confined and deepened estuaries, which considerably amplified both the tidal range (Van der Spek, 1997) and the risk of inundation in the upstream direction. Moreover, embankment strongly reduces the foreshore width, which is linked to less attenuation of wave energy (Möller et al., 1996; Zhang et al., 2021) and a higher risk of severe dike erosion (Zhu et al., 2020). Lastly, embankment impedes the natural process of floodplain aggradation that would otherwise balance background subsidence and soil compaction (Berendsen, 2004; Kirwan and Megonigal, 2013). Accordingly, embanked land slowly subsides, which raises issues with groundwater seepage (e.g. Chen et al., 2015). Therefore, especially in view of future

sea-level rise, sustainable flood defences are needed that not only reduce flood risk but also drive land-level rise and improve ecological value.

Part of the solution to more sustainable flood defences was explored in Chapter 6, which is the practice of transitional polders between double dikes. This practice enables land-level rise with mud and vegetation in a sheltered environment between a primary landward dike and smaller secondary dikes, and may be closed and used as arable land after sufficient land-level rise (Van Belzen et al., 2021). While a transitional polder is open, it influences the estuary morphology and tidal amplification by means of two mechanisms. Firstly, the added storage volume increases flood dominance in estuaries with moderate to high friction, which favours marine sediment import and shallowing of tidal channels. The shallower channels increase friction in the vertical sense, which dampens the tidal range. Secondly, the added intertidal width locally enhances friction in the lateral sense, which also dampens the tidal range. These mechanisms become more pronounced for transitional polders located further upstream, where they reduce flood water levels and potential flood risk. So, fewer dike reinforcements are needed to maintain a certain level of safety against flooding.

Besides reducing flood risk, transitional polders between double dikes also allow for the development of ecologically invaluable intertidal and supratidal areas, which can offset the expected loss of such areas within estuaries due to sea-level rise (Chapter 5). A natural example that clearly illustrates this potential for land-level rise and the renewed development of salt marshes is the "Drowned Land of Saeftinghe". This former embankment in the Western Scheldt Estuary (NL) was breached during a storm in 1570 and reintroduced to the tide. Consequently, tidal floodplains with tidal creeks started developing again, raising the drowned land into the highest parcel of land along the estuary, 4 m higher than the lowest embankments. This development of land-level rise equals observations of recently breached embankments in the same estuary (e.g. Eertman et al., 2002; Gourgue et al., 2022). Such building of new land may develop faster by the use of gate culverts to capture more fines (Marijnissen et al., 2021). Similar to field observations, the modelling in Chapter 6 indicates that land-level rise in transitional polders is a process that takes decades, and is therefore only a viable option as long as the mean rate of sediment accumulation in a polder (few millimetres to centimetres per year) exceeds the (increasing) rate of sea-level rise.

The aimed result of transitional polders is a much wider flood defence between the water and the land. Instead of a single high dike, a wider, albeit less high, flood defence is formed of tidal floodplains that are bounded by dikes. This will not completely safeguard the low-lying hinterland but will require much more reworking and scouring in the event of a breach than a single dike (Zhu et al., 2020), which will greatly reduce flood risk. Furthermore, transitional polders may offer a number of services that could increase public support and should be investigated further, including aquaculture, wildlife habitat and leisure. Yet, the practice of transitional polders requires sufficient sediment supply, which is not the case for all estuaries and may be compromised by further estuary drowning due to sea-level rise.

The closure of transitional polders after sufficient land-level rise may raise issues that need to be addressed before polders may be used for arable land again. For example, a newly developed salt marsh will also have formed tidal creeks for drainage, which are crucial for reaching the full ecological and geomorphological functioning of salt marshes and managed realignment sites (e.g. Chirol et al., 2022). However, such relief may not be compatible with agriculture. This may be resolved by levelling the land or by embanking only the higher salt marshes, in turn allowing the creeks to fill in and develop into salt marshes themselves. The latter resembles the embankment of the Western Scheldt Estuary from 1300 y AD onwards (Fig. 6.2) (e.g. Van der Spek, 1997). Another issue focuses on the salinity of the soil and groundwater, which either asks for saline agriculture or requires time for the groundwater to become fresh.

To understand how sea-level rise will impact estuary management, it is key to determine how estuaries are naturally shaped by their initial and boundary conditions and internal mechanisms. This

will form a basis of system knowledge from which the effects of e.g. artificial constructions and dredging can be inferred. On an inherited landscape and substrate (i.e. valley width, depth and geological constraints), an estuary imports or exports sediment to reach a steady state that is in balance with tidal floodplain formation and flood-dominant sediment import, provided the boundary conditions remain about constant. When an estuary is at a steady state, this also means estuary filling and the creation of accommodation are in balance. Then, an increase in accommodation by sea-level rise will remove an estuary (further) away from its steady state and results in a transgression. From a hypothetical point of view, an instantaneous sea-level rise could be considered an event that briefly sets back estuary development by creating accommodation, after which an estuary would develop again to its earlier steady state. However, a constant sea-level rise becomes a persistent boundary condition that may result in further drowning of estuaries, which was tested experimentally for wide filling estuaries in Chapter 5.

Rapid sea-level rise will result in the drowning of the middle reach of wide filling estuaries as fluvial and marine sediment supply reaches less far into an estuary (Chapter 5). The drowning in the middle reach was at the cost of tidal floodplains that were not able to keep up with the fast sea-level rise. Similar findings of drowning of the middle reach were found for novel experiments of confined estuaries (Fig. 7.2) (Cox et al., in review). To compensate for a reduced sediment supply and keep up with sea-level rise, confined estuaries were found to face enhanced bank erosion (Fig. 7.2). In natural systems, this will likely happen at the cost of ecologically rich salt marshes, and the consecutively larger cross-sectional area may dampen the tidal range (Leuven et al., 2019). However, in embanked

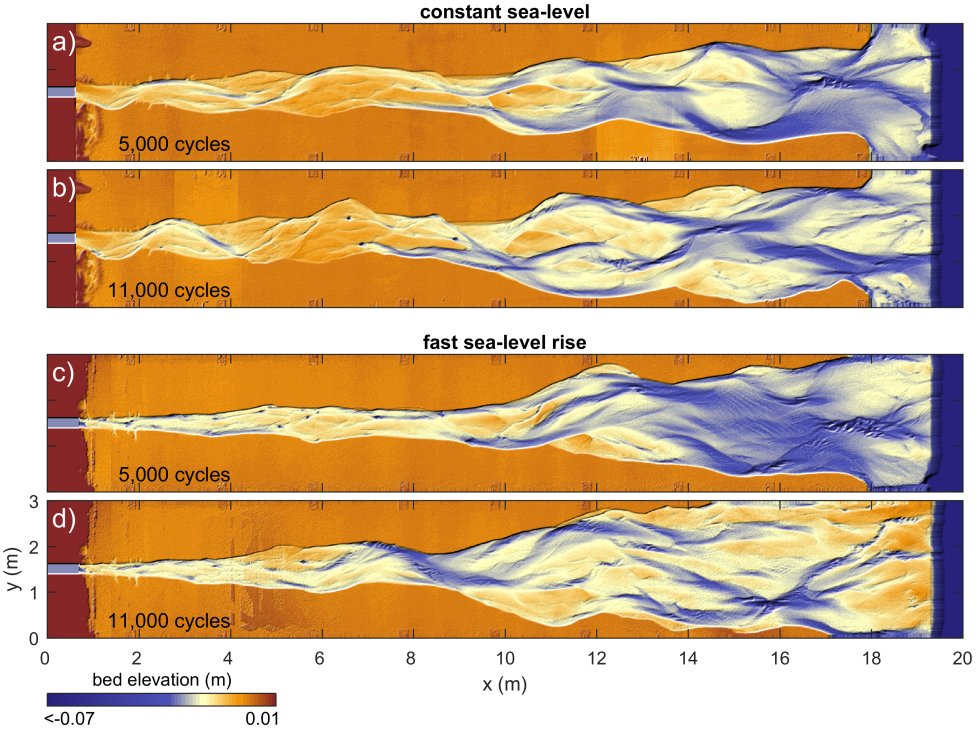

Figure 7.2 Digital elevation models of ingressive estuary experiments (a–b) with a constant sea-level and (c–d) with rapid sea-level rise (Cox et al., in review). Flow is from left to right. The ebb-tidal delta was obscured by the wave generator and was cut off from the digital elevation models at $x = 19.4$ m.

estuaries, it remains unclear how this will influence dike stability and flood risk, which requires further work.

So, rapid sea-level rise will probably pose problems related to flood risk and ecological habitats in estuaries (cf. Leuven et al., 2019). Deliberate breaching of dikes to create transitional polders has been argued in this thesis to be one of the possible strategies to adapt coastal regions to a rising sea-level. An alternative to drive land-level rise is peat formation, for which indications were found in the estuary experiments in Chapters 4 & 5. Although the vegetation species in the estuary experiments were unsuited for peat formation, areas with ponding water on the bay-head delta (see panel "vegetated levees" in Fig. 4.5) and high tidal wetlands showed possible locations for peat formation. The controlled drowning of near-coastal regions with fresh/brackish water favours the slow process of peat formation, which stores CO_2 and raises the land (e.g. Clymo, 1984; Smolders et al., 2002; Pierik et al., in prep.). This can be achieved by raising the groundwater table, which in many coastal regions is artificially maintained at a low level with pumps, for example for agricultural purposes. The benefits of a higher groundwater table and peat formation include a reduction in subsidence related to soil compaction and peat oxidation, and the development of a larger subterranean body of freshwater that hampers salt intrusion.

7.3 Advancements in modelling and experiments

To study how tidal floodplains in the form of mudflats and salt marshes influence the shape of estuaries, two advancements in numerical modelling and one advancement in scale experiments were undertaken in this thesis. Firstly, morphodynamics with a natural variability in morphological units needed to be reproduced in a numerical model to allow for the isolation of, and sensitivity analysis of, single boundary conditions. Literature showed natural morphodynamics may be achieved by time-varying perturbations on the boundary conditions in closed-system numerical models (Lanzoni and Seminara, 2006; Schuurman et al., 2016) and experiments (Van Dijk et al., 2013a). This thesis tested whether these perturbations also influence the morphodynamics and steady state of rivers in Chapter 2. Secondly, a numerical model was tested and validated to acquire flow data in scaled landscape experiments in Chapter 3. The resultant rich data set on water depths and flow velocities enabled the quantitative analysis of how tidal prism and tidal zonation developed over time in the filling estuary experiments. Thirdly, real vegetation in rivers and estuaries constitutes many species with different eco-engineering traits, yet scale experiments commonly only use one species, namely *Alfalfa*. So, to encompass the complex interplay of vegetation species on the morphological development, this thesis presented one of the first experiments that used multiple species (see also Kleinhans et al., 2022). Below, these three advancements are explained in further detail along with possible applications and new research opportunities.

7.3.1 Conditions for sustained natural dynamics

Natural rivers, estuaries and coasts are invariably subjected to changing boundary conditions, which cause ongoing morphodynamics and a natural variability in morphology. However, many numerical and experimental studies assume constant boundary conditions to reproduce (a part of) these systems, which tends to result in diminishing morphodynamic change (e.g. Braudrick et al., 2009; Van Oorschot et al., 2016). Still, new perturbations like bend and bar instabilities can develop within a modelled domain, but these take time and therefore distance to develop (Lanzoni and Seminara, 2006). Therefore, in order to reproduce ongoing morphodynamics without the need for an extensive domain, previous literature suggested that a perturbation needs to be imposed on the boundary conditions. For example, a time-varying wave direction in nearshore modelling causes a more natural variability of rip spacing, migration rate and direction (Castelle and Ruessink, 2011). And for

meandering rivers, a continuous perturbation of the river inflow causes dynamic meandering as found in scaled landscape experiments (Van de Lageweg et al., 2013; Van Dijk et al., 2013a; 2013b) and numerical modelling (Lanzoni and Seminara, 2006; Nicholas, 2013; Schuurman et al., 2016; Weiss, 2016).

As for rivers, most numerical modelling efforts with an inflow perturbation allowed for only one channel over the cross-section, so any perturbation would inevitably result in some form of meandering with neck-cutoffs. Accordingly, this raised the question to what extent an inflow perturbation forces the downstream channel and bar pattern. This thesis now demonstrates for a numerical meandering river with chute cutoffs (Chapter 2) that the direct influence of an inflow perturbation only extends to the first bend, whilst the channel and bar pattern further downstream is determined by the tendency to form floodplains. This is because perturbations dampen out within a few channel widths (Zolezzi and Seminara, 2001; Schuurman et al., 2016) and new bend and bar instabilities are generated at every bend (Struiksma et al., 1985; Crosato and Mosselman, 2009). Therefore, an inflow perturbation merely enables to attain and maintain natural dynamics close to the upstream boundary, strongly reducing the required length of a model domain.

However, this does not mean that all perturbations have a negligible effect on the overall morphodynamics. On the one hand, storm and flood events (e.g. Townend et al., 2007; Mariotti et al., 2010; Fruergaard et al., 2013; Swales et al., 2019) and perturbations like tectonics (Woolderink et al., 2022) often act as mere noise at the system scale, perpetuating the current steady state of a river or estuary. On the other hand, large enough triggers and persistent changes in boundary conditions may profoundly alter the steady state of a fluvial or tidal system. An example is the storm and subsequent dike breaches that formed the Dollard tidal embayment in the Ems Estuary (Van Maren et al., 2016; Pierik, 2021).

Some meandering rivers feed into estuaries, which raises the question whether estuaries with floodplain formation also need an inflow perturbation to produce sustained natural dynamics. In numerical modelling, this is already done by varying partitioned inflow to prevent scouring (e.g Braat et al., 2017; Brückner et al., 2021) but is still lacking in scaled landscape experiments of estuaries. Large meander bends in the upstream reach of estuaries seem to migrate much slower and have fewer cutoffs than their completely fluvial counterparts, which is probably related to the bidirectional flow (Leuven et al., 2018c). River discharge commonly constitutes only a small fraction of the tidal prism. And while this small contribution seems sufficient to influence the hydraulic geometry of channels in tidal deltas (Sassi et al., 2012) and estuaries (Shimozono et al., 2019), it is probably too small to directly influence the migration rate of meander bends. The addition of an inflow perturbation to an estuary experiment would likely result in a less semi-circular and more irregularly shaped bay-head delta with less floodplain but would otherwise not considerably affect the morphodynamics within an estuary. This ought to be tested in new scaled estuary experiments.

7.3.2 Integrating models and experiments

Scaled landscape experiments provide valuable insight about fluvial, tidal and coastal systems and make their morphodynamics more tangible. However, many previous studies experienced challenges to measure accurate and continuous data on the hydrodynamics, especially if multi-coloured sediments and vegetation were used. Whilst most studies used techniques including point gauging (e.g Friedkin, 1945; Mayor-Mora, 1977), dye (e.g. Gran and Paola, 2001; Kleinhans et al., 2012), ultrasounding (e.g. Tambroni et al., 2005; Tesser et al., 2007) and particle imaging velocimetry (PIV) (e.g. Peakall et al., 2007; Leuven et al., 2018b), so far only one research team (Tesser et al., 2007; Stefanon et al., 2010; 2012) instead modelled uniform shallow flow to acquire data on water depth and flow velocity. This modelling approach solved common issues like limitations of the measuring equipment and necessary simplifications during post-processing in previous techniques.

This thesis extended and validated the numerical modelling approach for unsteady non-uniform shallow flow in both fluvial and tidal (tilting) experiments (Chapter 3). The modelling requires as input a digital elevation model and a few flow boundary conditions to produce hydrodynamics (e.g. water depth, flow velocity and bed shear stress) at the same resolution as the elevation map with an overall performance similar to or higher than previous methods. Furthermore, vegetation effects can be included in the model as done for the filling estuary experiments presented in Chapters 4 & 5. So, the numerical modelling approach enables a quantitative and objective analysis of multiple hydrodynamic parameters, which allows for more in-depth analysis of future and past scaled landscape experiments.

The open-source modelling approach opens up faster and new ways to design and analyse scaled landscape experiments. Firstly, initial and boundary conditions can be tested in parallel prior to the physical experiments, which saves laboratory time. Secondly, inundation zones are readily derived from the modelled hydrodynamics and may be indicative of the spatial distribution of different floral and faunal species (Ysebaert et al., 2003). Consequently, scaled landscape experiments take on a more multi-disciplinary character, as experiments may now also be used to study, for instance, the impact of artificial constructions and dredging on life form habitat.

There is room for further development in flow modelling in experiments. The present model in Chapter 3 produces rather diffuse flow patterns. These provide sufficient information on the scale of an entire estuary, yet the modelling fails to capture the sharp flow curvatures around shallow bars. Improved modelling will result in a closer approximation of where vegetation may establish and where animals may thrive. Another development is to include substrate-dependent bed roughness. This requires additional input based on in-situ measurements or overhead imagery and will slightly improve flow modelling over shallow bars and bar tops. Since flow on bar tops is already very slow and more acting as intertidal volume storage, the large-scale flow patterns are probably not significantly influences by substrate-dependent bed roughness.

7.3.3 Vegetation in scaled landscape experiments

This thesis presented one of the first scaled landscape experiments with multiple vegetation species with different eco-engineering traits. Besides the commonly used *Alfalfa* (e.g. Gran and Paola, 2001; Braudrick et al., 2009; Van Dijk et al., 2013b), the novel filling estuary experiments also included *Lotus pedunculatus* and *Veronica beccabunga* (Lokhorst et al., 2019). Based on their different ideal sprouting conditions relative to the hydroperiod, *Alfalfa* represents riparian vegetation and *Lotus* and *Veronica* represent salt marsh and reed-like vegetation. *Veronica* was typically the pioneering species on intertidal bars because of its tiny seed size. However, a known issue with *Alfalfa* is its large and strong roots that sometimes prevent its removal by erosion, even in a channel. Conversely, the *Lotus* and *Veronica* species were strong enough to persist on intertidal and supratidal bars but were easily removed when inundation stress increased. The experiments in this thesis show that *Lotus* and *Veronica* behaved like natural vegetation in the scale experiments, suggesting that these species will also provide interesting results in fluvial landscape experiments.

7.4 Future work

This thesis focused on the first stages of estuary filling in scale experiments and land-level rise along meandering rivers and estuaries in numerical models. Together, these studies demonstrated the importance of floodplain formation, which confines and elevates fluvial and tidal systems, and how these effects may be negated by sea-level rise. This thesis generally focused on natural alluvial systems, thereby ignoring the human factor. Before the effects of artificial constructions and measures can be determined, it is crucial to understand the natural dynamics in rivers and estuaries. This thesis

advanced this understanding and led to a number of topics in both alluvial and managed estuaries that are deemed worth investigating and outlined below.

7.4.1 Estuary filling

The scaled landscape experiments in Chapter 4 showed the development of partly filled estuaries with mud and vegetation from an initially drowned and largely subtidal basin. Mud and especially vegetation proved effective at raising land and confining the subtidal channels in the upstream direction. However, the experiments remained partly filled and did not develop towards a completely filled estuary or an overfilled delta. Accordingly, it remains untested whether rapidly expanding reed, salt marshes and peatlands can start a positive feedback loop towards complete estuary filling like hypothesised for the Old Rhine Estuary (NL) (Beets and Van der Spek, 2000; De Haas et al., 2018; Pierik, 2021). This suggests that a larger tendency to form floodplains is needed, which may be achieved through an increased supply of fines. In nature, the deposition of fines is promoted by flocculation and the capture of vegetation, which are probably essential for the hypothesised rapid expansion of e.g. reeds and climax tidal vegetation. Therefore, new experiments are needed to test to what extent clastic material is needed to fill estuaries.

Mudflats in scale experiments to date tended to form mainly on mid-channel bars (Braat et al., 2019a; Chapters 4 & 5). In contrast, field observations (Dalrymple and Choi, 2007) and numerical modelling (Braat et al., 2017) show that mudflats can also flank the outer banks of an estuary, where they limit erosion of the outer banks. Braat et al. (2019a) hypothesised that the development of such shore-connected mudflats requires a net filling estuary, but the novel experiments of filling estuaries show a similar trend as in the ingressive estuary experiments. This may be related to the steep outer banks in these experiments (Braat et al., 2019a; Chapters 4 & 5), while more gentle slopes would create more space and smaller gradients that probably favour the deposition of shore-connected mudflats. Alternatively, the development of shore-connected mudflats may require a broader range of suspended sediment grain sizes (Boechat Albernaz et al., 2020) and diurnal variability, which necessitates further work.

Mudflats and salt marshes form a thin top layer on intertidal and supratidal bars relative to the deep subtidal channels. On a scale of a single bar or marsh, this has proven sufficient to strongly reduce tidal range and flow velocity. However, on a system scale, tidal floodplains are easily reworked by migrating channels. This raises the question whether increased bank strength is the dominant process that confines channels and reduces channel migration. Although an increased bank strength may result in less erosion on the fringes of mudflats and salt marshes, it seems unlikely that the added bank strength limits the channel migration of channels several tens of metres deep. In rivers, it was hypothesised that the main process that confines channels is instead a reduction in overland flow due to enhanced hydraulic roughness (Kleinhans et al., 2018), which prevents muddy and vegetated bars from being cut through. A similar hypothesis can be formulated for tidal floodplains, which tend to be difficult to erode (Spencer et al., 2016), and requires further work.

Sea-level rise will set back estuary filling in many estuaries as it negates the eco-engineering traits of vegetation and results in the drowning of ecologically invaluable intertidal and supratidal areas. Exploratory modelling (Chapter 6) suggests that new intertidal and supratidal areas can be formed along estuaries in transitional polders, which will also increase flood dominance and promote channel shallowing in estuaries with moderate to high friction. Therefore, the opening of transitional polders along estuaries could compensate part of the negative effects by sea-level rise. This subject remains underinvestigated to date and would benefit from future numerical and experimental studies.

Moreover, the drowning of the central reach of the experimental estuary happened due to rapid sea-level rise (Chapter 5). However, this is but one permutation of morphological response to sea-level rise. Alternatives, including complete transgression of an estuary and a complete drowning of the

entire estuary, were not reproduced and likely form with slower and faster sea-level rise (Chapter 5). New experiments and models with different rates of sea-level rise can show how the channel and bar pattern will change.

7.4.2 Estuary engineering

Estuaries form a gateway to the world and are therefore often heavily managed. The outer banks are commonly bounded by dikes that tend to force the locations of bars and channels (Leuven et al., 2018b) and leave little room for wide flanking mudflats and foreshores. Particularly in large estuaries with moderate to high friction, embankment has enhanced ebb-dominance. This culminated in deeper channels (Sherwood et al., 1990; Ahlhorn et al., 2012; Nnafie et al., 2019), which may be aggravated by dredging campaigns (e.g. Cox et al., 2021).

With sea-level on the rise and new policies that prioritise nature-based solutions (European Commission, 2021), there is an increasing interest in sustainable measures for flood safety that not only reduce flood risk but also increase ecological value and cause land-level rise (e.g. Esteves, 2014; Schoonees et al., 2019; Van den Hoven et al., 2022). Transitional polders between double dikes are one of these promising measures (Van Belzen et al., 2021) and require further investigation. Real-world findings indicate that the size and shape of managed realignment projects is important: larger and more elongated sites correlate with a higher species diversity because of smaller spatial gradients in habitat zones (Wolters et al., 2005). Furthermore, creek networks, either naturally developed or artificially dug, provide drainage that ensures the full ecological and geomorphological functioning of managed realignment sites (e.g. Chirol et al., 2022; Gourgue et al., 2022). Yet, (pre-carved) channels that are too high or too low with respect to the tidal range have little effect on the landward-to-seaward filling in managed realignment (Wallace et al., 2005) and may be less beneficial to the benefits of improved drainage. Additionally, it remains unclear what the optimum shape and size is of a transitional polder or managed realignment site to bring about fast land-level rise along with a rich biodiversity. This is probably specific to boundary conditions such as sediment supply and tidal range and requires more rigorous numerical modelling in both idealised and real-world estuaries.

On a more engineering level, gate culverts may be used to enhance mud deposition, and therefore land-level rise, in transitional polders. In the case of an open inlet, as used in the modelling of transitional polders in Chapter 6, the erosive power of ebb-dominant flows can remove part of the previously deposited mud. This slows down the desired process of land-level rise. In contrast, gate culverts enable a more controlled in- and outflow of water (e.g. Oosterlee et al., 2020; Van Belzen et al., 2021). This controlled tidal water exchange allows for a longer time of still-standing water and less erosion during ebb, which may promote mud deposition. However, the volume of water with suspended sediment that enters every tidal cycle during flood has a strong influence on the rate of mud deposition. Oosterlee et al. (2020) found that it is a larger water depth during flood and not a longer hydroperiod that correlates with mud deposition rates. In their example, the controlled inflow was minor and resulted in smaller deposition rates compared to an open inlet. This shows more research is needed into whether and how gate culverts can be used to promote mud deposition in combination with transitional polders.

References

Abel, N., Gorddard, R., Harman, B., Leitch, A., Langridge, J., Ryan, A. & Heyenga, S. (2011). Sea level rise, coastal development and planned retreat: analytical framework, governance principles and an Australian case study. *Environmental science & policy*, 14 (3), pp. 279–288.

Abrahim, G.M.S., Nichol, S.L., Parker, R.J. & Gregory, M.R. (2008). Facies depositional setting, mineral maturity and sequence stratigraphy of a Holocene drowned valley, Tamaki Estuary, New Zealand. *Estuarine, Coastal and Shelf Science*, 79 (1), pp. 133–142.

Adnan, M.S.G., Talchabhadel, R., Nakagawa, H. & Hall, J.W. (2020). The potential of tidal river management for flood alleviation in south western Bangladesh. *Science of the Total Environment*, 731, pp. 1–25.

Ahlhorn, F., Meyerdirks, J., Heiber, W. & Saathoff, S. (2012). Secondary Channels in European Estuaries. Occurrence and Importance of Secondary Channels in European Estuaries - Literature Study in the framework of the Interreg project TIDE. *Tech. Ref.*, 45 pp.

Allard, J., Chaumillon, E. & Féniès, H. (2009). A synthesis of morphological evolutions and Holocene stratigraphy of a wave-dominated estuary: The Arcachon lagoon, SW France. *Continental Shelf Research*, 29 (8), pp. 957–969.

Allen, G.P. & Posamentier, H.W. (1993). Sequence stratigraphy and facies model of an incised valley fill; the Gironde Estuary, France. *Journal of Sedimentary Research*, 63 (3), pp. 378–391.

Allen, J.R. (2000). Morphodynamics of Holocene salt marshes: a review sketch from the Atlantic and Southern North Sea coasts of Europe. *Quaternary Science Reviews*, 19 (12), pp. 1155–1231.

Arcement, G.J. & Schneider, V.R. (1989). *Guide for selecting Manning's roughness coefficients for natural channels and flood plains*.

Asahi, K., Shimizu, Y., Nelson, J. & Parker, G. (2013). Numerical simulation of river meandering with self-evolving banks. *Journal of Geophysical Research: Earth Surface*, 118, pp. 2208–2229. DOI:10.1002/JGRF.20150.

Ashmore, P.E. (1991). Channel morphology and bed load pulses in braided, gravel-bed streams. *Geografiska Annaler. Series A. Physical Geography*, 73 (1), pp. 37–52. DOI:10.1080/04353676.1991.11880331.

Ashworth, P.J., Best, J.L. & Leddy, J.O. (1994). *6 The Physical Modelling of Braided Rivers and Deposition of Fine-grained*. Vol. 8. Wiley.

Ashworth, P.J., Best, J.L. & Jones, M. (2004). Relationship between sediment supply and avulsion frequency in braided rivers. *Geology*, 32 (1), pp. 21–24.

Auerbach, L.W., Goodbred Jr, S.L., Mondal, D.R., Wilson, C.A., Ahmed, K.R., Roy, K., Steckler, M.S., Small, C., Gilligan, J.M. & Ackerly, B.A. (2015). Flood risk of natural and embanked landscapes on the Ganges-Brahmaputra tidal delta plain. *Nature Climate Change*, 5 (2), pp. 153–157.

Baar, A.W., Boechat-Albernaz, M., Van Dijk, W.M. & Kleinhans, M.G. (2019). Critical dependence of morphodynamic models of fluvial and tidal systems on empirical downslope sediment transport. *Nature communications*, 10 (1), pp. 1–12.

Baas, J.H., Jago, C., Macklin, M. & Team, C.C.C.R. (2008). *The river–estuarine transition zone (RETZ) of the Afon Dyfi (West Wales) as test bed for sediment transfer between river catchments and coastal environments*. BSRG 2008, 14–17th December.

Baker, W.L. (1989). Macro- and micro-scale influences on riparian vegetation in Western Colorado. *Annals of the Association of American Geographers*, 79 (1), pp. 65–78.

Bamber, J.L., Oppenheimer, M., Kopp, R.E., Aspinall, W.P. & Cooke, R.M. (2019). Ice sheet contributions to future sea-level rise from structured expert judgment. *Proceedings of the National Academy of Sciences*, 116 (23), pp. 11195–11200.

Baptist, M.J., Babovic, V., Rodríquez Uthurburu, J., Keijzer, M., Uittenbogaard, R.E., Mynett, A. & Verwey, A. (2007). On inducing equations for vegetation resistance. *Journal of Hydraulic Research*, 45 (4), pp. 435–450. DOI:10.1080/00221686.2007.9521778.

Baptist, M.J., Dankers, P., Cleveringa, J., Sittoni, L., Willemsen, P.W.J.M., Van Puijenbroek, M.E.B., De Vries, B., Leuven, J.R.F.W., Coumou, L., Kramer, H. & Elschot, K. (2021). Salt marsh construction as a nature-based solution in an estuarine social-ecological system. *Nature-Based Solutions*, 1, p. 100005.

Barbier, E.B. (2007). Valuing ecosystem services as productive inputs. *Economic policy*, 22 (49), pp. 178–229.

Barbier, E.B., Georgiou, I.Y., Enchelmeyer, B. & Reed, D.J. (2013). The value of wetlands in protecting southeast Louisiana from hurricane storm surges. *PloS one*, 8 (3), e58715.

Barbier, E.B., Hacker, S.D., Kennedy, C., Koch, E.W., Stier, A.C. & Silliman, B.R. (2011). The value of estuarine and coastal ecosystem services. *Ecological monographs*, 81 (2), pp. 169–193.

Baumgardner, S. (2016). *Quantifying Galloway: fluvial, tidal and wave influence on experimental and field deltas*. PhD thesis, University of Minnesota.
Beets, D.J. & Van der Spek, A.J.F. (2000). The Holocene evolution of the barrier and the back-barrier basins of Belgium and the Netherlands as a function of late Weichselian morphology, relative sea-level rise and sediment supply. *Netherlands Journal of Geosciences*, 79 (1), pp. 3–16.
Bendix, J. & Hupp, C.R. (2000). Hydrological and geomorphological impacts on riparian plant communities. *Hydrological processes*, 14 (6), pp. 2977–2990.
Benoit, L.K. & Askins, R.A. (2002). Relationship between habitat area and the distribution of tidal marsh birds. *The Wilson Bulletin*, 114 (3), pp. 314–323.
Berends, K.D., Straatsma, M.W., Warmink, J.J. & Hulscher, S.J.M.H. (2019). Uncertainty quantification of flood mitigation predictions and implications for interventions. *Natural hazards and Earth system sciences*, 19 (8), pp. 1737–1753.
Berendsen, H.J.A. (2004). *De vorming van het land*. (in Dutch) *English translation: The development of the Earth's surface*. Uitgeverij Van Gorcum.
Best, J. & Ashworth, P. (1994). A high-resolution ultrasonic bed profiler for use in laboratory flumes. *Journal of Sedimentary Research*, 64 (3), pp. 674–675.
Birch, G.F., Murray, O., Johnson, I. & Wilson, A. (2009). Reclamation in Sydney estuary, 1788–2002. *Australian Geographer*, 40 (3), pp. 347–368.
Blanton, J.O., Lin, G. & Elston, S.A. (2002). Tidal current asymmetry in shallow estuaries and tidal creeks. *Continental Shelf Research*, 22 (11-13), pp. 1731–1743.
Blum, M.D. & Törnqvist, T.E. (2000). Fluvial responses to climate and sea-level change: a review and look forward. *Sedimentology*, 47 (SUPPL. 1), pp. 2–48.
Boechat Albernaz, M. & Kleinhans, M.G. (in prep.). Tidal basin development with mud and vegetation.
Boechat Albernaz, M., Roelofs, L., Pierik, H.J. & Kleinhans, M.G. (2020). Natural levee evolution in vegetated fluvial-tidal environments. *Earth Surface Processes and Landforms*, 45 (15), pp. 3824–3841.
Bolla Pittaluga, M., Repetto, R. & Tubino, M. (2003). Channel bifurcation in braided rivers: equilibrium configurations and stability. *Water Resources Research*, 39 (3). DOI:10.1029/2001WR001112.
Bouma, T.J., Van Belzen, J., Balke, T., Zhu, Z., Airoldi, L., Blight, A.J., Davies, A.J., Galvan, C., Hawkins, S.J., Hoggart, S.P., et al. (2014). Identifying knowledge gaps hampering application of intertidal habitats in coastal protection: Opportunities & steps to take. *Coastal Engineering*, 87, pp. 147–157.
Boyd, R., Dalrymple, R. & Zaitlin, B.A. (1992). Classification of clastic coastal depositional environments. *Sedimentary Geology*, 80 (3-4), pp. 139–150.
Braat, L., Leuven, J.R.F.W., Lokhorst, I.R. & Kleinhans, M.G. (2019a). Effects of estuarine mudflat formation on tidal prism and large-scale morphology in experiments. *Earth Surface Processes and Landforms*, 44 (2), pp. 417–432.
Braat, L., Van Dijk, W.M., Pierik, H.-J., Van de Lageweg, W., Brückner, M.Z.M., Wagner-Cremer, F. & Kleinhans, M.G. (2019b). *Tidal bar accretion by mudflat sedimentation*. preprint on EarthArXiv. https://doi.org/10.31223/osf.io/gq9pt.
Braat, L., Van Kessel, T., Leuven, J.R.F.W. & Kleinhans, M.G. (2017). Effects of mud supply on large-scale estuary morphology and development over centuries to millennia. *Earth Surface Dynamics*, 5 (4), pp. 617–652.
Braudrick, C.A., Dietrich, W.E., Leverich, G.T. & Sklar, L.S. (2009). Experimental evidence for the conditions necessary to sustain meandering in coarse-bedded rivers. *Proceedings of the National Academy of Sciences*, 106 (40), pp. 16936–16941. DOI:10.1073/PNAS.0909417106.
Brückner, M.Z.M., Braat, L., Schwarz, C. & Kleinhans, M.G. (2020). What came first, mud or biostabilizers? Elucidating interacting effects in a coupled model of mud, saltmarsh, microphytobenthos, and estuarine morphology. *Water Resources Research*, 56 (9), e2019WR026945.
Brückner, M.Z.M., Mcmahon, W.J. & Kleinhans, M.G. (2021). Muddying the waters: modeling the effects of early land plants in paleozoic estuaries. *Palaios*, 36 (5), pp. 173–181.
Brückner, M.Z.M., Schwarz, C., Van Dijk, W.M., Van Oorschot, M., Douma, H. & Kleinhans, M.G. (2019). Salt marsh establishment and eco-engineering effects in dynamic estuaries determined by species growth and mortality. *Journal of Geophysical Research: Earth Surface*, 124 (12), pp. 2962–2986.
Byrne, R.J., Gammisch, R.A. & Thomas, G.R. (1980). Tidal prism-inlet area relations for small tidal inlets. In: *Coastal Engineering 1980*, pp. 2517–2533.
Camporeale, C., Perona, P., Porporato, A. & Ridolfi, L. (2005). On the long-term behavior of meandering rivers. *Water Resources Research*, 41 (12), W12403. DOI:10.1029/2005WR004109.
Carbonneau, P.E., Lane, S.N. & Bergeron, N. (2006). Feature based image processing methods applied to bathymetric measurements from airborne remote sensing in fluvial environments. *Earth Surface Processes and Landforms: The Journal of the British Geomorphological Research Group*, 31 (11), pp. 1413–1423.

Castellarin, A., Domeneghetti, A. & Brath, A. (2011). Identifying robust large-scale flood risk mitigation strategies: A quasi-2D hydraulic model as a tool for the Po river. *Physics and Chemistry of the Earth, Parts A/B/C*, 36 (7-8), pp. 299–308.

Castelle, B. & Ruessink, B.G. (2011). Modeling formation and subsequent nonlinear evolution of rip channels: Time-varying versus time-invariant wave forcing. *Journal of Geophysical Research: Earth Surface*, 116 (F4). DOI:10.1029/2011JF001997.

Chen, Y., Overeem, I., Kettner, A.J., Gao, S. & Syvitski, J.P. (2015). Modeling flood dynamics along the superelevated channel belt of the Yellow River over the last 3000 years. *Journal of Geophysical Research: Earth Surface*, 120 (7), pp. 1321–1351.

Chirol, C., Haigh, I.D., Pontee, N., Thompson, C.E. & Gallop, S.L. (2022). Morphological evolution of creek networks in 10 restored coastal wetlands in the UK. *Scientific Data*, 9 (1), pp. 1–16.

Chmura, G.L., Anisfeld, S.C., Cahoon, D.R. & Lynch, J.C. (2003). Global carbon sequestration in tidal, saline wetland soils. *Global biogeochemical cycles*, 17 (4).

Clement, A.J.H., Fuller, I.C. & Sloss, C.R. (2017). Facies architecture, morphostratigraphy, and sedimentary evolution of a rapidly-infilled Holocene incised-valley estuary: The lower Manawatu valley, North Island New Zealand. *Marine Geology*, 390, pp. 214–233.

Clymo, R.S. (1984). The limits to peat bog growth. *Philosophical Transactions of the Royal Society of London. B, Biological Sciences*, 303 (1117), pp. 605–654.

Coen, I (1988). Ontstaan en ontwikkeling van de Westerschelde. *Water*, 43 (1), pp. 156–162.

Constantine, J.A., Dunne, T., Piégay, H. & Kondolf, M.G. (2010). Controls on the alluviation of oxbow lakes by bed-material load along the Sacramento River, California. *Sedimentology*, 57 (2), pp. 389–407. DOI:10.1111/j.1365-3091.2009.01084.x.

Corenblit, D., Steiger, J., Gurnell, A.M., Tabacchi, E. & Roques, L. (2016). Seed retention by pioneer trees enhances plant diversity resilience on gravel bars: Observations from the river Allier, France. *Advances in Water Resources*, 93, pp. 182–192. DOI:10.1016/j.advwatres.2016.02.015.

Cox, J.R., Dunn, F.E., Nienhuis, J.H., Van der Perk, M. & Kleinhans, M.G. (2021). Climate change and human influences on sediment fluxes and the sediment budget of an urban delta: the example of the lower Rhine–Meuse delta distributary network. *Anthropocene Coasts*, 4 (1), pp. 251–280.

Cox, J.R., Lingbeek, J., Weisscher, S.A.H. & Kleinhans, M.G. (in review). Effects of sea-level rise on dredged estuary morphology. *Journal of Geophysical Research: Earth Surface*.

Cox, T., Maris, T., De Vleeschauwer, P., De Mulder, T., Soetaert, K. & Meire, P. (2006). Flood control areas as an opportunity to restore estuarine habitat. *Ecological Engineering*, 28 (1), pp. 55–63.

Crosato, A. (2009). Physical explanations of variations in river meander migration rates from model comparison. *Earth Surface Processes and Landforms*, 34, pp. 2078–2086. DOI:10.1002/esp.1898.

Crosato, A. & Mosselman, E. (2009). Simple physics-based predictor for the number of river bars and the transition between meandering and braiding. *Water Resources Research*, 45 (3), W03424. DOI:10.1029/2008WR007242.

D'Alpaos, A., Lanzoni, S., Marani, M. & Rinaldo, A. (2009). On the O'Brien–Jarrett–Marchi law. *Rendiconti Lincei*, 20 (3), pp. 225–236.

Dalrymple, R.W., Boyd, R. & Zaitlin, B.A. (1994). History of research, types and internal organisation of incised-valley systems: introduction to the volume. *SEPM Society for Sedimentary Geology*, 51, pp. 1–10.

Dalrymple, R.W. & Choi, K. (2007). Morphologic and facies trends through the fluvial–marine transition in tide-dominated depositional systems: a schematic framework for environmental and sequence-stratigraphic interpretation. *Earth-Science Reviews*, 81 (3-4), pp. 135–174.

Dalrymple, R.W., Zaitlin, B.A. & Boyd, R. (1992). Estuarine facies models; conceptual basis and stratigraphic implications. *Journal of Sedimentary Research*, 62 (6), pp. 1130–1146.

Dam, G, Van der Wegen, M., Labeur, R.J. & Roelvink, D. (2016). Modeling centuries of estuarine morphodynamics in the Western Scheldt estuary. *Geophysical Research Letters*, 43 (8), pp. 3839–3847.

De Haas, T., Pierik, H.-J., Van der Spek, A.J.F., Cohen, K.M., Van Maanen, B. & Kleinhans, M.G. (2018). Holocene evolution of tidal systems in The Netherlands: Effects of rivers, coastal boundary conditions, eco-engineering species, inherited relief and human interference. *Earth-Science Reviews*, 177, pp. 139–163.

De Haas, T., Van der Valk, L., Cohen, K.M., Pierik, H.-J., Weisscher, S.A.H., Hijma, M.P., Van der Spek, A.J.F. & Kleinhans, M.G. (2019). Long-term evolution of the Old Rhine estuary: Unravelling effects of changing boundary conditions and inherited landscape. *The Depositional Record*, 5 (1), pp. 84–108.

De Vet, P.L.M., Van Prooijen, B.C. & Wang, Z.B. (2017). The differences in morphological development between the intertidal flats of the Eastern and Western Scheldt. *Geomorphology*, 281, pp. 31–42.

De Villiers, G., Kleinhans, M.G. & Postma, G. (2013). Experimental delta formation in crater lakes and implications for interpretation of Martian deltas. *Journal of Geophysical Research E: Planets*, 118 (4), pp. 651–670. DOI:10.1002/jgre.20069.

Defina, A. (2000). Two-dimensional shallow flow equations for partially dry areas. *Water Resources Research*, 36 (11), pp. 3251–3264.
Deltares (2020). *Svn repository*. https://svn.oss.deltares.nl/repos/delft3d/tags/delft3d4/7545.
Depreiter, D., Lanckriet, T., Van Holland, G., Vanlede, J., Beirinckx, K. & Maris, T. (2015). Mud disposal and suspended sediment concentration in the lower sea Scheldt: towards a hyperturbid system? In: *E-proceedings of the 36th IAHR World Congress*, pp. 7430–7444.
Dijkema, K.S. (1987). Changes in salt-marsh area in the Netherlands Wadden Sea after 1600. In: *Vegetation between land and sea*. Springer, pp. 42–51.
Dissanayake, D.M.P.K., Roelvink, J.A. & Van der Wegen, M. (2009). Modelled channel patterns in a schematized tidal inlet. *Coastal Engineering*, 56 (11-12), pp. 1069–1083.
Dixon, M., Morris, R.K.A., Scott, C., Birchenough, A. & Colclough, S. (2008). Managed realignment–lessons from Wallasea, UK. In: *Proceedings of the Institution of Civil Engineers-Maritime Engineering*. Vol. 161. 2. Thomas Telford Ltd, pp. 61–71.
Dronkers, J. (1986). Tidal asymmetry and estuarine morphology. *Netherlands Journal of Sea Research*, 20 (2-3), pp. 117–131.
Dronkers, J. (2017). Convergence of estuarine channels. *Continental Shelf Research*, 144, pp. 120–133.
Du, J., Shen, J., Zhang, Y.J., Ye, F., Liu, Z., Wang, Z., Wang, Y.P., Yu, X., Sisson, M. & Wang, H.V. (2018). Tidal response to sea-level rise in different types of estuaries: The Importance of Length, Bathymetry, and Geometry. *Geophysical Research Letters*, 45 (1), pp. 227–235.
Duarte, C.M., Losada, I.J., Hendriks, I.E., Mazarrasa, I. & Marbà, N. (2013). The role of coastal plant communities for climate change mitigation and adaptation. *Nature Climate Change*, 3 (11), pp. 961–968.
Eertman, R.H.M., Kornman, B.A., Stikvoort, E. & Verbeek, H. (2002). Restoration of the Sieperda tidal marsh in the Scheldt estuary, the Netherlands. *Restoration Ecology*, 10 (3), pp. 438–449.
Elias, E.P.L., Van der Spek, A.J.F., Wang, Z.B. & De Ronde, J. (2012). Morphodynamic development and sediment budget of the Dutch Wadden Sea over the last century. *Netherlands Journal of Geosciences*, 91 (3), pp. 293–310. DOI:10.1017/S0016774600000457.
Elschot, K. & Bakker, J.P. (2016). Dynamics of small-scale topographic heterogeneity in European sandy salt marshes. *Journal of Marine Science and Engineering*, 4 (1), p. 21.
Engelund, F. (1974). Flow and bed topography in channel bends. *Journal of the Hydraulics Division*, 100 (Proc. Paper 10963), pp. 1631–1648.
Esteves, L.S. (2014). What is Managed Realignment? In: *Managed Realignment: A Viable Long-Term Coastal Management Strategy?* Springer, pp. 19–31.
European Commission (2021). Communication from the Commission to the European Parliament, the Council, the European Economic and Social Committee and the Committee of the Regions; Forging a climate-resilient Europe - the new EU Strategy on Adaptation to Climate Change. *COM/2021/82 final*.
Fagherazzi, S., Kirwan, M.L., Mudd, S.M., Guntenspergen, G.R., Temmerman, S., D'Alpaos, A., Van De Koppel, J., Rybczyk, J.M., Reyes, E., Craft, C., et al. (2012). Numerical models of salt marsh evolution: Ecological, geomorphic, and climatic factors. *Reviews of Geophysics*, 50 (1), RG1002.
Fagherazzi, S., Mariotti, G., Wiberg, P.L. & McGlathery, K.J. (2013). Marsh collapse does not require sea level rise. *Oceanography*, 26 (3), pp. 70–77.
Ferguson, R. (1987). Hydraulic and sedimentary controls of channel pattern. In: *River Channels: Environment and Process*. Richards K. (ed.). Institute of British Geographers Special Publication 18. Blackwell: Oxford; 129–158.
Fisk, H.N. (1947). Fine-grained alluvial deposits and their effects on Mississippi River activity. Volume 1. *Corps of Engineers Vicksburg Miss.*
FitzGerald, D.M., Fenster, M.S., Argow, B.A. & Buynevich, I.V. (2008). Coastal impacts due to sea-level rise. *Annual Review of Earth and Planetary Sciences*, 36, pp. 601–647.
FitzGerald, D.M., Hein, C.J., Hughes, Z., Kulp, M., Georgiou, I. & Miner, M. (2018). Runaway barrier island transgression concept: Global case studies. In: *Barrier dynamics and response to changing climate*. Springer, pp. 3–56.
FitzGerald, D.M. & Hughes, Z. (2019). Marsh processes and their response to climate change and sea-level rise. *Annual Review of Earth and Planetary Sciences*, 47, pp. 481–517.
Fortunato, A.B. & Oliveira, A. (2005). Influence of intertidal flats on tidal asymmetry. *Journal of Coastal Research*, 21 (5), pp. 1062–1067.
French, P.W. (2006). Managed realignment–the developing story of a comparatively new approach to soft engineering. *Estuarine, Coastal and Shelf Science*, 67 (3), pp. 409–423.
French, P. (1999). Managed retreat: a natural analogue from the Medway estuary, UK. *Ocean & Coastal Management*, 42 (1), pp. 49–62.
Friedkin, J. (1945). *A laboratory study of the meandering of alluvial rivers*. U.S. Army Corps of Engineers, U.S. Waterways Experiment Station, Vicksburg, Mississippi, USA.

Friedrichs, C.T. (1995). Stability shear stress and equilibrium cross-sectional geometry of sheltered tidal channels. *Journal of Coastal Research*, 11 (4), pp. 1062–1074.
Friedrichs, C.T. (2010). Barotropic tides in channelized estuaries. In: *Contemporary Issues in Estuarine Physics*. Cambridge University Press Cambridge, UK, pp. 27–61.
Friedrichs, C.T. (2011). Tidal flat morphodynamics: a synthesis. *Coastal and Estuarine Research Federation, 21st Biennial Conference, Daytona Beach, FL*.
Friedrichs, C.T. & Aubrey, D.G. (1988). Non-linear tidal distortion in shallow well-mixed estuaries: a synthesis. *Estuarine, Coastal and Shelf Science*, 27 (5), pp. 521–545.
Fruergaard, M., Andersen, T.J., Johannessen, P.N., Nielsen, L.H. & Pejrup, M. (2013). Major coastal impact induced by a 1000-year storm event. *Scientific Reports*, 3 (1), pp. 1–7.
Furbish, D.J. (1988). River-bend curvature and migration: How are they related? *Geology*, 16 (8), pp. 752–755. DOI:10.1130/0091-7613(1988)016<0752:RBCAMH>2.3.CO;2.
Féniès, H. & Faugères, J.-C. (1998). Facies and geometry of tidal channel-fill deposits (Arcachon Lagoon, SW France). *Marine Geology*, 150 (1-4), pp. 131–148.
Gardner, J.T. & Ashmore, P.E. (2011). Geometry and grain-size characteristics of the basal surface of a braided river deposit. *Geology*, 39 (3), pp. 247–250.
Gay, G.R., Gay, H.H., Gay, W.H., Martinson, H.A., Meade, R.H. & Moody, J.A. (1998). Evolution of cutoffs across meander necks in Powder River, Montana, USA. *Earth Surface Processes and Landforms*, 23 (7), pp. 651–662. DOI:10.1002/(SICI)1096-9837(199807)23:7<651::AID-ESP891>3.0.CO;2-V.
Gedan, K.B., Kirwan, M.L., Wolanski, E., Barbier, E.B. & Silliman, B.R. (2011). The present and future role of coastal wetland vegetation in protecting shorelines: answering recent challenges to the paradigm. *Climatic change*, 106 (1), pp. 7–29.
Geerling, G.W., Ragas, A.M.J., Leuven, R.S.E.W., Van den Berg, J.H., Breedveld, M., Liefhebber, D. & Smits, A.J.M. (2006). Succession and rejuvenation in floodplains along the river Allier (France). *Hydrobiologia*, 565 (1), pp. 71–86. DOI:10.1007/1-4020-5367-3_5.
Glenn, J.L. (1978). *Sediment sources and Holocene sedimentation history in Tillamook Bay, Oregon; data and preliminary interpretations*. Tech. rep. US Geological Survey.
Gourgue, O., Van Belzen, J., Schwarz, C., Vandenbruwaene, W., Vanlede, J., Belliard, J.-P., Fagherazzi, S., Bouma, T.J., Van de Koppel, J. & Temmerman, S. (2022). Biogeomorphic modeling to assess resilience of tidal marsh restoration to sea level rise and sediment supply. *Earth Surface Dynamics*, 10 (3), pp. 531–553.
Gran, K. & Paola, C. (2001). Riparian vegetation controls on braided stream dynamics. *Water Resources Research*, 37 (12), pp. 3275–3283.
Grasmeijer, B., Dam, G. & Taal, M. (2013). Actualisatierapport Delft3D Schelde-estuarium (in Dutch). *Technical Report (International Marine & Dredging Consultants)*.
Gregoire, G., Le Roy, P., Ehrhold, A., Jouet, G. & Garlan, T. (2017). Control factors of Holocene sedimentary infilling in a semi-closed tidal estuarine-like system: the bay of Brest (France). *Marine Geology*, 385, pp. 84–100.
Groen, P. (1967). On the residual transport of suspended matter by an alternating tidal current. *Netherlands Journal of Sea Research*, 3 (4), pp. 564 –574. DOI:HTTPS://DOI.ORG/10.1016/0077-7579(67)90004-X.
Heap, A.D. & Nichol, S.L. (1997). The influence of limited accommodation space on the stratigraphy of an incised-valley succession: Weiti River estuary, New Zealand. *Marine Geology*, 144 (1-3), pp. 229–252.
Hickin, E.J. & Nanson, G.C. (1975). The character of channel migration on the Beatton River, northeast British Columbia, Canada. *Geological Society of America Bulletin*, 86 (4), pp. 487–494. DOI:10.1130/0016-7606(1975)86<487:TCOCMO>2.0.CO;2.
Hijma, M.P. & Cohen, K.M. (Mar. 2010). Timing and magnitude of the sea-level jump preluding the 8200 yr event. *Geology*, 38 (3), pp. 275–278.
Hooke, J.M. (2004). Cutoffs galore!: occurrence and causes of multiple cutoffs on a meandering river. *Geomorphology*, 31 (3), pp. 225–238. DOI:10.1016/J.GEOMORPH.2003.12.006.
Horton, B.P., Khan, N.S., Cahill, N., Lee, J.S., Shaw, T.A., Garner, A.J., Kemp, A.C., Engelhart, S.E. & Rahmstorf, S. (2020). Estimating global mean sea-level rise and its uncertainties by 2100 and 2300 from an expert survey. *NPJ climate and atmospheric science*, 3 (1), pp. 1–8.
Hoyal, D.C.J.D. & Sheets, B.A. (2009). Morphodynamic evolution of experimental cohesive deltas. *Journal of Geophysical Research: Earth Surface*, 114 (F2). DOI:10.1029/2007JF000882.
Huggett, R.J. (2016). *Fundamentals of Geomorphology*. Routledge.
Iwasaki, T., Shimizu, Y. & Kimura, I. (2016). Numerical simulation of bar and bank erosion in a vegetated floodplain: A case study in the Otofuke River. *Advances in Water Resources*, 93, pp. 118–134. DOI:10.1016/J.ADVWATRES.2015.02.001.
Iwasaki, T., Shimizu, Y. & Kimura, I. (2013). Modelling of the initiation and development of tidal creek networks. In: *Proceedings of the Institution of Civil Engineers-Maritime Engineering*. Vol. 166. 2. Thomas Telford Ltd, pp. 76–88.
Jarrett, J.T. (1976). *Tidal prism: inlet area relationships*. Vol. 3. US Army Engineer Waterways Experiment Station.

Jeuken, M.C.J.L. (2000). On the morphologic behaviour of the tidal channels in the Westerschelde estuary (PhD thesis). *Universiteit Utrecht*.
Jeuken, M.C.J.L. & Wang, Z.B. (2010). Impact of dredging and dumping on the stability of ebb–flood channel systems. *Coastal Engineering*, 57 (6), pp. 553–566.
Job, T., Penny, D., Morgan, B., Hua, Q., Gadd, P. & Zawadzki, A. (2021). Multi-stage Holocene evolution of the River Murray Estuary, South Australia. *The Holocene*, 31 (1), pp. 50–65.
Jongepier, I., Wang, C., Missiaen, T., Soens, T. & Temmerman, S. (2015). Intertidal landscape response time to dike breaching and stepwise re-embankment: A combined historical and geomorphological study. *Geomorphology*, 236, pp. 64–78.
Kadiri, M., Spencer, K.L., Heppell, C.M. & Fletcher, P. (2011). Sediment characteristics of a restored saltmarsh and mudflat in a managed realignment scheme in Southeast England. *Hydrobiologia*, 672 (1), pp. 79–89.
Kiedrzyńska, E., Kiedrzyński, M. & Zalewski, M. (2015). Sustainable floodplain management for flood prevention and water quality improvement. *Natural Hazards*, 76 (2), pp. 955–977.
Kiesel, J., Schuerch, M., Christie, E.K., Möller, I., Spencer, T. & Vafeidis, A.T. (2020). Effective design of managed realignment schemes can reduce coastal flood risks. *Estuarine, Coastal and Shelf Science*, 242, p. 106844.
King, S.E. & Lester, J.N. (1995). The value of salt marsh as a sea defence. *Marine pollution bulletin*, 30 (3), pp. 180–189.
Kirwan, M.L., Guntenspergen, G.R., D'Alpaos, A., Morris, J.T., Mudd, S.M. & Temmerman, S. (2010). Limits on the adaptability of coastal marshes to rising sea level. *Geophysical Research Letters*, 37 (23), p. L23401.
Kirwan, M.L. & Megonigal, J.P. (2013). Tidal wetland stability in the face of human impacts and sea-level rise. *Nature*, 504 (7478), pp. 53–60.
Kleinhans, M.G. (2010). Sorting out river channel patterns. *Progress in Physical Geography*, 34 (3), pp. 287–326. DOI:10.1177/0309133310365300.
Kleinhans, M.G., Braudrick, C., Van Dijk, W.M., Van de Lageweg, W.I., Teske, R. & Van Oorschot, M. (2015a). Swiftness of biomorphodynamics in Lilliput- to Giant-sized rivers and deltas. *Geomorphology*, 244, pp. 56–73. DOI:10.1016/J.GEOMORPH.2015.04.022.
Kleinhans, M.G., De Vries, B.M.L., Braat, L. & Van Oorschot, M. (2018). Living Landscapes: Muddy and vegetated floodplain formation effects on fluvial pattern in an incised river. *Earth Surface Processes and Landforms*, 43 (14), pp. 2948–2963.
Kleinhans, M.G., Ferguson, R.I., Lane, S.N. & Hardy, R.J. (2013). Splitting rivers at their seams: bifurcations and avulsion. *Earth Surface Processes and Landforms*, 38 (1), pp. 47–61. DOI:10.1002/ESP.3268.
Kleinhans, M.G., Jagers, H.R.A., Mosselman, E. & Sloff, C.J. (2008). Bifurcation dynamics and avulsion duration in meandering rivers by one-dimensional and three-dimensional models. *Water Resources Research*, 44 (8), W08454. DOI:10.1029/2007WR005912.
Kleinhans, M.G. & Van den Berg, J.H. (2011). River channel and bar patterns explained and predicted by an empirical and a physics-based method. *Earth Surface Processes and Landforms*, 36 (6), pp. 721–738. DOI:10.1002/ESP.2090.
Kleinhans, M.G., Van Dijk, W.M., Van de Lageweg, W.I., Hoyal, D.C.J.D., Markies, H., Van Maarseveen, M., Roosendaal, C., Van Weesep, W., Van Breemen, D., Hoendervoogt, R. & Cheshier, N. (2014a). Quantifiable effectiveness of experimental scaling of river- and delta morphodynamics and stratigraphy. *Earth-Science Reviews*, 133, pp. 43–61. DOI:10.1016/J.EARSCIREV.2014.03.001.
Kleinhans, M.G., Van Rosmalen, T.M., Roosendaal, C. & Van der Vegt, M. (2014b). Turning the tide: mutually evasive ebb-and flood-dominant channels and bars in an experimental estuary. *Advances in Geosciences*, 39, pp. 21–26.
Kleinhans, M.G., Leuven, J.R.F.W., Braat, L. & Baar, A.W. (2017a). Scour holes and ripples occur below the hydraulic smooth to rough transition of movable beds. *Sedimentology*, 64 (5), pp. 1381–1401.
Kleinhans, M.G., Roelofs, L., Weisscher, S.A.H., Lokhorst, I.R. & Braat, L. (2022). Estuarine morphodynamics and development modified by floodplain formation. *Earth Surface Dynamics*, 10 (2), pp. 367–381.
Kleinhans, M.G., Van der Vegt, M., Van Scheltinga, R.T., Baar, A.W. & Markies, H. (2012). Turning the tide: experimental creation of tidal channel networks and ebb deltas. *Netherlands Journal of Geosciences*, 91 (3), pp. 311–323.
Kleinhans, M.G., Van Der Vegt, M., Leuven, J.R.F.W., Braat, L., Markies, H., Simmelink, A., Roosendaal, C., Van Eijk, A., Vrijbergen, P. & Van Maarseveen, M. (2017b). Turning the tide: comparison of tidal flow by periodic sea level fluctuation and by periodic bed tilting in scaled landscape experiments of estuaries. *Earth Surface Dynamics*, 5 (4), pp. 731–756.
Kleinhans, M.G., Van Scheltinga, R.T., Van Der Vegt, M. & Markies, H. (2015b). Turning the tide: Growth and dynamics of a tidal basin and inlet in experiments. *Journal of Geophysical Research: Earth Surface*, 120 (1), pp. 95–119.

Kleinhans, M.G., Weerts, H.J.T. & Cohen, K.M. (2010). Avulsion in action: reconstruction and modelling sedimentation pace and upstream flood water levels following a Medieval tidal-river diversion catastrophe (Biesbosch, The Netherlands, 1421–1750 AD). *Geomorphology*, 118 (1-2), pp. 65–79.
Lanzoni, S. & Seminara, G. (2006). On the nature of meander instability. *Journal of Geophysical Research: Earth Surface*, 111 (F4). DOI:10.1029/2005JF000416.
Lanzoni, S. & Seminara, G. (2002). Long-term evolution and morphodynamic equilibrium of tidal channels. *Journal of Geophysical Research: Oceans*, 107 (C1), pp. 1–13.
Lawrence, P.J., Smith, G.R., Sullivan, M.J. & Mossman, H.L. (2018). Restored saltmarshes lack the topographic diversity found in natural habitat. *Ecological Engineering*, 115, pp. 58–66.
Leduc, P., Peirce, S. & Ashmore, P. (2019). Short communication: Challenges and applications of structure-from-motion photogrammetry in a physical model of a braided river. *Earth Surface Dynamics*, 7, pp. 97–106.
Leopold, L.B. & Wolman, M.G. (1957). *River channel patterns: braided, meandering, and straight*. Geological Survey professional paper 282-B. US Government Printing Office, Washington, DC.
Lesser, G.R., Roelvink, J.A., Van Kester, J.A.T.M. & Stelling, G.S. (2004). Development and validation of a three-dimensional morphological model. *Coastal engineering*, 51 (8-9), pp. 883–915.
Leuven, J.R.F.W., De Haas, T., Braat, L. & Kleinhans, M.G. (2018a). Topographic forcing of tidal sandbar patterns for irregular estuary planforms. *Earth Surface Processes and Landforms*, 43 (1), pp. 172–186.
Leuven, J.R.F.W. & Kleinhans, M.G. (2019). Incipient tidal bar and sill formation. *Journal of Geophysical Research: Earth Surface*, 124 (7), pp. 1762–1781.
Leuven, J.R.F.W., Braat, L., Van Dijk, W.M., De Haas, T., Van Onselen, E.P., Ruessink, B.G. & Kleinhans, M.G. (2018b). Growing forced bars determine nonideal estuary planform. *Journal of Geophysical Research: Earth Surface*, 123 (11), pp. 2971–2992.
Leuven, J.R.F.W., Pierik, H.-J., Van der Vegt, M., Bouma, T.J. & Kleinhans, M.G. (2019). Sea-level-rise-induced threats depend on the size of tide-influenced estuaries worldwide. *Nature Climate Change*, 9 (12), pp. 986–992.
Leuven, J.R.F.W., Van Maanen, B., Lexmond, B.R., Van der Hoek, B.V., Spruijt, M.J. & Kleinhans, M.G. (2018c). Dimensions of fluvial-tidal meanders: Are they disproportionally large? *Geology*, 46 (10), pp. 923–926.
Leuven, J.R.F.W., Verhoeve, S.L., Van Dijk, W.M., Selaković, S. & Kleinhans, M.G. (2018d). Empirical assessment tool for bathymetry, flow velocity and salinity in estuaries based on tidal amplitude and remotely-sensed imagery. *Remote Sensing*, 10 (12), pp. 1–32.
Lokhorst, I.R., Braat, L., Leuven, J.R.F.W., Baar, A.W., Van Oorschot, M., Selaković, S. & Kleinhans, M.G. (2018). Morphological effects of vegetation on the tidal-fluvial transition in Holocene estuaries. *Earth Surface Dynamics*, 6 (4), pp. 883–901.
Lokhorst, I.R., De Lange, S.I., Van Buiten, G., Selaković, S. & Kleinhans, M.G. (2019). Species selection and assessment of eco-engineering effects of seedlings for biogeomorphological landscape experiments. *Earth Surface Processes and Landforms*, 44 (14), pp. 2922–2935.
Luhar, M., Rominger, J. & Nepf, H. (2008). Interaction between flow, transport and vegetation spatial structure. *Environmental Fluid Mechanics*, 8 (5), pp. 423–439. DOI:10.1007/s10652-008-9080-9.
Marani, M., Belluco, E., D'Alpaos, A., Defina, A., Lanzoni, S. & Rinaldo, A. (2003). On the drainage density of tidal networks. *Water Resources Research*, 39 (2), ESG.
Marciano, R., Wang, Z.B., Hibma, A., De Vriend, H.J. & Defina, A. (2005). Modeling of channel patterns in short tidal basins. *Journal of Geophysical Research: Earth Surface*, 110 (F1).
Marijnissen, R.J.C., Kok, M., Kroeze, C. & Van Loon-Steensma, J.M. (2021). Flood risk reduction by parallel flood defences–Case-study of a coastal multifunctional flood protection zone. *Coastal Engineering*, 167, p. 103903.
Mariotti, G., Fagherazzi, S., Wiberg, P.L., McGlathery, K.J., Carniello, L. & Defina, A. (2010). Influence of storm surges and sea level on shallow tidal basin erosive processes. *Journal of Geophysical Research: Oceans*, 115 (C11), pp. 1–17.
Mariotti, G. & Fagherazzi, S. (2010). A numerical model for the coupled long-term evolution of salt marshes and tidal flats. *Journal of Geophysical Research: Earth Surface*, 115 (F1).
Marra, W.A., Braat, L., Baar, A.W. & Kleinhans, M.G. (2014). Valley formation by groundwater seepage, pressurized groundwater outbursts and crater-lake overflow in flume experiments with implications for Mars. *Icarus*, 232, pp. 97–117.
Masselink, G., Hanley, M.E., Halwyn, A.C., Blake, W., Kingston, K., Newton, T. & Williams, M. (2017). Evaluation of salt marsh restoration by means of self-regulating tidal gate–Avon estuary, South Devon, UK. *Ecological engineering*, 106, pp. 174–190.
Matsubara, Y., Howard, A.D., Burr, D.M., Williams, R.M.E., Dietrich, W.E. & Moore, J.M. (2015). River meandering on Earth and Mars: A comparative study of Aeolis Dorsa meanders, Mars and possible terrestrial analogs of the Usuktuk River, AK, and the Quinn River, NV. *Geomorphology*, 240, pp. 102–120.
Maximova, T., Ides, S., De Mulder, T. & Mostaert, F. (2009). LTV O&M thema veiligheid: deelproject 1. Verbetering hydrodynamisch NEVLA model ten behoeve van scenario-analyse (in Dutch). *WL Rapporten*, 756.

Mayor-Mora, R.E. (1977). *Laboratory investigation of tidal inlets on sandy coasts.* Tech. rep. California Univ Berkeley Hydraulic Engineering Lab.
Meyer-Peter, E. & Müller, R. (1948). Formulas for bed-load transport. In: *IAHSR 2nd meeting, Stockholm, appendix 2*. IAHR.
Mietta, F., Chassagne, C., Manning, A.J. & Winterwerp, J.C. (2009). Influence of shear rate, organic matter content, pH and salinity on mud flocculation. *Ocean Dynamics*, 59 (5), pp. 751–763.
Minderhoud, P.S.J., Erkens, G., Pham, V.H., Bui, V.T., Erban, L., Kooi, H. & Stouthamer, E. (2017). Impacts of 25 years of groundwater extraction on subsidence in the Mekong delta, Vietnam. *Environmental research letters*, 12 (6), p. 064006.
Möller, I, Spencert, T & French, J. (1996). Wind wave attenuation over saltmarsh surfaces: preliminary results from Norfolk, England. *Journal of Coastal Research*, 12 (4), pp. 1009–1016.
Möller, I., Kudella, M., Rupprecht, F., Spencer, T., Paul, M., Van Wesenbeeck, B.K., Wolters, G., Jensen, K., Bouma, T.J., Miranda-Lange, M., et al. (2014). Wave attenuation over coastal salt marshes under storm surge conditions. *Nature Geoscience*, 7 (10), pp. 727–731.
Moore, R.D., Wolf, J., Souza, A.J. & Flint, S.S. (2009). Morphological evolution of the Dee Estuary, Eastern Irish Sea, UK: a tidal asymmetry approach. *Geomorphology*, 103 (4), pp. 588–596.
Mori, N. & Chang, K.-A. (2003). Experimental study of a horizontal jet in a wavy environment. *Journal of engineering mechanics*, 129 (10), pp. 1149–1155.
Morris, J.T., Sundareshwar, P., Nietch, C.T., Kjerfve, B. & Cahoon, D.R. (2002). Responses of coastal wetlands to rising sea level. *Ecology*, 83 (10), pp. 2869–2877.
Morris, R.K.A. (2012). Managed realignment: A sediment management perspective. *Ocean & coastal management*, 65, pp. 59–66.
Morris, R.K.A. (2013). Managed realignment as a tool for compensatory habitat creation–a re-appraisal. *Ocean & coastal management*, 73, pp. 82–91.
Mossman, H.L., Davy, A.J. & Grant, A. (2012). Does managed coastal realignment create saltmarshes with 'equivalent biological characteristics' to natural reference sites? *Journal of Applied Ecology*, 49 (6), pp. 1446–1456.
Mudd, S.M., Howell, S.M. & Morris, J.T. (2009). Impact of dynamic feedbacks between sedimentation, sea-level rise, and biomass production on near-surface marsh stratigraphy and carbon accumulation. *Estuarine, Coastal and Shelf Science*, 82 (3), pp. 377–389.
Munsch, S.H., Cordell, J.R. & Toft, J.D. (2017). Effects of shoreline armouring and overwater structures on coastal and estuarine fish: opportunities for habitat improvement. *Journal of Applied Ecology*, 54 (5), pp. 1373–1384.
Muto, T. & Steel, R.J. (2001). Autostepping during the transgressive growth of deltas: results from flume experiments. *Geology*, 29 (9), pp. 771–774. DOI:10.1130/0091-7613(2001)029<0771:ADTTGO>2.0.CO;2.
Nagata, T., Watanabe, Y., Yasuda, H. & Ito, A. (2014). Development of a meandering channel caused by the planform shape of the river bank. *Earth Surface Dynamics*, 2, pp. 255–270.
Nagata, T., Watanabe, Y., Yasuda, H., Ito, A. & Kuwamura, T. (2013). Development of a meandering channel caused by the plane shape of the river bank in the low-water channel. *Monthly Report of Civil Engineering Research Institute for Cold Region*, 721. (in Japanese), pp. 2–11.
Nanson, G.C. & Knighton, A.D. (1996). Anabranching rivers: their cause, character and classification. *Earth Surface Processes and Landforms*, 21 (3), pp. 217–239. DOI:10.1002/(SICI)1096-9837(199603)21:3<217::AID-ESP611>3.0.CO;2-U.
Neary, V., Sotiropoulos, F & Odgaard, A. (1999). Three-dimensional numerical model of lateral-intake inflows. *Journal of Hydraulic Engineering*, 125 (2), pp. 126–140.
Nichol, S.L. (1991). Zonation and sedimentology of estuarine facies in an incised valley, wave-dominated, microtidal setting, New South Wales, Australia. In: *Tidal Sedimentology*. CSPG Special Publications, pp. 41–58.
Nicholas, A. (2013). Modelling the continuum of river channel patterns. *Earth Surface Processes and Landforms*, 38 (10), pp. 1187–1196. DOI:10.1002/esp.3431.
Nicholls, R.J., Brown, S., Goodwin, P., Wahl, T., Lowe, J., Solan, M., Godbold, J.A., Haigh, I.D., Lincke, D., Hinkel, J., et al. (2018). Stabilization of global temperature at 1.5 C and 2.0 C: implications for coastal areas. *Philosophical Transactions of the Royal Society A: Mathematical, Physical and Engineering Sciences*, 376 (2119), p. 20160448.
Nnafie, A., De Swart, H.E., De Maerschalck, B., Van Oyen, T., Van der Vegt, M. & Van der Wegen, M. (2019). Closure of secondary basins causes channel deepening in estuaries with moderate to high friction. *Geophysical Research Letters*, 46 (22), pp. 13209–13216.
Nnafie, A., Van Oyen, T., De Maerschalck, B., Van der Vegt, M. & Van der Wegen, M. (2018). Estuarine channel evolution in response to closure of secondary basins: An observational and morphodynamic modeling study of the Western Scheldt Estuary. *Journal of Geophysical Research: Earth Surface*, 123 (1), pp. 167–186.
O'Brien, M.P. (1931). Estuary tidal prisms related to entrance areas. *Civil Engineering*, 1 (8), pp. 738–739.

O'Brien, M.P. (1969). Equilibrium flow areas of inlets on sandy coasts. *Journal of the Waterways and Harbors Division*, 95 (1), pp. 43–52.
Olabarrieta, M., Geyer, W.R., Coco, G., Friedrichs, C.T. & Cao, Z. (2018). Effects of density-driven flows on the long-term morphodynamic evolution of funnel-shaped estuaries. *Journal of Geophysical Research: Earth Surface*, 123 (11), pp. 2901–2924.
Oosterlee, L., Cox, T.J.S., Temmerman, S & Meire, P (2020). Effects of tidal re-introduction design on sedimentation rates in previously embanked tidal marshes. *Estuarine, Coastal and Shelf Science*, 244, p. 106428.
Paola, C. (2000). Quantitative models of sedimentary basin filling. *Sedimentology*, 47, pp. 121–178.
Parker, G. (1976). On the cause and characteristic scales of meandering and braiding in rivers. *Journal of Fluid Mechanics*, 76 (3), pp. 457–480. DOI:10.1017/S0022112076000748.
Partheniades, E. (1965). Erosion and deposition of cohesive soils. *Journal of the Hydraulics Division*, 91 (1), pp. 105–139.
Peakall, J., Ashworth, P.J. & Best, J.L. (2007). Meander-bend evolution, alluvial architecture, and the role of cohesion in sinuous river channels: a flume study. *Journal of Sedimentary Research*, 77 (3), pp. 197–212. DOI:10.2110/JSR.2007.017.
Perucca, E., Camporeale, C. & Ridolfi, L. (2007). Significance of the riparian vegetation dynamics on meandering river morphodynamics. *Water Resources Research*, 43 (3). DOI:10.1029/2006WR005234.
Peterson, C. (2014). Late Holocene Geomorphology of the Columbia River Estuary, Oregon and Washington, USA. *Journal of Geography and Geology*, 6 (2), pp. 1–27.
Pethick, J. (2002). Estuarine and tidal wetland restoration in the United Kingdom: policy versus practice. *Restoration Ecology*, 10 (3), pp. 431–437.
Pierik, H.-J. (2021). Landscape changes and human–landscape interaction during the first millennium AD in the Netherlands. *Netherlands Journal of Geosciences*, 100 (e11), pp. 1–14.
Pierik, H.-J., Cohen, K.M., Vos, P.C., Van der Spek, A.J.F. & Stouthamer, E. (2017). Late Holocene coastal-plain evolution of the Netherlands: the role of natural preconditions in human-induced sea ingressions. *Proceedings of the Geologists' Association*, 128 (2), pp. 180–197.
Pierik, H.-J., Moree, J.I.M., Roelofs, L., Boechat-Albernaz, M., Wilbers, A., Van der Valk, L., Van Dinter, M., De Haas, T. & Kleinhans, M.G. (in prep.). Vegetation composition and peat accumulation steer Holocene tidal-fluvial basin filling and overbank sedimentation along the Old Rhine River, the Netherlands.
Pinter, N., Jemberie, A.A., Remo, J.W.F., Heine, R.A. & Ickes, B.S. (2008). Flood trends and river engineering on the Mississippi River system. *Geophysical Research Letters*, 35 (23), pp. 1–5.
Plancke, Y.M.G., Ides, S.J., Vos, G.R., Roose, F. & Peters, J.J. (2010). A new disposal strategy for the Western Scheldt, conciliating port accessibility and nature preservation. In: *32nd PIANC Congress, 125th anniversary PIANC - setting the course, Liverpool, UK, Liverpool Arena and Convention Centre, 10 - 14 May 2010: PIANC MMX book of abstracts. pp. 173.*
Postma, H. (1961). Transport and accumulation of suspended matter in the Dutch Wadden Sea. *Netherlands Journal of Sea Research*, 1 (1), pp. 148 –190. DOI:HTTPS://DOI.ORG/10.1016/0077-7579(61)90004-7.
Remo, J.W.F., Carlson, M. & Pinter, N. (2012). Hydraulic and flood-loss modeling of levee, floodplain, and river management strategies, Middle Mississippi River, USA. *Natural hazards*, 61 (2), pp. 551–575.
Reynolds, O. (1889). Report of the committee appointed to investigate the action of waves and currents on the beds and foreshores of estuaries by means of working models, British Association Report. *Papers on mechanical and physical subjects*, 2, pp. 380–481.
Reynolds, O. (1891). Third report of the committee appointed to investigate the action of waves and currents on the beds and foreshores of estuaries by means of working models, British Association Report. *Papers on mechanical and physical subjects*, 2, pp. 482–518.
Rijke, J., Van Herk, S., Zevenbergen, C. & Ashley, R. (2012). Room for the River: delivering integrated river basin management in the Netherlands. *International journal of river basin management*, 10 (4), pp. 369–382.
Roep, T. & Van Regteren Altena, J. (1988). Paleotidal levels in tidal sediments (3800-3635 BP); compaction, sea level rise and human occupation (3275-2620BP) at Bovenkarspel, NW Netherlands. *Tide-Influenced Sedimentary Environments and Facies*, pp. 215–231.
Roy, P.S., Thom, B.G. & Wright, L.D. (1980). Holocene sequences on an embayed high-energy coast: an evolutionary model. *Sedimentary Geology*, 26 (1-3), pp. 1–19.
Sassi, M.G., Hoitink, A.J.F., De Brye, B. & Deleersnijder, E. (2012). Downstream hydraulic geometry of a tidally influenced river delta. *Journal of Geophysical Research: Earth Surface*, 117 (F4).
Savenije, H.H.G. (2015). Prediction in ungauged estuaries: An integrated theory. *Water Resources Research*, 51 (4), pp. 2464–2476.
Schoonees, T., Gijón Mancheño, A., Scheres, B., Bouma, T.J., Silva, R., Schlurmann, T. & Schüttrumpf, H. (2019). Hard structures for coastal protection, towards greener designs. *Estuaries and Coasts*, 42 (7), pp. 1709–1729.

Schramkowski, G., Schuttelaars, H. & De Swart, H. (2002). The effect of geometry and bottom friction on local bed forms in a tidal embayment. *Continental Shelf Research*, 22 (11-13), pp. 1821–1833.
Schrijvershof, R. & Vroom, J. (2016). Effecten van Realistische (extreme) Stortstrategieën in de Westerschelde. *Deltares report 1220094*.
Schuerch, M., Spencer, T., Temmerman, S., Kirwan, M.L., Wolff, C., Lincke, D., McOwen, C.J., Pickering, M.D., Reef, R., Vafeidis, A.T., et al. (2018). Future response of global coastal wetlands to sea-level rise. *Nature*, 561 (7722), pp. 231–234.
Schumm, S.A. & Khan, H. (1972). Experimental study of channel patterns. *Geological Society of America Bulletin*, 83 (6), pp. 1755–1770.
Schumm, S.A., Mosley, M.P. & Weaver, W (1987). *Experimental fluvial geomorphology*. John Wiley and Sons Inc., New York, NY.
Schuurman, F., Marra, W.A. & Kleinhans, M.G. (2013). Physics-based modeling of large braided sand-bed rivers: Bar pattern formation, dynamics, and sensitivity. *Journal of geophysical research: Earth Surface*, 118 (4), pp. 2509–2527. DOI:10.1002/2013JF002896.
Schuurman, F., Shimizu, Y., Iwasaki, T. & Kleinhans, M.G. (2016). Dynamic meandering in response to upstream perturbations and floodplain formation. *Geomorphology*, 253, pp. 94–109. DOI:10.1016/J.GEOMORPH.2015.05.039.
Schwarz, C., Bouma, T.J., Zhang, L.Q., Temmerman, S., Ysebaert, T. & Herman, P.M.J. (2015). Interactions between plant traits and sediment characteristics influencing species establishment and scale-dependent feedbacks in salt marsh ecosystems. *Geomorphology*, 250, pp. 298–307.
Schwarz, C., Gourgue, O., Van Belzen, J., Zhu, Z., Bouma, T.J., Van De Koppel, J., Ruessink, G., Claude, N. & Temmerman, S. (2018). Self-organization of a biogeomorphic landscape controlled by plant life-history traits. *Nature Geoscience*, 11 (9), pp. 672–677.
Seabergh, W.C., King, D.B. & Stephens, B.E. (2001). *Tidal inlet equilibrium area experiments, inlet laboratory investigations*. Vol. 1. US Army Corps of Engineers, Engineer Research, Development Center, Coastal, and Hydraulics Laboratory.
Sherwood, C.R., Jay, D.A., Harvey, R.B., Hamilton, P. & Simenstad, C.A. (1990). Historical changes in the Columbia River estuary. *Progress in Oceanography*, 25 (1-4), pp. 299–352.
Shi, Z. & Lamb, H.F. (Oct. 1991). Post-glacial sedimentary evolution of a microtidal estuary, Dyfi Estuary, west Wales, U.K. *Sedimentary Geology*, 73 (3-4), pp. 227–246.
Shimizu, Y., Inoue, T., Hamaki, M. & Iwasaki, T. (2013). *iRIC Software, Changing River Science, Nays2D Solver Manual*. iRIC.
Shimozono, T., Tajima, Y., Akamatsu, S., Matsuba, Y. & Kawasaki, A. (2019). Large-scale Channel Migration in the Sittang River estuary. *Scientific reports*, 9 (1), pp. 1–9.
Simon, A. & Collinson, A.J. (2002). Quantifying the mechanical and hydrologic effects of riparian vegetation on streambank stability. *Earth Surface Processes and Landforms*, 27 (5), pp. 527–546. DOI:10.1002/ESP.325.
Siviglia, A., Stecca, G., Vanzo, D., Zolezzi, G., Toro, E.F. & Tubino, M. (2013). Numerical modelling of two-dimensional morphodynamics with applications to river bars and bifurcations. *Advances in Water Resources*, 52, pp. 243–260.
Smolders, A.J.P., Tomassen, H.B.M., Lamers, L.P.M., Lomans, B.P. & Roelofs, J.G.M. (2002). Peat bog restoration by floating raft formation: the effects of groundwater and peat quality. *Journal of Applied Ecology*, 39 (3), pp. 391–401.
Solari, L., Van Oorschot, M., Belletti, B., Hendriks, D., Rinaldi, M & Vargas-Luna, A. (2016). Advances on modelling riparian vegetation-hydromorphology interactions. *River Research and Applications*, 32 (2), pp. 164–178. DOI:10.1002/RRA.2910.
Sonke, W., Kleinhans, M.G., Speckmann, B., Van Dijk, W.M. & Hiatt, M. (2022). Alluvial connectivity in multi-channel networks in rivers and estuaries. *Earth Surface Processes and Landforms*, 47 (2), pp. 477–490.
Spearman, J. (2011). The development of a tool for examining the morphological evolution of managed realignment sites. *Continental Shelf Research*, 31 (10), S199–S210.
Speer, P.E. & Aubrey, D.G. (1985). A study of non-linear tidal propagation in shallow inlet/estuarine systems Part II: Theory. *Estuarine, Coastal and Shelf Science*, 21 (2), pp. 207–224.
Spencer, T., Möller, I., Rupprecht, F., Bouma, T.J., Van Wesenbeeck, B.K., Kudella, M., Paul, M., Jensen, K., Wolters, G., Miranda-Lange, M., et al. (2016). Salt marsh surface survives true-to-scale simulated storm surges. *Earth Surface Processes and Landforms*, 41 (4), pp. 543–552.
Stefanon, L., Carniello, L., D'Alpaos, A. & Lanzoni, S. (2010). Experimental analysis of tidal network growth and development. *Continental Shelf Research*, 30 (8), pp. 950–962.
Stefanon, L., Carniello, L., D'Alpaos, A. & Rinaldo, A. (2012). Signatures of sea level changes on tidal geomorphology: Experiments on network incision and retreat. *Geophysical Research Letters*, 39 (12), pp. 1–6.

Stella, J.C., Hayden, M.K., Battles, J.J., Piégay, H., Dufour, S. & Fremier, A.K. (2011). The role of abandoned channels as refugia for sustaining pioneer riparian forest ecosystems. *Ecosystems*, 14 (5), pp. 776–790. DOI:10.1007/S10021-011-9446-6.

Struiksma, N., Olesen, K.W., Flokstra, C. & de Vriend, H.J. (1985). Bed deformation in curved alluvial channels. *Journal of Hydraulic Research*, 23 (1), pp. 57–79. DOI:10.1080/00221688509499377.

Swales, A., Reeve, G., Cahoon, D.R. & Lovelock, C. (2019). Landscape evolution of a fluvial sediment-rich Avicennia marina mangrove forest: insights from seasonal and inter-annual surface-elevation dynamics. *Ecosystems*, 22 (6), pp. 1232–1255.

Symonds, A.M. & Collins, M.B. (2007). The development of artificially created breaches in an embankment as part of a managed realignment, Freiston Shore, UK. *Journal of Coastal Research*, Special Issue 50, pp. 130–134.

Symonds, A.M. & Collins, M.B. (2005). Sediment dynamics associated with managed realignment; Freiston Shore, The Wash, UK. In: *Coastal Engineering 2004: (In 4 Volumes)*. World Scientific, pp. 3173–3185.

Syvitski, J.P., Kettner, A.J., Overeem, I., Hutton, E.W., Hannon, M.T., Brakenridge, G.R., Day, J., Vörösmarty, C., Saito, Y., Giosan, L., et al. (2009). Sinking deltas due to human activities. *Nature Geoscience*, 2 (10), pp. 681–686.

Tal, M. & Paola, C. (2010). Effects of vegetation on channel morphodynamics: results and insights from laboratory experiments. *Earth Surface Processes and Landforms*, 35 (9), pp. 1014–1028. DOI:10.1002/ESP.1908.

Tal, M. & Paola, C. (2007). Dynamic single-thread channels maintained by the interaction of flow and vegetation. *Geology*, 35 (4), pp. 347–350.

Tambroni, N., Bolla Pittaluga, M. & Seminara, G. (2005). Laboratory observations of the morphodynamic evolution of tidal channels and tidal inlets. *Journal of Geophysical Research: Earth Surface*, 110 (F4).

Temmerman, S., Bouma, T.J., Van de Koppel, J., Van der Wal, D., De Vries, M.B. & Herman, P.M.J. (2007). Vegetation causes channel erosion in a tidal landscape. *Geology*, 35 (7), pp. 631–634.

Temmerman, S., Govers, G., Wartel, S. & Meire, P. (2003). Spatial and temporal factors controlling short-term sedimentation in a salt and freshwater tidal marsh, Scheldt estuary, Belgium, SW Netherlands. *Earth Surface Processes and Landforms: The Journal of the British Geomorphological Research Group*, 28 (7), pp. 739–755.

Temmerman, S., Meire, P., Bouma, T.J., Herman, P.M., Ysebaert, T. & De Vriend, H.J. (2013). Ecosystem-based coastal defence in the face of global change. *Nature*, 504 (7478), pp. 79–83.

Temmink, R.J.M., Lamers, L.P., Angelini, C., Bouma, T.J., Fritz, C., Van de Koppel, J., Lexmond, R., Rietkerk, M., Silliman, B.R., Joosten, H., et al. (2022). Recovering wetland biogeomorphic feedbacks to restore the world's biotic carbon hotspots. *Science*, 376 (6593), eabn1479.

Tesser, G., D'Alpaos, A & Lanzoni, S. (2007). Morphological characteristics of laboratory generated tidal networks. *River, Coastal and Estuarine Morphodynamics (RCEM 2007), Enschede, Netherlands*, pp. 771–777.

Thorn, C.E. & Welford, M.R. (1994). The equilibrium concept in geomorphology. *Annals of the Association of American Geographers*, 84 (4), pp. 666–696.

Townend, I.H. (2012). The estimation of estuary dimensions using a simplified form model and the exogenous controls. *Earth Surface Processes and Landforms*, 37 (15), pp. 1573–1583.

Townend, I.H., Wang, Z.B. & Rees, J.G. (2007). Millennial to annual volume changes in the Humber Estuary. *Proceedings of the Royal Society A: Mathematical, Physical and Engineering Sciences*, 463 (2079), pp. 837–854.

Umitsu, M., Buman, M., Kawase, K. & Woodroffe, C.D. (2001). Holocene palaeoecology and formation of the Shoalhaven River deltaic-estuarine plains, Southeast Australia. *The Holocene*, 11 (4), pp. 407–418.

Van Belzen, J., Rienstra, G. & Bouma, T.J. (2021). *Dubbele dijken als robuuste waterkerende landschappen voor een welvarende Zuidwestelijke Delta.* Tech. rep. NIOZ Royal Netherlands Institute for Sea Research, 99 pp. DOI:10.25850/NIOZ/7B.B.KB.

Van de Lageweg, W.I., Schuurman, F., Cohen, K.M., Van Dijk, W.M., Shimizu, Y. & Kleinhans, M.G. (2016). Preservation of meandering river channels in uniformly aggrading channel belts. *Sedimentology*, 63 (3), pp. 586–608. DOI:10.1130/G35192.1.

Van de Lageweg, W.I., Van Dijk, W.M., Baar, A.W., Rutten, J. & Kleinhans, M.G. (2014). Bank pull or bar push: What drives scroll-bar formation in meandering rivers? *Geology*, 42 (4), pp. 319–322.

Van de Lageweg, W.I., Braat, L., Parsons, D.R. & Kleinhans, M.G. (2018). Controls on mud distribution and architecture along the fluvial-to-marine transition. *Geology*, 46 (11), pp. 971–974.

Van de Lageweg, W.I., Van Dijk, W.M. & Kleinhans, M.G. (2013). Channel belt architecture formed by a meandering river. *Sedimentology*, 60 (3), pp. 840–859.

Van de Broek, M., Baert, L, Temmerman, S. & Govers, G. (2019). Soil organic carbon stocks in a tidal marsh landscape are dominated by human marsh embankment and subsequent marsh progradation. *European Journal of Soil Science*, 70 (2), pp. 338–349.

Van den Hoven, K., Kroeze, C. & Van Loon-Steensma, J.M. (2022). Characteristics of realigned dikes in coastal Europe: Overview and opportunities for nature-based flood protection. *Ocean & Coastal Management*, 222, p. 106116.

Van der Spek, A.J.F. (1995). Reconstruction of tidal inlet and channel dimensions in the Frisian Middelzee, a former tidal basin in the Dutch Wadden Sea. *Tidal Signatures in Modern and Ancient Sediments*, 24, pp. 239–258.
Van der Spek, A.J.F. (1997). Tidal asymmetry and long-term evolution of Holocene tidal basins in The Netherlands: simulation of palaeo-tides in the Schelde estuary. *Marine geology*, 141 (1-4), pp. 71–90.
Van der Wal, D., Herman, P.M.J., Forster, R.M., Ysebaert, T., Rossi, F., Knaeps, E., Plancke, Y.M.G. & Ides, S.J. (2008). Distribution and dynamics of intertidal macrobenthos predicted from remote sensing: response to microphytobenthos and environment. *Marine Ecology Progress Series*, 367, pp. 57–72.
Van der Wegen, M. & Roelvink, J.A. (2008). Long-term morphodynamic evolution of a tidal embayment using a two-dimensional, process-based model. *Journal of Geophysical Research: Oceans*, 113 (C3), pp. 1–23.
Van der Deijl, E.C., Van der Perk, M. & Middelkoop, H. (2017). Factors controlling sediment trapping in two freshwater tidal wetlands in the Biesbosch area, The Netherlands. *Journal of Soils and Sediments*, 17 (11), pp. 2620–2636.
Van der Spek, A.J.F. & Beets, D.J. (1992). Mid-Holocene evolution of a tidal basin in the western Netherlands: a model for future changes in the northern Netherlands under conditions of accelerated sea-level rise? *Sedimentary Geology*, 80 (3-4), pp. 185–197. DOI:10.1016/0037-0738(92)90040-X.
Van der Spek, A. (1994). *Large-scale evolution of Holocene tidal basins in the Netherlands*, p. 189.
Van Dijk, M., Postma, G. & Kleinhans, M.G. (2009). Autocyclic behaviour of fan deltas: an analogue experimental study. *Sedimentology*, 56 (5), pp. 1569–1589.
Van Dijk, W.M., Schuurman, F., Van de Lageweg, W.I. & Kleinhans, M.G. (2014). Bifurcation instability and chute cutoff development in meandering gravel-bed rivers. *Geomorphology*, 213, pp. 277–291.
Van Dijk, W.M., Teske, R., Van de Lageweg, W.I. & Kleinhans, M.G. (2013b). Effects of vegetation distribution on experimental river channel dynamics. *Water Resources Research*, 49 (11), pp. 7558–7574.
Van Dijk, W.M., Van de Lageweg, W.I. & Kleinhans, M.G. (2012). Experimental meandering river with chute cutoffs. *Journal of Geophysical Research: Earth Surface*, 117 (F3). DOI:10.1029/2011JF002314.
Van Dijk, W.M., Van de Lageweg, W.I. & Kleinhans, M.G. (2013a). Formation of a cohesive floodplain in a dynamic experimental meandering river. *Earth Surface Processes and Landforms*, 38 (13), pp. 1550–1565.
Van Dijk, W.M., Cox, J.R., Leuven, J.R.F.W., Cleveringa, J., Taal, M., Hiatt, M.R., Sonke, W., Verbeek, K., Speckmann, B. & Kleinhans, M.G. (2021). The vulnerability of tidal flats and multi-channel estuaries to dredging and disposal. *Anthropocene Coasts*, 4 (1), pp. 36–60.
Van Dijk, W.M., Hiatt, M., Van der Werf, J. & Kleinhans, M.G. (2019). Effects of shoal margin collapses on the morphodynamics of a sandy estuary. *Journal of Geophysical Research: Earth Surface*, 124 (1), pp. 195–215.
Van Dijk, W.M., Mastbergen, D.R., Van den Ham, G.A., Leuven, J.R.F.W. & Kleinhans, M.G. (2018). Location and probability of shoal margin collapses in a sandy estuary. *Earth Surface Processes and Landforms*, 43 (11), pp. 2342–2357.
Van Heijst, M.W. & Postmal, G. (2001). Fluvial response to sea-level changes: A quantitative analogue, experimental approach. *Basin Research*, 13 (3), pp. 269–292. DOI:10.1046/j.1365-2117.2001.00149.x.
Van Kessel, T. & Vanlede, J. (2010). Impact of harbour basins on mud dynamics Scheldt estuary in the framework of LTV. *Deltares: Delft*, pp. 1–29.
Van Kessel, T., Vanlede, J. & De Kok, J. (2011). Development of a mud transport model for the Scheldt estuary. *Continental Shelf Research*, 31 (10), S165–S181.
Van Ledden, M., Van Kesteren, W.G.M. & Winterwerp, J.C. (2004). A conceptual framework for the erosion behaviour of sand–mud mixtures. *Continental Shelf Research*, 24 (1), pp. 1–11.
Van Maren, D.S., Oost, A.P., Wang, Z.B. & Vos, P.C. (2016). The effect of land reclamations and sediment extraction on the suspended sediment concentration in the Ems Estuary. *Marine Geology*, 376, pp. 147–157.
Van Oorschot, M.V., Kleinhans, M.G., Geerling, G. & Middelkoop, H. (2016). Distinct patterns of interaction between vegetation and morphodynamics. *Earth Surface Processes and Landforms*, 41, pp. 791–808. DOI:10.1002/esp.3864.
Van Putte, N., Temmerman, S., Verreydt, G., Seuntjens, P., Maris, T., Heyndrickx, M., Boone, M., Joris, I. & Meire, P. (2020). Groundwater dynamics in a restored tidal marsh are limited by historical soil compaction. *Estuarine, Coastal and Shelf Science*, 244, p. 106101.
Van Rijn, L.C. (2007). Unified View of Sediment Transport by Currents and Waves. I: Initiation of Motion, Bed Roughness, and Bed-Load Transport. *Journal of Hydraulic Engineering*, 133 (6), pp. 649–667. DOI:10.1061/(ASCE)0733-9429(2007)133:6(649).
Van Rijn, L.C. (1997). Sediment transport and budget of the central coastal zone of Holland. *Coastal Engineering*, 32 (1), pp. 61–90.
Vandenbruwaene, W., Schwarz, C., Bouma, T.J., Meire, P. & Temmerman, S. (2015). Landscape-scale flow patterns over a vegetated tidal marsh and an unvegetated tidal flat: Implications for the landform properties of the intertidal floodplain. *Geomorphology*, 231, pp. 40–52.

Vlaswinkel, B.M. & Cantelli, A. (2011). Geometric characteristics and evolution of a tidal channel network in experimental setting. *Earth Surface Processes and Landforms*, 36 (6), pp. 739–752.
Vos, P., De Koning, J. & Van Eerden, R. (2015). Landscape history of the Oer-IJ tidal system, Noord-Holland (the Netherlands). *Netherlands Journal of Geosciences*, 94 (4), pp. 295–332.
Vos, P., Meulen, M., Weerts, H. & Bazelmans, J. (2018). *Atlas van Nederland in het Holoceen. Landschap en bewoning vanaf de laatste ijstijd tot nu*. Prometheus: Amsterdam.
Vos, P. (2015). *Origin of the Dutch coastal landscape: long-term landscape evolution of the Netherlands during the Holocene, described and visualized in national, regional and local palaeogeographical map series*. Barkhuis.
Vos, P.C. & Van Kesteren, W.P. (2000). The long-term evolution of intertidal mudflats in the northern Netherlands during the Holocene; natural and anthropogenic processes. *Continental Shelf Research*, 20 (12-13), pp. 1687–1710.
Vroom, J., De Vet, P.L.M. & Van der Werf, J. (2015). Validatie Waterbeweging Delft3D NeVla Model Westerscheldemonding. *Technical Report*. Deltares.
Vuik, V., Jonkman, S.N., Borsje, B.W. & Suzuki, T. (2016). Nature-based flood protection: The efficiency of vegetated foreshores for reducing wave loads on coastal dikes. *Coastal engineering*, 116, pp. 42–56.
Wallace, K.J., Callaway, J.C. & Zedler, J.B. (2005). Evolution of tidal creek networks in a high sedimentation environment: a 5-year experiment at Tijuana Estuary, California. *Estuaries*, 28 (6), pp. 795–811.
Wang, Z.B., Jeuken, C & De Vriend, H.J. (1999). Tidal asymmetry and residual sediment transport in estuaries. *Delft Hydraulics report Z2749*.
Wang, Z.B. & Townend, I.H. (2012). Influence of the nodal tide on the morphological response of estuaries. *Marine Geology*, 291, pp. 73–82.
Watts, C.W., Tolhurst, T.J., Black, K.S. & Whitmore, A.P. (2003). In situ measurements of erosion shear stress and geotechnical shear strength of the intertidal sediments of the experimental managed realignment scheme at Tollesbury, Essex, UK. *Estuarine, Coastal and Shelf Science*, 58 (3), pp. 611–620.
Weiss, S.F. (2016). *Meandering river dynamics*. PhD dissertation. University of Illinois.
Weitbrecht, V., Kühn, G. & Jirka, G.H. (2002). Large scale PIV-measurements at the surface of shallow water flows. *Flow Measurement and Instrumentation*, 13 (5-6), pp. 237–245.
Westoby, M.J., Brasington, J., Glasser, N.F., Hambrey, M.J. & Reynolds, J.M. (2012). 'Structure-from-Motion' photogrammetry: A low-cost, effective tool for geoscience applications. *Geomorphology*, 179, pp. 300–314.
Wheeler, D., Tan, S., Pontee, N. & Pygott, J. (2008). Alkborough scheme reduces extreme water levels in the Humber Estuary and creates new habitat. In: *FLOODrisk 2008-The European Conference on Flood Risk Management Research in to Practice 30 September–2 October 2008 Keble College, Oxford, UK*.
Williams, P.B. & Orr, M.K. (2002). Physical evolution of restored breached levee salt marshes in the San Francisco Bay estuary. *Restoration Ecology*, 10 (3), pp. 527–542.
Wilson, K., Berryman, K., Cochran, U. & Little, T. (2007). A Holocene incised valley infill sequence developed on a tectonically active coast: Pakarae River, New Zealand. *Sedimentary Geology*, 197 (3-4), pp. 333–354.
Wolters, M., Garbutt, A. & Bakker, J.P. (2005). Salt-marsh restoration: evaluating the success of de-embankments in north-west Europe. *Biological Conservation*, 123 (2), pp. 249–268.
Woodroffe, C.D., Rogers, K., McKee, K.L., Lovelock, C.E., Mendelssohn, I. & Saintilan, N. (2016). Mangrove sedimentation and response to relative sea-level rise. *Annual Review of Marine Science*, 8, pp. 243–266.
Woodruff, J.D., Martini, A.P., Elzidani, E.Z., Naughton, T.J., Kekacs, D.J. & MacDonald, D.G. (2013). Off-river waterbodies on tidal rivers: Human impact on rates of infilling and the accumulation of pollutants. *Geomorphology*, 184, pp. 38–50.
Woolderink, H.A.G., Weisscher, S.A.H., Kleinhans, M.G., Kasse, C. & Van Balen, R.T. (2022). Modelling the effects of normal faulting on alluvial river meandering. *Earth Surface Processes and Landforms*, 47 (5), pp. 1252–1270.
Yabe, T., Ishikawa, T., Kadota, Y. & Ikeda, F. (1990). A multidimensional cubic-interpolated pseudoparticle (CIP) method without time splitting technique for hyperbolic equations. *Journal of the Physical Society of Japan*, 59 (7), pp. 2301–2304. DOI:10.1143/JPSJ.59.2301.
Yang, B.C., Dalrymple, R.W. & Chun, S.S. (2005). Sedimentation on a wave-dominated, open-coast tidal flat, south-western Korea: summer tidal flat–winter shoreface. *Sedimentology*, 52 (2), pp. 235–252.
Ysebaert, T., Herman, P.M.J., Meire, P., Craeymeersch, J., Verbeek, H. & Heip, C.H.R. (2003). Large-scale spatial patterns in estuaries: estuarine macrobenthic communities in the Schelde estuary, NW Europe. *Estuarine, coastal and shelf Science*, 57 (1-2), pp. 335–355.
Zanichelli, G., Caroni, E. & Fiorotto, V. (2004). River bifurcation analysis by physical and numerical modeling. *Journal of Hydraulic Engineering*, 130 (3), pp. 237–242.
Zecchin, M., Brancolini, G., Tosi, L., Rizzetto, F., Caffau, M. & Baradello, L. (2009). Anatomy of the Holocene succession of the southern Venice lagoon revealed by very high-resolution seismic data. *Continental Shelf Research*, 29 (10), pp. 1343–1359.

Zhang, M., Dai, Z., Bouma, T.J., Bricker, J., Townend, I., Wen, J., Zhao, T. & Cai, H. (2021). Tidal-flat reclamation aggravates potential risk from storm impacts. *Coastal Engineering*, 166, p. 103868.

Zhou, Z., Coco, G., Jiménez, M., Olabarrieta, M., Van der Wegen, M. & Townend, I.H. (2014). Morphodynamics of river-influenced back-barrier tidal basins: The role of landscape and hydrodynamic settings. *Water Resources Research*, 50 (12), pp. 9514–9535.

Zhou, Z., Coco, G., Townend, I., Olabarrieta, M., Van Der Wegen, M., Gong, Z., D'Alpaos, A., Gao, S., Jaffe, B.E., Gelfenbaum, G., et al. (2017). Is "morphodynamic equilibrium" an oxymoron? *Earth-Science Reviews*, 165, pp. 257–267.

Zhu, Z., Vuik, V., Visser, P.J., Soens, T., van Wesenbeeck, B., van de Koppel, J., Jonkman, S.N., Temmerman, S. & Bouma, T.J. (2020). Historic storms and the hidden value of coastal wetlands for nature-based flood defence. *Nature Sustainability*, 3 (10), pp. 853–862.

Zinger, J.A., Rhoads, B.L., Best, J.L. & Johnson, K.K. (2013). Flow structure and channel morphodynamics of meander bend chute cutoffs: A case study of the Wabash River, USA. *Journal of Geophysical Research: Earth Surface*, 118 (4), pp. 2468–2487. DOI:10.1002/JGRF.20155.

Zolezzi, G. & Seminara, G. (2001). Downstream and upstream influence in river meandering. Part 1. General theory and application to overdeepening. *Journal of Fluid Mechanics*, 438, pp. 183–211.

Zong, L. & Nepf, H. (2011). Spatial distribution of deposition within a patch of vegetation. *Water Resources Research*, 47 (3), W03516. DOI:10.1029/2010WR009516.

Acknowledgements

This thesis and the past four-and-a-half years of my PhD project would have looked very different if not for the contributions of many friends and colleagues. Below, I wish to thank the people who supported me and my work.

Maarten, jij was de drijvende kracht (*pun intended*) die mij deed inzien hoe verwonderlijk water en zand ons aardoppervlak vormen. Ik wil je graag bedanken voor je enorme enthousiasme voor mijn onderzoek en jouw bodemloze put aan ideeën. Ons kantoor leek wel een fruitgaard met al het "laaghangend fruit" dat je overal zag hangen. Dat laaghangend fruit bleek met regelmaat toch zwaar op de maag te vallen en langer te verwerken dan voorzien. Desondanks heb ik met onder andere jouw hulp en inzicht hier spreekwoordelijk een paar mooie appeltaarten (lees: artikelen) van kunnen bakken. Over bakken gesproken: **Anne**. We leerden elkaar kennen toen ik bij jou mij masteronderzoek kwam doen en weet nog goed hoe ik wekenlang zand zat te zeven in een klein kamertje in de Zonneveldvleugel voor een uitgebreide data set die we later samen publiceerden. Je hebt een natuurlijke gave om mensen te motiveren (voor jou) aan de slag te gaan met jouw oneindige vrolijkheid en oprechte interesse op professioneel en persoonlijk vlak. Ik vond het daarom altijd onzettend fijn om ook tijdens mijn promotieonderzoek met je samen te werken en lekker bij te kletsen.

This journey wouldn't have been possible without my close colleagues that helped me through thick and thin. No matter what PhD-life threw at us, we reminded each other to celebrate our wins, no matter how little they were. And what better way to do so than having a well-deserved pancake at the Rhijnauwen pancake house? **Frances**, **Jana**, **Job**, **Lonneke**, **Safaa**, **Tatjana**, and others, thank you for this great tradition. And while we are at the topic of food, I also wish to express my gratitude for the occasional potluck evenings I had with many of my former colleagues: **Anne**, **Jasper**, **Harm-Jan**, **Lisanne**, **Marcio**, **Müriel**, **Sanja**, **Will** and **Wout**, thank you for these joyful evenings. Besides indulging in food, desserts and what not, I could of course also rely on my PhD colleagues in other ways and would like to thank a few here. **Jana** (and **Julien**), I loved the many afternoons and evenings we played board games together and caught up on work and life, mostly the latter. And let's not forget about you properly introducing me to Eurovision. **Tatjana**, it has been wonderful getting to know you, I admire your optimism and I enjoyed our chats about life, gardening, yoga and knitting. **Lonneke**, with you there was never a dull moment and for support, laughs and lunch breaks you were never far away, for which I am very pleased. **Danghan**, thank you for your positive vibe in and around the office and I like how we got to know each other better towards the end of our PhD projects. **Lisanne**, I am really pleased you made a short informative video of my research that I have since used in many media outlets to show and explain my work. **Chloe**, I enjoyed our time at EGU and would like to thank you for the many uplifting and joyous conversations. Also many thanks to all of you who helped shovelling sand and cleaning the Metronome so I could conduct my flume experiments. It was tiring work but the many ABBA medleys and biscuits made it fun all the same, right, **Anne**?

I wish to thank the members of the exam committee: **Katja Philippart**, **Iris Möller**, **Stijn Temmerman**, **Ad van der Spek**, **Ton Hoitink** and **Tjeerd Bouma**. Thank you for your time and investment in evaluating my thesis and acting as opponents during the public defence.

Shimizu-sensei and **Kyuka-san**, thank you for giving me the opportunity for doing an internship at Hokkaido University and teaching me the numerical model Nays2D which I have used in many of my papers since. I have learnt a lot from you on Japanese river management and am very grateful I was given the floor to present my work on meandering rivers to the local ministries in Obihiro. It was a wonderful and insightful experience that I will never forget. 感謝の申し上げようございません。

Verder wil ik graag de lab technici **Arjan**, **Bas**, **Marcel**, **Mark** en **Henk** bedanken voor jullie inzet om mijn experimenten in de kantelende stroomgoot de Metronoom mogelijk te maken. De Metronoom en alle omhangende software en apparatuur vereisten de nodige, uitgebreide handleidingen en er ging soms ook wat mis, maar mede dankzij jullie hebben we een paar prachtige riviermondingen kunnen nabootsen. Uiteindelijk blijft het professioneel spelen in een zandbak.

Kim, **Robert**, **Jordy**, **Josephien**, **Jelle**, **Pelle** en **Jan-Eike**, bedankt voor jullie bijdrage aan ons onderzoek met jullie BSc en MSc projecten. Veel van jullie projecten hebben aan de grondslag gelegen van huidige en toekomstige publicaties.

Met veel plezier heb ik tijdens m'n promotietraject onderwijs gegeven en ondersteund. **Esther**, **Hans**, **Kim**, **Maarten** en **Wim**, bedankt voor de prettige samenwerking tijdens het geven van jullie cursussen. Mede door het geven van veel onderwijs tijdens m'n promotietraject en daarvoor als junior docent heb ik mijn BKO mogen behalen. **Martin** en **Maarten**, bedankt dat jullie dit mogelijk hebben gemaakt. **Elisabeth**, al sinds het Honours College Geowetenschappen werkte ik in verschillende rollen met je samen en ik kon altijd bij jou terecht voor een goed gesprek, of dat nu ging over werk of alles behalve. Bedankt voor je hulp, advies en gezelligheid. **Stefan**, bedankt voor het helpen uitdragen van ons onderzoek naar het grotere publiek via verschillende media. Echt een kers op de taart om zo je onderzoek te mogen afronden.

Eveline, **Franca** en **Suzanne**, dankjulliewel voor het meehelpen opzetten van de PhD introductie dagen. En **Eveline**, wat was het een klus om de enquête over het welzijn van promovendi AVG in elkaar te draaien, maar het is ons gelukt en vormt nu de basis voor enquêtes in andere faculteiten.

Margriet, **Noraini** en **Rianne**, fijn dat we elkaar sinds onze studietijd op de IBB zijn blijven zien, telkens weer onder het genot van een goed boek en lekkere hapjes. **Lennart**, bedankt voor de leuke ervaringen en overvloedige filmtips. Fijn dat we zoveel met elkaar kunnen delen. **Laura**, **Bente** en **Erik**, hoewel onze wegen scheidden na onze studie zijn we elkaar blijven zien, waarbij de meeste keren het ook onbedoeld een soort housewarming was bij een van ons. We verhuizen wat af met elkaar! Leuk om zo steeds weer een nieuw stukje Nederland te ontdekken. Ook wil ik graag **Felicia** en **Martine** bedanken voor jullie steun wanneer ik dat nodig had. Ik heb veel van jullie over mezelf geleerd. **Rob** en **Annerie**, jullie enthousiasme over en interesse voor alles dat met onderzoek en natuur te maken heeft, inspireert mij. Het is altijd gezellig als we bij elkaar zijn en iedere keer leer ik weer bij over wat de natuur ons allemaal te bieden heeft.

Pap, **mam** en **Roos**, bedankt dat jullie er altijd voor me zijn. Van kinds af aan steunen jullie mij in alles wat ik doe en met al mijn verhalen en ervaringen kan ik bij jullie terecht. Onder het genot van een borrel buiten onder de plataan, een wandeling op de hei of een film op de bank, we hebben meer dan genoeg manieren om te ontspannen en van het leven te genieten. Ik kijk dan ook terug op prachtige ervaringen thuis en op vakantie die ik lang zal koesteren.

Als laatste, **Jasper**: met jou kan ik de wereld aan en met volle teugen van het leven genieten. Je hebt het beste met me voor en staat altijd klaar met goed advies als ik dat nodig heb, ook al ben ik soms te eigenwijs om dat te volgen. We hebben prachtige ervaringen opgedaan in en rondom ons nieuwe huis en op de vele vakanties en ik kijk enorm uit naar wat voor moois de toekomst ons nog meer te bieden heeft.

About the author

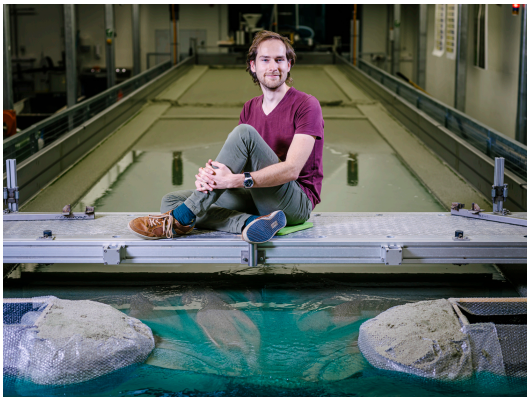

I was born in Roosendaal, The Netherlands on 23 December 1993. Although I developed a natural curiosity for rocks and geology from a young age, I was swayed into studying the natural development of rivers, estuaries and coasts during my Bachelor Earth Sciences at Utrecht University. I continued my studies at Utrecht University with a Masters Earth Surface and Water in 2015, focusing on river and coastal dynamics. For my master thesis, I conducted experiments on sediment sorting in river bends. My babbling to my supervisors about learning Japanese in my free time earned me a six-month internship at Hokkaido University in Japan, where I worked on the numerical modelling of meandering rivers with vegetation. Back in the Netherlands and after graduating cum laude in 2017, I worked as a junior teacher at the department of Physical Geography at Utrecht University for four months. Then, I was given the opportunity to start my PhD project with Maarten Kleinhans (and later also Anne Baar) in February 2018 on building and raising land along meandering rivers and estuaries using scale experiments and numerical modelling. Throughout my studies and PhD project, I enjoyed supervising bachelor and master students in thesis writing and teaching multiple courses. For science outreach, I publicised my work in multiple national media and acted as a program developer for an annual summer school for primary school children.

List of publications

Journal articles as first author

Weisscher, S. A. H., Adema, P. H., Rossius, J.-E. & Kleinhans, M. G. (in review). The effect of sea-level rise on estuary filling in scaled laboratory experiments. *The Depositional Record*.

Weisscher, S. A. H., Baar, A. W., Van Belzen, J., Bouma, T. J. & Kleinhans, M. G. (2022). Transitional polders between double dikes: driving land-level rise and reducing flood propagation. *Nature-Based Solutions*, 2, 100022, 15 pp DOI: 10.1016/j.nbsj.2022.100022.

Weisscher, S. A. H., Van den Hoven, K., Pierik, H.-J. & Kleinhans, M. G. (2022). Building and raising land: mud and vegetation effects in infilling estuaries. *Journal of Geophysical Research*, 127(1), 1–24. DOI: 10.1029/2021JF006298.

Weisscher, S. A. H., Boechat-Albernaz, M., Leuven, J. R. F. W., Van Dijk, W. M., Shimizu, Y., & Kleinhans, M. G. (2020). Complementing scale experiments of rivers and estuaries with numerically modelled hydrodynamics. *Earth Surface Dynamics*, 8(4), 955–972. DOI: 10.5194/esurf-8-955-2020.

Weisscher, S. A. H., Shimizu, Y., & Kleinhans, M. G. (2019). Upstream perturbation and floodplain formation effects on chute-cutoff-dominated meandering river pattern and dynamics. *Earth Surface Processes and Landforms*, 44(11), 2156–2169. DOI: 10.1002/esp.4638.

Journal articles as co-author

Cox, J. R., Lingbeek, J., **Weisscher, S. A. H.** & Kleinhans, M. G. (in review). Effects of sea-level rise on dredged estuary morphology. *Geophysical Research Letters*.

Kleinhans, M. G., Roelofs, L., **Weisscher, S. A. H.**, Lokhorst, I. R. & Braat, L. (2022). Estuarine morphodynamics and development modified by floodplain formation. *Earth Surface Dynamics*, 10(2), 367–381. DOI:10.5194/esurf-10-367-2022.

Woolderink, H. A. G., **Weisscher, S. A. H.**, Kleinhans, M. G., Kasse, C. & Van Balen, R. T. (2022). Modelling the effects of normal faulting on alluvial river meandering. *Earth Surface Processes and Landforms*, 47(5), 1252‐-1270. DOI:10.1002/esp.5315.

Baar, A. W., **Weisscher, S. A. H.**, & Kleinhans, M. G. (2020). Interaction between lateral sorting in river bends and vertical sorting in dunes. *Sedimentology*, 67(1), 606–626. DOI:10.1111/sed.12656.

De Haas, T., Van der Valk, L., Cohen, K. M., Pierik, H. J., **Weisscher, S. A. H.**, Hijma, M. P., Van der Spek, A. J. F. & Kleinhans, M. G. (2019). Long-term evolution of the Old Rhine estuary: Unravelling effects of changing boundary conditions and inherited landscape. *The Depositional Record*, 5(1), 84–108. DOI:10.1002/dep2.56.

Leuven, J.R.F.W., Kleinhans, M.G., **Weisscher, S.A.H.** & Van der Vegt, M. (2016). Tidal sand bar dimensions and shapes in estuaries. *Earth-Science Reviews* (invited review), 161, 204–223. DOI:10.1016/j.earscirev.2016.08.004.

Outreach

Selected news articles

Janssen, C. (2021). Investeer anders: 'dijken geen oplossing tegen stijgende zeespiegel'. *Foodlog*. (28-12-2021) Available at: foodlog.nl.

Schreuder, W. (2021). Kronkelende rivieren stoten minder CO2 uit dan rechte. *New Scientist*. (10-12-2021). Available at: newscientist.nl.

Van der Linden, W. X. (2021). Wat kunnen we leren van een overstroming van 6 eeuwen geleden om Nederland te beschermen. *EenVandaag*. (09-12-2021). Available at: eenvandaag.avrotros.nl.

Van Mersbergen, C. (2021). 600 jaar na de vloed: 'Absurd dat we gewoon doorbouwen alsof er niets aan de hand is'. *Algemeen Dagblad*. (18-11-2021). Availabel at: ad.nl.

Television reports

Omroep Zeeland (19-07-2022) - regional tv program on land-level rise in the province of Zeeland in The Netherlands in collaboration with photography artist Rem van den Bosch and story teller J. Zinkweg of *Zand & Zink film and tv*.

EenVandaag (10-12-2021) - national news item on the Sint-Elisabeths flood in collaboration with K. De Moed and W. X. Van der Linden.

Algemeen Dagblad (18-11-2021) - online news item on the Sint-Elisabeths flood and land-level rise.

Radio performances

NPO Radio 1 EenVandaag (10-12-2021 16:30) - 8-minute interview on the Sint-Elisabeths flood and land-level rise.

Utrecht University
Faculty of Geosciences
Department of Physical Geography

ISSN 2211-4335